5-2009

Sands through the hourglass the structural and functional diversity of major intrinsic proteins

Ian Stuart Wallace
University of Tennessee

To the Graduate Council:

I am submitting herewith a dissertation written by Ian Stuart Wallace entitled "Sands through the hourglass the structural and functional diversity of major intrinsic proteins." I have examined the final electronic copy of this dissertation for form and content and recommend that it be accepted in partial fulfillment of the requirements for the degree of Doctor of Philosophy, with a major in Biochemistry and Cellular and Molecular Biology.

Daniel M. Roberts, Major Professor

We have read this dissertation and recommend its acceptance:

Accepted for the Council:

Carolyn R. Hodges

Vice Provost and Dean of the Graduate School

(Original signatures are on file with official student records.)

To the Graduate Council:

I am submitting herewith a dissertation written by Ian Stuart Wallace entitled "Sands Through the Hourglass: The Structural and Functional Diversity of Major Intrinsic Proteins." I have examined the final electronic copy of this dissertation for form and content and recommend that it be accepted in partial fulfillment of the requirements for the degree of Doctor of Philosophy, with a major in Biochemistry, Cellular, and Molecular Biology.

_____
Daniel M. Roberts, Major Professor

We have read this dissertation
and recommend its acceptance:

Albrecht G. von Arnim_____

Cynthia B. Peterson_____

Kurt Lamour_____

(Original signatures are on file with official student records)

Accepted for the Council:

Carolyn R. Hodges_____

Vice Provost and Dean of the Graduate School

Sands Through the Hourglass: The Structural and Functional Diversity of Major Intrinsic Proteins

A Dissertation

Presented for the

Doctor of Philosophy

Degree

The University of Tennessee, Knoxville

Ian Stuart Wallace

May, 2009

Acknowledgements

I have thought about what I would say on this page for the last four and a half years, but upon reaching this point I am at a loss for words. It would require another 200-page dissertation to properly thank all of the people and describe all of the experiences that I have had in this part of my life. I do not have that kind of space, so I will just do the best that I can.

I met Daniel "Bossman" Roberts as an undergraduate here at the University of Tennessee, and he immediately struck me as an intellectual force to be reckoned with. I decided to join Dan's lab in the fall of 2001 due to the influence and taunts of Dr. Jim Guenther (who we will get to in a bit), and that decision allowed me to truly figure out what I wanted for my education, my occupation, and my life. A few years later, Dan convinced me (through the lens of a 32 oz. Dos Equis dark) to remain at UT in his lab, and I will never regret that decision (unlike some of the other ones that I have made through the lens of a 32 oz. Dos Equis dark). Dan has always told me that when I leave, I will take the parts of him that I like and leave the ones that I don't to my next position. So I will take the neurotic attention to detail, the respect for biochemistry in all of its forms, the sharp tongue, the passion for teaching, and the ability to analyze any scientific question from one hundred different angles. However, some of his musical tastes and opinions on mine might not make the trip. On a more serious note, I will be eternally grateful to Dan for the time that he has spent with me imparting the many secrets of successful science.

I would also like to thank my committee for providing guidance and constructive criticism during my time in graduate school. I chose Albrecht von

Arnim, Kurt Lamour, and Cynthia Peterson to serve in this capacity because I regard them all as excellent scientists, and I knew that they would provide a diverse and rigorous gauntlet of knowledge to aid me through my doctoral research. I would also like to thank Dr. Elizabeth Howell for having a number of insightful conversations with me concerning enzyme kinetics, thermodynamics, and life in general. Finally, I would like to thank my collaborators Mayuki Tanaka, Toru Fujiwara, Angela Douglas, and Ally Shakesby for giving me the opportunity to work on the NIP6;1 boric acid transport and aphid aquaporin projects, respectively. These projects allowed me to perform truly international collaborative science, and I am sure that these experiences will prove to be crucial in my development as a researcher. I am indebted to these people and I will not forget the many pieces of advice that you have given me.

I blame Jim Guenther for getting me into this business. In my opinion, Jim parallels Tom Maniatis as a technical resource for methods in molecular biology, and he taught me how even the simplest experiments can be rewarding. My first unambiguous positive result was collected in his presence and it was at that moment that I decided I wanted to be a scientist. Jim rarely ever gave me a direct answer to a question, but rather made me figure out how to do things on my own, then teased me until I got it right. Though his lessons could be cruel, they were valuable and taught me the importance of becoming an independent scientist. Jim is also not the kind of person to befriend people lightly, but his friendship to me has been one of (brutal but fair) honesty and he truly does have “big wings”.

I have had the fortune to work with a number of people in the lab who have also provided me with knowledge, good company, and preservation of sanity over the past seven years. Won-Gyu Choi will always be my good friend and never ceases to amaze me. His devotion to his work and family as well as his ability to work for hours without sleep are admirable and I wish I could be more like him. I would like to thank Eric Vincill for his constant source of amusement, his green thumb, and for throwing up on my rug during his bachelor party. I have enjoyed working with Jin Ha Hwang in the lab over the past three years, and I am sure that his attention to detail in research will serve him well. I would also like to thank him for the occasional cigarette that got me through the last year of graduate school.

As I am leaving, I have bequeathed part of my work that is near and dear to my heart to Pintu Masalkar, and I hope that he will nourish this work through his time and efforts. Judging by the work that he has been able to accomplish in only a year's time, I think that this project is in safe hands. I see great promise in Ansul Lokdarshi, and I look forward to seeing him mature as a scientist (especially because I want to hire him as a postdoc when he graduates). Despite his taste for warm peanut butter and pea sandwiches, I feel that Ansul has much to offer the lab and that he will have a productive career in science. I want to thank John McReynolds and Tian Li for taking over the aphid and plant aquaporin projects, respectively. Both of these students have a passion for science and it greatly pleases me to know that they will continue the work that I have toiled with for so long. Finally, I would like to thank all of the talented undergraduates and rotation students that helped me in the lab at one time or another (Derek Slagle, Wes Gideon, Travis Farmer, Rebecca Wilson, Hee-

Youn Yang, and others). I hope that they are content with their chosen paths and I thank them for their time in the lab.

I would also like to thank my friends and family whom I have neglected for more years than I can count due to long hours in the lab. I thank them for putting up with my BS and loving me anyway and for all of their support (emotional and occasional financial). I truly could not have done this without you and I thank you from the bottom of my heart. I would finally like to dedicate this dissertation to my grandparents who came from meager beginnings to provide their families with the opportunity to do whatever they wanted in life.

ABSTRACT

Major Intrinsic Proteins (MIPs) are an ancient family of integral membrane proteins that mediate the bidirectional flux of water and small solutes across cellular membranes. Genomic and phylogenetic analyses indicate that plants contain more MIP genes than their animal and microbial counterparts. An analysis of MIP structure also indicates that plant MIPs structurally diverse at the regions that control selectivity of these proteins. Homology modeling was performed using all 35 members of the MIP family from *Arabidopsis thaliana*. This analysis revealed that MIPs can be divided into 8 functional subgroups based on the amino acids in their selectivity determining ar/R regions. A broader phylogenetic analysis of all available MIP sequences indicates that 92 ar/R regions exist in this dataset, and that much of the diversity arises from plant sources.

Homology modeling indicated that the Nodulin 26-like intrinsic protein (NIP) family of Arabidopsis could be divided into two subgroups based on ar/R classification: NIP subgroup I and II. Functional analysis indicates that these two subgroups are functionally distinct. NIP subgroup I forms aquaglyceroporin channels that are also permeable to ammonia, while NIP subgroup II channels are impermeable to water and capable of transporting larger solutes, such as urea. Site-directed mutagenesis studies were used to rationally interconvert the selectivity of these proteins by amino acid substitutions in the ar/R region. Finally, it was demonstrated that members of NIP subgroup II in Arabidopsis form physiologically relevant boric acid channels at the plasma membrane.

Nodulin 26, the archetypal NIP, is phosphorylated by a calcium dependant protein kinase (CDPK) at Ser 262 in its C-terminus. This study demonstrates that nodulin 26 phosphorylation increases the water permeability of the channel. In addition, the C-terminus was found to constitute a protein interaction site for nodule cytosolic glutamine synthetase.

Finally, the study was extended to characterize MIP channels from the common pea aphid (ApAQP1 and ApAQP2). The results indicate that ApAQP1 is a water-selective aquaporin that is involved in aphid gut osmoregulation, while ApAQP2 is a water channel that is permeable to an array of linear polyols. The potential physiological function of this channel is also discussed.

COMPREHENSIVE ABSTRACT

Major Intrinsic Proteins (MIPs) mediate the bi-directional flux of water and small neutral solutes across cellular membranes. MIPs have classically been divided into two functional categories: the water-specific aquaporins, and aquaglyceroporins, which are permeable to water as well as other solutes, such as glycerol. Several recent structural analyses of MIPs indicate that these proteins have a three-dimensional fold that is structurally conserved from bacteria to higher eukaryotes, and this protein fold consists of six membrane-spanning α-helices interrupted by five loop regions (loops A-E). Structural analysis and molecular dynamics simulations have implicated a tetrad of residues consisting of amino acids from helix 2 (H2), helix 5 (H5), and loop E (LE_1 and LE_2) in determining the substrate selectivity and transport rate of these proteins, and this region of the pore is known as the aromatic/ arginine (ar/R) selectivity filter.

Phylogenetic and homology modeling analyses from the present work indicate that plants show a considerably greater ar/R diversity. By using Arabidopsis as a test system, the complete MIP complement of this organism was modeled and the ar/R regions were analyzed. The 35 Arabidopsis MIPs could be grouped into a total of 8 different functional subfamilies based on the identity of the amino acids at their ar/R regions. Subsequent phylogenetic analysis using a MIP sequence database composed of 1000 sequences from all known eukaryotic and prokaryotic kingdoms indicated that a total of 92 classes of ar/R regions were observed. These results indicate that the structural diversity of the ar/R region in MIPs is much greater than previously

conceived, and that these novel ar/R regions could result in MIPs that have been evolutionarily recruited to perform new physiological functions.

To test this hypothesis, we used a combination of homology modeling, functional analysis, and site-directed mutagenesis to characterize new members of the plant MIP family and determine the residues that contribute to their substrate specificity. This analysis led to the discovery of two ar/R subgroups of the Nodulin-26-like Intrinsic Proteins (NIPs): NIP subgroup I and II. These subgroups differ by only a single nonconservative substitution at the H2 position their ar/R region of Trp (NIP subgroup I) and Ala (NIP subgroup II). Functional analysis indicates that representative members of NIP subgroup I (nodulin 26) and NIP subgroup II (AtNIP6;1) have distinct transport properties. Nodulin 26 is an aquaglyceroporin that is permeable to water, glycerol, ammonia, and formamide, but is impermeable to urea. In contrast, AtNIP6;1 is completely impermeable to water, but is capable of transporting the larger test solutes, with the essential plant micronutrient boric acid identified as the physiologically relevant solute.

AtNIP6;1 is predominantly expressed phloem tissues within the stem nodes in the aerial organs of Arabidopsis, and phenotypic analysis of AtNIP6;1 T-DNA mutants indicate that these plants exhibit severe leaf developmental abnormalities under boric acid-limiting conditions. A model is proposed in which AtNIP6;1 is involved in preferentially distributing boric acid to these developing aerial tissues, and this model relates AtNIP6;1 to other Arabidopsis boric acid channels to provide a comprehensive understanding of plant boric acid transport.

To understand features outside of the ar/R region that influence MIP transport, we investigated the effect of post-translational modifications on nodulin 26 water permeability. Nodulin 26 is a NIP subgroup I protein that is specifically targeted to the symbiosome membrane of nitrogen-fixing root nodules in soybean. Nodulin 26 is phosphorylated by a symbiosome membrane-associated Calcium Dependent Protein Kinase (CDPK) on Ser 262. Functional analysis of nodulin 26 in *Xenopus laevis* oocytes and in isolated symbiosome membrane vesicles indicate that phosphorylation of nodulin 26 at Ser 262 increases the water permeability of this channel by three-fold. In addition, we determined that the cytosolically exposed C-terminal region of nodulin 26 that encompasses this phosphorylation site also serves as a protein interaction site for soybean nodule glutamine synthetase. Interaction of native and recombinant soybean cytosolic glutamine synthetases with intact nodulin 26 was demonstrated in isolated soybean symbiosome membranes as well as by split-ubiquitin yeast two-hybrid analysis. A model is presented in which glutamine synthetase, may interact with nodulin 26, an ammonia channel, to form a "metabolic funnel" that serves to rapidly assimilate the fixed nitrogen escaping the symbiosome.

Finally, we applied homology modeling analysis techniques developed for plant MIPs to two aquaporin channels (ApAQP1 and ApAQP2) isolated from the common pea aphid (*Acyrthosiphon pisum*). Homology modeling analysis indicates that ApAQP1 contains all of the ar/R amino acids necessary to form a water-selective transport, while the ApAQP2 ar/R region contains nonconservative substitutions at the H5 and LE_1 positions that suggest it is capable of transporting solutes other than water. Functional analysis indicates that ApAQP1 is a water-selective channel that

exhibits a low activation energy for water transport and is inhibited by the classical aquaporin inhibitor mercury (II) chloride. ApAQP2 was also permeable to water, but this channel was unaffected by mercurial inhibitors and was able to transport a wide range of linear polyols in addition to water.

Real-time PCR expression analysis and in situ hybridization experiments indicate that ApAQP1 is expressed in the stomach and distal intestine of the aphid gut, while ApAQP2 is expressed in a specialized cell type termed the bacteriocyte, which houses metabolically-essential aphid symbionts (*Buchnera aphidicola*), suggesting that each of these proteins play different roles in aphid physiology. Overall, this study demonstrates that MIPs from plants and insects are more structurally diverse than their vertebrate animal as well as microbial counterparts with respect to the amino acids that compose their ar/R regions. This study also links this selectivity filter diversity to the ability of plants MIPs to transport novel physiological solutes. Finally, this study highlights the importance of posttranslational phosphorylation as a regulatory mechanism for MIPs, and suggests that protein interactions may be a previously unidentified component in the molecular function of MIPs.

TABLE OF CONTENTS

CHAPTER **PAGE**

CHAPTER **PAGE**

LIST OF TABLES

TABLES **PAGE**

LIST OF FIGURES

FIGURE **PAGE**

FIGURE **PAGE**

FIGURE **PAGE**

FIGURE **PAGE**

Chapter I

Introduction

Water and the experimental evidence for the existence of water channels

Due to its unique density, cohesive, adhesive, and temperature-associated properties, water is a unique and appropriate solvent for life. Water, which is present at 55.5 M in solution, is the most abundant molecule in cells, and all biological processes must be adapted to take place in the context this molecule. In addition, the interaction of water and phospholipids provides cells with a unique and essential opportunity to compartmentalize cellular processes by the formation of biological membranes (Deamer et al., 1994). Phospholipid bilayer membranes are characteristic of all living cells, and the formation of internal membranes in eukaryotic cells has contributed at a fundamental level to the complexity of eukaryotic organisms. Biological membranes are selectively permeable in that they allow small hydrophobic compounds to passively diffuse through the hydrophobic core of the lipid bilayer, while restricting the diffusion of hydrophilic compounds, such as carbohydrates, proteins, and nucleic acids. One complication of this selective permeability is that cells must manufacture proteins that can serve as selective conduits for the transport of essential ions and compounds that are not allowed to pass through the lipid bilayer.

Twenty-five years ago, it was widely accepted that water passively diffused across biological membranes because naked phospholipids bilayers were found to be quite permeable to water. However, the passive diffusion of water through membranes could not account for the high water permeability of certain cell types

(Finkelstein, 1987), most notably erythrocytes (Paganelli and Solomon, 1957; Sidel and Solomon, 1957), renal collecting duct cells (White and Rolf, 1963; Morgan and Berliner, 1968), and the toad urinary bladder (Kachadorian et al., 1977).

Water permeability can be quantitatively described by two biophysical parameters: the osmotic permeability coefficient (P_f) is a measure of the water permeability rate in an osmotic gradient, and the diffusional water permeability coefficient (P_d) is the rate of water diffusion under isoosmotic conditions. Passive diffusion of water through a phospholipids bilayer is characterized by a P_f/ P_d ratio that approaches unity. In contrast, a P_f/P_d ratio much greater than 1 indicates facilitated water transport through either a proteinacious or organized lipid component of the membrane. Human erythrocytes were found to have a P_f/ P_d ratio that was much greater than 1 (Brahm, 1982), and it was proposed that this observation resulted from the presence of a membrane water channel.

In addition, the energetics of water transport provided evidence that diffusion of water through lipids could not solely account for the water permeability of some biological membranes. Diffusion of water through lipid bilayers is characterized by a large activation energy (E_a) of 10 kcal/ mol or more (Cohen, 1975). This result indicates that as temperature increases, the lipids in the membrane bilayer will become more mobile and will allow water to flow through the membrane at a greater rate. In contrast, some membranes were found to have water transport activation energies of 3-5 kcal/mol, a characteristic that is indicative of water flowing through an aqueous conduit and an observation that indicates that water transport was much less dependent on temperature (Dicker and Elliot, 1967). These results again suggest

the existence of a low energy pathway that allows the facilitated flux of water across cellular membranes.

Finally, pharmacological evidence suggested the existence of membrane water channels. The water permeability of the toad urinary bladder plasma membrane as well as the mammalian renal collecting duct (Bourguet et al., 1976; Brown and Orci, 1983) drastically increases upon stimulation with the antidiuretic hormone vasopressin, indicating that cells can modulate their water permeability selectively and in response to hormonal stimuli through a proposed shuttling mechanism of membrane water channels (Wade et al., 1981). Pharmacological evidence also indicated that the water permeability of some membranes was acutely and reversibly inhibited by mercurial compounds (Macey and Farmer, 1970). Inhibition by mercurial compounds resulted in an increase in the E_a of water transport, presumably through the modification of the sulfhydryl side chain of cysteine residues in proteinacious water channels (Macey, 1984).

Overwhelmingly, the characteristics of rapid water permeability in certain cell types suggested the presence of integral membrane proteins that would transport water in an osmotic gradient. These initial experiments also predicted that any candidate water channel would have a P_f/ P_d ratio much greater than 1, an E_a for water transport between 3-5 kcal/ mol, and the channel would at least be sensitive to mercurial compounds.

The isolation of the first water channels

Early arguments suggested that water channels might be formed by organized lipid domains (Brown and Orci, 1983), but several experiments decidedly indicated water channels were proteinacious. Expression of isolated RNA from mammalian erythrocytes, renal papilla, and renal collecting ducts in *Xenopus laevis* oocytes indicated that these RNA populations encoded a protein that satisfied all water channel criteria (Zhang et al., 1990; Tsai et al., 1991). In addition, X-ray inactivation studies of water permeability in renal proximal tubule indicated that a protein of 30 kDa was responsible for the water permeability of these membranes (van Hoek et al., 1991).

Isolation of water channel proteins was very difficult due to the lack of specific modification reagents, the lack of a technique for their detection that was analagous to patch clamping of ion channels, and the relatively high permeability of naked bilayer membranes to water. Candidate proteins, including the band 3 anion exchange protein from red blood cells (Solomon et al., 1983) and the GLUT1 glucose transporter (Fischbarg et al., 1989; Fischbarg et al., 1990), were proposed to facilitate water transport across cell membranes, but these proteins did not satisfy the biochemical and biophysical criteria that had previously been ascribed to water channels (Zhang et al., 1991). As is the case in many great biological discoveries, the elucidation of the molecular identity of the water channel was serendipitous (Saboori et al., 1988).

The first water channel protein was isolated as a 28 kDa purification byproduct of the Rhesus (Rh) antigen from erythrocytes (Saboori et al., 1988). The byproduct was postulated to be a protein degradation fragment of the Rh antigen, but

subsequent amino acid analysis, peptide fragment mapping, differential antibody reactivity, and localization of the 28 kDa protein to non-erythroid tissues like the mammalian kidney suggested that this hypothesis was incorrect (Denker et al., 1988). The cDNA of this 28 kDa protein was isolated from a human bone marrow cDNA library by degenerate PCR (Preston and Agre, 1991) and was predicted to encode a 269 amino acid protein. In agreement with previous peptide mapping data (Denker et al., 1988), hydropathy plot analysis indicated that this 28 kDa peptide was an integral membrane protein with a predicted topology of six membrane-spanning domains with cytosol-exposed amino and carboxyl termini. This protein was dubbed Channel-forming Integral membrane Protein of 28 kDa, or CHIP28 and was immediately recognized to have high amino acid sequence identity with the Major Intrinsic Protein (MIP26) of the bovine optical lens fiber membrane (Gorin et al., 1984) as well as MIP26 homologues in bacteria (Muramatsu and Mizuno, 1989; Sweet et al., 1990), plants (Sandal and Marcker, 1988; Johnson et al., 1990; Guerrero et al., 1990; Yamamoto et al., 1990), and insects (Rao et al., 1990). Structural similarities between MIP26 and CHIP28 also appeared at the biochemical level when two different groups demonstrated that these proteins form tetramers in detergent micelles (Aerts et al., 1990; Smith and Agre, 1991).

Preston et al. (1992) was the seminal paper of early water channel research. The authors demonstrated that when CHIP28 RNA was expressed in *Xenopus laevis* oocytes, the water permeability of the oocyte plasma membrane dramatically increased in the presence of hypotonic solution. In addition, it was demonstrated that the water permeability conferred upon CHIP28-expressing oocytes was inhibited by

mercury compounds and that this inhibition could be rescued by pre-incubation with excess reducing agent. Interestingly, this simple and yet elegant assay remains a staple of water channel research even today. Subsequently, purified CHIP28 was reconstituted into liposome vesicles and was shown to increase water permeability of these vesicles over 50-fold (Zeidel et al., 1992). In addition, the water permeability of CHIP28 liposomes exhibited all of the characteristics of previously biochemically characterized water channels because it was sensitive to mercurial compounds and showed a low activation energy for water transport (Zeidel et al., 1992). These results cemented the identification of CHIP28 as a molecular water channel, and this protein was subsequently renamed aquaporin-1 (AQP1).

When aquaporin-1 was functionally characterized, only two other homologous protein sequences had been assigned functional activity. Bovine MIP26 was suggested to form gap junction ion channels in the mammalian eye (Shen et al., 1991) and the bacterial glycerol facilitator protein GlpF was shown to transport glycerol and other small polyols (Heller et al., 1980; Sweet et al., 1990; Maurel et al., 1993). Since a water transport function could not be ascribed to all members of the family, these genes were described by their sequence homology to MIP26, and were therefore dubbed the Major Intrinsic Protein (MIP) family (Reizer et al., 1993).

MIP structure and the conserved hourglass fold

Soon after AQP1 was demonstrated to be the first water channel, various groups began to probe the structure of this protein to determine the molecular mechanism of water transport. Early biochemical studies based on hydropathy

analysis, mutagenesis, and water permeability studies of MIPs from a variety of sources suggested that these proteins contain six membrane-spanning α-helices interrupted by five loop regions (loops A-E). Hydropathy plot analysis also indicated that two highly conserved asparagine-proline-alanine (NPA) motifs in loops B and E were part of a secondary structural element that had a high hydrophobicity index and these regions were also postulated to constitute part of the pore (Jung et al., 1994). The N and C terminal halves of the MIP sequence were found to be very similar, and were proposed to have originated by a gene duplication event (Reizer et al., 1993) that could potentially lead to an obverse two-fold structural symmetry. Based on these observations, Jung et al. (1994) proposed a topological model of MIP structure that resembled an hourglass, with the transmembrane domains forming the outside of the hourglass and the B as well as E loops forming the constriction. Although this model was proposed in the absence of structural data, the "hourglass model" of MIP structure was largely and remarkably verified by subsequent structural analyses.

Early structural studies of MIPs using electron diffraction of two-dimensional crystalline arrays (Jap and Li, 1995; Ren et al., 2000; Ren et al., 2001), atomic force microscopy (Walz et al., 1996), and cryo-electron microscopy (Daniels et al., 1999) indicated that MIPs from plant as well as animal origins formed a tilted helical bundle containing six transmembrane domains, as had been predicted in the hourglass model. However, it was not until the high-resolution X-ray crystal structures of bovine AQP1 (Sui et al., 2001) and the bacterial glycerol facilitator protein GlpF (Fu et al., 2000) that atomic resolution was obtained providing a clearer picture of "the hourglass". Both of these proteins share a common fold that is remarkably conserved from

bacteria to higher eukaryotes and contains six membrane-spanning α-helices (Helix 1-6) organized into a right-handed helical bundle surrounding a central pore (Figure **1.1A** and **1.1B**). The transmembrane domains are interrupted by five loop regions (loops A-E). Loops B and E contain the highly conserved NPA motifs, and form small 12 amino acid α-helices that fold back into the core of the protein to form a seventh pseudo-helix. The Pro and Ala residues in the NPA motifs interdigitate to orient the Asn residues in the center of the pore, and this group of amino acids forms one of the two major pore constrictions referred to as the NPA region (Fu et al., 2000; Sui et al., 2001).

Since the three-dimensional fold of these proteins is very similar, it is remarkable that they have such different functional properties, with AQP1 forming a water-selective channel and GlpF forming a channel with a specific substrate specificity for glycerol. A mechanism for this distinct substrate selectivity was postulated based upon comparison of the two structures. In particular, it was observed that a tetrad of amino acids from helix 2 (H2), helix 5 (H5), and loop E (LE_1 and LE_2) form a second pore constriction that resides 8 angstroms away from the NPA region on the extracellular side of the pore (Figure **1.1C**). In AQP1, this group of amino acids is composed of a Phe residue at H2, a His at H5, a Cys at LE_1, and an Arg residue at LE_2, while in GlpF the H2, H5, and LE_1 residues are Trp, Gly, and Phe, respectively, with the Arg at LE_2 position being unchanged. Due to the high prevalence of aromatic amino acids as well as the presence of a highly conserved Arg residue in this part of the protein, this part of the pore was dubbed the aromatic/ arginine (ar/R) region (Fu et al., 2000).

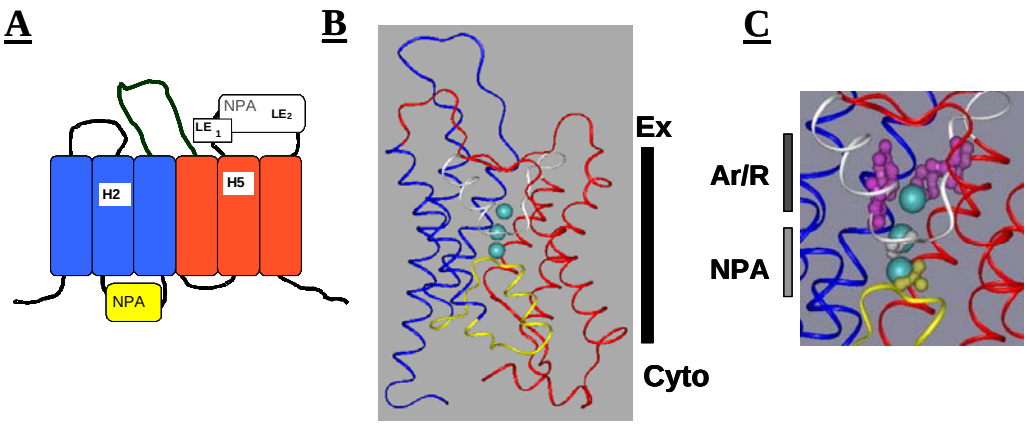

Figure 1.1: Major Intrinsic Protein structure and membrane topology: **A.** A one-dimensional topology map of Major Intrinsic proteins is shown. The first three transmembrane domains are colored in blue, and the last three are colored in red. Loops B and E containing the highly conserved NPA motifs are indicated in yellow and white, respectively. The relative position of the key ar/R selectivity filter residues at H2, H5, LE_1, and LE_2 are also indicated. **B.** The three-dimensional structure of bovine AQP1 (1J4N) is shown using the same color-coded regions shown in A. The position of the extracellular and cytosolic compartments is indicated to the right of the figure and the bar represents the position of the membrane bilayer. The positions of three co-crystallized pore water molecules are represented as aqua space filling spheres **C.** A magnified image of the NPA and ar/R region of bovine AQP1 is shown with the asparagine residues of the N-terminal as well as C-terminal NPA motif shown in yellow and white, respectively. The key ar/R residues are shown labeled in magenta. The position of the ar/R relative to the NPA region is indicated to the left of the figure.

The potential of this region for forming the structural basis of selectivity was initially noted because the proposed substrates of each channel (glycerol for GlpF; water for bovine AQP1) co-crystallized at this site in each of the structures (Fu et al., 2000; Sui et al., 2001). An analysis of the molecular interactions between protein and substrate led to a physical model that describes the ability of each channel to transport these substrates.

In bovine AQP1, the water at the ar/R region is coordinated by the ε2 nitrogen of His 182, the peptide backbone carbonyl of Cys 191, and the guanido group of Arg 197 (Figure **1.2**). The Phe 58 residue at the helix 2 position of the ar/R is suggested to orient water, such that it forms maximal hydrogen bonding overlap with all other hydrogen bond donors and acceptors in the ar/R region (Sui et al., 2001). In this model, water would form three hydrogen bonds with the protein at the ar/R region, which is the average number of hydrogen bonds formed between water molecules in solution. Therefore, this area of the protein would be able to effectively desolvate bulk water molecules so that they can pass through the channel in a single file manner. In contrast to the AQP1 ar/R region, the GlpF ar/R filter is much more hydrophobic. In this channel, the H2 Trp 48 and LE_1 Phe 200 residues interact with the methylene backbone of glycerol, while the LE_2 Arg 206 residue hydrogen bonds to the hydroxyl groups of glycerol (Figure **1.2**). The substitution of the H5 His in AQP1 for Gly 191 in GlpF results in a smaller amino acid that allows the close approach of the Phe residue at LE_1 and maintains the conformation necessary for this amino acid to interact with glycerol (Fu et al., 2000).

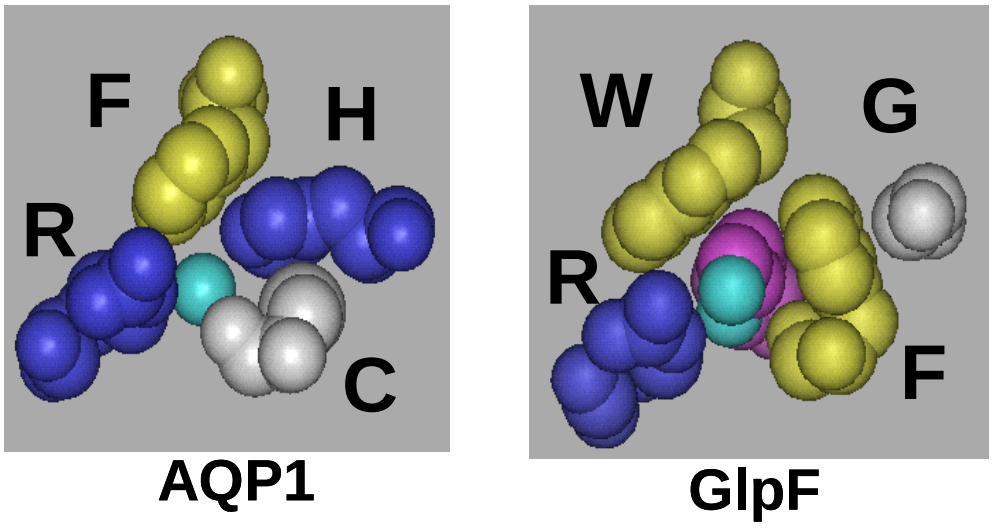

Figure 1.2: Structural comparison of the AQP1 and GlpF ar/R selectivity filters: The selectivity filter residues of bovine AQP1 and *E. coli* GlpF are shown. The helix 2 (H2), helix 5 (H5), loop E_1 (LE_1), and loop E_2 (LE_2) residues are shown clockwise starting from the top left residue. Residues of the ar/R region are indicated by their single letter amino acid code and colored according to the following color scheme: yellow- hydrophobic; blue- basic; white- small hydrophilic. The positions of crystallized substrates are also indicated. Water is represented as a single aqua sphere, while glycerol is shown with the methylene backbone in magenta and the hydroxyl groups in aqua.

In addition to the differences in amino acid composition, the residues of the GlpF ar/R region make it wider (3.7 angstroms) compared to the corresponding ar/R region of AQP1 (2.8 angstroms). The widening of the GlpF pore allows this channel to transport the larger glycerol molecule, while the ar/R region of AQP1 is just large enough to transport a single water molecule (radius of 2.4 angstroms). Therefore, the ar/R regions serve as both a size exclusion filter, and a structural filter that recognizes the specific chemical properties of the substrate using the amino acids of the ar/R, providing van der Waals interactions or hydrogen bonds depending on the nature of the substrate.

The mechanism of water/ solute transport and proton exclusion

Although the mechanism of substrate selectivity was proposed from the analysis of static crystal structures, the structural basis of MIP substrate selectivity was further investigated in molecular dynamics simulations of water and glycerol permeation events through AQP1 as well as GlpF (de Groot and Grubmuller, 2001; Jensen et al., 2002; Tajkhorshid et al., 2002; Lu et al., 2003). In addition, MIPs were demonstrated to be completely impermeable to ions, including protons (Zeidel et al., 1992; Maurel et al., 1993), which are known to traverse single file columns of water via the Grotthuss mechanism (de Grotthuss, 1806; Agmon, 1995; Tuckerman et al., 1997; Marx et al., 1999). Molecular dynamics simulations were therefore critical to determine the basis of selectivity of these channels and were made possible by the large number of full solute permeation events on the molecular dynamics timescale (de Groot and Grubmuller, 2001).

Molecular dynamics simulations of water flux through the experimental structures of AQP1 and GlpF in hydrated POPE bilayers (de Groot and Grubmuller, 2001) provided the molecular detail for the structural elements in the water permeation pathway as well as the mechanism for water permeation through protein channels. These simulations indicate that water hydrogen bonds to a line of peptide backbone carbonyls donated by the highly conserved His (residue 74 in AQP1), Ala (73), as well as Gly (72) residues preceding the first NPA motif, and these residues lead directly to the first intimate interaction site in the protein: the NPA region. Both asparagine residues of the NPA motif hydrogen bond with the transported water molecule, and these residues are apposed by the hydrophobic side chains of Phe 24, Val 176, and Ile 191 in the AQP1 structure. The transported water molecule forms a second intimate interaction with the AQP1 channel at the ar/R region, forming hydrogen bonds with His 182, Cys 189, and Arg 195. Thermodynamic calculations from these simulations also suggested that the largest energetic barrier to water transport occurs at the ar/R region, implying that the transition state of substrate transport occurs at this region and that the structural properties of this constriction are critical in discriminating the substrates that translocate the MIP channel.

Glycerol conduction follows a similar pathway along the analogous residues of GlpF (Fu et al., 2000; Jensen et al., 2002). The His 66, Ala 65, and Gly 64 peptide backbone carbonyls preceding the first NPA (analogous to the residues in AQP1) also form hydrogen bonds with the hydroxyl groups of glycerol, while a symmetrically related set of peptide backbone carbonyls donated by Ala 201, Phe 200, and Gly 199 perform the same task on the other side of the channel. Again, major protein-glycerol

interactions are formed at the NPA asparagine residue side chains, and at the ar/R region. The suggested model resulting from the structural observation of the GlpF ar/R region (Fu et al., 2000) was also validated by subsequent molecular dynamics simulations (Jensen et al., 2002). The ar/R selectivity filter is also responsible for the observed strict stereospecificity of GlpF to larger alditols (Fu et al., 2000). The shape of the ar/R opening provides a selective pore that is only capable of transporting alditols with hydroxyl groups in the same stereochemical conformation. In fact, GlpF is able to select prochiral forms of glycerol (Fu et al., 2000) and other conformations of glycerol are transported much more slowly in molecular dynamics simulations (Jensen et al., 2002; Lu et al., 2003). Compounds like xylitol, which have multiple hydroxyl group stereochemistries in the same molecule, must rotate about a carbon-carbon bond to pass through the ar/R region, and this conformational rearrangement increases the occupancy time of these molecules at the ar/R region, resulting in a lower transport rate. These observations define the entire substrate translocation pathway for these channels and were among the first molecular dynamics simulations of channels that could be performed on the first principles of molecular mechanics.

In addition to the substrate translocation pathway, molecular dynamics simulations have played an integral role in determining the molecular basis for the exquisitely low permeability of MIP channels to ions even as small as protons and hydronium ions (Zeidel et al., 1992; Maurel et al., 1993). The highly conserved NPA motifs serve to reorient the dipole of water molecules passing through this region of the protein by specifically forming hydrogen bonds between the asparagine side chain amide hydrogens and the oxygen of the transported water molecule (de Groot and

Grubmuller, 2001). This "dipole-flipping" mechanism prevents protons from being transferred along the water column via the Grotthuss mechanism and preserves transmembrane proton gradients necessary for active transport processes as well as ATP synthesis. In addition, the highly conserved Arg residue of the ar/R region as well as the positively charged helical dipoles of the NPA half-helices serve as strong electrostatic barriers against the transport of positively charged ions through the MIP pore (de Groot and Grubmuller, 2001; Jensen et al., 2002; Tajkhorshid et al., 2002). These studies provide the mechanistic basis of rapid MIP-mediated transport of water and small solutes like glycerol, while simultaneously excluding ion transport, and provide an argument for the structural conservation of the hourglass pore as well as the two conserved pore nodes (ar/R and NPA regions) that interact with an array of transported substrates.

Phylogenetic and functional diversity of the MIP superfamily: Animals and Microbes

In the wake of the discovery of molecular water channels, numerous proteins constituting the MIP superfamily have been isolated, and these proteins are represented in all kingdoms of life. In general, MIPs can be subdivided into two categories based on phylogenetic analysis and function: the aquaporins (represented by AQP1 discussed above) and aquaglyceroporins (represented by GlpF discussed above). The sequenced genomes in a variety of organisms have provided a wealth of information concerning the absolute number and biological diversity of these proteins. For example, the sequenced genome of *E. coli* contains two MIPs: the well

characterized glycerol facilitator GlpF (Heller et al., 1980; Sweet et al., 1990) and the water-selective channel AqpZ (Calamita et al., 1995). A broader phylogenetic analysis of sequenced bacterial genomes indicates that bacteria typically contain 1 to 3 MIP genes, and all of these proteins are similar to either AqpZ or GlpF (Hohmann et al., 2000). Similarly, the sequenced genome of *Saccharomyces cerevisiae* contains a single glyceroporin (Fps1p; Van Aelst et al., 1991; Luyten et al., 1995), as well as two aquaporin homologues (AQY1 and AQY2; Bonhivers et al., 1998; Carbrey et al., 2001). Interestingly, AQY1 was apparently inactivated during the evolution of yeast under laboratory conditions due to point mutations in the core MIP fold (Bonhivers et al., 1998).

Multicellular eukaryotic organisms typically contain a wider array of MIP genes. Each isoform is specifically expressed in a characteristic cellular localization pattern and is specifically adapted to perform the necessary transport functions in these tissues. The *C. elegans* genome contains eight MIP isoforms (Aqp-1 through Aqp-8), and these proteins are capable of water, glycerol, and urea transport (Campbell et al., 2008). Interestingly, worms containing the *aqp-2, aqp-3, aqp-4, aqp-8* quadruple genetic lesion are phenotypically normal, suggesting that these proteins are not essential for osmoregulation in this organism, or that other mechanisms compensate for MIPs to maintain osmotic homeostasis (Huang et al., 2007).

The human genome contains 11 canonical MIP genes (AQP0-AQP10), and these proteins also adhere to the typical aquaporin/ aquaglyceroporin paradigm (Agre and Kozono, 2003). AQP0, AQP1, AQP2, AQP4, and AQP5 proteins form water-

selective channels (Preston et al., 1992; Fushimi et al., 1993; Jung et al., 1994; Raina et al., 1995; Meinild et al., 1998), while AQP3, AQP7, and AQP9 are permeable to water, glycerol, and urea (Echevarria et al., 1994; Ishibashi et al., 1994; Ishibashi et al., 1997; Kuriyama et al., 1997). AQP8 is permeable to water, urea, and ammonia (Ma et al., 1997; Koyama et al., 1998). Interestingly, AQP6 shows unusual transport properties. At neutral pH it is an aquaporin, however at acidic pH it acquires the ability to transport anions (Yasui et al., 1999a). Thus, this channel is the only member of the mammalian MIP family that displays ion channel activity. AQP6 is localized to internal vesicles in the renal epithelia (Yasui et al., 1999a; Yasui et al., 1999b). The conductance through this protein is gated by acidic pH, and the AQP6 transcript is regulated by acid/ base homeostasis, suggesting that this channel serves a physiological role in pH homeostasis (Promeneur et al., 2000).

Mammalian aquaporin function has been associated with a variety of developmental defects and disease states, such as nephrogenic diabetes (AQP2; Deen et al., 1994; van Lieburg et al., 1994), brain edema (AQP4; Vizuete et al., 1999; Manley et al., 2000), and congenital cataracts (AQP0; Francis et al., 2000a; Francis et al., 2000b; Shiels et al., 2001). These observations suggest that MIPs affect a variety of processes involving osmoregulation and rapid water transport in mammalian tissues.

Compared to other animal species, analysis of insects show that they possess an extremely diverse and understudied complement of MIPs. The first insect MIP to be functionally characterized was *Drosophila melanogaster* Big Brain (BIB), a channel protein that is expressed in neuroblast tissues of the developing central

nervous system (Rao et al., 1990). BIB is a unique MIP because it forms a non-selective cation channel when heterologously expressed in *Xenopus* oocytes (Yanochko and Yool, 2002) and contains a 400 amino acid extension at the C-terminus of the protein. The C-terminus of most MIP superfamily members is less than 50 amino acid residues, suggesting that this domain may be responsible for the observed gating of the nonselective cation channel activity (Yanochko and Yool, 2002). BIB-like aquaporins are conserved in a number of insect species (e.g. *A. mellifera, T. castaneum,* and *A. aegypti*) suggesting that their role in neural development may be conserved in other insects (Campbell et al., 2008).

In addition to the BIB-like MIPs, the sequenced genomes of insects contain MIPs that are similar to classical aquaporins, of which Drosphila DRIP is the familial archetype (Kaufman et al., 2005). This protein forms water-selective channels when heterologously expressed in *Xenopus* oocytes or yeast secretory vesicles and is localized to the Malphigian tubules, a fluid excretory organ similar to the mammalian kidney. DRIP is proposed to mediate rapid water transport in this insect organ to handle the large volumes of fluid that are excreted from the insect after feeding, and DRIP-like proteins are conserved in a variety of different insects as well as (Campbell et al., 2008). Recently, a third family of insect MIPs were observed by phylogenetic analysis, and these proteins were dubbed the *P. rufa* integral proteins since they were initially isolated from this organism (Campbell et al., 2008). The only functionally characterized members of this subfamily were isolated from the sleeping chironomid (*Polypedilum vanderplanki*), and these proteins form water-selective channels that are suggested to be involved in preserving osmotic homeostasis under dehydration stress

(Kikawada et al., 2008). Thus, insect MIPs constitute a structurally diverse and unique group of proteins that have conserved biochemical as well as physiological functions, but these channels have been drastically understudied (Campbell et al., 2008).

Phylogenetic and functional diversity of the MIP superfamily: plants

Due to their sessile nature, plants are much more susceptible to osmotic stresses, such as salinity, drought, and cold, because they cannot move away from the site of the stress to avoid it (Chrispeels and Maurel, 1994). In light of these adaptive challenges, it comes as no surprise that the available sequenced genomes of higher plants contain 3-4 times as many MIP genes as their mammalian counterparts (Chaumont et al., 2001; Johanson et al., 2001; Quigley et al., 2001; Sakurai et al., 2005). Plant MIPs can be divided into four subfamilies (Figure **1.3**) based on phylogenetic analysis: the plasma membrane intrinsic proteins (PIPs), the tonoplast intrinsic proteins (TIPs), the nodulin 26-like intrinsic proteins (NIPs), and the small basic intrinsic proteins (SIPs). Each of these MIP family subgroups are represented in all sequenced higher plant genomes, and this diversity of MIP family members highlights the challenges associated with plant water relations. Below, a summary of the characteristics of each of these plant MIP subfamilies is presented.

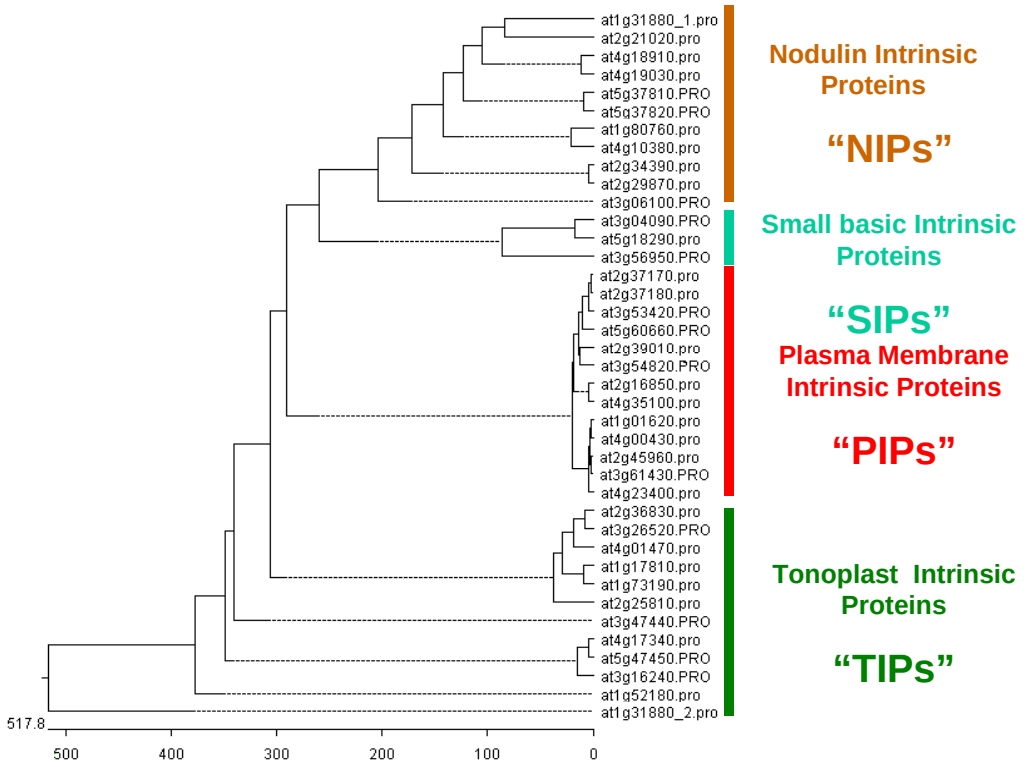

Figure 1.3: The phylogeny of the Arabidopsis MIP family: The 35 full-length MIP subfamily members from the sequenced Arabidopsis genome were aligned by the ClustalW algorithm and assembled into a phylogenetic tree using DNAstar software. The four plant MIP subgroups are indicated to the right of the tree with the NIP subgroup indicated in brown, the SIP subgroup in aqua, the PIP subgroup in red, and the TIP subgroup in green. The members of each subfamily are indicated by their Arabidopsis genome accession number. The axis below the tree indicates the relative number of substitutions necessary to produce the tree.

The Plasma membrane Intrinsic Proteins (PIPs)

The first PIP subfamily member (RD28) was originally identified in *Arabidopsis thaliana* (Daniels et al., 1994) and was demonstrated to form water-selective channels when heterologously expressed in *Xenopus* oocytes. RD28 was localized to the plasma membrane of root and leaf cells at constitutively high expression levels, but these levels were further increased under conditions that alter the turgor pressure of the plant cell (Yamaguchi-Shinozaki and Shinozaki, 1993). PIP subfamily members were subsequently isolated from a variety of monocotyledonous (Liu et al., 1994; Malz and Sauter, 1999; Li et al., 2000; Chaumont et al., 2001) and dicotyledonous plants (Qi et al., 1995; Johansson et al., 1996; Ruiter et al., 1997; Biela et al., 1999). Additional functional analysis indicates that PIPs are not permeable to test solutes like glycerol and urea (Chaumont et al., 2000), suggesting that they are uniquely adapted for water transport and represent water-specific aquaporins rather than aquaglyceroporins.

Interestingly, PIPs phylogenetically group into two subfamilies (PIP1 and PIP2) with distinct functional properties. The PIP2 members are water-selective aquaporins with a high intrinsic P_f whereas PIP1 members show a much lower water transport rate (Chaumont et al., 2000). The structural basis for the disparity in water permeability is currently unknown and extremely perplexing, considering that sequence analysis indicates that these proteins are greater than 70 % identical at the amino acid level and contain identical amino acids in the key pore-forming regions of the protein. In accordance with their proposed function as water channels, physiological studies indicate that PIP isoforms are involved in a number of plant

processes that necessitate the rapid transport of water, including adaptation to drought, salinity, and flooding stress, as well as seed rehydration and embolism recovery (Martre et al., 2002; Aharon et al., 2003; Javot et al., 2003; Sakr et al., 2003; Schuurmans et al., 2003; Tournaire-Roux et al., 2003; Lian et al., 2004). Therefore, the PIP subfamily can be considered as a highly conserved group of water-selective aquaporins that are used for various water transport processes occurring at the plasma membrane.

The Tonoplast Intrinsic Proteins (TIPs)

Members of the TIP subfamily were among the first water channels to be characterized in plants (Maurel et al., 1993), and phylogenetic analysis indicates that these proteins form a large and diverse group of channels in all sequenced higher plant genomes (Chaumont et al., 2001; Johanson et al., 2001; Quigley et al., 2001; Sakurai et al., 2005). The first TIP (α-TIP) was originally identified from screens of cDNA libraries of various plant seeds (Johnson et al., 1989). The α-TIP cDNA encodes a 27 kDa protein with 6 putative transmembrane domains and amino acid sequence homology to GlpF as well as AQP0 (Johnson et al., 1990). Subsequent analysis of α-TIP showed that this it is localized to the protein storage vacuole of dessicated seed tissue. Further cDNA screens resulted in the identification of β-TIP (Johnson et al., 1990), an isoform which is also expressed in seed tissue, γ-TIP (Hofte et al., 1992), that is expressed throughout the plant body, and δ-TIP (Daniels et al., 1996), which is expressed throughout the aerial tissue.

Functional analysis of TIP subfamily members upon heterologous expression in *Xenopus* oocytes showed that they also form aquaporin channels (Maurel et al., 1993; Maurel et al., 1994). However, these proteins are distinguished from PIPs since they also transport larger test solutes such as urea (Gerbeau et al., 1999; Klebl et al., 2003; Liu et al., 2003) as well as ammonia (Jahn et al., 2004; Holm et al., 2005; Dynowski et al., 2008). Members of the TIP subfamily were consistently localized to the tonoplast membrane, and specific isoforms were targeted to unique vacuoles suggesting that subcellular localization might play a role in the functional diversification of these proteins (Jauh et al., 1998). The sequenced Arabidopsis genome defined the total complement of TIPs in this organism, and phylogenetic analysis indicated that α- and β-TIP group into the same evolutionary clade, while γ- and δ-TIP group into evolutionarily distinct clades. Each of these TIP clades has three members that share high amino acid sequence identity, and these genes are proposed to have arisen by gene duplication of an ancestral TIP gene (Chaumont et al., 2001; Johanson et al., 2001; Quigley et al., 2001). In addition, the annotated genome of Arabidopsis revealed a fourth TIP subgroup that is represented by the Arabidopsis protein AtTIP5;1. This protein has not been functionally characterized, but AtTIP5;1 has homologues in corn (Chaumont et al., 2001) and rice (Sakurai et al., 2005), suggesting that its function has been conserved in higher plant evolution. While a specific function for members of the TIP family has not been described to date, these proteins are expressed in zones of cellular elongation and differentiation, suggesting that they may be involved in intercellular water transport through the enormous vacuole that develops in these tissues and participates in turgor-mediated

cell expansion (Barrieu et al., 1998; Chaumont et al., 1998; Karlsson et al., 2000). In addition, as noted by Maurel (1997) the P_f of the tonoplast is much higher than that of the plasma membrane, which is an important feature in regulation of turgor and cytosolic cell volume in plant cells. Thus, the presence of TIPs as a major component of the tonoplast may be important as part of the water transport mechanism guiding this osmoregulation.

The Small basic Intrinsic Proteins (SIPs)

The newest addition to the plant MIP superfamily are the small basic intrinsic proteins (SIPs), and their existence was only elucidated through an examination of the sequenced Arabidopsis genome (Johanson et al., 2001; Quigley et al., 2001) as well as a massive expressed sequence tag (EST) database from corn (Chaumont et al., 2001). Nevertheless, SIP family members seem to be conserved in higher plants (Sakurai et al., 2005) as well as in nonvascular plants, such as the moss *Physcomitrella patens* (Borstlap, 2002), suggesting that SIPs were acquired before the onset of vascular plant development. While the biochemical and physiological functions of SIP subfamily members are currently unknown, their peculiarity has been highlighted because they possess nonconservative amino acid substitutions at many key structural positions of the MIP fold (Johanson and Gustavsson, 2002). These residue substitutions occur throughout the putative substrate translocation pathway as well as in the highly conserved NPA regions of the protein, implying that SIP subgroup members may be permeable solutes outside of typical MIP substrates. It is also interesting to note that phylogenetic analysis of corn, rice, and Arabidopsis

(Chaumont et al., 2001; Johanson et al., 2001; Quigley et al., 2001; Sakurai et al., 2005) indicate that the SIP subfamily is consistently divided into two groups (SIP1 and SIP2) suggesting that each of these subgroups has a conserved and necessary physiological function.

The Nodulin 26-like Intrinsic Proteins (NIPs)

The NIP subfamily is the fourth phylogenetic subgroup of plant MIPs and is named for the familial archetype nodulin 26, a symbiosome-specific protein from nitrogen-fixing root nodules. Since this subfamily was the major focus that led to the initiation of this study, the details of symbiotic nitrogen fixation and the role of nodulin-26 in the symbiosis are considered in more detail in the subsequent section.

Nodulin 26: A nitrogen-fixing root nodule-specific MIP

Under limiting conditions of soil nitrogen, members of the *Rhizobiaceae* family of diazotrophic bacteria can form symbiotic interactions with the roots of leguminous plants, resulting in the formation of a novel plant organ termed the nodule (reviewed in Limpens and Bisseling, 2003; Oldroyd and Downie, 2008). Inside the nodule, the bacteria are housed in specialized infected cells, where they are enclosed in a symbiosis-specific organelle termed the symbiosome (Roth et al., 1988). The symbiosome is delimited by a membrane of plant origin, the "symbiosome membrane", which sequesters the nitrogen-fixing bacteria from the plant cytosol and necessarily controls the metabolic communication between the host plant and the bacterial symbiont (reviewed in Udvardi and Day, 1997). Inside the symbiosome, the

bacteria reduce atmospheric nitrogen to ammonia through the activity of the MoFe protein nitrogenase, and this reduced source of nitrogen passes through the symbiosome membrane into the plant cytosol, where it is assimilated to glutamine through the enzymatic action of glutamine synthetase (Miflin and Habash, 2002). In return, the host plant provides the bacteria with essential compounds that are necessary to maintain the nitrogen fixation process, including a source of reduced carbon in the form of C4 dicarboxylates (Udvardi and Day, 1997; Day et al., 2001).

Various transport activities have been ascribed to the symbiosome membrane (Table **1.1**), including the channel-mediated transport of water, glycerol, ammonia/ ammonium, and positively charged monovalent as well as divalent cations (Tyerman et al., 1995; Rivers et al., 1997; Dean et al., 1999; Niemietz and Tyerman, 2000; Roberts and Tyerman, 2002). In addition, transporters for divalent heavy metals, dicarboxylates, inorganic anions, and Ca^{2+} are present on the symbiosome membrane, and proteins responsible for some of these activities are now known (Ouyang et al., 1990; Andreev et al., 1999; Moreau et al., 2002; Kaiser et al., 2003; Vincill et al., 2005; summarized in Table **1.1**). Finally, a P-type proton pumping ATPase activity has been biochemically observed on the symbiosome membrane (Udvardi and Day, 1989; Corzo et al., 1997; Fedorova et al., 1999), and this protein is hypothesized to serve a pivotal role in energizing the symbiosome membrane to drive the active transport processes for metabolite transport.

Ammonia/ ammonium is the end product of the nitrogenase reaction, and the transport of these compounds out of the symbiosome has been subject to some debate (Day et al., 2001).

Table 1.1: Documented transport activities on the symbiosome membrane

Transporter	Transport activities	Reference
GmN70	Chloride, nitrite, nitrate	Vincill et al., 2005
Non-selective cation channel	Ammonium, potassium, calcium	Tyerman et al., 1995; Obermeyer and Tyerman, 2005
H^+-ATPase	Protons (ATP dependent)	Day et al., 1989
Nodulin 26	Water, glycerol, ammonia	Rivers et al., 1997; Dean et al., 1999
GmZIP1	Zinc	Moreau et al., 2002
Ca^{2+}- ATPase	Calcium (Magnesium, ATP dependent)	Andreev et al., 1999
GmDMT1	Fe^{3+}, Mn^{2+}, Cu^{2+}, Zn^{2+}	Kaiser et al., 2003
Dicarboxylate transporter	Malate, succinate	Ouyang et al., 1990

There are at least three putative mechanisms for ammonia efflix from the symbiosome space. Because of its ability to diffuse across lipid bilayers as well as the high proposed concentrations of ammonia that accumulate inside the symbiosome (Streeter, 1989), it was initially proposed that uncharged ammonia was released by passive diffusion (Udvardi and Day, 1990). However, the P-type ATPase activity associated with the symbiosome membrane is suggested to acidify the lumen of the symbiosome, indicating that NH_4^+ is the predominant form of fixed nitrogen in the symbiosome space. Consequently, a voltage-gated inwardly-rectified non-selective cation channel permeable to ammonium was described by patch clamp recordings in isolated symbiosome membranes of soybean (*Glycine max*; Tyerman et al., 1995) and later in the model legume *Lotus japonicus* (Roberts and Tyerman, 2002). The ammonium permeability of this channel is regulated by the divalent cations Ca^{2+} and Mg^{2+}, which serve as "gating particles" on the cytosolic side of the membrane (Tyerman et al., 1995; Kaiser et al., 1998; Roberts and Tyerman, 2002; Obermeyer and Tyerman, 2005) and confer the voltage-dependence as well as inward rectification properties of the channel. Upon hyperpolarization of the membrane by the proton pumping ATPase, the gating particle is displaced, and ammonium ion is transported from the symbiosome space to the cytosol (Tyerman et al., 1995; Kaiser et al., 1998; Roberts and Tyerman, 2002), facilitating the efflux and assimilation of fixed NH_4^+.

Passive flux of uncharged ammonia has also been observed on the symbiosome membrane by stopped-flow fluorimetry (Niemietz and Tyerman, 2000). This study revealed that NH_3 was rapidly transported through a proposed

proteinacious pathway that exhibited a low activation energy for NH_3 transport. This transport pathway was also sensitive to $HgCl_2$, and inhibition could be reversed in the presence of β-mercaptoethanol. As discussed previously, reversible mercury inhibition is a hallmark of MIP mediated transport. Combined with the high water permeability of the symbiosome membrane (Rivers et al., 1997; Dean et al., 1999), these observations suggest the presence of a multifunctional MIP channel on the symbiosome membrane.

Nodulin-26 is the only known MIP channel on the symbiosome membrane. This protein was first described by Verma and co-workers (Fortin et al., 1987) and was suggested to be a major protein component of the symbiosome membrane. Subsequent analyses provided support for this hypothesis, demonstrating that nodulin 26 constitutes 10-15% of the symbiosome membrane protein mass (Weaver et al., 1991; Dean et al., 1999). Early sequence comparisons revealed the similarity of nodulin-26 to MIP26 (Sandal and Marcker, 1988), and this protein was among the first MIP sequences identified in plants. Before the details of its functional properties became apparent, nodulin-26 was demonstrated to be a major phosphoprotein on the symbiosome membrane that is uniquely phosphorylated by a symbiosome membrane-associated Calcium Dependent Protein Kinase (CDPK) on Ser 262 (Weaver et al., 1991; Weaver and Roberts, 1992). CDPKs are a plant specific class of protein kinases that contain a kinase domain fused to a calmodulin-like EF-hand containing domain (Saterlee and Sussman, 1998). These proteins are activated by transient increases in the cytosolic $[Ca^{2+}]$ resulting from a variety of developmental as well as stress-induced phenomena (reviewed in Harper et al., 2004; Harper and Harmon,

2005), and the activated protein kinase phosphorylates downstream targets that are involved in these processes. Phosphorylation represents a common regulatory mechanism in MIPs, and nodulin-26 was among the first of these proteins that were decisively shown to be subject to this type of modification as well as one of the first substrates identified for CDPK (Weaver et al., 1991; Weaver and Roberts, 1992).

Expression of nodulin 26 was found to coincide with a rapid burst of membrane biosynthesis that precedes endocytosis and development of the symbiosome membrane (Fortin et al., 1987; Guenther et al., 2003). Given the numerous functional activities associated with the symbiosome membrane, and the selective targeting of nodulin 26 to this membrane, a transport role supporting symbiosis has been proposed. The transport activity of nodulin 26 has been the subject of extensive biochemical and biophysical characterization both in *Xenopus laevis* oocytes as well as in purified symbiosome membrane vesicles and reconstituted proteoliposomes (Rivers et al., 1997; Dean et al., 1999; Niemietz and Tyerman, 2000; Guenther et al., 2003). From these analyses it is clear that nodulin 26 possesses aquaporin activity with a low unitary water conductance compared to robust aquaporins such as mammalian aquaporin 1 (Rivers et al., 1997; Dean et al., 1999). Nevertheless, the high concentration of nodulin 26 confers a high osmotic water permeability (P_f = 0.05 cm/s) upon the symbiosome membrane. This water permeability shows all of the hallmarks of protein-facilitated water transport, including a low activation energy (3-4 kcal/ mol) and sensitivity to the classical aquaporin inhibitor $HgCl_2$ (Rivers et al., 1997; Dean et al., 1999) as well as to heavy metals such as $AgNO_3$ and $HAuCl_4$ (Niemietz and Tyerman, 2002). Nodulin 26 has

also been demonstrated to transport test solutes such as formamide and glycerol (Rivers et al., 1997; Dean et al., 1999) as well as ammonia (Niemietz and Tyerman, 2000) and was one of the first multifunctional aquaglyceroporins demonstrated in plants.

Nodulin 26 orthologues have been isolated on the symbiosome membranes of other legumes including the genetic models *Medicago truncatula* (Catalano et al., 2004) and *Lotus japonicus* (LjNod26; Guenther and Roberts, 2000), suggesting that this protein plays a conserved role during the nitrogen-fixing symbiosis in legumes. In light of the multifunctional nature of nodulin 26 transport and the lack of transgenic techniques that are applicable to soybean, this role has remained elusive. Given the high water permeability of the symbiosome, and the fact that this is the major organelle in the specialized infected cell, a potential role in osmoregulation has been proposed (Rivers et al., 1997; Dean et al., 1999). Thus, the high water permeability of the symbiosome membrane as a result of the large amount of nodulin 26 on this membrane could serve a role in regulation of cytosolic volume homeostasis and osmotic regulation, similar to the proposed role of TIPs on the central vacuole of other plant cells (reviewed in Maurel et al., 2002).

The biological significance of the glycerol transport activity of nodulin 26 is not as clear since there is no obvious need for glycerol transport in metabolic support of the symbiosis. However, given the importance of the symbiosome membrane in metabolic exchange during the symbiosis, the report of nodulin 26 providing facilitated transport of ammonia (Niemietz and Tyerman, 2000) is potentially significant. The transport mechanism for fixed nitrogen across the symbiosome

membrane is still a subject of debate with transport mechanisms for uncharged ammonia (Niemietz and Tyerman, 2000) and charged ammonium ion (Tyerman et al., 1995; Roberts and Tyerman, 2002; Obermeyer and Tyerman, 2005) being proposed. Both pathways provide discrete conduits for reduced nitrogen efflux, but their relative contribution would depend on both the pH and electrochemical gradients across the symbiosome membrane.

While nodulin 26 was originally isolated and characterized in the root nodules of leguminous plants (Fortin et al., 1987; Weaver et al., 1991; Weaver and Roberts, 1992; Rivers et al., 1997; Dean et al., 1999; Guenther and Roberts, 2000), it is increasingly evident that NIP subfamily members are present in nonleguminous as well as nonvascular plants (Weig et al., 1997; Weig and Jakob, 2000; Chaumont et al., 2001; Johanson et al., 2001; Quigley et al., 2001; Borstlap, 2002; Schuurmans et al., 2003). As described previously, nodulin 26 forms water channels in *Xenopus* oocytes as well as in native symbiosome membranes, and these channels are also permeable to glycerol, formamide, and ammonia (Rivers et al., 1997; Dean et al., 1999; Niemietz and Tyerman, 2000). *Arabidopsis thaliana* NIP1;1 and NIP1;2 were also demonstrated to form aquaglyceroporin channels in *Xenopus* oocytes and yeast (Weig et al., 1997; Weig and Jakob, 2000), suggesting that these functional properties are characteristic of the subfamily and distinct from other plant MIP subgroups. While the transport properties of these proteins are well established, the localization and physiological function of NIP subgroup members in nonleguminous plants remains less understood.

The evolutionary conservation of MIPs from prokaryotes to the most recently evolved eukaryotes suggests that these proteins are essential transport components of biological membranes. However, accumulating evidence suggests that while water transport remains a functional property of this protein family, some MIPs are capable of transporting solutes other than water. It is clear that plants and insects contain a greater number of structurally diverse MIP superfamily members than their mammalian as well as microbial counterparts, and preliminary phylogenetic analysis indicates that these MIPs contain more diverse combinations of amino acids at their selectivity-determining ar/R regions. In light of these observations, we used homology-based modeling, coupled with site-directed mutagenesis and functional analysis to investigate the structural determinants as well as substrate selectivity profiles of plant MIP channels with an emphasis on the NIP subfamily. In addition, we investigated how posttranslational modifications, specifically nodulin 26 phosphorylation, affect NIP channel permeability in the context of the ar/R region. Due to the relative lack of functional data available for insect MIPs, and their considerable ar/R region diversity, similar techniques were applied to these channels to investigate their unique functional properties. Finally, we used the computational and functional data obtained from these channels to strategically investigate the physiological function of MIPs in their native organism.

Chapter II

Materials and Methods

Plant materials and growth conditions

Arabidopsis thaliana Col-0 (L.) Heynh plants were obtained from the Fujiwara lab stocks and were grown as well as maintained as described as previously described (Takano et al., 2006). NIP6;1 T-DNA insertion lines were obtained from the SALK SIGnAL database (Alonso et al., 2003) and seeds for these lines were purchased from the Arabidopsis Biological Resource Center (ABRC). For the routine growth of the wild type Arabidopsis plants, seeds were sterilized in 50 % (v/v) ethanol for 1 minute, followed by incubation in 50 % (v/v) sodium hypochlorite, 0.1 % (v/v) Tween-20 for 20 minutes. The seeds were washed 5 times in sterile water and were sewn on ½ strength Murashige and Skoog (MS) agar media containing 1 % (w/v) sucrose (Sigma catalog number M9274). The seeds were stratified at 4^0 C and were grown under long-day conditions (16 hr light/ 8 hr dark cycle) for 10 days in a growth chamber. Plants were then transferred to pots containing Pro-mix soil and were grown in a growth chamber under long-day conditions until they were 6 weeks old. Root, stem, leaf, flower, and silique tissue was harvested from these plants and stored at -80^0 C until the tissue was used for RNA isolation as described below.

Nodulated soybean (*Glycine max* cv Bragg) were grown and maintained as previously described (Weaver et al., 1991). *Bradyrhizobium japonicum* USDA110 was cultured in BMM media and was used to inoculate germinated soybeans as

previously described (Weaver et al., 1991; Guenther et al., 2003). Plants were grown under greenhouse conditions in vermiculite, and were watered during alternative weeks with water or Herridge's solution as described previously (Weaver et al., 1991; Guenther et al., 2003).

Arabidopsis plants that were used for phenotypic studies as well as boric acid uptake analysis were grown in hydroponic culture as previously described (Fujiwara et al., 1992; Takano et al., 2002) at 22^0 C. For boric acid-dependent growth, the content of the boric acid in the growth medium was varied using a defined growth medium as previously described (Takano et al., 2006). Arabidopsis plants were grown under short-day conditions (10 hr light/ 14 hr dark cycle) to investigate vegetative growth and under long-day conditions to observe the reproductive plant stages. NIP6;1-GFP expressing plants were grown in MS-agar medium containing 1% (w/v) sucrose and 1.5% (w/v) gellan gum.

For analysis of the boric acid dependence of AtNIP5;1 and AtNIP6;1 expression, Arabidopsis Col-0 plants were grown under long-day conditions in solid MS medium supplemented with 100 μM boric acid for 29 days. These plants were transferred to hydroponic culture in medium supplemented with 100 μM boric acid for 17 days and then to hydroponic culture solutions containing 100 or 0.1 μM boric acid for 24 hrs prior to sample collection.

RNA extraction and cDNA synthesis

Stem, leaf, root, and flower tissue from six-week old Arabidopsis plants grown under long day conditions were ground in a mortar with a pestle cooled with

liquid nitrogen. Total RNA was extracted from the resulting tissue powder by incubation for 10 minutes at 25^0 C with 500 μL of Plant RNA Extraction Reagent (Invitrogen). Samples were centrifuged at 10,000 x g, and the supernatant was transferred to a new tube. Chloroform (300 μL) and 4 M NaCl (125 μL) were added, and the resulting mixture was centrifuged at 12,000 x g for 10 minutes at 25^0 C. Equal volumes of the top phase of this solution and 100 % isopropanol were mixed, and the RNA was precipitated at -80^0 C for 20 minutes. The solution was centrifuged at 12,000 x g for 10 minutes at 25^0 C, and the resulting RNA pellet was washed with 500 μL of 80 % (v/v) ethanol. The supernatant was removed, and the RNA was resuspended in 100 μL of sterile "DEPC" water (treated with 0.1 % [v/v] diethylpyrocarbonate). Total RNA from 35-day-old nodules was prepared in an identical manner.

Genomic DNA contamination was removed from the RNA sample by incubation with 2 units of RNAse-free DNAseI (Ambion) for 40 minutes at 37^0 C. The reaction was terminated by the addition of 5 μL of DNAseI stop reagent followed by incubation for 10 minutes at 25^0 C. The sample was centrifuged at 10,000 x g for 2 minutes to remove the DNAseI stop reagent. The integrity of total RNA was assessed by observation of the ribosomal RNA bands after electrophoresis on a 0.8 % (w/v) agarose gel in the presence of 0.4 ng/ mL ethidium bromide run in 1 X Tris-acetate EDTA buffer (Sambrook et al., 1989).

Total RNA from plant samples was reverse transcribed to cDNA using the Superscript III reverse transcription kit (Invitrogen). Two μg of total RNA sample were combined with 2 μL of 10 mM dNTP mix as well as 0.5 μL of poly dT primer

and incubated at 65^0 C for 10 minutes. After cooling on ice, the following buffer components were added: 4 μL of 10X Superscript III reverse transcriptase buffer, 8 μL of 25 mM $MgCl_2$, 4 μL of 100 mM dithiothreitol, 1 μL of RNAse Out, and 1 μL of Superscript III reverse transcriptase. The reactions were incubated for 15 minutes at 25^0 C, 90 minutes at 45^0 C, then 15 minutes at 72^0 C. One μL of RNAse H was then added to these samples and incubated for an additional 30 minutes at 37^0 C. The cDNA samples were stored at -20^0 C until further use.

Total RNA was extracted from dissected adult aphid gut, bacteriocyte, fat body, and head tissue by homogenization in ice-cold TRIzol reagent (Invitrogen) using the manufacturer's instructions. To remove contaminating DNA, the RNA was incubated with RNAse-free DNAseI (Roche) for 30 minutes at 37^0 C then at 75^0 C for 15 minutes before purification with the RNAeasy minikit (Qiagen) using the RNA cleanup protocol. First-strand cDNA synthesis of aphid total RNA samples was performed using the Superscript II reverse transcriptase kit (Invitrogen) following the manufacturer's instructions.

Cloning methods for *Xenopus laevis* oocyte expression

The LjNod26 (Guenther and Roberts, 2000) and nodulin-26 (Fortin et al., 1987; Rivers et al., 1997) cDNAs and constructs for *Xenopus* oocyte expression were prepared as previously described. All cDNAs were cloned into the *Bgl*II site of the pXβG-ev1 *Xenopus* oocyte expression vector (Preston et al., 1992) between the 5' and 3' untranslated regions (UTR) of *Xenopus* β-globin and downstream from the T3 RNA polymerase promoter.

An N-terminal FLAG epitope tag was inserted into the pXβG-ev1 expression vector by combining FLAG epitope F and FLAG epitope R primers (Table **2.1**) to form a cassette. The cassette contains cohesive ends complementary to *Bgl*II or *Bam*HI overhangs at the 5' and 3' end. This cassette also contains an *Eco*RI restriction site at the 5' end, followed by the coding sequence for the FLAG epitope (MDYKDDDDK). The cassette oligonucleotides (240 ng/ μL) were phosphorylated by T4 polynucleotide kinase (Fisher Scientific) at 37^0 C for 30 minutes, followed by an enzyme denaturation step at 65^0 C for 15 minutes. pXβG-ev1 was digested with *Bgl*II and dephosphorylated with shrimp alkaline phosphatase (SAP; Promega). The phosphorylated FLAG epitope cassette was ligated into the vector using the Takara ligation kit version II (Takara), and the resulting ligated plasmids were transformed into *Escherichia coli* DH5α. Positive clones were verified as described in the analytical methods section by automated DNA sequencing. This plasmid will be referred to as pXβG-FLAG.

AtNIP6;1 was cloned from Arabidopsis stem cDNA samples by PCR using ExTaq DNA polymerase (Takara) as well as NIP6;1 F and NIP6;1 R (Table **2.1**) gene-specific primers. These primers were designed to amplify the AtNIP6;1 open-reading frame (ORF) flanked by *Bgl*II sites. The AtNIP6;1 ORF was amplified under the following PCR conditions: 5 minutes of initial denaturation at 94^0 C followed by 30 cycles at 94^0 C (30 s), 55^0 C (30 s), 72^0 C (75 s), and a final extension at 72^0 C (7 min). The PCR product was resolved by electrophoresis on a 1 % (w/v) low-melting agarose gel and was purified by using the QiaQuick gel purification kit (Qiagen).

Table 2.1: Oligonucleotide primers used for *Xenopus* expression constructs

Primer name	Direction	Sequence[a]	Comments[b]
FLAG epitope	**Forward**	GATCCGAATTCATGGACTACAAAGACGACG ACGACAAAA	*Bam*HI overhang
FLAG epitope	**Reverse**	GATCTTTTGTCGTCGTCGTCTTTGTAGTCC ATGAATTCG	*Bgl*II overhang
AtNIP5;1	**Forward**	AGATCTATGGCTCCACCGGAGGCT	*Bgl*II site
AtNIP5;1	**Reverse**	AGATCTTTAACGAAAGCTCCT	*Bgl*II site
AtNIP6;1	**Forward**	GGAAGATCTATGGATCATGAGGAAATT CCATCCACG	*Bgl*II site
AtNIP6;1	**Reverse**	GGAAGATCTTCATCTTCTGAAGCTCCT CCTCTCTTTGGG	*Bgl*II site
AtNIP6;1 A119W	**Forward**	TGCGCCGCCTCGTGGGGTTTGGCGGTT	Mutagenesis
AtNIP6;1 A119W	**Reverse**	AACCGCCAAACCCCACGAGGCGGCGCA	Mutagenesis
AtNIP6;1 V252A	**Forward**	TCGATGAACCCTGCAAGAACACTGGGT	Mutagenesis
AtNIP6;1 V252A	**Reverse**	ACCCAGTGTTCTTGCAGGGTTCATCGA	Mutagenesis
LjNod W77H	**Forward**	GGTATTGCACTTGTCCATGGACTGGCTGTG ATGG	Mutagenesis
LjNod W77H	**Reverse**	CCATCACAGCCAGTCCATGGACAAGTGC AATACC	Mutagenesis
ApAQP1	**Forward**	ATCCTTTGATTAGTGGTA	None
ApAQP1	**Reverse**	CCTAAGTTAAATGATATG	None
ApAQP1 *Xenopus*	**Forward**	GGATCCATGAAGGAATACGGTACATTC	*Bam*HI site
ApAQP1 *Xenopus*	**Reverse**	GGATCCTCAAAG ATCATAAGAGCTTGC	*Bam*HI site
ApAQP2 *Xenopus*	**Forward**	AGATCTATGAACCACACAGCGTTG	*Bgl*II site
ApAQP2 *Xenopus*	**Reverse**	AGATCTTTATTTTACTCGTTCATCGTT	*Bgl*II site

[a]All primer sequences are in the 5' to 3' direction.

[b]Underlined portions of the sequences represent restriction sites.

Gel-purified AtNIP6;1 DNA was inserted into the pCR2.1-TOPO cloning vector (Invitrogen) by incubating 100 ng of AtNIP6;1 PCR product with 0.5 μL of pCR2.1-TOPO vector at 25^0 C for 10 minutes. The resulting clones were transformed into *E. coli* DH5α. Colonies were screened for the presence of the AtNIP6;1 insert by blue/ white screening on LB-ampicillin plates containing 200 μL of 40 mg/ mL X-gal (5-bromo-4-chloro-3-indolyl-beta-D galactopyranoside). White colonies were grown in Luria Broth (LB) media supplemented with 100 μg/ mL ampicillin for 16 hours at 37^0 C with shaking. Plasmids were purified from these bacterial cultures using the Wizard SV miniprep kit (Promega) following the manufacturer's instructions. The AtNIP6;1 cDNA was removed from pCR2.1-TOPO by *Bgl*II digestion and was ligated into pXβG-ev1 with or without the N-terminal FLAG epitope tag using the Takara ligation kit version II (Takara).

AtNIP5;1 was amplified from the pOO2 plasmid (Takano et al., 2006) using the NIP5;1 F and NIP5;1 R gene-specific primers (Table **2.1**), which also contain *Bgl*II restriction sites. The AtNIP5;1 PCR product was cloned into pXβG-FLAG by the same method described above for AtNIP6;1.

Site-directed mutants of AtNIP6;1 were generated directly in the AtNIP6;1/ pXβG-FLAG vector using the Quickchange method (Stratagene). The LjNod26 W77H mutation was generated using the LjNod26/ pXβG-ev1 vector as a template. Oligonucleotide primers were synthesized to produce the AtNIP6;1 A119W mutation (NIP6;1 A119W F and NIP6;1 A119W R; Table **2.1**), the AtNIP6;1 V252A mutation (NIP6;1 V252A F and NIP6;1 V252A R; Table **2.1**) as well as LjNod26 W77H (LjNod26 W77H F and LjNod26 W77H R; Table **2.1**). Five hundred nanograms of

each primer were combined with 100 ng of each template in a PCR reaction containing 2.5 units of *Pfu* polymerase (Stratagene), and the mutant plasmids were amplified by PCR using the following cycling conditions: initial denaturation at 94^0 C for 10 minutes, 30 cycles of 94^0 C (30s), 60^0 C (30s), 72^0 C (8 min), with a final extension at 72^0 C for 7 minutes. The entire PCR reaction was desalted in an Amicon spin-filter (Millipore) and was digested with *Dpn*I for 16 hrs at 37^0 C to remove the original plasmid template. Five μL of the resulting solution was transformed into *E. coli* DH5α cells. Mutations were verified by automated DNA sequencing.

The soybean nodulin-26 wild-type cDNA and phosphorylation null mutant with a substitution of an Ala for Ser-262 (S262A) were generated as previously described (Lee et al., 1995) and were cloned into the *Bgl*II site pXβG-ev1 under the control of the T3 promoter.

ApAQP1 was isolated from aphid gut cDNA by PCR amplification using gene specific primers (ApAQP1 F and ApAQP1 R; Table **2.1**) and KOD Hot Start DNA Polymerase (Toyobo). The reaction conditions were 31 cycles of 94^oC for 1 min, 35^oC for 1 min, and 72^oC for 2 min 30 sec. The denaturing step was extended to 5 min in the first cycle and the extension time increased to 8 min in the last cycle. PCR products were separated by electrophoresis in a 1% (w/v) agarose gel and stained with ethidium bromide before visualisation under ultraviolet light. The ApAQP1 cDNA was extracted from the gel by the QIAquick Gel Extraction kit (Qiagen) and was cloned into the pCR®-Blunt II-TOPO® plasmid vector (Invitrogen) following the manufacturers' instructions. The recombinant vectors were transformed into One Shot® TOP10 chemically-competent *E. coli* cells. Plasmids were purified by the

Qiaprep Spin Miniprep kit (Qiagen). Plasmids containing inserts were identified by automated DNA sequencing.

The *ApAQP1* open reading frame in the Blunt II-TOPO® vector was amplified by PCR with ExTaq polymerase (Takara) and gene-specific primers containing *Bam*HI restriction sites (*ApAQP1* Xenopus F and *ApAQP1* Xenopus R; Table **2.1**). The cycling conditions were: initial denaturation at 94^0C for 10 min, followed by 30 cycles with 94^oC (30 s), 55^oC (30 s), 72^oC (2 min), and a final extension for 7 min at 72^oC. The amplified PCR product was resolved on a 1.0% (w/v) low melting point agarose gel and was purified using the Qiaquick gel extraction kit (Qiagen) and was cloned into the pCR2.1-TOPO vector (Invitrogen). The cDNA fragment was excised by *Bam*HI digestion and was cloned into the *Bgl*II site of the pXβG-FLAG vector as described previously. The final expression construct contained the *ApAQP1* cDNA with a N-terminally fused FLAG epitope tag. The correct sequence of the construct was verified by automated DNA sequencing. The *ApAQP2*/ pXβG-FLAG construct was generated in exactly the same manner using gene-specific PCR primers for pXβG-FLAG cloning (*ApAQP2* Xenopus F and *ApAQP2* Xenopus R; Table **2.1**).

Cloning of soybean cytosolic glutamine synthetases

Cytosolic glutamine synthetase isoforms were cloned from soybean nodule cDNA by designing primers against the conserved 5' end of the glutamine synthetase cDNA (GS cytosolic F and GS nodule F; Table **2.2**) as well as gene specific primers against the 3'untranslated region of each isoform (Table **2.2**; Morey et al., 2002).

Table 2.2: Oligonucleotide primers used for soybean glutamine synthetase cloning

Primer name	Direction[a]	Sequence
GS cytosolic F	Forward	CGAGCTCATGTCTCTCTGCTCTCAGATCTC
GS nodule F	Forward	CGCGGATCCATGTCGTTGCTCTCCGATCTT
GS β_1 3'-UTR R	Reverse	CGAGCTCTCATGGCTTCACAGAATGGTT
GS β_2 3'-UTR R	Reverse	CGCGGATCCATTTGGTTTCCAAGAATGGT
GS γ_1 3'-UTR R	Reverse	TCCTCGCTTGGTAATCATGAG
GS γ_2 3'-UTR R	Reverse	ATTCTTCACTTCAGTACTACC

[a]All primer sequences are in the 5' to 3' direction.

These primers were used to amplify each isoform by PCR using ExTaq polymerase (Takara) and the following PCR cycling conditions: initial denaturation at 94^0 C for 10 minutes, 30 cycles of 94^0 C for 30 seconds, 55^0 C for 30 seconds, and 72^0 C for 2 minutes and 15 seconds, followed by a final extension of 72^0 C for 7 minutes. The PCR products were resolved on a 1.0% (w/v) agarose gel run in Tris-acetate EDTA buffer (Sambrook et al., 1989) containing 10 ng/ mL ethidium bromide.

The resulting PCR products were cloned into the pCR2.1-TOPO vector as described above. Ten white colonies from each transformation reaction were sequenced as described in the analytical methods section, and the resulting nucleotide sequences indicated the presence of four unique glutamine synthetase isoforms that are subsequently referred to as *Glycine max* glutamine synthetase 1;1, 1;2, 1;3, and 1;4 (GmGS1;1-1;4).

Expression of channel constructs in *Xenopus laevis* oocytes

Oocytes were harvested and prepared for microinjection essentially as previously described (Rivers et al., 1997; Guenther and Roberts, 2000). Stage V and VI oocytes were surgically removed from female oocyte positive *Xenopus laevis* frogs (Xenopus Express) in Frog Ringers solution (96 mM NaCl, 2 mM KCl, 5 mM $MgCl_2$, 5 mM HEPES-NaOH pH 7.6). The collagen layer around the oocytes was removed by incubation of these oocytes in Frog Ringers solution supplemented with 1 mg/ mL collagenase (Sigma; catalog number C9891) for 1-2 hrs at 25^0 C with shaking. The oocytes were washed 5-7 times in 15 mL of Frog Ringers solution, and

were equilibrated in Frog Ringers supplemented with 0.6 mM $CaCl_2$ for at least 2 hrs at 18^0 C.

5'-capped cRNA was generated by linearizing the oocyte expression vectors with *Xba*I (AtNIP5;1-FLAG, AtNIP6;1-FLAG, AtNIP6;1 A119W-FLAG, AtNIP6;1 V252A-FLAG, Nodulin 26-FLAG, LjNod26 W77H), *Bam*HI (ApAQP1-FLAG), or *Sma*I (AQP1, ApAQP2). Linearized plasmids (1 μg) were used as templates in the T3 mMessage mMachine in vitro transcription kit (Ambion). The plasmids were incubated in the presence of T3 polymerase enzyme mix for 1 hour at 37^0 C, followed by incubation with 1 unit of RNAse-free DNAse I for 15 minutes at 37^0 C. The cRNA was precipitated in 3 M LiCl at -80^0 C for 1 hour and was centrifuged at 10,000 x g for 30 minutes at 4^0 C. The supernatant was removed and the pellet was washed with 100 μL of 70 % (v/v) ethanol, and was collected by centrifugation at 10,000 x g for 15 minutes at 4^0 C. The supernatant was removed, and the pellet was resuspended in 10 μL of DEPC-treated sterile water. The absorbance of the sample at 260 nm (1 absorbance unit = 40 μg/ mL) was used to quantify the concentration of the cRNA in solution, and all samples were adjusted to a 1 μg/ μL stock concentration. The integrity of the RNA was determined by electrophoresis on a 0.8 % (w/v) agarose gel in Tris-acetate EDTA buffer in the presence of 0.4 ng/ mL ethidium bromide. The integrity of the cRNA was checked by visualization of the bands on a transilluminator. Samples were stored in 5 μL aliquots at -80^0 C until further use.

Oocytes were injected with 46 nL of cRNA (1 μg/ μL) with a Nanoject II microinjector (Drummond). Uninjected oocytes or oocytes injected with 46 nL of

sterile DEPC water were used as negative controls. Oocytes were incubated in individual wells of a 96-well plate in 200 μL of oocyte medium (Frog Ringers solution supplemented with 0.6 mM $CaCl_2$ and 1000 U penicillin-streptomycin) for 72-96 hrs at 18^0 C prior to assay.

Oocyte water permeability assays

The osmotic water permeability of *Xenopus* oocytes was determined at 15^0 C by video microscopy using a Nikon Alphaphot YS microscope and NIH Image software essentially as previously described (Rivers et al., 1997; Guenther and Roberts, 2000). Serial images of oocytes were captured using a specialized algorithm obtained from Dr. Jim Hall at the University of California, Irvine. Oocytes were placed in a bath solution cooled by a custom microscopy stage containing Frog Ringers solution diluted to 30 % of its initial osmolarity (60 mOsm/ kg). The rate of oocyte swelling [$d(V/V_0)/dt$] was used to calculate the osmotic permeability coefficient (P_f) using the following equation (Equation 1):

$$P_f = \frac{V_0(dV/V_0)dt}{\left(\frac{S_{\text{real}}}{S_{\text{sphere}}}\right)V_w(\text{osm}_{\text{in}} - \text{osm}_{\text{out}})} \qquad \text{eq. 1}$$

where V_0 is the surface area of the oocyte at time 0, osm_{in} is the osmolarity inside the oocyte, osm_{out} is the osmolarity of the bath solution, V_w is the partial molar volume of water (18 cm^3/ mol), S_{real} is the actual surface area of the oocyte, and S_{sphere} is the area calculated by assuming the oocyte is a sphere. Based on morphological estimates, an S_{real}/ S_{sphere} value of 9 was used to correct for the increase in the oocyte plasma

membrane surface area caused by the presence of folds and microvilli (Zampighi et al., 1995). The basal water permeability of the oocyte plasma membrane was determined by performing the same assays with uninjected oocytes, or oocytes injected with 46 nL of sterile water.

Inhibition of ApAQP1 by mercury (II) chloride was investigated by pre-incubating oocytes in oocyte medium supplemented with 1 mM $HgCl_2$ for 5 min at 25^{o}C, followed by immediate water permeability assay. Control experiments confirmed that this treatment did not affect the basal water permeability of uninjected oocytes, indicating that $HgCl_2$ at this dose did not have nonspecific deleterious effects on the oocytes or any effect on the diffusive water permeability through the oocyte membrane.

For activation energy (E_a) measurements, the temperature of the bath solution used in the oocyte water permeability assay was varied from 6 to 18^{o}C. Natural logarithms of the P_f values collected at these temperatures were plotted against the inverse of the absolute temperature (K), and linear regression analysis was used to fit the data to the Arrhenius equation (Equation 2):

$$\ln(P_f) = \left(\frac{-E_a}{R}\right)\left(\frac{1}{T}\right) + \ln(A) \qquad \text{eq. 2}$$

where E_a is the activation energy for water transport, R is the universal gas constant, and A is the Arrhenius pre-exponential factor.

To test the effects of phorbol esters or okadaic acid on water permeability, oocytes were incubated in full-strength Frog Ringers solution supplemented with 0.6 mM $CaCl_2$ containing either 10 nM phorbol-12-myristate-13-acetate (Calbiochem) or

25-50 nM okadaic acid (Calbiochem) for 30 minutes at 25^0 C followed by immediate water permeability assay.

Oocyte solute permeability assays

Xenopus oocytes expressing a variety of MIP channels were assayed for solute permeability by several different methods. Nonradiolabeled solute uptake assays were performed by equilibrating oocytes in full-strength Frog Ringers solution supplemented with 0.6 mM $CaCl_2$ and measuring the oocyte swelling rate by video microscopy of these oocytes at 15^0 C in a solution that contained an isoosmotic Frog Ringers solution with the NaCl component replaced by 200 mM test solute. In this case, solute uptake results in an inwardly-directed osmotic gradient resulting in water uptake and oocyte swelling. The rate of solute uptake is reported as an oocyte swelling rate [$d(V/V_0)/ dt$] determined by video microscopy as described above.

Radiolabeled glycerol uptake assays were performed by incubating groups of 9 oocytes in glycerol assay buffer (200 mM glycerol, 60 μCi/ mL [^{3}H] glycerol [ICN], 2 mM KCl, 5 mM $MgCl_2$, 0.6 mM $CaCl_2$, and 5 mM HEPES-NaOH at pH 7.6) for 10 minutes at 25^0 C. The oocytes were subsequently washed with 2 x 10 mL of ice-cold glycerol assay buffer without radiolabeled glycerol. Oocytes were separated into groups of three in scintillation vials and were lysed by the addition of 300 μL of 10 % (w/v) sodium dodecylsulfate. The uptake of radioactive glycerol was quantified by scintillation counting in 10 mL of Scintiverse II aqueous scintillation cocktail (Fisher Scientific) using a Beckman LS 3801 scintillation counter.

Radiolabeled urea and mannitol uptake assays were performed in a similar manner. Groups of 9 oocytes were incubated in either urea assay buffer (200 mM urea, 30 μCi/ mL [^{14}C] urea [MP Biomedicals], 2 mM KCl, 5 mM $MgCl_2$, 0.6 mM $CaCl_2$, and 5 mM HEPES-NaOH pH 7.6) or mannitol assay buffer (200 mM mannitol, 20 μCi/ mL [^{14}C] mannitol [MP Biomedicals], 2 mM KCl, 5 mM $MgCl_2$, 0.6 mM $CaCl_2$, 5 mM HEPES-NaOH pH 7.6) for 10 minutes at 25^0 C. The oocytes were washed with 20 mL of ice-cold assay buffer without radiolabeled substrate and were processed and assayed for radioisotope uptake in exactly the same manner as described above for glycerol uptake assays.

Direct uptake of boric acid was performed by incubating groups of 9 oocytes in Frog Ringers solution supplemented with 0.6 mM $CaCl_2$ as well as 2 mM boric acid. Assays were conducted at 15^0 C. For time-dependent uptake assays, oocytes were removed at 0, 5, 10, and 20 minutes and were washed with a total of 30 mL of ice-cold Frog Ringers solution without the test metalloid compound. These oocytes were separated into groups of 3 in eppendorf tubes, lyophilized, and subjected to inductively coupled plasma mass spectrometry (ICP-MS) in an SPQ-9000 instrument (Sieko Instruments) to quantitate the amount of metalloid compound in the sample as previously described (Takano et al., 2002).

Stopped-flow fluorimetry analysis of nodulin-26 water permeability

Intact symbiosomes were isolated from 28-day-old nodules by the Percoll step gradient method as described previously (Weaver et al., 1991). Symbiosome membrane vesicles were prepared and loaded with 20 mM carboxyfluorescein (Rivers

et al., 1997) by vortexing the isolated symbiosomes in loading buffer (20 mM carboxyfluorescein, 25 mM 3-(N-morpholino)-propanesulfonic acid (MOPS)-NaOH pH 7.0, 3 mM $MgSO_4$, and 200 mM mannitol, 262 mOsm/kg). The P_f of these membrane vesicles was determined by stopped-flow fluorimetry by abruptly doubling the osmolarity of the extravesicular solution by injection into an equal volume of 25 mM MOPS-NaOH pH 7.0, 3 mM $MgSO_4$, and 700 mM sucrose while monitoring the time-dependent fluorescent quenching of entrapped carboxyfluorescein. Experiments were performed on a Bio-Logic SFM-3 stopped-flow apparatus (Biologix) with a MPS-51 power supply fitted with a TC-100/ 10 cuvette, 15 mL syringes, and a HDS mixer. This apparatus was run at a total flow rate of 2 mL/ s (80 μL/ injection) with a measured dead time of 7 ms.

The fluorimeter was controlled by the Bio-Kine software V3.20 (Biologix) and 1000 points of fluorescence data (λ_{ex} = 490 nm, emission filtered with a 515 nm cutoff filter) were collected at time intervals of 0.1 and 1 ms. At least 10 individual traces were averaged to reduce the signal-to-noise ratio and were fitted to a single exponential curve. The amplitude and end-point values from this curve were used to relate the relative fluorescence to relative volume based on a linear relationship between fluorescence and intravesicular volume (Harris et al., 1990) and the assumption that the internal volume of the vesicle reaches 50 % of the initial volume at the end of the experiment. The P_f was calculated from the time course of relative fluorescence using the osmotic water permeability equation (Equation 3):

$$\frac{dV(t)}{dt} = P_f \bullet SAV \bullet V_w \left\{ \frac{\mathrm{osm_{in}}}{V_{(t)}} - \mathrm{osm_{out}} \right\} \quad \text{eq. 3}$$

Where V(t) is the relative volume of the vesicles at time t, P_f is the osmotic permeability coefficient, SAV is the vesicle surface-to-volume ratio, V_w is the molar volume of water (18 cm^3/ mol), osm_{in} is the osmolarity of the vesicle lumen, and osm_{out} is the osmolarity of the extravesicular media. The diameter of the vesicles used in these experiments were calculated by their 90^0 light-scattering intensity using a Brookhaven Instruments BI-200 goniometer, and these data were used to calculate the SAV ratio.

For analysis of the effects of phosphorylation on the nodulin-26 P_f, isolated vesicles (13.1 μg protein/ mL) were incubated at 30^0 C for 30 minutes in either loading buffer without carboxyfluorescein, kinase buffer (loading buffer supplemented with 3 mM ATP) or loading buffer supplemented with 30 units/ mL of calf intestinal alkaline phosphatase (Promega). The level of nodulin-26 phosphorylation was assayed by protein gel blot analysis using a nodulin-26 S262 phosphorylation-specific antibody as previously described (Guenther et al., 2003).

Transition state analysis of water transport

The thermodynamic parameters describing the transition state of water transport through the nodulin-26 and AQP1 channels were calculated by previously described methods (Sogami et al., 2001) using the following equations:

$$P_f = \left(\frac{\lambda^2}{\delta}\right)\left(\frac{kT}{h}\right)e^{\left(\frac{-\Delta G^{\ddagger}}{RT}\right)} \qquad \text{eq. 4A}$$

$$\Delta H^{\ddagger} = E_a - RT \qquad \text{eq. 4B}$$

$$\Delta G^{\ddagger} = \Delta H^{\ddagger} - T\Delta S^{\ddagger} \qquad \text{eq. 4C}$$

where λ is the average distance between energy minima when a molecule moves across a membrane, δ is the membrane thickness, *k* is Boltzmann's constant, *T* is the absolute temperature, *h* is Planck's constant, *R* is the ideal gas constant, E_a is the activation energy, and $\Delta G^{\ddagger}$, $\Delta H^{\ddagger}$, $\Delta S^{\ddagger}$ and are the free energy, enthalpy, and entropy of the transition state, respectively. In all calculations, δ is assumed to be 50 Å and λ is assumed to be 2.5 Å.

Immunochemical techniques

For expression analysis of various MIP constructs in *Xenopus*, Western blots were performed using a monoclonal antibody directed against the FLAG epitope tag (Stratagene). *Xenopus* oocyte lysates were prepared by homogenizing five oocytes in 100 μL of oocyte homogenization buffer (20 mM Tris-HCl pH 7.4, 5 mM $MgCl_2$, 5 mM NaH_2PO_4, 80 mM sucrose, 1 mM EDTA, 1 mM dithiothreitol, 1 mM phenylmethyl sulfonyl fluoride, 5 μg/ mL leupeptin, and 5 μg/ mL pepstatin A) in an eppendorf tube at 4^0 C with a Teflon pestle. The samples were centrifuged at 250 x g for 10 minutes to remove yolk protein, and the lysate supernatant was saved for Western blot analysis.

Lysate proteins were separated by electrophoresis on a 12.5 % (w/v) polyacrylamide gel (SDS-PAGE) and were electrophoretically transferred onto polyvinylidene fluoride membranes (Immobilion) for 12 hrs at 4^0 C in transfer buffer (0.2 M zwitterionic glycine, 25 mM Tris-HCl, and 20 % [v/v] methanol). Membranes were incubated in blocking solution (10 % [w/v] non-fat dry milk, 137 mM NaCl, 2.7

mM KCl, 10 mM NaH_2PO_4, and 2 mM K_2HPO_4 [PBS] at pH 7.2) for 2 hrs at 37^0 C with shaking. The membranes were washed three times for 5 minutes in PBSt (PBS at pH 7.2 and 0.01 % [v/v] Tween-20). The membrane was then incubated with primary antibody solution (1:1000 mouse anti-FLAG antibody [Stratagene] in 1 % [w/v] non-fat dry milk and PBS pH 7.2) for 1 hr at 37^0 C. The membranes were washed in PBSt as described above, and were incubated in secondary antibody solution (1:2000 horseradish peroxidase coupled horse anti-mouse antibody [Vector Biotechnologies], 1 % [w/v] non-fat dry milk, and PBS pH 7.2). The membrane was washed again with PBSt as described above and was developed with 1.25 mM luminol, 0.2 mM p-coumaric acid, 0.009 % [v/v] H_2O_2, and 100 mM Tris-HCl pH 8.0. The chemiluminescent signal was detected by exposure to Fuji HR-HA 30 X-ray film.

Biochemical isolation of nodulin-26 interacting proteins by affinity chromatography

Immobilized peptide resins were prepared by m-maleimidobenzoyl-N-hydroxysuccinimide coupling, essentially as previously described (Guenther et al., 2003). Four mL of ω-aminohexyl agarose (Sigma) was washed with 150 mL of 0.01 M $NaPO_4$ pH 7.0 and was resuspended in 7 mL of the same buffer. Fifteen mg of the heterobifunctional cross-linking reagent 3-maleimidobenzoyl-N-hydroxysuccinimide (MBS; Pierce) was dissolved in 100 μL of dimethyl formamide (Sigma) and was added to the resin. The resin mixture was incubated at 25^0 C for 30 minutes and was then washed with 200 mL of 0.01 M $NaPO_4$ pH 7.0. The resin was resuspended in 7

mL of the same buffer, and 15 mg of sulfhydryl-containing peptides comprising the entire C-terminus of nodulin-26 (CK-25), the C-terminal phosphorylation site of LIMP2 (CI-14), or the partial C-terminus of the unrelated protein Arabidopsis SIP2;1 (CP-13) were added to the solution. All peptide sequences are shown in Table **2.3**. This mixture was incubated at 25^0 C for 4 hrs with shaking. After incubation, the resin was washed with 250 mL of 0.01 M $NaPO_4$ buffer pH 7.0 and was stored at 4^0 C in the same buffer.

Nodule soluble proteins were isolated by crushing 40 g of 40-day-old nodule tissue in 40 mL of 25 mM MOPS-NaOH at pH 7.0, 350 mM mannitol, 10 mM $MgSO_4$, 15 mM sodium ascorbate, 1 % [w/v] polyvinylpyrrolidine-40, 5 mM DTT, 10 mM EDTA, 1 mM PMSF in a glass mortar with a pestle. The extract was filtered through two layers of miracloth (Calbiochem) and was layered on top of a Percoll step gradient as previously described (Weaver et al., 1991). The gradients were centrifuged at 5,500 rpm in an HS-4 rotor (Sorvall) for 15 minutes at 4^0 C, and the top layer containing nodule soluble proteins as well as smaller membrane fragments was removed. The membrane fragments were separated from the soluble protein fraction by centrifuging this sample at 100,000 x g for 1 hr at 4^0 C in a Ti-60 rotor (Beckman). Five mL of the resulting clarified extract was applied to 200 μL of peptide-coupled affinity resins. The resins were extensively washed with 50 mM Tris-HCl pH 7.5, 150 mM NaCl and bound proteins were eluted from the resin with 10 mM Tris-HCl pH 7.5, 6 M urea. Proteins in the eluted fractions were separated on 12.5 % SDS-PAGE gels and were stained with Coomassie blue solution.

Table 2.3: MIP C-terminal peptides used for glutamine synthetase purification experiments:

Peptide name[a]	Sequence[b]
CI-14	**CREITKNVSFLKGI**
CP-13	**CVFKPLTEEQEKP**
CK-25	**CRYTDKPLSEITKSASFLKGRAASK**

[a] Peptides are designated by their first residue, last residue, and peptide length.

[b] The sequence of each peptide is shown from the amino to the carboxyl terminus.

Partial purification of native glutamine synthetase from soybean root nodules

Thirty-two grams of 35-day-old soybean root nodules were homogenized in 100 ml of 100 mM Tris-HCl pH 8.4, 10 mM magnesium acetate, 10% (v/v) glycerol, 0.5% Triton X-100 (v/v), 1 mM PMSF, and 1 μg/ mL leupeptin by a using polytron mixer (Kinematica GmbH) at 4^0C. The extract was centrifuged at 34,000 x g in an SS-34 rotor for 30 min at 4^0 C. An equal volume of chilled acetone was added to the supernatant, and the mixture was stirred at 4^0C for 20 min. The precipitated proteins were separated by centrifugation at 34,000 x g in an SS-34 rotor (Sorvall) for 15 min at 4^0 C. The pellet was dried on ice under an air stream and was resuspended in resuspension buffer (10 mM Tris-HCl pH 7.5, 10 mM magnesium acetate, 10% [v/v] glycerol). Saturated ammonium sulfate was added drop-wise to the resuspended sample to 30% saturation while stirring at 4^0C for 15 min. The sample was centrifuged as described above and the supernatant was decanted. Ammonium sulfate was added to the supernatant to 60% saturation, and the sample was centrifuged as described above. The pellet was resuspended in 5 mL of resuspension buffer and centrifuged at 200,000 x g in a Ti-80 rotor (Beckman) for 30 min at 4^0 C.

The supernatant from this sample was applied to a Sephacryl S-300 molecular exclusion column (dimensions 50 cm x 2 cm) equilibrated in resuspension buffer. The column was run in resuspension buffer at a flow rate of 0.5 mL/ min and 3 mL fractions were collected and were assayed for glutamine synthetase activity. Fractions exhibiting the highest glutamine synthetase activity were analyzed by SDS-PAGE. The samples were pooled and stored in aliquots at -80^0 C.

Symbiosome membrane and peptide affinity resin association of glutamine synthetase activity

For resin association assays, 50 μL of CI-14, CP-13, and CK-25 conjugated agarose resins or underived ω-aminohexyl agarose were equilibrated with 7 mL of binding buffer (20 mM Tris-HCl pH 7.5, 150 mM NaCl, 5 mM $MgCl_2$). The supernatant was removed and 50 units (1U = 1 μmol of γ-glutamyl hydroxamate produced per minute at 37^0 C) of soybean nodule glutamine synthetase was incubated with the resins at 25^0 C for 30 minutes. After incubation, the resin samples were centrifuged at 5000 x g for 10 seconds to pellet the resin. The supernatant was transferred to a new tube, and the resin was washed with 10 mL of binding buffer. The glutamine synthetase enzymatic activity in the unadsorbed supernatant fraction and the bound resin fractions was subsequently measured.

Symbiosome membrane glutamine synthetase association assays were conducted by incubating 100 μg of isolated soybean symbiosome membranes with 50 units of purified soybean glutamine synthetase in binding buffer for 1 hr at 4^0 C. The membranes were washed three times with 5 mL of binding buffer with membranes collected by centrifugation at 100,000 x g for 1 hr at 4^0 C in a Ti-80 rotor after each wash (Beckman). The symbiosome membrane samples were divided into groups of three aliquots, and were assayed for glutamine synthetase activity. As a negative control, untreated symbiosome membranes were washed as described above and were assayed for glutamine synthetase enzymatic activity. Peptide inhibition of the glutamine synthetase membrane interaction was assayed by the addition of 10 μM CI-14 peptide to the incubation mixture.

Matrix assisted laser desorption ionization- time of flight (MALDI-TOF) and tandem MS analysis of nodulin-26 interacting proteins

Proteins eluting from the affinity chromatography resins were resolved by SDS-PAGE and were stained with Coomassie blue. Protein bands were excised using surgical scalpel blades. A piece of gel was cut from a blank region of the gel and was processed in parallel to serve as a background control. The excised gel pieces were washed and destained by the following regime: 100 μL deionized distilled water (ddH_2O) for 15 min, 100 μL 50% (v/v) acetonitrile for 15 min, 100% acetonitrile for 30 seconds, and 100 mM NH_4HCO_3 for 5 min followed by addition of 100 μL of acetonitrile. After incubation in acetonitrile for 15 min, the supernatant was removed, and the excised gel pieces were dried in a SpeedVac centrifuge (Savant). Proteins were reduced and alkylated. Fifty μL of 10 mM DTT in 100 mM NH_4HCO_3 was added, and the proteins were reduced for 1 hr at 56°C. After cooling to room temperature, the DTT solution was replaced with the same volume of 55 mM iodoacetamide in 100 mM NH_4HCO_3. The alkylation reaction was performed for 45 min at 25^0 C in the dark. The gel pieces were washed with 100 μL of 100 mM NH_4HCO_3 for 5 min, and were dehydrated by addition of 100 % acetonitrile. After removing the acetonitrile, the gel pieces were rehydrated in 100 mM NH_4HCO_3, and were dehydrated again by addition of the same volume of acetonitrile. The liquid solution was removed, and the gel pieces were completely dried in a SpeedVac centrifuge.

Trypsin (Pierce) pretreated with L-1-tosylamido-2-phenylethyl chloromethyl ketone (TPCK) was used for digestion of protein gel samples. Four μL of 0.05 μg/μL trypsin was added, and the sample was incubated at 4^0 C for 1 hr. The residual trypsin solution was removed, and the gel pieces were incubated in 50 μL of 25 mM NH_4HCO_3, and 2 mM $CaCl_2$ at 37°C for 16 hr. One μL of trifluoroacetic acid (TFA) was added to kill residual trypsin activity, and the solution was decanted to a new tube. Fifty μL of 1% (v/v) TFA in 60% (v/v) acetonitrile was added and the sample was taken to dryness in a SpeedVac centrifuge.

ZipTip pipette tips (Millipore), which contain C18 bonded spherical silica (15 μm, 200 Å pore size) in a 0.6 μL bed volume, were used for the desalting of the tryptic peptides. The tips were first washed with 100% acetonitrile, then in nano-pure ddH_2O, and then were equilibrated with 0.1% (v/v) trifluoroacetic acid. The dried pellet containing the tryptic peptides was dissolved in 15 μL of 0.1% (v/v) trifluoroacetic acid, and the peptides were bound to the pre-equilibrated ZipTip by fully depressing the pipette plunger. Samples were pipetted up and down through the ZipTip 10 times. The ZipTip was washed twice with 0.1% (v/v) trifluoroacetic acid and 10% (v/v) acetonitrile. The digested peptides were eluted using 5 μL of saturated α-cyano-4-hydroxy-cinnamic acid in 60% (v/v) acetonitrile: and 0.1% TFA, 1:1 (v/v).

MALDI-TOF mass spectra were acquired at either the University of Georgia Proteomics Facility (initial experiments) or by analysis at the University of Tennessee on a Bruker microflex time-of-flight mass spectrometer (Bruker Daltonics) with a nitrogen laser operating at 337 nm in the positive-ion mode. Prior to each analysis in the reflectron method, the mass spectrometer was externally calibrated using the

calculated masses of peptide calibration standard II (Bruker Daltonics); bradykinin fragment 1-7, angiotensin I and II, substance P, bombesin, porcine renin substrate tetradecapeptide, ACTH clip fragments 1-17 and 18-39, and somatostatin 28. A one μL droplet of the desalted sample was spotted directly onto the AnchorChip target plate (Bruker Daltonics) of the mass spectrometer. The acceleration voltage was set to 20 kV, and the pressure in the TOF analyzer was 6×10^{-7} bar. Tandem MS sequencing analysis was performed at the University of Georgia Proteomics Facility.

The masses of tryptic peptides were analyzed by searching the NCBI nonredundant protein database with ProFound provided by Laboratory of Mass Spectrometry and Gaseous Ion Chemistry at Rockefeller University (http://prowl.rockefeller.edu/prowl-cgi/profound.exe). Peptide masses were assumed to be monoisotopic, and methionine residues were assumed to be partially oxidized. A maximum number of two missed cleavages for tryptic digests were allowed, and the mass tolerance was set to 0.2 dalton.

Split-ubiquitin yeast two-hybrid methods

Split-ubiquitin yeast two-hybrid experiments were performed using the yeast strains and methods previously described (Obrdlik et al., 2004). THY.AP4 [*MATa, ura3, leu2, trp1, lexA:: LacZ, LexA:: HIS3, LexA:: ADE2*] and THY.AP5 [*MATα, URA3, leu2, trp1, his3, loxP:: ADE2*] *Saccharomyces cerevisiae* strains as well as the pMetYCgate, pNXgate 32, pNubWT, KAT1/ pMetYCgate, and KAT1/ pNXgate 32 vectors were obtained from the ABRC. The relevant features of pMetYCgate and pNXgate 32 vectors are described (Figure **2.1**). Untransformed yeast cells were

streaked on YPD agar (1 % [w/v] yeast extract, 2 % [w/v] peptone, 2 % [w/v] dextrose, 1.5 % [w/v] bactoagar) and were grown for 2 days at 30^0 C. The presence of the ADE2 gene mutation in both of these strains causes them to have a red color on YPD media. Bacterial contamination of the yeast stocks was examined by light microscopy using a Nikon Alphaphot YS microscope.

The pMetYCgate and pNXgate32 vectors are designed for recombination-based cloning and must be linearized before transformation (Figure **2.2**). To prepare these vectors for transformation, pMetYCgate was digested with *Pst*I and *Hind*III, while the pNXgate32 vector was digested with *Eco*RI and *Sma*I. Both sets of digests were carried out at 37^0 C for 4 hrs, and the resulting plasmid fragments were gel purified from a 1 % (w/v) low melting point agarose gel by using the Qiaquick gel extraction kit (Qiagen).

Soybean glutamine synthetase cDNAs were amplified by PCR from sequenced pCR2.1-TOPO vectors containing each insert using ExTaq polymerase (Takara) and gene-specific primers containing the necessary B1 and B2 recombination sites (Table **2.4**). Nodulin-26 was amplified from the Nodulin-26/ pXβG-ev1 (Rivers et al., 1997) using ExTaq DNA polymerase (Takara) gene specific primers containing the necessary B1 as well as B2 sites (Table **2.4**). The PCR products were separated on a 1 % (w/v) low melting point agarose gel, and were purified using the Qiaquick gel extraction kit (Qiagen).

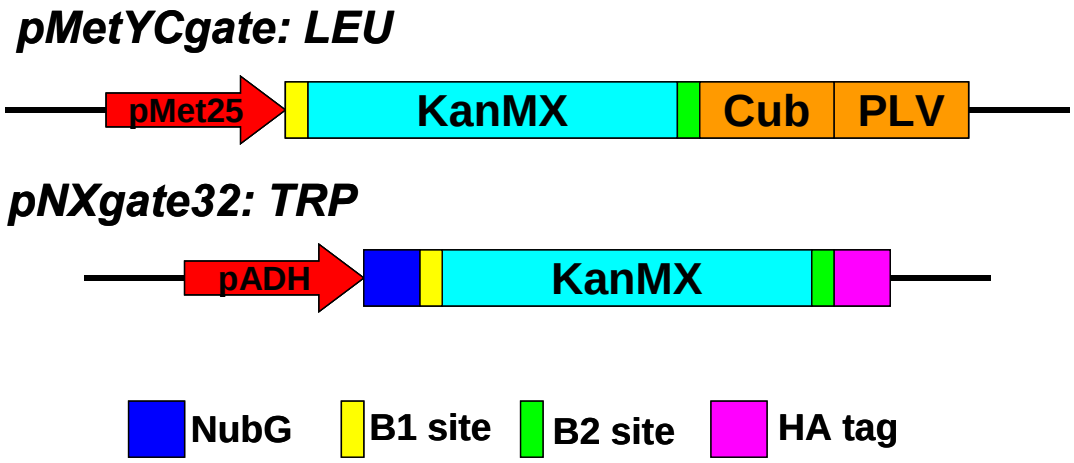

Figure 2.1: Relevant features of the pMetYCgate and pNXgate32 vectors: The pMetYCgate and pNXgate32 plasmids contain a gentamicin resistance cassette (KanMX) that is removed upon digestion with *Pst*I/ *Hind*III (pMetYCgate) or *Eco*RI/ *Sma*I (pNXgate32). pMetYCgate is transcriptionally controlled by the methionine repressible MET25 promoter, while pNXgate32 is under the control of the constitutive alcohol dehydrogenase promoter. The positions of the B1 and B2 recombination sites are shown in yellow and green, respectively. The positions of the Cub/ PLV (orange), Nub (blue), and 3xHA epitope tag (purple) translational fusions are indicated. Both plasmids contain ampicillin resistance markers for routine selection during routine cloning in *E. coli*. pMetYCgate contains the LEU2 gene for selection of yeast on synthetic media without leucine, while the pNXgate32 plasmid contains the TRP1 gene to select for yeast on synthetic media lacking tryptophan.

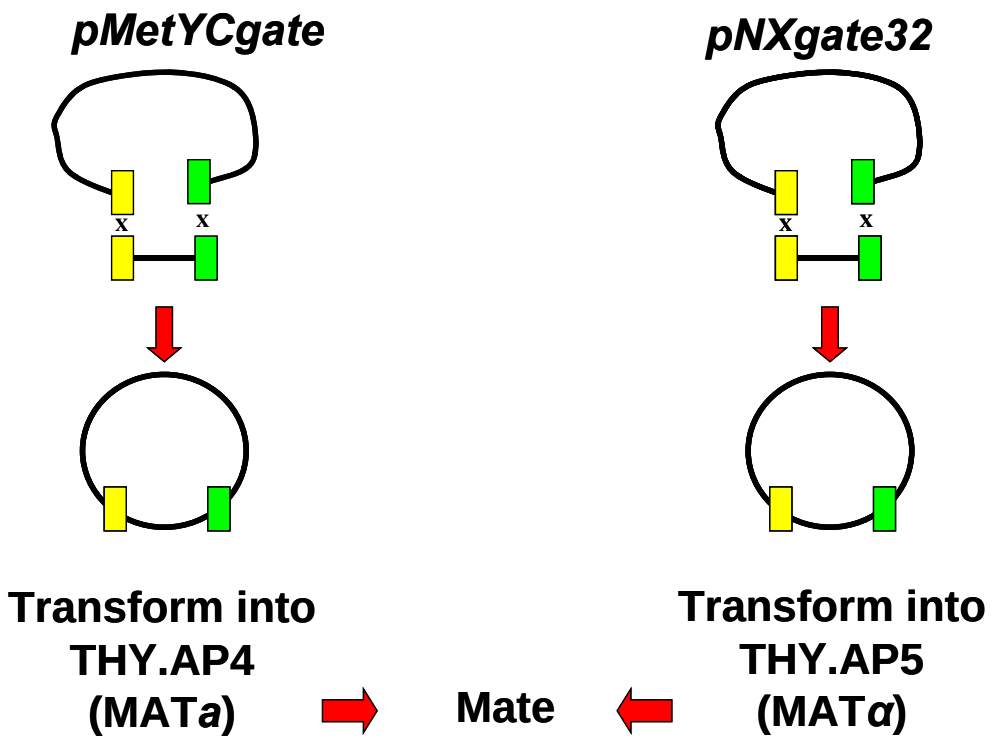

Figure 2.2: Cloning and mating scheme for split-ubiquitin yeast two-hybrid: The pMetYCgate and pNXgate32 vectors are designed for yeast in vivo cloning using their B1 and B2 recombination sites. These vectors were linearized and were co-transformed with PCR products containing complementary B1 and B2 sites. The PCR products of bait and prey constructs are inserted into the vector through yeast in vivo recombination in the proper orientation and in frame with the necessary translational fusion elements present in the vectors. The pMetYCgate constructs are transformed into the THY.AP4 strain (MATa), while the pNXgate32 constructs are transformed into the THY.AP5 strain (MATα). These strains are then mated under selection as described in materials and methods to produce a strain containing both plasmids and all reporter genes necessary to perform the interaction assays.

Table 2.4: Oligonucleotide primers used for split-ubiquitin two-hybrid interaction assays

Primer name	Direction	Sequence[a]	Comments[b]
Nodulin-26 mbSUS	Forward	ACAAGTTTGTACAAAAAAGCAGGCTCT CCAACCACCATGGCTGATTATTCAGCA	B1 Linker
Nodulin-26 mbSUS	Reverse	TCCGCCACCACCAACCACTTTGTACAAGAA AGCTGGGTATTTGGAGGCAGCACGGCC	B2 Linker
GmGS1;1 mbSUS	Forward	ACAAGTTTGTACAAAAAAGCAGGCTCT CCAACCACCATGTCTCTGCTCTCAGAT	B1 Linker
GmGS1;1 mbSUS	Reverse	TCCGCCACCACCAACCACTTTGTACAA GAAAGCTGGGTACAGAATGGTTGTGTCTGC	B2 Linker
GmGS1;2 mbSUS	Forward	ACAAGTTTGTACAAAAAAGCAGGCTCT CCAACCACCATGTCTCTGCTCTCAGAT	B1 Linker
GmGS1;2 mbSUS	Reverse	TCCGCCACCACCAACCACTTTGTACAA GAAAGCTGGGTACAGAATGGTTGTGTCTGC	B2 Linker
GmGS1;3 mbSUS	Forward	ACAAGTTTGTACAAAAAAGCAGGCTCTCCA ACCACCATGTCGTTGCTCTCCGAT	B1 Linker
GmGS1;3 mbSUS	Reverse	TCCGCCACCACCAACCACTTTGTACAAGAA AGCTGGGTAGTAACGGCCGCCAGTGTG	B2 Linker
GmGS1;4 mbSUS	Forward	ACAAGTTTGTACAAAAAAGCAGGCTCTCCA ACCACCATGTCGTTGCTCTCCGAT	B1 Linker
GmGS1;4 mbSUS	Reverse	TCCGCCACCACCAACCACTTTGTACAAGAA AGCTGGGTATGGTTTCCAAAGAATAGT	B2 Linker

[a]All primer sequences are in the 5' to 3' direction.

[b]Underlined regions represent sequences coding for the B1 and B2 linker regions necessary for yeast in vivo cloning

For transformation, 10 mL YPD starter cultures of each strain were grown overnight with shaking in YPD media at 28^0 C. These cultures were used to seed 100 mL of YPD media, which were grown to mid-log phase (OD_{600} = 0.8-1.6). The cells were harvested by centrifugation at 2500 x g for five minutes in a Sorvall GLC-1 centrifuge. The supernatant was removed and the cell pellet was resuspended in 30 mL of TE buffer (10 mM Tris-HCl pH 7.5, 1 mM EDTA). The cells were centrifuged as described above, and were resuspended in 15 mL of LiAc/ TE solution (10 mM Tris-HCl, 100 mM lithium acetate, 1 mM EDTA, pH 7.5) and were centrifuged again as described above. The supernatant was removed and the yeast cells were resuspended in 0.6 mL of LiAc/ TE solution. These competent cells were incubated for 30 minutes at 25^0 C before use in yeast transformations.

Yeast transformation reactions were carried out by combining test DNA samples with 20 μL of 10 mg/ mL boiled salmon sperm DNA (Sigma), 4.5 μL of 1 M lithium acetate, 50 μL of competent cells, and 300 μL of 40% (w/v) polyethylene glycol-3350 in LiAc/TE solution. In transformations containing intact plasmid DNA, 1 μg of DNA was used, while reactions containing linear plasmids with inserts to be recombined contained 100 ng of gel-purified plasmid as well as 300 ng of gel-purified insert. All pMetYCgate constructs were transformed into the THY.AP4 strain, and all pNXgate 32 as well as pNubWT constructs were transformed into the THY.AP5 strain. After all transformation components were combined, they were mixed by tapping the eppendorf tube and were incubated for 30 minutes at 28^0 C with shaking. The cells were heat shocked by incubation at 42^0 C for 20 minutes, and were centrifuged at 2500 x g for 1 min. The supernatant was removed, and the yeast

cells were resuspended in 100 μL of TE buffer and were plated onto selective media lacking leucine for THY.AP4 transformants or on media lacking tryptophan for THY.AP5 transformants. Yeast transformants were allowed to grow for 2 days at 30^0 C on selective media.

The mating-based split-ubiquitin yeast two-hybrid system requires mating of the yeast strains containing the individual bait and prey plasmids to combine both plasmids in a single yeast strain. For mating reactions, five to ten positive transformants were combined and grown in 5 mL of liquid synthetic media lacking leucine (THY.AP4 clones) or tryptophan (THY.AP5 clones) at 28^0 C for 16 hrs. The cultures were centrifuged at 2500 x g for 5 minutes, and the cell pellet was resuspended in 1 mL of TE buffer. Fifteen μL of the appropriate THY.AP4 and THY.AP5 transformant solutions were mixed in individual wells of a 96 well plate, and 5 μL of this cell mixture were plated onto YPD agar plates. The strains were allowed to mate for 8 hrs at 30^0 C. Mated yeast were selected by resuspending a small amount of each colony in 100 μL of sterile water and transferring 5 μL of this solution onto synthetic media plates lacking tryptophan, leucine, and uracil (SC/ -trp, leu, ura), and growing for 2 days at 30^0 C.

β-galactosidase assays were performed by an X-gal overlay assay. The assay solution was prepared by dissolving 0.25 g of agarose in 50 mL of 60 mM Na_2HPO_4, 45 mM NaH_2PO_4, 10 mM KCl, and 1 mM $MgSO_4$ pH 7.0, allowing the solution to cool below 50^0 C, and adding 0.2 % (w/v) SDS and 2 mg/ mL X-gal. The solution was stirred and poured over the yeast colonies. After the agarose solidified, the plates were incubated at 37^0 C for 16 hrs and color development was assayed.

Activation of HIS3 was determined by assessing the growth of yeast containing different bait/ prey plasmid combinations on synthetic media lacking histidine. Yeast were transferred from SC/ -trp, leu, ura media to synthetic media also lacking histidine (SC/ -trp, leu, ura, his) and were grown for 2 days at 30^0 C. Growth was scored after this incubation period by comparison of yeast colonies to the growth of yeast containing empty pMetYCgate and pNXgate vectors. The unmodified N-terminal fragment of ubiquitin (pNubWT) was used as a positive control.

Real-time PCR expression analysis

Root, rosette leaf, and stem tissues were collected from three independent plants and total RNA was extracted using the RNeasy Plant Mini Kit (Qiagen) according to the manufacturer's instructions. Five hundred ng of total RNA from each tissue was reverse transcribed into cDNA in a 20 μL reaction using the Primescript RT reagent kit (Takara) with an oligo dT-16 primer.

Real-time PCR expression analysis was performed using a Thermal Cycler Dice (Takara) with SYBR green Premix ExTaq II (Takara). Each set of reactions was conducted using gene-specific primers (Table **2.5**) with elongation factor 1-α (EF1-α) as a standardization control. Specific amplification of target genes was confirmed by both melting-curve analyses of the PCR products using the Thermal Cycler Dice instrument as well as by agarose gel electrophoresis. The relative levels of AtNIP5;1 and AtNIP6;1 were calculated using the standard curve method and standardized using EF1-α as a calibrator.

Table 2.5: Oligonucleotide primers for real-time PCR expression analysis

Primer name	Direction	Sequence[a]
AtNIP5;1 RT	**Forward**	CACCGATTTTCCCTCTCCTGAT
AtNIP5;1 RT	**Reverse**	GCATGCAGCGTTACCGATTA
AtNIP6;1 RT	**Forward**	GGCAATGGTTACAGCCGGAT
AtNIP6;1 RT	**Reverse**	GGAGCTGAGACGCTTATTGGTT
Elongation Factor 1-α RT	**Forward**	CCTTGGTGTCAAGCAGATGA
Elongation Factor 1-α RT	**Reverse**	TGAAGACACCTCCTTGATGATTT
ApAQP1 RT	**Forward**	AGCCAACCGAAGCAACATAGTT
ApAQP1 RT	**Reverse**	GGTGGGCGGCAGCAA
ApAQP2 RT	**Forward**	TGAACCACACAGCGTTG
ApAQP2 RT	**Reverse**	TTTTACTCGTTCATCGTT
GAPDH RT	**Forward**	AGATGAAGTTGTGTCTTCCGACTTT
GAPDH RT	**Reverse**	GACAAATTGGTCGTTCAATGAAATC
β-tubulin RT	**Forward**	GGCCAAGGGTCATTACACTGA
β-tubulin RT	**Reverse**	TGCGAACCACGTCCAACA
Ribosomal protein 32 RT	**Forward**	CGTCTTCGGACTCTGTTGTCAA
Ribosomal protein 32 RT	**Reverse**	CAAAGTGATCGTTATGACAAACTCAA

[a]All primers are in the 5’ to 3’ direction

For analysis of aphid tissues, the isolation of total RNA was performed as described above, and these RNA samples were used to generate cDNA using Superscript II reverse transcriptase (Invitrogen) and $p(dN)_6$ random hexamers (Roche). All assays included control reactions without reverse transcriptase.

Real-time quantification of cDNAs was performed with an ABI Prism 7900 Sequence Detection System (Applied Biosystems). The comparative Ct method was applied to determine the abundance of ApAQP1 as well as ApAQP2. Gene-specific primers for ApAQP1 and ApAQP2 (Table **2.5**) were designed using the Primer Express software (Applied Biosystems). The slope of the template titration curves were -3.3 ± 0.1, equivalent to > 95% amplification efficiency. The reaction mixtures contained 1x Power SYBR Green MasterMix (Applied Biosystems), gene-specific primers (optimized at 0.1-0.2 μM depending on the primer set), and 2 μL of cDNA template in a final reaction volume of 25 μL. Thermal cycling conditions were 2 min at 50^0 C, 10 min 95^0 C followed by 40 cycles of 15s at 95^0 C, and 1 min at 60^0 C. The assays included a dissociation curve (95^0 C for 30 sec followed by a 60-95^0 C temperature ramp in increments of 0.5^0 C for 1 min each), which confirmed that all detectable fluorescence was derived from specific products. All experimental samples were assayed in triplicate, with template free and –RT controls.

The relative expression of ApAQP1 and ApAQP2 was assessed by determining the threshold cycle (C_t), and each transcript was normalized to the expression of three reference genes: glyceraldehyde-3-dehydrogenase (GAPDH), β-tubulin (βTUB), and ribosomal protein L32 (RPL32) because the expression of some reference genes can vary across animal tissues (Thellin et al., 1999). The relative

expression of each aphid MIP isoform was displayed as the geometric mean after normalization to the three reference genes (Vandesompele et al., 2002) and standardized to the expression level of the transcript in the whole aphid body.

AtNIP6;1 subcellular localization studies

The AtNIP6;1 genomic DNA clone was amplified from Arabidopsis Col-0 genomic DNA by PCR using gene-specific primers (NIP6;1-genomic F and NIP6;1-genomic R; Table **2.6**). The resulting fragment was cloned into the pGEM-T easy vector (Promega) according to the manufacturer's instructions, and the sequence of the cloned PCR product was confirmed by automated DNA sequencing. The AtNIP6;1 genomic construct was then amplified from the above plasmid using PCR primers (NIP6;1-GFP gateway F and NIP6;1-GFP gateway R; Table **2.6**) containing the CACC sequence at the 5' end of the PCR product to facilitate directional cloning into the pENTR/ D-TOPO vector (Invitrogen) via the TOPO cloning reaction. The cloned genomic fragment was subcloned into the pMDC43 plasmid (Curtis and Grossniklaus, 2003), which contains a dual cauliflower mosaic virus 35S RNA promoter, a synthetic green fluorescent protein mutant (sGFP; S65T), and a nopaline synthase transcriptional terminator (Nos T). Subcloning was performed using Gateway LR clonase (Invitrogen) according to the manufacturer's instructions.

Wild-type Arabidopsis Col-0 plants were transformed with this construct using the floral-dip method (Clough and Bent, 1998). Homozygous T_3 transgenic lines were vertically grown for 10 days on solid MS medium containing 100 μM boric acid.

Table 2.6: Oligonucleotide primers used for plant expression constructs

Primer name	Direction	Sequence[a]	Comments[b]
AtNIP6;1 genomic DNA	**Forward**	CCTCGCATGGATCATGAGG	**None**
AtNIP6;1 genomic DNA	**Reverse**	TAATATAGAAGCGAGTGTTTTTC	**None**
AtNIP6;1-GFP gateway	**Forward**	CACCGATCATGAGGAAATTCCATCCAC	**Gateway Site**
AtNIP6;1-GFP gateway	**Reverse**	TCATCTTCTGAAGCTCCTCCTCTCT	**None**
AtNIP6;1 promoter gateway	**Forward**	CACCTCGAACGACGATTAATGGAG	**Gateway Site**
AtNIP6;1 promoter gateway	**Reverse**	GTCGAGGGTAGAGAGATAGATGAGATC	**None**

[a]All primer sequences are in the 5' to 3' direction.

[b]Underlined regions represent oligonucleotide sequences necessary for directional cloning into the pENTR/ D-TOPO vector.

For staining of the tonoplast, plants were incubated in 20 μM FM4-64 (Molecular Probes) for 5 min, washed three times in water, and incubated on solid MS medium for 18 hr in the dark. Cell walls were stained by incubating the root tissue in 10 μg/ mL propidium iodide (Molecular Probes). The 488 nm (Ar laser) excitation wavelengeth of a FLUOVIEW500 laser scanning confocal microscope was used to observe the AtNIP6;1-GFP fluorescence (emission filter 515-545 nm), FM4-64 fluorescence (excitation filter 560 nm), and propidium iodide fluorescence (excitation filter 610 nm).

Histochemical methods

The 2355 base pair promoter region upstream of the AtNIP6;1 initiation codon was amplified from Arabidopsis Col-0 genomic DNA by PCR using specific primers (pNIP6;1 Gateway F and pNIP6;1 Gateway R; Table **2.6**). The amplified DNA fragment was subcloned into the pENTR/ D-TOPO vector via the Gateway cloning reaction (Invitrogen). The cloned promoter was subcloned into pMDC162 containing the β-glucuronidase gene (GUS) with LR clonase enzyme (Invitrogen) using the manufacturer's instructions.

This construct was transformed into Arabidopsis Col-0 plants by the floral dip method as described above. Homozygous T_3 transgenic lines were grown hydroponically for 28 days under long-day conditions prior to histochemical analysis, and GUS staining was performed as described previously (Shibagaki et al., 2002). Cross sections of petioles as well as stems were prepared by incubating in fixation solution (50 mM PIPES-NaOH, 5 mM EGTA, 0.2 % [v/v] Triton X-100, and 4 %

[w/v] paraformaldehyde) for 8 hrs. Samples were washed in 50 mM PIPES-NaOH, 5 mM EGTA, 0.2 % (v/v) Triton X-100, and 2 % sucrose (w/v) two times for 15 minutes, and were cut into small pieces. The samples were thoroughly dehydrated through a graded ethanol series and embedded in Technovit 7100 (Heraeus Kulzer GmbH) according to the manufacturer's protocol. Five μm sections were cut with a microtome.

For analysis of AtNIP6;1 plants, nip6;1-1 and nip6;1-2 were grown alongside wild-type Arabidopsis Col-0 in hydroponic medium containing 1 μM boric acid for 28 days under short-day conditions. The fifth leaves from the base of the seedling were harvested and referred to as "old leaves", while the sixteenth to nineteenth leaves from the base were also harvested and referred to as "young leaves". Leaf samples were fixed in fixation solution as described above, were dehydrated through an ethanol series, and were embedded in Technovit 7100 as described above. Five μm sections were cut with a microtome and stained with 0.05 % (w/v) toluidiene blue at 50^0 C for 30 seconds.

Aphid guts and embryos were dissected from adult aphids into 0.9 % (w/v) NaCl and were prepared for in situ hybridization experiments as described previously described (Price et al., 2007). The sense and antisense DIG-dUTP labeled RNA probes were prepared from ApAQP1 or ApAQP2 cDNA in the Blunt-II-TOPO plasmid vector by using previously described methods (Price et al., 2007). Hybridization was visualized using BM Purple alkaline phosphatase substrate (Roche) with 1 mM levamisole added to the color substrate solution to inhibit the enzymatic activity of endogenous alkaline phosphatases. Microscopic analysis was

performed using a Zeiss SteREO Lumar V12 microscope fitted with a 1.5 x NeoLumar lens and imaged with an Axiocam MRc5 camera. The analysis was restricted to embryos >175 μm long and the gut region from the esophagus to the intestine.

Boric acid tracer analysis

Wild-type Arabidopsis Col-0 plants as well as the nip6;1-1 and nip6;1-2 mutant plants were grown on solid medium containing 10 μM boric acid with 99 % enriched ^{11}B (Cambridge Isotope Laboratories) for 19 days until bolting occurred. These plants were transferred to hydroponic growth medium containing 10 μM ^{11}B boric acid for 8 days. Plants were then transferred to hydroponic culture solutions containing 0.1 μM ^{11}B enriched boric acid for an additional 24 hrs, and were then incubated in medium containing 0.3 μM or 100 μM 99 % ^{10}B enriched boric acid (Cambridge Isotope Laboratories) for 0 and 24 hr. Shoot apices, stems, rosette leaves, and roots were harvested from at least three independent plants after incubation and the tissue content of ^{10}B boric acid was measured by ICP-MS as discussed above.

dsRNA knockdown of ApAQP1 and aphid phenotypic analysis

Sequences of ApAQP1 in the Blunt-II-TOPO vector and the green fluorescent protein homologue GFP-citrine in the pET28a vector (Novagen) were amplified by PCR using gene-specific primers conjugated with 21 base pairs of the T7 polymerase promoter (Table **2.7**).

Table 2.7: Oligonucleotide primers used in aphid dsRNA knockdown experiments

Primer name	Direction	Sequence[a]
ApAQP1 dsRNA	**Forward**	TAATACGACTCACTATAGGGAGTC ACGGTTAGCTTTTTGGTG
ApAQP1 dsRNA	**Reverse**	TAATACGACTCACTATAGGGAGTG TGGACAGTTCCTCCAAGT
GFP dsRNA	**Forward**	TAATACGACTCACTATAGGGCCCT CGTGACCACCCTCGG
GFP dsRNA	**Reverse**	TAATACGACTCACTATAGGGCTTC TCGTTGGGGTCTTTGCTC

[a]All primer sequences are in the 5' to 3' direction

The amplified products were used as templates for dsRNA synthesis of each gene using the MEGAscript T7 kit (Ambion). The dsRNA was precipitated with isopropanol, resuspended in RNAse-free water, and were stored at -80^0 C. Prior to use, the integrity of the dsRNA was assessed by agarose gel electrophoresis and was quantified with a Nanodrop spectrophotometer. dsRNA samples were administered orally at 1 μg/ μL in the diet of 6-day-old aphids that were reared from birth on a chemically defined diet (Douglas, 2006). The hemolymph osmolarity of test aphid samples was determined by freezing point depression (Malone and Tomos, 1992) calibrated against 0-0.6 M NaCl standards.

General analytical methods

The osmolarity of all solutions for *Xenopus* oocyte assay was determined by freezing point depression using an Osmette S Automatic Osmometer (Precision Systems). General protein analyses of extracts and protein samples were performed using the bicinchoninic acid (BCA) assay (Pierce Endogen Chemicals). Analysis of DNA sequences was done by automated sequencing using a Perkin-Elmer Applied Biosystems 373 DNA sequencer and the Prism dye terminator reaction at the University of Tennessee Molecular Biology Resource Facility. Sodium dodecyl sulfate polyacrylamide gel electrophoresis (SDS-PAGE) was performed by using the discontinuous buffer system described by Laemmli (1971).

Glutamine synthetase enzymatic activity was assayed in a 200 μL reaction containing 50 mM imidazole pH 7.3, 50 mM sodium glutamate, 20 mM $MgCl_2$, 25 mM β-mercaptoethanol, 100 mM hydroxylamine, and 5 mM ATP and was initiated

by the addition of the enzyme sample. Assays were conducted for 30 minutes at 37^0 C. The reactions were quenched by the addition of 200 μL of 370 mM $FeCl_3$, 300 mM trichloroacetic acid, and 600 mM HCl. Insoluble material was removed by centrifugation at 10,000 x g for 1 minute, and the sample absorbance was measured by a Labsystems Multiscan MCC-340 ELISA plate reader (Fisher Scientific) at 492 nm. Glutamine synthetase activity was quantified by comparison to a standard curve of γ-glutamylhydroxamate (Sigma).

Homology modeling and model evaluation

All homology models were constructed using the Molecular Operating Environment software (MOE 2002.03; Chemical Computing Group, Montreal). Target sequences were aligned with the experimental structures of AQP1 (1J4N; Sui et al., 2001), GlpF (1FX8; Fu et al., 2000), SoPIP2;1 (2B5F; Tornroth-Horsefield et al., 2006), AQPZ (1RC2; Savage et al., 2003), or AQPM (2F2B; Lee et al., 2005) using MOE's sequence and structural alignment algorithm (Kelly, 1996; Kelly and Labute, 1996) with the structural alignment tool enabled and the blosum62 substitution matrix. Accession numbers for Arabidopsis MIP target sequences used were: AtPIP1;1, CAB71073; AtPIP1;2, AAC28529; AtPIP1;3, AAF81320; AtPIP1;4, AAF02782; AtPIP1;5, T05378; AtPIP2;1, CAB67649; AtPIP2;2, AAD18142; AtPIP2;3, AAD18141; AtPIP2;4, BAB09839; AtPIP2;5, T06738; AtPIP2;6, AAC79629; AtPIP2;7, CAA17774; AtPIP2;8, AAC64216; AtTIP1;1, AAD31569; AtTIP1;2, BAB01832; AtTIP1;3, T01947; AtTIP2;1, BAB01264; AtTIP2;2, F71442; AtTIP2;3, BAB09071; AtTIP3;1, AAF18716; AtTIP3;2, AAF97261; AtTIP4;1,

AAC42249; AtTIP5;1, T12999; AtSIP1;1, AAF26804; AtSIP1;2, BAB09487; AtSIP2;1, CAB72165; AtNIP1;1, AAM51272; AtNIP1;2, T05028; AtNIP2;l, T02327; AtNIP3;1, NP_174472; AtNIP4;1, BAB10360; AtNIP4;2, BAB10361; AtNIP5;1, T04053; AtNIP6;1, AAF14664; and AtNIP7;1, AAF30303. The accession number for soybean (*Glycine max*) nodulin-26 is CAA28471. The accession numbers for ApAQP1 and ApAQP2 are XP_001952020 and XP_001952198, respectively

Three-dimensional model building was performed using the MOE homology modeling program (Kelly, 1996) based on a segment matching procedure (Levitt, 1992) and a best intermediate algorithm with the option to refine each individual structure was enabled. A database of 10 structures was generated, and each structure was individually refined to a root mean squared (RMS) gradient of 1 angstrom.

The stereochemical quality of the models was assessed by using Ramachandran plot analysis and by using the Protein Report structural analysis function in the MOE Protein Structure Evaluation package. This program searches for disallowed bond angles, bond lengths, and side-chain rotamers. In all cases, the models had one or fewer residues in the disallowed region of the Ramachandran plot, and these residues were present in putative loop regions that do not contribute to the formation of the MIP pore. Homology models were further analyzed by superposition of each intermediate model onto the experimental structure of AQP1 to determine which models had the smallest RMS deviation from the experimental template. The model that best-suited all of these criteria was selected for further analysis.

The pore-forming regions of various MIP homology models were analyzed with the HOLE program (Smart et al., 1993), which uses a simulated annealing algorithm to find the optimal trajectory of a sphere with a variable radius through the pore of a protein. The AMBER van der Waals radius file was used during the run. Both a vector and initial point in the channel must be specified to start the program. An initial vector of <0, 0, 1> was used because the pore of each model was oriented along the z-axis. To determine an initial point in the channel, coordinates were taken from NPA as well as ar/R residues and averaged to produce a point between these regions in three-dimensional space. The output file was imaged on a Silicon Graphics workstation (Mountain View, CA) with the InsightII software (Biosym, San Diego).

Sequence alignment and phylogenetic analysis

The protein database at NCBI (*http://www.ncbi.nlm.nih.gov*) was screened for major intrinsic protein sequences by using the search term "aquaporin". This search recovered 2550 that were used to generate a phylogenetic tree using the Tree tool at the NCBI site (Figure 2.3). Sequences were recovered from 1791 eukaryotic genes or cDNAs representing animals (91 species), plants (100 species), fungi (26 species), and protozoa (15 species). In addition, 686 sequences were obtained from 345 species of bacteria. The sequences were downloaded as protein sequence files using the EditSeq program of the DNAstar Lasergene 8 software. Redundant sequences were eliminated from the database by performing sequence alignments of all amino acid sequences from the same organism in batches of 20 sequences and determining their percent amino acid identity.

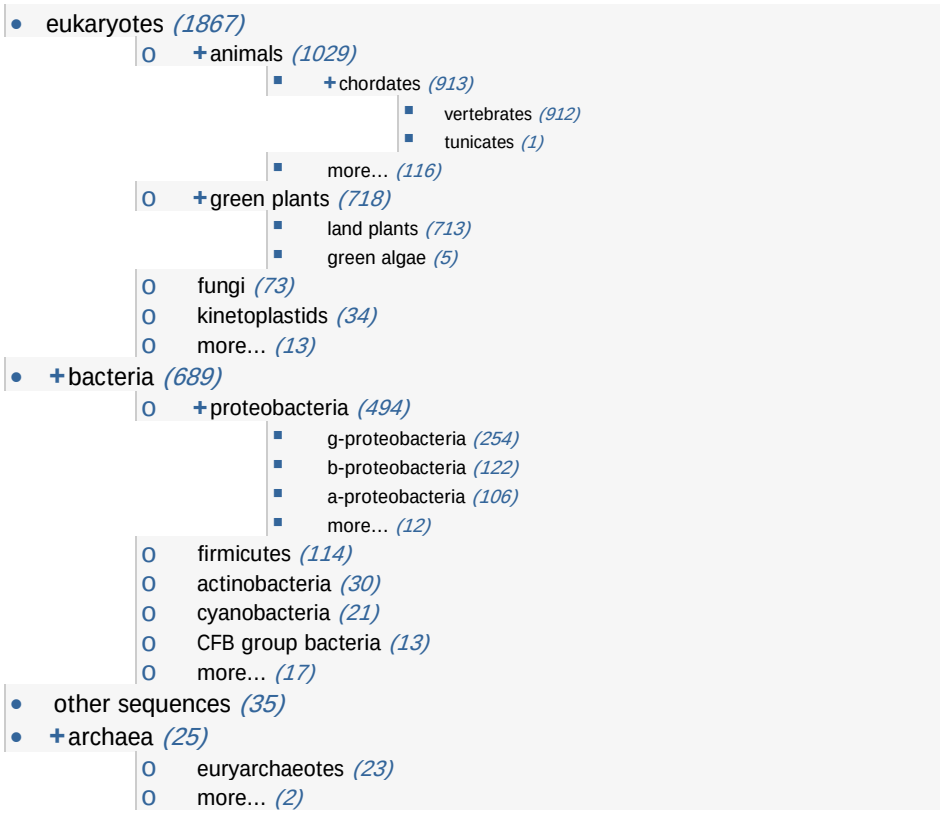

Figure 2.3: MIP sequences used for phylogenetic analysis: Tree of sequences from aquaporin search at the National Center for Biotechnology Information (NCBI) Protein Website. The webaddress for this search is: http://www.ncbi.nlm.nih.gov/sites/entrez?db=protein&cmd=historysearch&querykey=1.

Any sequences from the same organism that were 100 % identical to a previous sequence were discarded. The database of protein sequences was aligned using the Clustal W alignment algorithm in the DNAstart MegAlign software package. Ar/R residues for each sequence in the database were assigned by alignment with sequences of known structure (AQP1, SoPIP2, and AqpM), and these sequences were grouped according to their exact ar/R sequence. These groups were used to calculate the frequency of each amino acid at the different ar/R region positions. To simplify the data, the amino acids were grouped based on their similar chemical and structural properties as follows: small hydrophilic (Ala, Cys, Gly, Ser, Thr), aromatic (Trp, Phe, Tyr), hydrophobic (Leu, Met), β-branched hydrophobic (Ile, Val), and hydrophilix (Asn, Gln). His, Lys, Arg, and Pro were considered individually.

Ar/R "interconversion" was defined as any group of ar/R amino acids that can be interconverted to a second group of ar/R amino acids observed in the sequence dataset by a single substitution. The number of interconversions was determined at each ar/R position by systematically comparing each ar/R region to all others in the dataset to find ar/R amino acids that satisfied these criteria. A substitution was defined as conservative if the new amino acid was in the same structural subgroup or nonconservative if the new amino acid was in a different structural subgroup.

Chapter III

Results

Homology modeling of plant MIP pore regions

Homology modeling as a useful MIP structure prediction tool

The available crystal structures of multiple MIPs indicate that these proteins possess a highly conserved three-dimensional protein fold (Fu et al., 2000; Sui et al., 2001; Harries et al., 2004; Tornroth-Horsefield et al., 2006), suggesting that they may be particularly suited to structure prediction techniques such as homology modeling. Homology modeling is a sequence-based structure prediction algorithm that uses the experimentally determined structure of a protein (template) to predict the structure of homologous proteins with no available structural data (targets). The precision of the final model is dependent upon the accuracy of the initial sequence alignment used to model the target protein (Xu et al., 2000), but highly conserved regions of the protein can be used to generate accurate sequence alignments even in cases of low overall sequence identity. To investigate the possibility that homology modeling is a suitable technique for the prediction of MIP structure, the homology modeling algorithm was applied to MIP sequences of known structure and the resulting models were compared to the corresponding experimentally determined structures.

In addition to AQP1, AQP0, and GlpF, x-ray crystal structures are available for Spinach PIP2 (SoPIP2; Tornroth-Horsefield et al., 2006), *Escherichia coli* AqpZ

(Savage et al., 2003), and *Methanothermobacter marburgensis* AqpM (Lee et al., 2005). To determine the fidelity of the homology modeling approach the sequences of these proteins were used as homology modeling targets and bovine AQP1 (1J4N; Sui et al., 2001) was used as a modeling template. The Molecular Operating Environment (MOE) software was used to generate these homology models. The MOE homology modeling algorithm generated ten individually energy minimized structures that were superimposed on the initial AQP1 template, and the structure with the lowest root mean squared (RMS) deviation from the template, was chosen for further analysis.

To test the accuracy of the MOE homology modeling algorithm for the prediction of MIP structures, the best homology model structures of SoPIP2, AqpZ, and AqpM were generated and were superimposed on their respective x-ray structures. Figure **3.1** shows the results of this experiment. The homology models of AqpM, AqpZ, and SoPIP2 showed excellent agreement in the overall MIP fold when superimposed on their respective x-ray crystal structures (Figure **3.1A**) with an RMS deviation of less than 4 angstroms between the homology model and experimental structure. When the amino acid sequence identity of each target protein and the AQP1 template was plotted against the homology model RMS deviation from the experimental template over the entire protein, a linear relationship was observed over a wide range of amino acid sequence identity (Figure **3.1B**). When only the C_α carbons of the pore-forming ar/R and NPA residues are superimposed, the RMS deviation of these regions in all structures was less than 1 angstrom from the experimental template, and less than 2 angstroms when all atoms of these residues

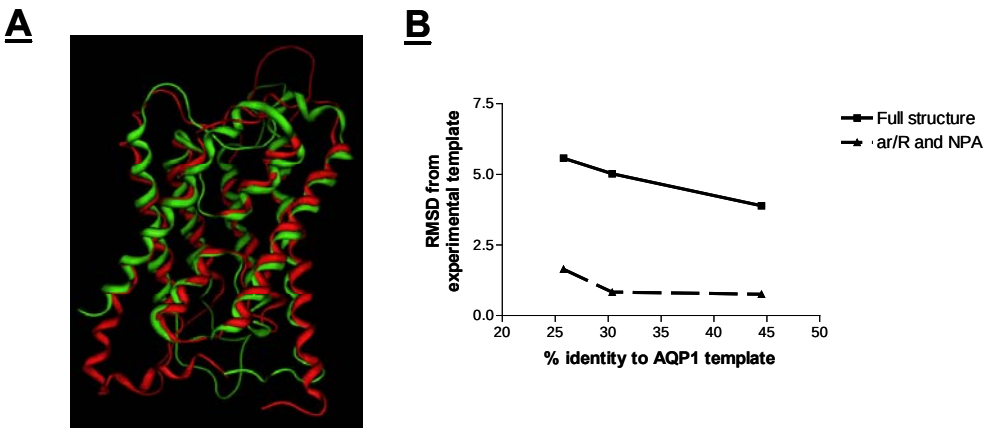

Figure 3.1: Homology modeling analysis control experiments with test MIP structures: **A.** A homology model of SoPIP2 was generated using the MOE software and the X-ray crystal structure of bovine AQP1 (PDB ID: 1J4N) as a template. The resulting model was superimposed onto the experimental structure of SoPIP2 (PDB ID: 2B5F). The SoPIP2 homology model is shown in red and the experimental structure is shown in green. **B.** Homology models of SoPIP2, AqpM, and AqpZ were generated using MOE software and the x-ray crystal structure of bovine AQP1 as a template. Each homology model was superimposed onto the respective experimental structure (PDB IDs: SoPIP2 open- 2B5F; *E. coli* AqpZ- 2ABM; *M. marburgensis* AqpM- 2F2B), and the RMS deviation of the peptide backbone C_α carbons from the full model (bold line) as well as the ar/R and NPA residues (dashed line) were plotted against the % amino acid identity of each sequence to the AQP1 template.

were considered. Structural analysis of the superimposed homology model-experimental structure pairs demonstrates that the majority of the structural deviation occurs in the loop regions between α-helices. These secondary structural elements are generally less conserved in MIPs and are not involved in pore formation, with the exception of loops B and E. These results suggest that homology modeling can be used to accurately model the pore-forming regions of MIPs.

Nodulin-26 as a homology modeling test case

The functional properties of nodulin-26 have been extensively biochemically as well as biophysically characterized, and the details of substrate selectivity as well as single channel permeability rates are available (Rivers et al., 1997; Dean et al., 1999). For these reasons, this protein was chosen as the first candidate for a homology modeling case study. To generate the homology model, the amino acid sequence of nodulin-26 was aligned with the bovine AQP1 template and homology modeling was performed.

Superposition of the nodulin-26 homology model on the AQP1 template indicates that the transmembrane domains of these protein structures show excellent alignment, with an overall RMS deviation of less than 1 angstrom (Figure **3.2**). A more detailed analysis of the nodulin-26 ar/R region indicates that this protein contains a Trp residue at H2, Val at H5, Ala at LE_1 and an Arg at LE_2 (Figure **3.3**). The Trp and Arg residues of the nodulin-26 ar/R region are similar to the analogous residues in the GlpF ar/R region. The presence of a Val at the nodulin-26 H5 position compared to His in AQP1 suggests that this substitution will result in an apparent widening of the pore and will remove a potential hydrogen bonding acceptor, while

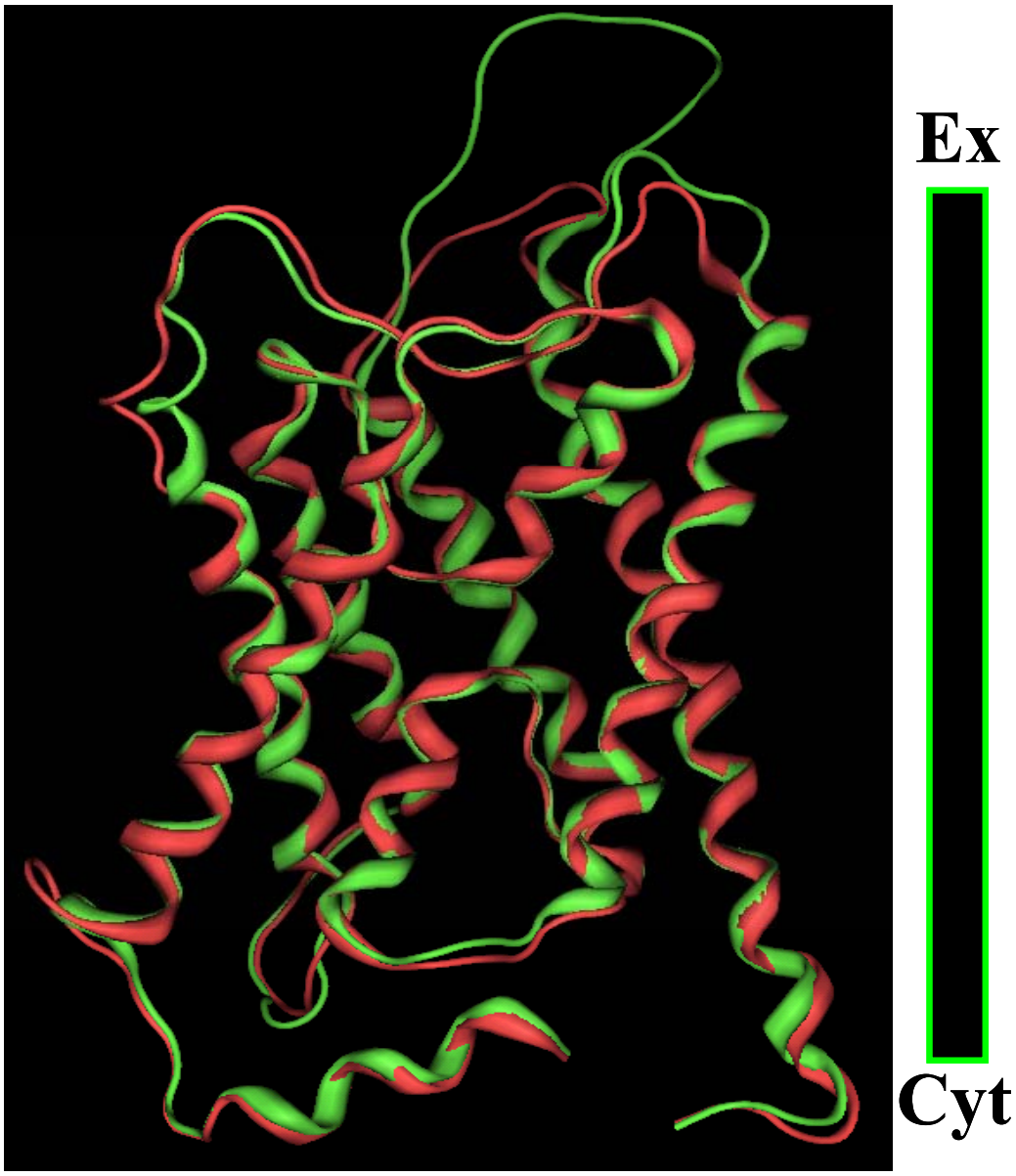

Figure 3.2: Nodulin-26 homology modeling analysis: A homology model of nodulin-26 was generated using MOE software and the x-ray crystal structure of bovine AQP1 (PDB ID: 1J4N) as a template. The backbone ribbons of nodulin-26 (red) superimposed on bovine AQP1 (green) are shown with the position of the extracellular and cytosolic compartments indicated to the right of the figure.

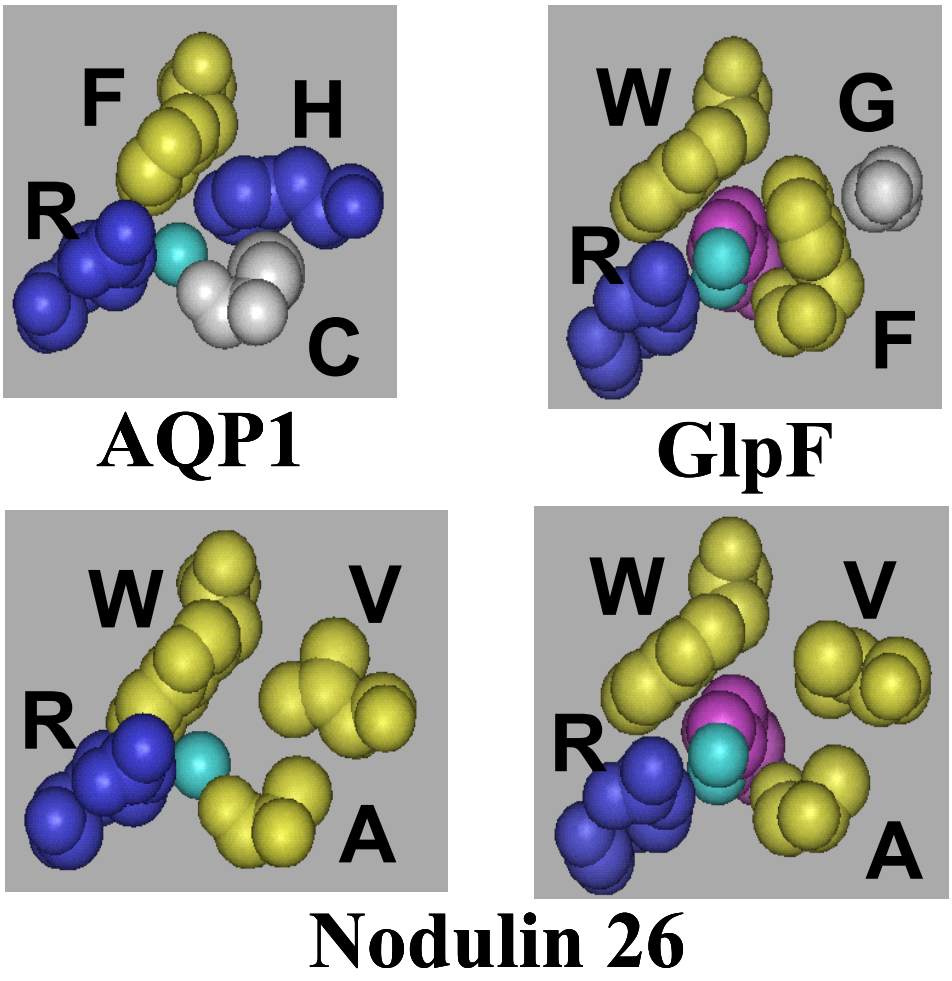

Figure 3.3: Structural comparison of the AQP1, GlpF, and nodulin-26 ar/R regions: The ar/R regions of bovine AQP1, *E. coli* GlpF, and a soybean nodulin 26 homology model are shown viewed down the pore from the extracellular side of the membrane. The ar/R positions are H2, H5, LE_1, and LE_2 starting from the top left and moving clockwise. The amino acid residues of the ar/R region are indicated with their single letter designations and are colored according to the following scheme: blue-basic, yellow-hydrophobic, white-small hydrophilic. A co-crystallized water molecule in the AQP1 ar/R region is shown as an aqua sphere. The methylene backbone of the GlpF ar/R glycerol molecule is colored magenta while the hydroxyl groups are aqua. The absolute coordinates of each of these substrates were superposed into the ar/R regions of the nodulin-26 homology model.

simultaneously increasing the hydrophobicity of the channel. These observations suggest that, similar to GlpF, the nodulin-26 ar/R has the amphipathic properties as well as the larger pore diameter necessary to accommodate transport of glycerol. Conversely, the nodulin-26 ar/R lacks crucial hydrogen bonding ar/R residues (e.g. His at H5 in AQP1) necessary for rapid water transport.

Detailed functional analysis of nodulin-26 water permeability are in agreement with the functional predictions made by homology modeling. Water permeability measurements of nodulin-26 indicate that this protein is a water channel, but its unitary water conductance rate (p_f) is 30-fold lower than the corresponding value for AQP1 (Table **3.1**; Zeidel et al., 1992; Dean et al., 1999). To further investigate these water permeability discrepancies, transition state analysis of water transport was performed to investigate the thermodynamic properties of the pores of these channels.

Molecular dynamics simulations have demonstrated that the passage of water through the ar/R region is the rate-limiting transition state for water flux in AQP1 (de Groot and Grubmuller, 2001), so the differences in unitary conductance rate between nodulin-26 and AQP1 are proposed to result from amino acid differences at the ar/R region. The enthalpy, entropy, and free energy of the transition state for water transport are related to the activation energy and the osmotic permeability coefficient (P_f) (Sogami et al., 2001). Water permeability and activation energy measurements for water transport through nodulin-26, AQP1, and bare lipid bilayers were used to calculate the thermodynamic parameters of the transition state of water transport, and these results are presented in Table **3.1**.

Table 3.1: Water transport transition state analysis for nodulin-26 and AQP1

Membrane[a]	E_a (kJ/mol)[b]	$\Delta H^{\ddagger}$ (kJ/mol)[c]	$\Delta S^{\ddagger}$ (e.u.)	p_f (cm^3/s)[d]
Control liposomes	61.9	59.4	24.1	
AQP1 proteoliposomes	9.20	6.65	-19.6	11.4×10^{-14}
Nodulin-26 proteoliposomes	17.0	14.6	-17.5	0.38×10^{-14}

[a]Nodulin-26 reconstitution experiments were performed in Dean et al. (1999). The AQP1 proteoliposome data was taken from van Hoek et al. (1992).

[b]Activation energies were calculated from Arrhenius plots as in Dean et al. (1999).

[c] The $\Delta H^{\ddagger}$ and $\Delta S^{\ddagger}$ for water transport were calculated by the approach described in Sogami et al. (2001).

[d] The unitary water conductance rate for AQP1 as well as nodulin-26 were calculated in Zeidel et al. (1992) and Dean et al. (1999), respectively.

The results demonstrate that MIP-mediated water transport differs from water transport through a lipid bilayer in several respects. First, MIP-mediated water transport shows a highly negative $\Delta S^{\ddagger}$ suggesting that water molecules traversing the MIP pore are highly organized. Second, the $\Delta H^{\ddagger}$ for water transport through MIPs is much lower than the corresponding value for a bare lipid bilayer, indicating that water-transporting MIPs provide protein contacts at the ar/R region that compensate for the dehydration of transported water molecules. Interestingly, the AQP1 and nodulin-26 $\Delta H^{\ddagger}$ for water transport differs by the energy of approximately one hydrogen bond. This difference is predicted by the His to Val substitution at the ar/R H5 position elucidated in the previous homology modeling experiments.

Homology modeling of the Arabidopsis MIPs and Classification based on the ar/R region

Phylogenetic analyses of plant MIPs suggested that these proteins are diverse and can be divided into four subfamilies based on amino acid sequence alone. To investigate whether this phylogenetic diversity is reflected in diversity of the ar/R region and possibly channel function, homology models were generated for all 35 MIP family members of the model genetic organism *Arabidopsis thaliana* using the AQP1 experimental structure as a template (Table **3.2**). In conjunction with published functional analysis experiments for these channels, these models were used to classify the Arabidopsis MIPs into 8 subfamilies based on their ar/R region characteristics (Table **3.3**). The results of these experiments suggest that the ar/R regions of plant MIPs are much more structurally diverse than their animal and

Table 3.2 Conserved ar/R signatures of Arabidopsis MIPs

ar/R[a] subgroup	Helix 2[b]	Helix 5	Loop E_1	Loop E_2	rms deviation[c] Å
PIP	F	H	T	R	0.91
TIP					
Group I	H	I	A	V	0.67
Group IIA	H	I	G	R	1.03
Group IIB	H	I	A	R	0.72
Group III	N	V	G	C	1.56[d]
NIP					
Group I	W	I, V	A	R	0.92
Group II	A	I, V	A or G	R	0.97
SIP					
Group I	T	F, V, I[e]	P	I	1.39
Group II	S	H	G	A	1.86

[a] The bold designations represent each of the subfamilies of plant MIPs as described in (Quigley et al., 2001; Johanson et al., 2001). Under each heading ar/R subcategories are listed based on the representative member of each subfamily.

[b] The conserved consensus residue at each position of the ar/R tetrad based on sequence alignment and homology modeling is listed.

[c] The root mean square deviation of the α-carbon backbone of the homology model of the indicated MIP from the backbone of the AQP1 template is listed. Similar homology modeling results were obtained with GlpF (rmsd 1.5 to 2 Å, data not shown).

[d]The TIP5;1 homology model shows a shorter α-helix 1(21 residues) compared to the AQP template

Table 3.3: Distribution of specific *Arabidopsis thaliana* MIP gene products among the eight ar/R subcategories

ar/R subgroup[a]	Members in *A. thaliana*[b]
PIP	PIP1;1 1;2 1;3 1;4 1;5 PIP2:1 2:2 2;3 2;4 2;5 2;6 2;7 2;8
TIP Group I	TIP1;1, TIP1;2, TIP1;3
TIP Group II	TIP2;1 TIP2;2, TIP2;3 TIP3;1 TIP3;2 TIP4;1
TIP Group III	TIP5;1
NIP Group I (nodulin 26-like)	NIP1;1, NIP1;2, NIP2;1, NIP3;1, NIP4;1, NIP4;2,
NIP Group II	NIP5;1 NIP6;1 NIP7;1
SIP Group I	SIP1;1, SIP1;2
SIP Group II	SIP2;1

[a]Each of the eight ar/R subgroups based on sequence alignment and homology modeling are listed.

[b]Members of each ar/R subgroup in *Arabidopsis thaliana* based on the nomenclature of Quigley et al., (2001) and Johanson et al. (2001).

microbial counterparts, and that these plant MIPs may have evolved new functions by conserving the MIP fold while altering key pore selectivity regions. The eight ar/R subfamilies of Arabidopsis are individually discussed in detail below.

The Plasma Membrane Intrinsic Proteins

Sequence alignment and phylogenetic analysis indicate that the PIP family is the largest MIP subgroup in Arabidopsis (Johanson et al., 2001; Quigley et al., 2001) as well as in rice and corn (Chaumont et al., 2001; Sakurai et al., 2005). Homology modeling and structural analysis of all 13 Arabidopsis PIP isoforms (Table **3.2**) indicate that these proteins are homogenous with respect to their ar/R region amino acids and contain a Phe residue at H2, a His at H5, a Thr at LE_1, and an Arg at LE_2 (Figure **3.4B**). The PIP and AQP1 ar/R regions are very similar and differ by only a single substitution of Thr at the LE_1 position in PIPs to Cys in AQP1. This substitution is not likely to affect water transport because the peptide backbone carbonyl is suggested to act as a hydrogen bond acceptor at this position, and several functionally characterized mammalian as well as microbial aquaporins contain residue substitutions at this position (Jung et al., 1994). Therefore, homology modeling suggests that PIP isoforms contain all the structural determinants necessary to perform water-selective transport.

The Tonoplast Intrinsic Proteins

The TIP family is the second largest MIP subfamily in Arabidopsis, with 10 full-length sequences present in the genome (Quigley et al., 2001). Homology modeling analysis indicates that the TIP subfamily is highly diverse with respect to

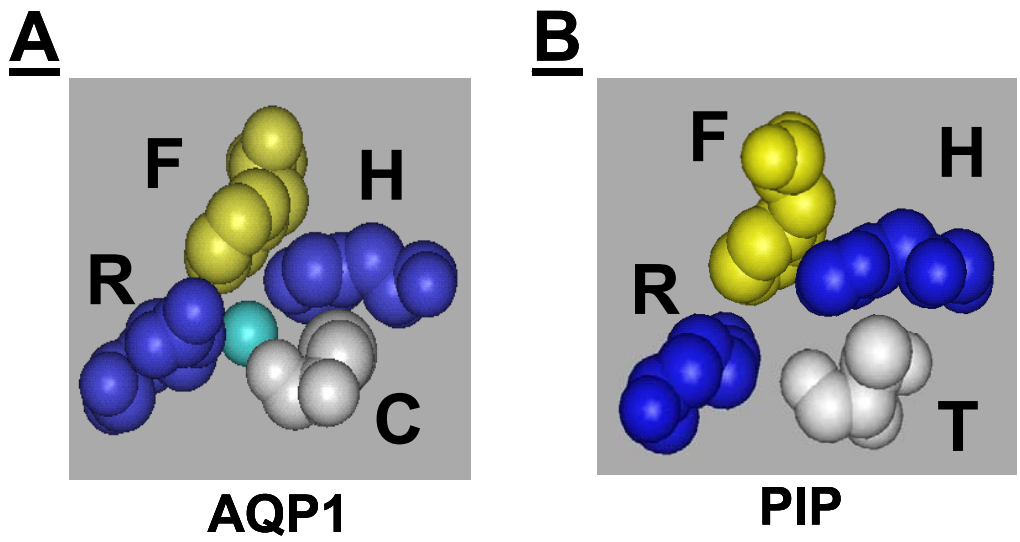

Figure 3.4: Structural comparison of the AQP1 and PIP family ar/R regions: The structure of the AQP1 **(A)** and PIP subfamily **(B)** ar/R regions are shown with their H2, H5, LE_1 and LE_2 amino acid residues indicated by single letter designations. The residues proceed starting at the top left with H2 and moving clockwise. The amino acids are color coded as follows: yellow-hydrophobic, blue-basic, white-small hydrophilic. The position of a water molecule crystallized in the AQP1 ar/R is shown with water represented as an aqua sphere.

the the ar/R region, and that these proteins can be classified into three groups (Table **3.3**) based on their ar/R amino acids: TIP subgroup I, TIP subgroup IIA and IIB, and TIP subgroup III.

All members of the TIP ar/R subgroups I and II contain a His residue at H2, an Ile/ Val at H5, and the orientation of these residues results in the exact opposite pattern of hydrophobic and hydrophilic amino acids present the in AQP1 ar/R (Figure **3.5A-C**). TIP subgroup IIA and IIB are distinguished by the presence of either an Ala (Group IIA) or Gly (Group IIB) at the LE_1 position of the ar/R. These substitutions are unusual compared to the APQ1 structural paradigm, however HOLE analysis indicates that the pore diameter of TIP3;1 is similar to AQP1 at the ar/R region (Figure **3.6C**), suggesting that this region is still the major constriction of the pore. The main difference between TIP subgroups I and II occurs at LE_2 where TIP subgroup I members have a Val substitution in place of the highly conserved Arg residue in TIP subgroup II members that normally occurs at this position (Figure **3.5B**). Arabidopsis TIP5;1 is the sole member of TIP subgroup III, and this protein possesses a completely novel ar/R region, with an Asn residue at H2, a Val at H5, a small flexible Gly at LE_1, and a Cys residue replacing the highly conserved Arg at LE_2 (Figure **3.5E**). The homology model of TIP5;1 indicates that these unusual ar/R residues form a much wider pore with a reduced capacity to form hydrogen bonds compared to AQP1. HOLE analysis of the TIP5;1 homology model indicates that these residue substitutions result in a pore that is wider than that of AQP1, as well as other members of the TIP subfamily (Figure **3.6B**) These results suggest that TIP5;1 may transport solutes that are not conventionally permeable to other MIP channels.

Figure 3.5: Structural comparisons of TIP subgroup ar/R regions to AQP1: The structure of the AQP1 **(A)**, TIP subgroup I **(B)**, TIP subgroup IIA **(C)**, TIP subgroup IIB **(D)**, and TIP subgroup III **(E)** ar/R regions are shown. The amino acids at the H2, H5, LE_1 and LE_2 positions of the ar/R region are indicated with their single letter amino acid designations. The residues are oriented with the H2 position at the top of each panel, and the other residues of the ar/R region proceeding clockwise. The amino acid residues are colored according to the following color scheme: yellow-hydrophobic, blue-basic, white-small hydrophilic

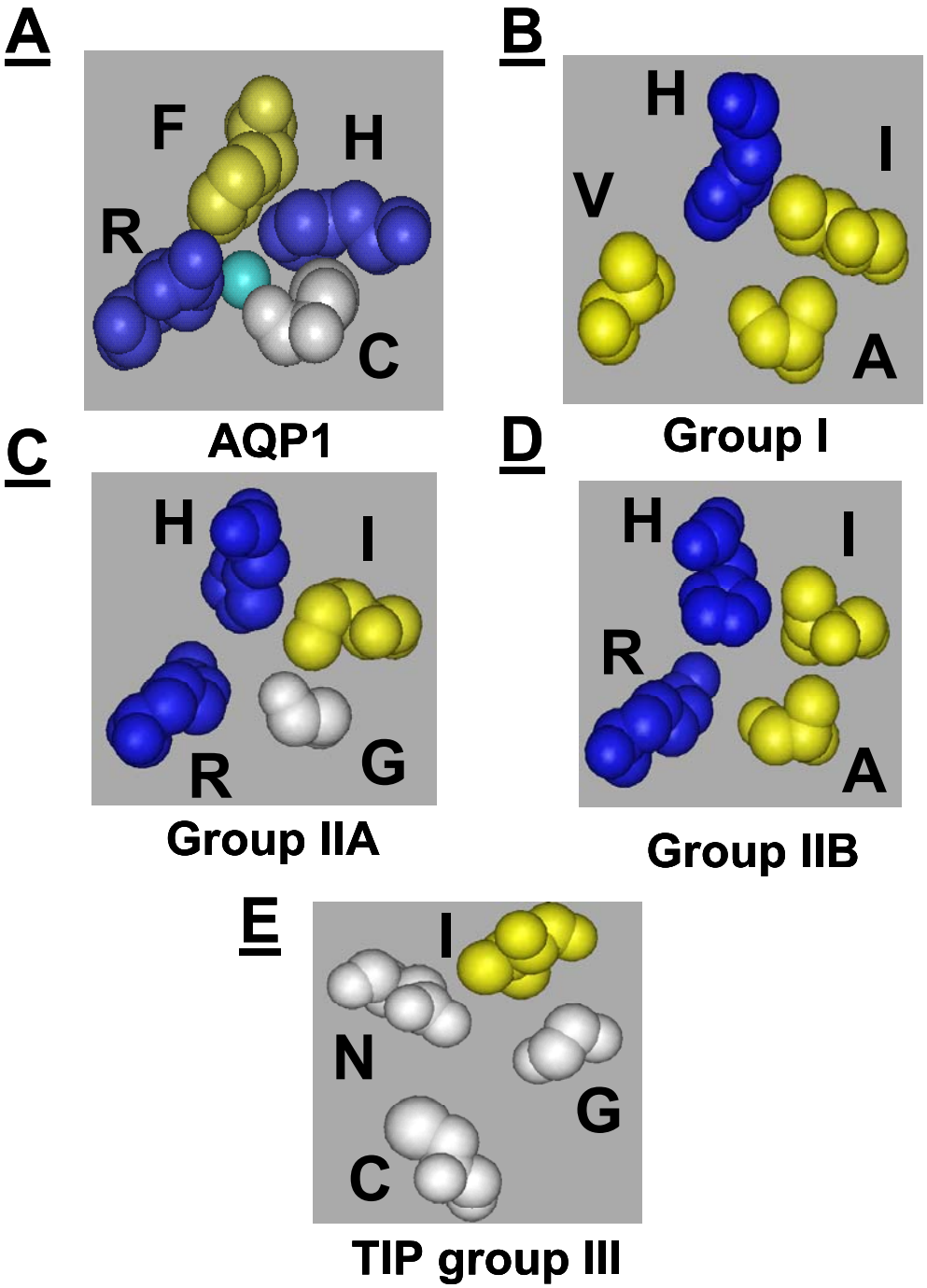
A
F
H
R
C
AQP1
B
H
I
V
A
Group I
C
H
I
R
G
Group IIA
D
H
I
R
A
Group IIB
E
I
N
G
C
TIP group III

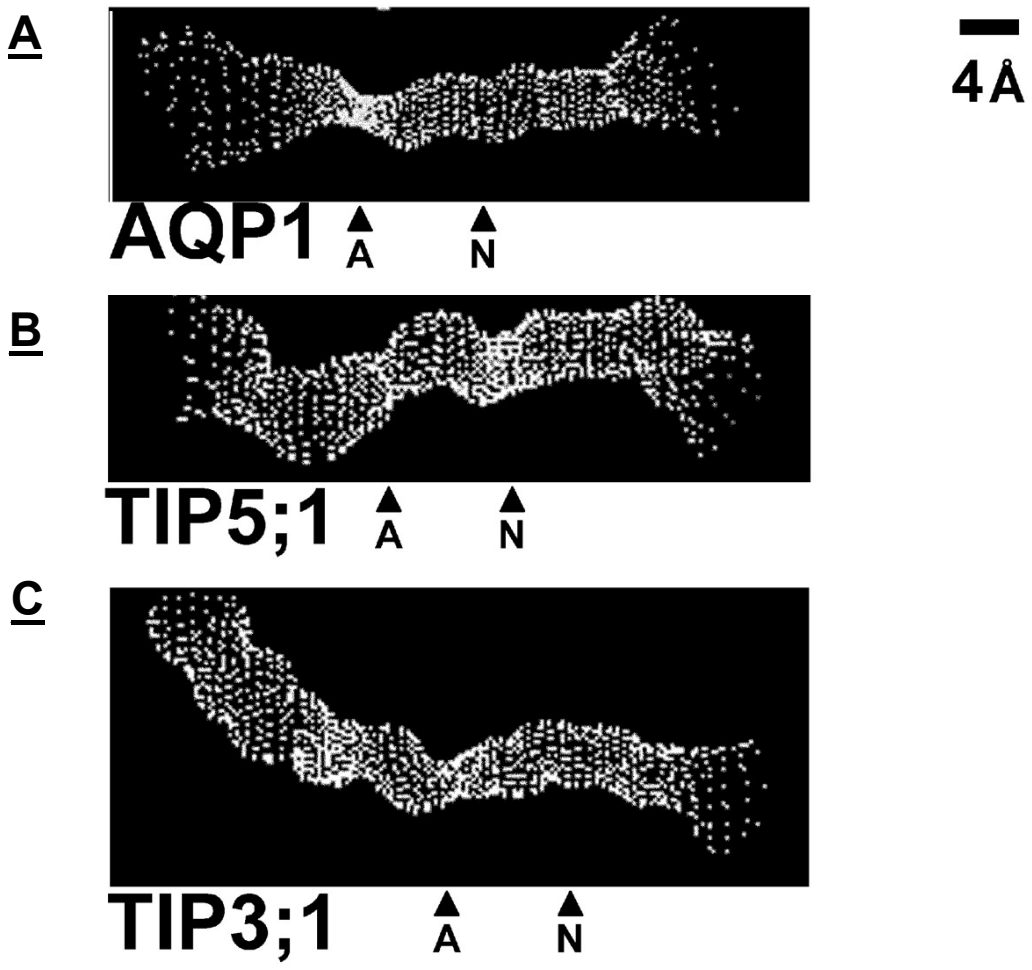

Figure 3.6: HOLE analysis of TIP subfamily members: HOLE computational analysis (Smart et al., 1993) was used to determine the pore diameter of the AQP1 experimental structure (**A**) as well as the diameters of the TIP5;1 (**B**) and TIP3;1 (**C**) homology models. The white mesh diagram indicates the pore diameter along the z-axis of the channel. The positions of the ar/R (A) and NPA (N) regions are indicated at the bottom of each figure. A size bar of 4 angstroms is shown for reference.

The Small basic Intrinsic Proteins

Unlike other Arabidopsis MIPs, the homology modeling of SIP subfamily members is difficult because these proteins share only 15% amino acid identity with the AQP1 template. However, elements of the pore surrounding the ar/R and NPA regions of these proteins are conserved, allowing alignment constraints to be imposed that resulted in homology models showing less than 2 angstroms of RMS deviation from the AQP1 template (Table **3.2**).

Analysis of the putative SIP ar/R regions suggests that these proteins can be classified into two subgroups based on their ar/R amino acids (SIP subgroup I and II). SIP subgroup I contains two members in Arabidopsis (SIP1;1 and SIP1;2) while SIP subgroup II contains a single member (SIP2;1). SIP subgroup I members contain a hydrophobic amino acid at H5 (Val in SIP1;1 and Phe in SIP1;2) similar to the aliphatic amino acids observed in TIPs, but the remaining ar/R amino acids are unique. SIP subgroup I ar/R regions typically contain a hydrophilic Thr residue at H2, a conserved Pro at LE_1, and an Ile at LE_2 (Figure **3.7A**), resulting in a putative ar/R region that is much more hydrophobic compared to AQP1. In contrast, the ar/R region of SIP subgroup II is highly hydrophilic, with a Ser residue at H2, a His at H5, a Gly at LE_1, and an Ala at LE_2 (Figure **3.7B**).

The Nodulin-26 like Intrinsic Proteins

The Arabidopsis genome contains nine full-length NIP family members, and homology modeling analysis indicates that these proteins can be divided into two ar/R subgroups (NIP subgroup I and II) differing mainly at the ar/R H2 position.

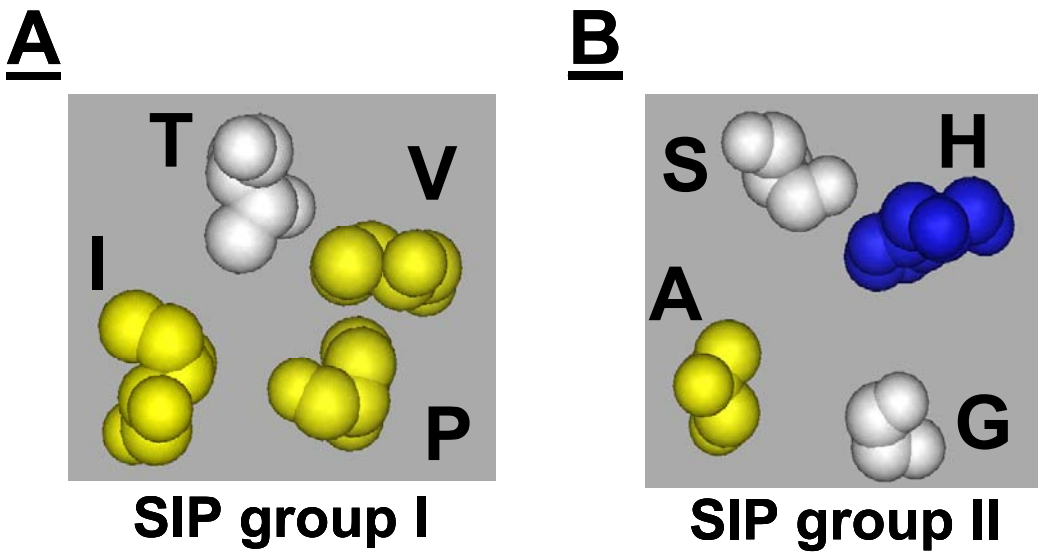

Figure 3.7: Structure of the SIP family ar/R regions: The structure of the SIP subgroup I **(A)** and SIP subgroup II **(B)** ar/R regions are shown with single letter amino acid code indicating each amino acid. The H2, H5, LE_1 and LE_2 positions start from the top with the H2 residue and proceed clockwise. The amino acid residues are colored according to the following scheme: yellow-hydrophobic, blue-basic, white-small hydrophilic.

NIP subgroup I and II contain similar amino acids to TIP subgroup II throughout most of the ar/R region, including a Val or Ile at H5, an Ala residue at LE_1, and the highly conserved Arg residue at LE_2 (Figure **3.8A**). The single nonconservative substitution that discriminates these subgroups occurs at the H2 position. NIP subgroup I members, including nodulin-26, contain a large Trp residue at the H2 position, while NIP subgroup II members contain a small Ala residue (Figure **3.8A** and **B**).

Further structural analysis of representative NIP subgroup I (nodulin 26) and NIP subgroup II (NIP6;1) members using HOLE (Smart et al., 1993) indicates that these proteins have markedly different pore apertures (Figure **3.8C** and **D**). The nodulin-26 homology model has a predicted minimum pore aperture of about 2.5 angstroms at the ar/R region, while NIP6;1 has a predicted pore that is roughly two times wider. This larger pore aperture is due to the much smaller Ala residue at the ar/R H2 position in NIP subgroup II members and would presumably allow NIP6;1 to transport much larger solutes than NIP subgroup I members, suggesting that NIP subgroup I an II are functionally distinct. Details on the functional properties of NIP subgroup I and II is presented in section III below.

Phylogeny of NIP subgroup I and II

To investigate the species distribution and prevalence of NIP subgroup I and II members, the available NIP sequences from a variety of plant species were aligned and compiled into a phylogenetic tree (Figure **3.9**). NIP subgroup I and II members were classified by the amino acids present at their ar/R regions.

Figure 3.8: Structural analysis of the NIP subfamily ar/R regions: The structure of the NIP subgroup I **(A)** and NIP subgroup II **(B)** ar/R regions are shown with single letter designations indicating the amino acid residues. The position of the H2, H5, LE_1, and LE_2 ar/R positions are shown starting from the top left of the figure and proceeding clockwise. The amino acids are colored according to the following scheme: yellow-hydrophobic, blue-basic. HOLE computational analysis (Smart et al., 1993) was used to predict the pore diameter of nodulin-26 **(C)** and NIP6;1 **(D)** homology models. The white mesh diagram indicates pore diameter along the channel axis. A size bar of 4 angstroms is shown to the right of the figure for reference. The relative position of the ar/R and NPA residues are also indicated at the bottom of the figure. **E.** The pore diameter values generated from HOLE analysis are plotted against the distance along the z-axis. The blue line indicates pore data for the nodulin-26 homology model, and the black line indicates the values for NIP6;1. The positions of the ar/R and NPA regions are shown.

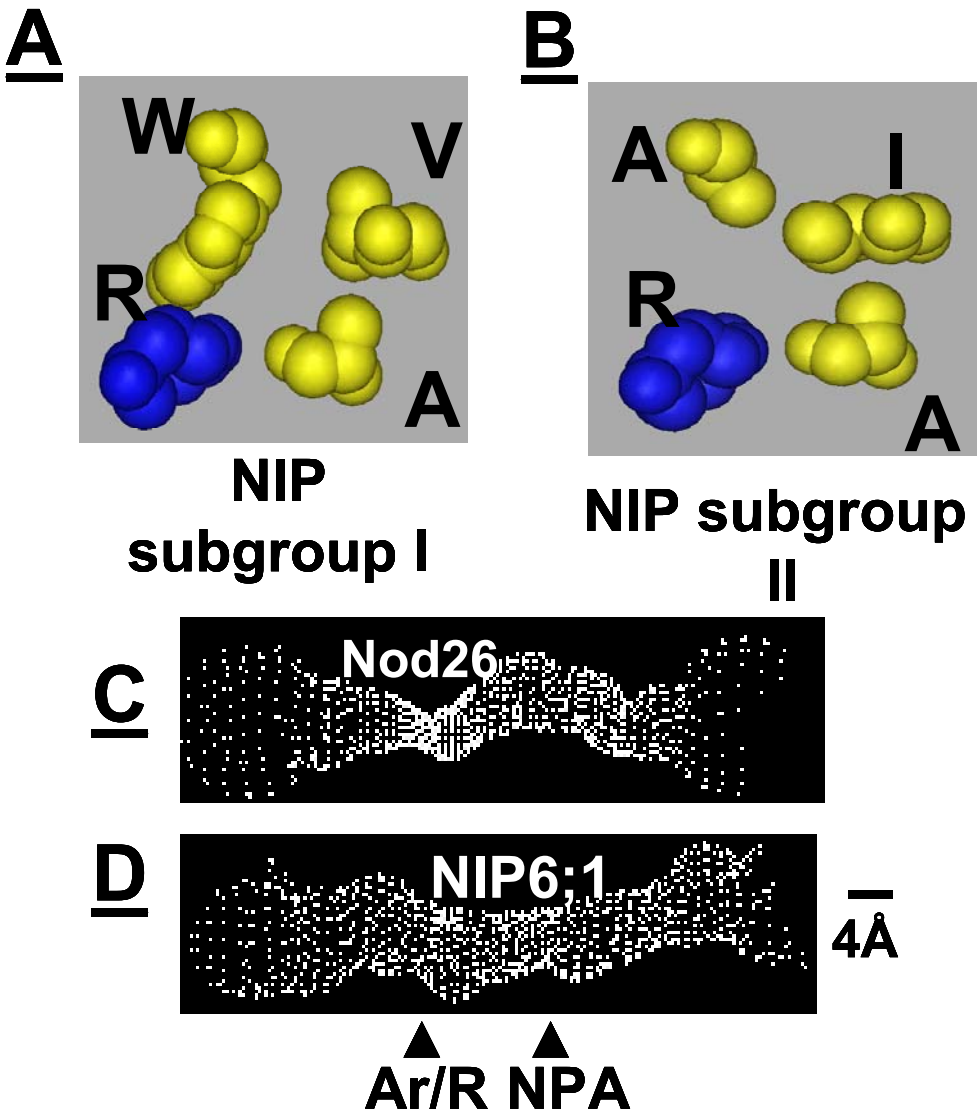
A
W
V
R
A
NIP
subgroup I
B
A
I
R
A
NIP subgroup
II
C
Nod26
D
NIP6;1
4Å
Ar/R
NPA
E
pore diameter (Å)
10.0
7.5
5.0
2.5
0.0
0.0
0.5
1.0
1.5
channel coordinate (z)
ar/R
NPA
Nodulin 26
NIP6;1

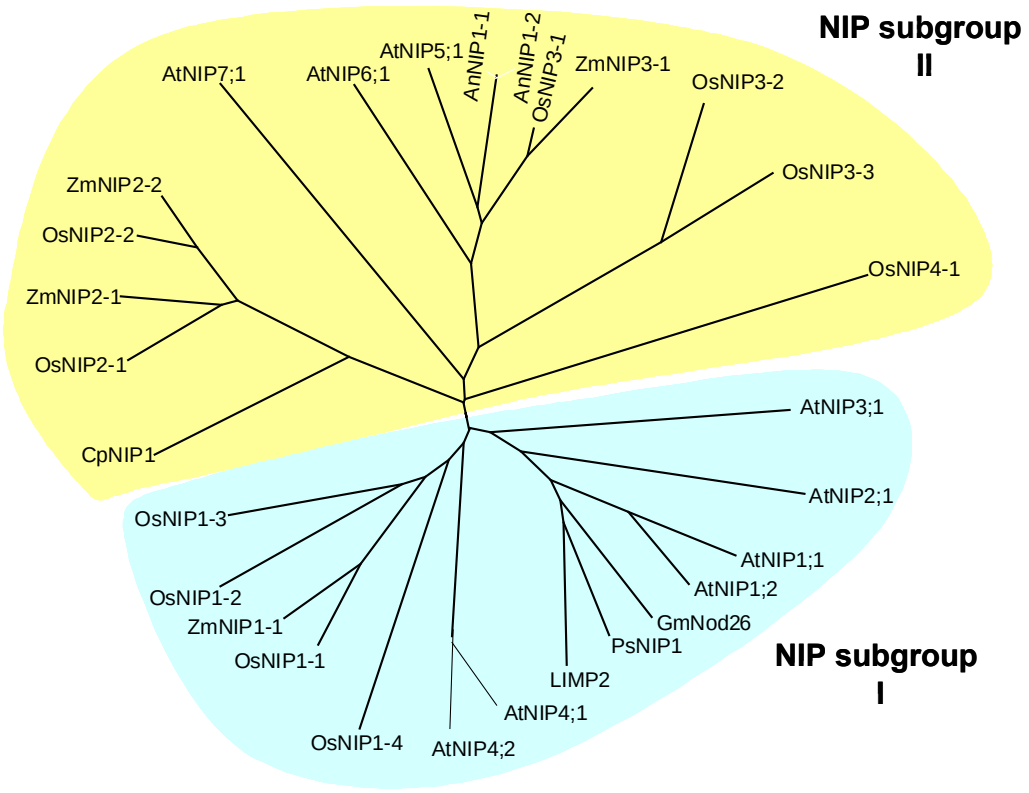

Figure 3.9: Phylogenetic analysis of NIP subgroup I and II: Sequences of NIP subfamily members from rice, corn, Arabidopsis, *Atriplex nummularia*, *Curcubita pepo*, *Lotus japonicus*, and soybean were aligned using Clustal W, and this sequence alignment was used to generate an unrooted dendrogram. The ar/R residues of each sequence were examined in the sequence alignment to assign these proteins into either the NIP subgroup I (blue), or NIP subgroup II (yellow).

The results of this analysis indicate that NIP subgroup I and II members are present in all higher plant genomes examined and that these proteins form separate groups in the phylogenetic tree, suggesting evolutionary divergence. These results also suggest that NIP subgroup I and II are widespread and that these proteins are present in leguminous as well as non-leguminous plants.

Phylogenetic analysis and evolution of the MIP ar/R region

Amino acid distribution of the residues comprising the MIP ar/R region

Due to the importance of the ar/R region in determining MIP substrate selectivity, and considering the unexpected diversity of this motif in higher plants, a massive MIP phylogenetic analysis was performed to investigate the distribution and properties of the ar/R amino acids across the MIP family. One thousand non-redundant amino acid sequences comprising MIPs from animal, plant, bacteria, fungi, as well as protist origins were identified as described in materials in methods and were aligned to examine the distribution of amino acids present at the ar/R region as well as the overall ar/R region diversity.

The amino acid sequences of MIPs in the phylogenetic analysis were aligned with bovine AQP1, Spinach SoPIP2, *E. coli* GlpF, and *Methanothermobacter marburgensis* AqpM using the ClustalW algorithm. Since the structures of these proteins have been observed by X-ray crystallography and their ar/R residues can be accurately assigned in the alignment, they serve as alignment controls to accurately assign the ar/R residues in the test sequences. In addition, the alignment of the two highly conserved NPA motifs was used as a second criterion to determine the

accuracy of the overall alignment. From the resulting alignments, the amino acids comprising the ar/R region of each protein were assigned by comparison with the control sequences above, and these sequences were placed into categories based on their exact ar/R sequence. This analysis identified 92 non-redundant ar/R residue combinations, including a number of ar/R tetrads that are novel and functionally uncharacterized. The sequences were assigned a four-letter designation corresponding to the single letter amino acid code at the H2, H5, LE_1, and LE_2 positions of the ar/R (e.g. FHCR).

To determine the most common combinations of ar/R residues, the dataset of sequences was probed for all ar/R regions that represented a frequency of more than 1% of the total ar/R sequences in the dataset (i.e. 10 sequences). This analysis identified 11 ar/R combinations that constitute 85% of the total sequences analyzed (Figure **3.10**). The FHTR ar/R region, which is characteristic of the plant PIP family, is the most commonly observed ar/R region in the dataset, comprising 51% of the observed amino acid sequences. The related "water-selective" ar/R combinations FHAR, FHCR, and FHSR were also frequently observed, and the total number of sequences bearing these ar/R amino acid combinations constitute 13.1% of the dataset protein sequences. MIPs containing the plant TIP-like ar/R combinations HIAR, HIGR, and HIAV are also highly represented in the phylogenetic analysis, comprising a total of 13.6% of the total sequences. Finally, the aquaglyceroporin-like ar/R regions WVAR, WGYR, and YVPR represent 4.2% of the sequences used in the analysis. These results indicate that certain combinations of ar/R amino acid residues are over-represented in the MIP amino acid sequence database used for this analysis,

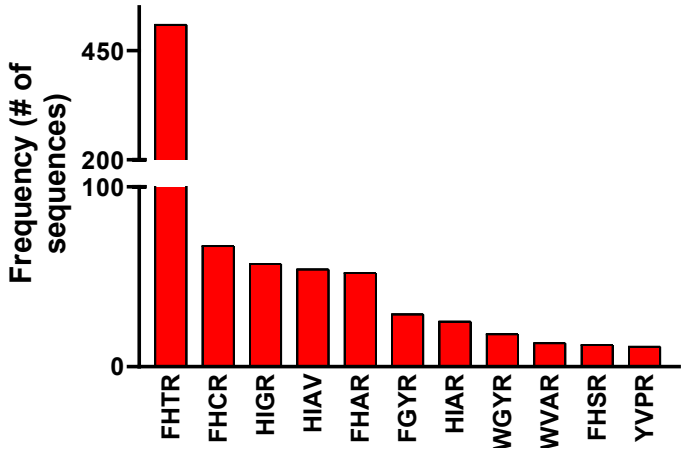

Figure 3.10: Commonly observed ar/R combinations in MIPs: A database of 1000 MIP sequences from GenBank were compiled and aligned with bovine AQP1, SoPIP2, AqpM, and GlpF using the ClustalW alignment algorithm as described in Materials and Methods. The residues comprising the ar/R region were assigned for each sequence based on this alignment and grouped into categories according to the exact ar/R sequence. The frequency of ar/R region groups that represent more than 1% (10 sequences or greater) of the overall dataset are plotted with their ar/R composition represented below. The sequence of letters below each bar represented the single letter code for each amino acid appearing at the ar/R region. The order of positions is helix 2, helix 5, loop E_1, and loop E_2.

and suggest that multiple organisms are under selective pressure to maintain these types of ar/R combinations. These results also suggest that during MIP evolution, selection of particular amino acid residues at each position of the ar/R region occurred, presumably due to the necessary transport functions of these channels. To test this hypothesis, the frequency of each amino acid was observed at all four ar/R region positions, and the results of this analysis are shown in figure **3.11**.

Lys was the only amino acid that was not observed at any position of the 1000 ar/R regions analyzed, but the remaining 19 amino acids show distinct occurrence frequencies at certain positions within the ar/R region. For example, Arg is found exclusively at the LE_2 position of the ar/R region, while His occurs frequently at both the H2 and H5 positions. Both of these amino acids are basic, but their substitution pattern within the ar/R is completely different, suggesting that the structure of each amino acid is uniquely suited to form channels with the substrate selectivity patterns necessary for each protein.

To account for the similar properties of certain residues, the amino acid frequencies were recalculated at each ar/R region position by grouping these residues according to their chemical and structural properties. Each amino acid was grouped into one of the following categories based on the properties of their side chains: small hydrophilic (Ala, Gly, Ser, Cys, Thr), aromatic hydrophobic (Phe, Trp, Tyr), acidic (Asp, Glu), β-branched aliphatic hydrophobic (Ile, Val), unbranched hydrophobic (Leu, Met), and amide (Asn, Gln). The amino acids Arg, Lys, His, as well as Pro were each considered separately because of their unique structural and chemical properties. Figure **3.12** illustrates the results of this analysis.

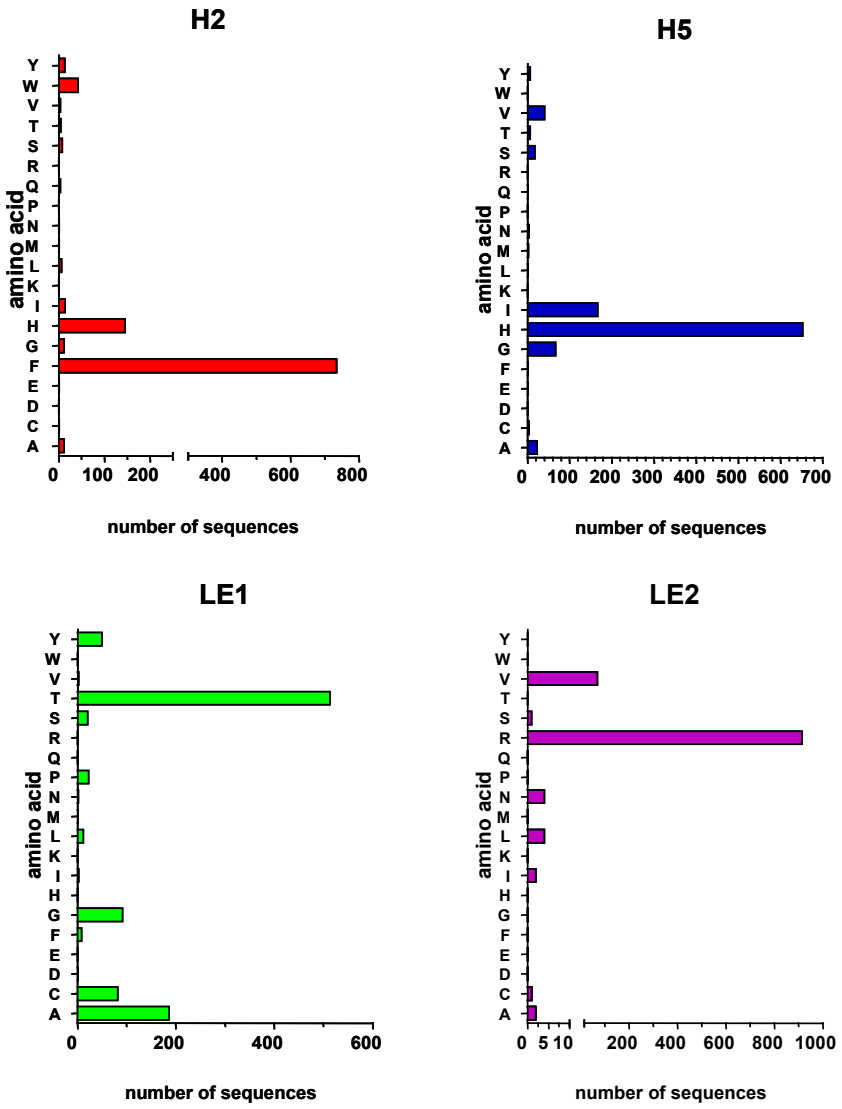

Figure 3.11: Amino acid preferences at each position of the ar/R region: **A.** The frequency of all 20 natural amino acids at each position of the ar/R region was calculated from a dataset of 1000 MIP sequences as described in Materials and Methods. The colored bars represent the frequency at each position of the ar/R according to the following scheme: red; helix 2 position, blue; helix 5 position, green; loop E_1 position, magenta; loop E_2 position.

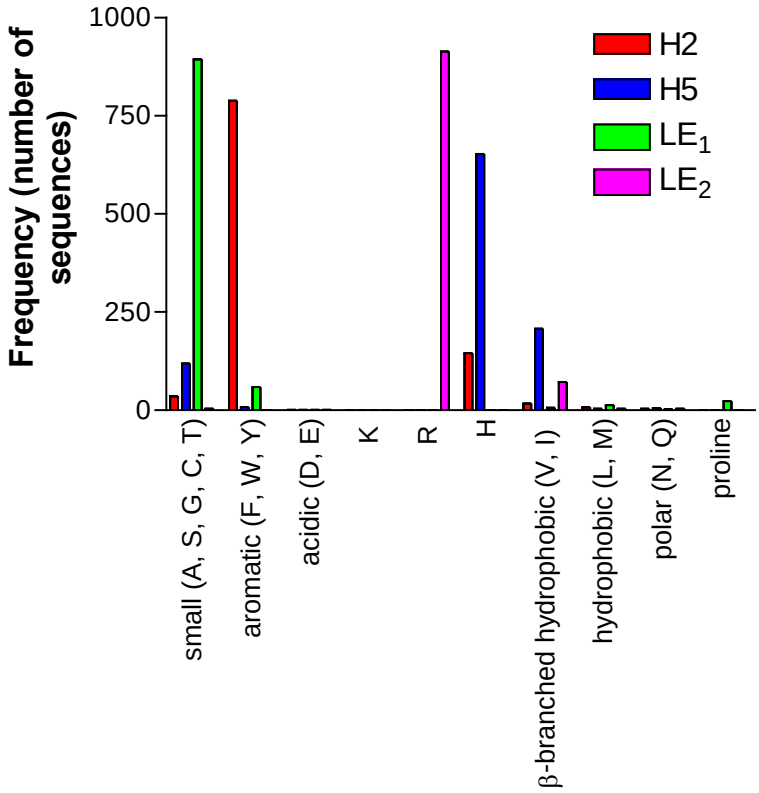

Figure 3.12: Analysis of chemical properties of common amino acids at the ar/R region: The 20 natural amino acids were grouped according to their chemical properties, and the frequency of each amino acid group was calculated for the four positions of the ar/R region from a database of 1000 sequences as described in materials and methods. The small hydrophilic (Ala, Ser, Gly, Cys, and Thr), hydrophobic and aromatic (Phe, Trp, Tyr), β-branched hydrophobic (Val, Ile), hydrophobic (Leu, Met), acidic (Asp, Glu), and amide containing (Asn, Gln) amino acids were grouped together according to chemical properties. Lysine, arginine, histidine, and proline were considered separately in this analysis. The colored bars represent the frequency at each position of the ar/R according to the following scheme: red; helix 2 position, blue; helix 5 position, green; loop E_1 position, magenta; loop E_2 position.

The ar/R H2 position predominantly contains the large aromatic residues Phe, Trp, and Tyr, with 78.9 % of the sequences in the dataset possessing one of these three residues at the H2 position. Histidine, small hydrophilic, and β-branched hydrophobic amino acids are also represented at this position in 14.5, 3.5, and 1.7 % of the dataset sequences, respectively. The H5 position of the ar/R is dominated by the presence of histidine in 65.3 % of the MIP amino acid sequences. An additional 20.8 % of these sequences contain a β-branched hydrophobic residue, and 11.9 % contain a small hydrophilic residue at the ar/R H5 position.

The most commonly observed amino acids at the LE_1 position are small hydrophilic residues, with 89.4 % of the sequences containing one of the five residues in this category. Additionally, 5.9 % of these sequences contain a hydrophobic aromatic residue, and 2.3 % of sequences contain a Pro residue at this position. Interestingly, LE_1 is the only ar/R position where Pro appears in the sequences comprising this dataset.

The LE_2 position of the ar/R is the most highly conserved and almost exclusively contains an Arg or β-branched hydrophobic residue. Of the sequences used for this study, 91.4 % contain an Arg residue at the LE_2 position, while an additional 7.3 % contain a β-branched hydrophobic residue, usually Val. The remaining 1.6% of the sequences have equal frequencies of small hydrophilic, hydrophobic, and Asn/Gln residues at LE_2. Although Lys is similar to Arg in its structural and chemical properties, it is never observed at LE_2 or any other position in the ar/R region. In addition, the acidic amino acids Asp and Glu were only observed

in three out of the 1000 sequences used in this study, suggesting that acidic residues are structurally unsuitable in the ar/R region.

The results of this analysis suggest that there is a selection pressure for certain amino acids in the ar/R region over others, as evidenced by the low abundance of ar/R combinations containing Lys, Asp, and Glu. In addition, these results imply that particular amino acids commonly found in the ar/R region have a higher frequency of occurrence at particular ar/R positions. For example, Arg is exclusively found at the LE_2 position of the ar/R region, while large aromatic amino acids are generally found at the H2 position. These frequencies suggest an evolutionary pressure exists to conserve these amino acids in discrete positions of the ar/R region in order to maintain the biological function of the channel.

The amino acid frequency analysis presented above has two important implications regarding the evolution of the ar/R region. First, these results suggest that single rather than multiple amino acid substitutions at the ar/R region are more likely to occur. Second, the observation that only a narrow range of amino acids are tolerated at each ar/R position suggests that only certain amino acid substitutions are allowed at each position. For example, if a MIP contains an Arg at the ar/R LE_2 position, then amino acid frequency analysis predicts that the most likely tolerated substitution is a Val, since these two amino acids are nearly the only two found at this position. To test these hypotheses, the number of ar/R regions in the pool of 92 ar/R sequences that could be interconverted by a single conservative or nonconservative substitution was determined. Figure **3.13** indicates that single nonconservative substitutions at the

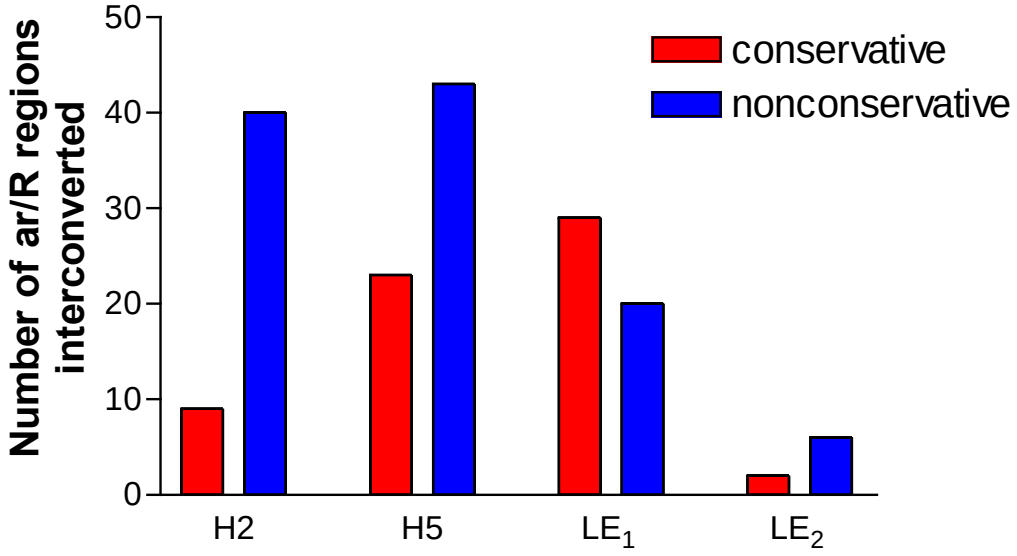

Figure 3.13: Frequencies of conservative and nonconservative substitutions at the ar/R region: The number of ar/R regions that could be interconverted by single conservative (red bars) or nonconservative (blue bars) substitutions were determined using the 92 ar/R combinations identified from a database containing 1000 MIP sequences. In this analysis, a conservative substitution is defined as a substitution that occurs within the amino acid categories defined in materials and methods, while a nonconservative substitution occurs between two amino acid categories. Each ar/R position is labeled at the bottom of the figure.

H2 position of the ar/R region account for nearly 40 of the ar/R regions observed in the dataset. A similar result (43 ar/R regions interconverted) was observed for amino acid substitutions at the H5 position. In contrast, conservative substitutions at these positions of the ar/R region are less frequent. For example, 9 (H2) and 23 (H5) ar/R regions can be interconverted by a single substitution.

The frequency of conservative and nonconservative substitutions at the loop E ar/R positions are nearly equal and show a much lower frequency compared to the H2 and H5 positions. When all ar/R positions are considered, 71 out of the 92 ar/R combinations observed in the MIP dataset can be interconverted by a single nonconservative substitution in the ar/R region.

The frequency and chemical properties of nonconservative amino acid substitutions occurring at each position of the ar/R region were analyzed (Figure **3.14)**. At the H2 position, the most common substitutions are aromatic to small hydrophilic residues or aromatic residues to histidine. These observations are interesting in light of the fact that these types of substitutions allow the H2 position to be interconverted between the most commonly observed H2 residues in the plant NIP and TIP subfamilies. The H5 position is also very diverse with respect to the types of residue substitutions that are observed. The most commonly observed substitutions are small hydrophilic residues to either beta branched hydrophobic residues or histidine. In addition, substitutions of β-branched hydrophobic residues to histidine or aromatic residues are also commonly observed.

A large number of ar/R regions can be interconverted by single conservative substitutions at the LE_1 position, but the most commonly observed nonconservative

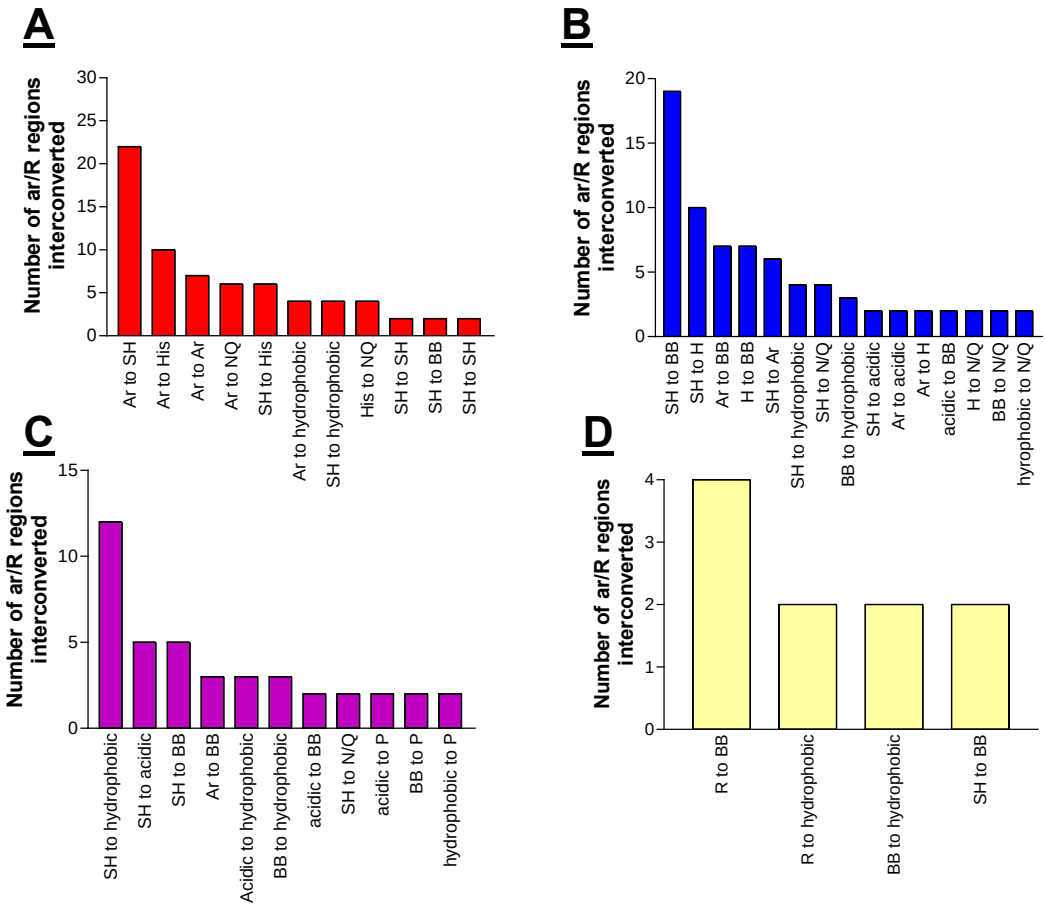

Figure 3.14: Frequency of ar/R interconversion classes: The types of nonconservative substitutions for the H2 (A), H5 (B), LE_1 (C), and LE_2 (D) positions of the ar/R region were determined. The abbreviations for each class are as follows: Ar; aromatic, SH; small hydrophilic, BB; beta branched; His; histidine, R; arginine, N/Q; asparagine or glutamine, P; proline, hydrophobic;

substitution is a small hydrophilic residue to a hydrophobic residue. In addition, there are a small number of ar/R regions that can be interconverted by a substitution of Pro at this position to acidic, β-branched, or hydrophobic residues. Interestingly, LE_1 is the only ar/R position where Pro is observed. The comparatively large number of conservative amino acid substitutions observed at this position may reflect the fact that this position typically contributes a backbone carbonyl oxygen as a hydrogen bond acceptor to the transported substrate, so MIPs can afford to have a larger number of possible residues at this position.

Finally, LE_2 is the ar/R position that is least likely to have nonconservative substitutions. The most common nonconservative substitution at this position is an Arg for β-branched hydrophobic residues, usually Val. However, the Arg at the LE_2 position is so highly conserved in the ar/R region that very few ar/R regions containing a Val substitution are observe. Overall, these results suggest that the majority of single nonconservative amino acid substitutions in the ar/R region occur within the confines of the amino acid preferences for each ar/R position and imply that these single nonconservative substitutions could allow for a majority of the observed structural diversity at the ar/R region.

Functional properties and the structural determinants of selectivity in NIP and TIP subgroup members

Comparative functional analysis of NIP subgroup I and II

To examine the detailed structural mechanisms by which plant MIPs determine their functional properties, representative NIP subgroup I, NIP subgroup II, and TIP subgroup II proteins were analyzed. Nodulin-26 is a NIP subgroup I protein that has been extensively characterized. Functional analysis shows that nodulin 26 is an aquaglyceroporin that is permeable to water as well as to uncharged solutes such as formamide, glycerol, and ammonia (Rivers et al., 1997; Dean et al., 1999; Guenther and Roberts, 2000; Niemietz and Tyerman, 2000). Several other members of NIP subgroup I have similar permeabilities (Weig et al., 1997; Weig and Jakob, 2000; Guenther and Roberts, 2000). Because modeling studies in the previous sections revealed the presence of a separate conserved ar/R tetrad for NIP subgroup II members, the functional properties of NIP subgroup II were investigated in *Xenopus* oocytes using Arabidopsis NIP6;1 as a representative for this subgroup. AtNIP6;1 expressing oocytes were assayed for water as well as solute permeability as described below.

AtNIP6;1 oocytes were assayed for water permeability using a standard osmotic water permeability assay that measures the rate of oocyte water uptake after hypoosmotic challenge (Preston et al., 1992). This rate is used to calculate the osmotic permeability coefficient (P_f), which is a useful comparison of water permeability among MIP channels. In contrast to members of NIP subgroup I, water permeability assays indicate that NIP6;1 is completely impermeable to water (Figure **3.15A**). Expression of both NIP6;1 and nodulin-26 in oocytes was verified by fusing a FLAG epitope tag to the N-terminus of these proteins and performing Western blot analysis of oocyte lysates (Figure **3.15C**).

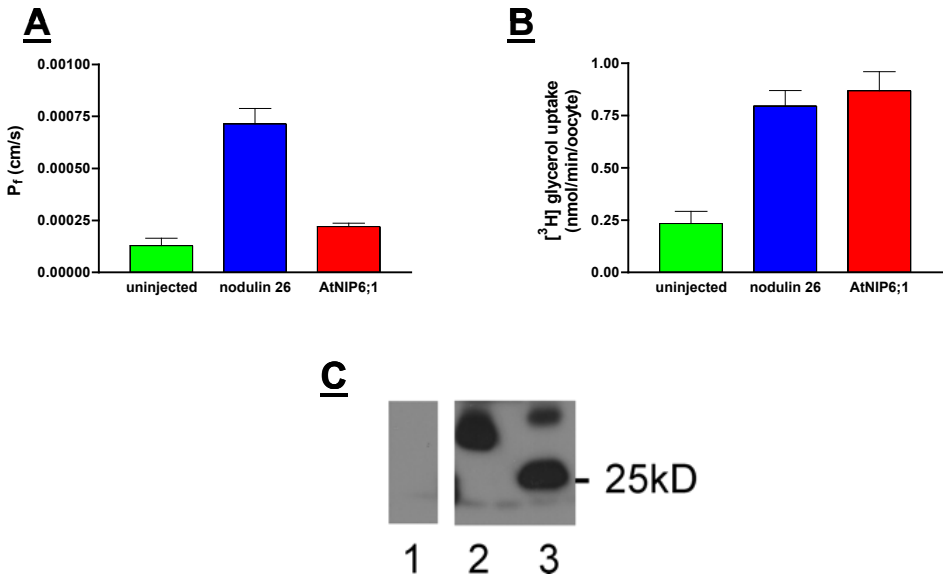

Figure 3.15: Water and glycerol permeabilities of NIP subgroup NIP6;1: *Xenopus* oocytes were injected with 46 ng of cRNA encoding nodulin-26 or NIP6;1 translationally fused to an N-terminal FLAG epitope tag and cultured as previously described (Rivers et al., 1997). These oocytes were assayed for water **(A)** as well as glycerol **(B)** permeability. Uninjected oocytes were used as negative controls. Error bars in panel A represent standard deviation (n=5-9). Error bars in panel B represent SEM (n=3). **C.** Ten micrograms of uninjected (lane 1), NIP6;1 (lane 2), and nodulin-26 (lane 3) oocyte lystate protein were separated on a 12.5% SDS-PAGE gel and probed with an anti-FLAG antibody. The position of the 25 kDa molecular weight marker is indicated to the right of the figure.

This experiment indicates that these proteins are properly expressed in oocytes, and that the lack of observed water permeability is not due to lack of channel expression. Subsequent glycerol uptake assays indicate that NIP6;1 is a glycerol permease that has a glycerol uptake rate that is identical compared to nodulin-26 (Figure **3.15B**). These data show that AtNIP6;1 is a glyceroporin with no detectable aquaporin activity.

HOLE analysis of the NIP6;1 homology model (see Figure **3.8D**) indicates that NIP subgroup II members have a much wider pore aperture than their NIP subgroup I counterparts, suggesting that these proteins may be permeable to larger solutes. To further investigate the substrate selectivity of NIP subgroup II proteins, NIP6;1 was tested for formamide as well as urea permeability. These solutes were selected because they are uncharged compounds of defined van der Waals volume (formamide = 24.8 cm^3/ mol; urea = 32.8 cm^3/ mol), they have similar structural properties, and they were previously used to probe the pore size of the prototypical NIP subgroup I channel nodulin-26 (Rivers et al., 1997). These assays were conducted by transferring NIP6;1-expressing oocytes to an isoosmotic assay solution in which the test solute replaced NaCl in a base frog Ringers buffer. Formamide and urea permeability were measured by swelling of these oocytes resulting from the sympathetic flux of water following the solute as it is transported into the oocyte down its concentration gradient.

Figure **3.16A** illustrates the results of these experiments. NIP6;1 is equally permeable to both formamide and urea. This selectivity profile contrasts with nodulin 26, which transports formamide but excludes urea.

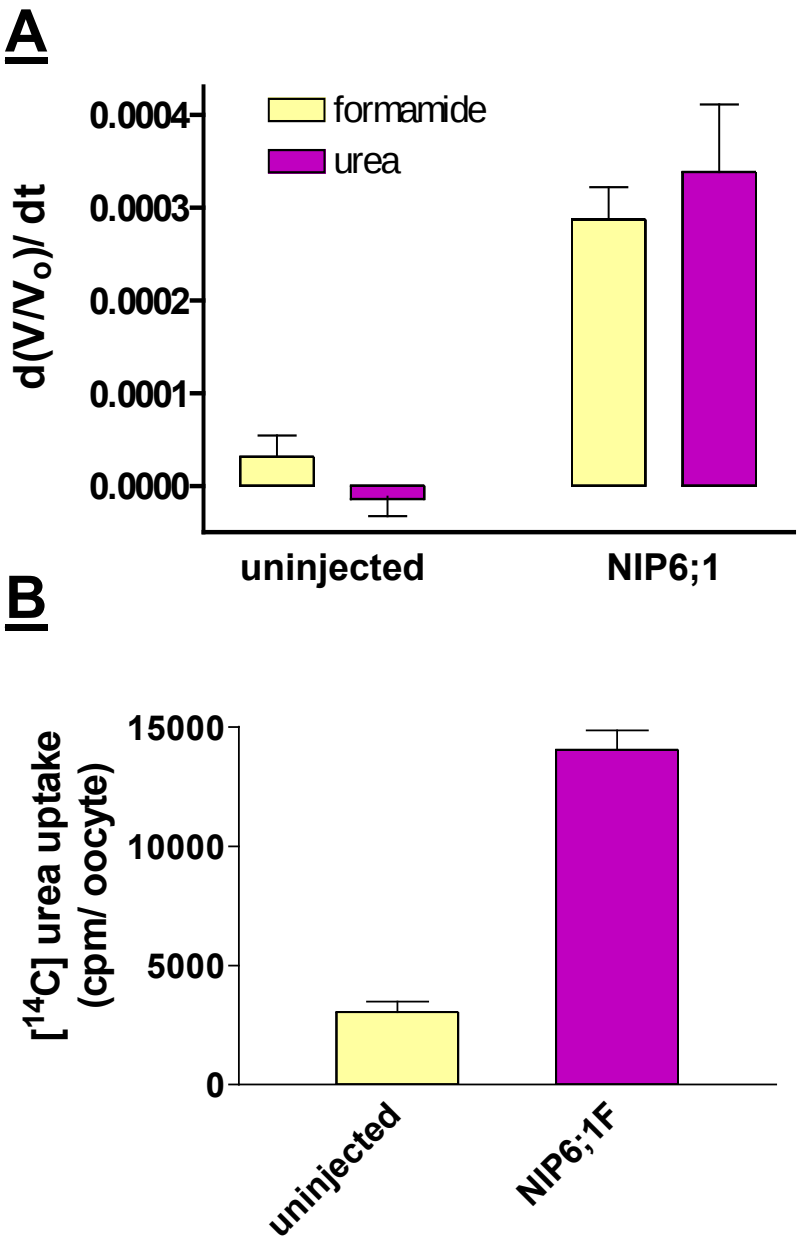

Figure 3.16: NIP subgroup II permeability to urea and formamide: *Xenopus* oocytes were injected with 46 ng of cRNA encoding NIP6;1 and cultured as previously described (Rivers et al., 1997). **A.** Oocytes were assayed for formamide (yellow bars) and urea permeability (magenta bars) by the modified oocyte swelling assay as described in the result section text. Uninjected oocytes were used as negative controls. Error bars represent SEM (n=5). **B.** Urea permeability of NIP6;1-expressing oocytes was assayed by isoosmotic uptake of ^{14}C-labeled urea. Uninjected oocytes were used as negative controls. Error bars represented SEM (n=3).

Subsequent direct uptake assays indicate that NIP6;1-expressing oocytes were 3.5 fold more permeable to ^{14}C-labeled urea than uninjected control oocytes (Figure **3.16B**), supporting the urea-induced swelling analyses observed by video microscopy. These results again demonstrate that NIP subgroup II members are functionally distinct from NIP subgroup I members. In conjunction with the previous homology modeling and pore-sizing computational analysis, these results also suggest that the novel substrate selectivity of NIP subgroup II members is linked to the composition of the ar/R region.

The structural determinants of NIP and TIP selectivity

Functional analysis experiments suggest that NIP and TIP family members have discrete selectivity profiles to water and other transported solutes including glycerol, urea, and ammonia (Klebl et al., 2003; Liu et al., 2003; Dynowski et al., 2008; reviewed in Wallace et al., 2006). These differential substrate selectivity profiles as well as the ar/R region homology models generated above provide a unique opportunity to investigate the structural determinants of selectivity between these proteins.

NIP subgroup I and II, and TIP subgroup II proteins, contain conserved H5, LE_1, and LE_2 ar/R residues, but these proteins show class-specific differences at the H2 residue. TIP subgroup II members contain a His residue at this position, NIP subgroup I members have a Trp, and NIP subgroup II members have an Ala residue (Table **3.3**). The H2 Trp residue of the NIP subgroup I ar/R is highly conserved among glyceroporins (Froger et al., 1998) whereas this residue is a conserved His

residue in glycerol-impermeant TIPs, suggesting that this residue may contribute to glycerol substrate selectivity in NIP subgroup I members. To test this hypothesis, the ar/R H2 Trp of LjNod26, a nodulin-26 orthologue from *Lotus japonicus* (Guenther and Roberts, 2000), was converted to a TIP-like His residue by site-directed mutagenesis. This mutant was expressed in *Xenopus* oocytes and assayed for water as well as glycerol permeability.

When expressed in *Xenopus* oocytes, LjNod26 forms a channel that shows indistinguishable water and glycerol permeabilities from nodulin-26 (Guenther and Roberts, 2000; Figure **3.17A**). When the H2 ar/R Trp residue of LjNod26 was converted to His (LjNod26 W77H), the mutant channel has an osmotic water permeability nearly identical to that of wild-type LjNod26. However, radio-isotopic glycerol uptake assays indicate that the LjNod26 W77H mutation decreases the glycerol permeability of this mutant channel by greater than 5-fold (Figure **3.17B**). These results suggest that the Trp residue at the H2 position of the ar/R is a critical structural determinant for glycerol selectivity in NIP subgroup I members and conversely, that the presence of a His residue at the H2 position confers a greater selectivity for water over glycerol observed for TIP subgroup II members.

Since the H2 ar/R residue appears to exert a drastic influence on transported substrate selectivity and NIP subgroup II members differ from NIP subgroup I members at the critical H2 residue, we investigated the structural determinants that confer the unique substrate selectivity of NIP subgroup II members. NIP subgroup II members also contain identical H5, LE_1, and LE_2 positions of the ar/R region when compared to NIP subgroup I as well as TIP subgroup II members, but contain a single

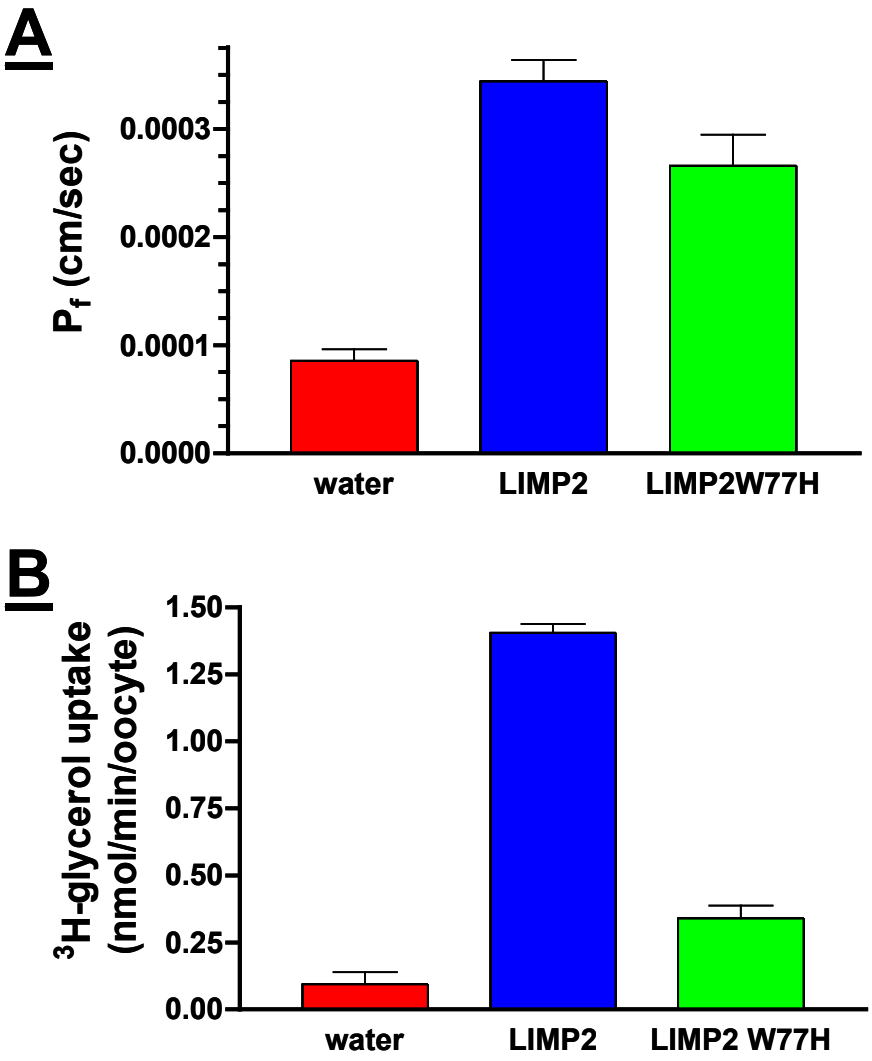

Figure 3.17: Effects of substitution at the H2 ar/R residue on glycerol and water selectivity in TIP and NIP subgroup I members: *Xenopus* oocytes were injected with 46 ng of wild-type LIMP2 (blue bars) or LIMP2 W77H mutant (green bars) cRNA and cultured as previously described (Rivers et al., 1997). These oocytes were assayed for water permeability **(A)** and radio-labeled glycerol uptake **(B)** as previously described (Guenther and Roberts, 2000). Error bars represent SEM (n=29 for water permeability, n=9 for glycerol uptake). Oocytes injected with 46 nL of DEPC treated water (red bars) were used as negative controls.

nonconservative substitution of Ala at H2 instead of the NIP subgroup I Trp residue that is a selectivity determinant for glycerol transport. In addition to the differences at the ar/R region, NIP subgroup II members have a Val substitution for the highly conserved alanine residue in the C-terminal NPA motif. Analysis of the effects of these substitutions on pore architecture is apparent when one considers the pore diameter calculated for nodulin-26 (NIP-I) and AtNIP6;1 (NIP-II) homology models (Figure **3.8C-E**). As mentioned previously, the alanine substitution results in a widening of the pore (from 3.7 angstroms in NIP-I to 7 angstroms in NIP-II members), so that nearly two water molecules can fit side by side in the ar/R filter. At the same time, the substitution of a Val residue in the second NPA motif results in a slight narrowing of the pore around this region. To test the contribution of these residues to NIP subgroup II selectivity, the Ala at the H2 ar/R position of AtNIP6;1 was mutated to a Trp residue, which is characteristic of NIP subgroup I members (NIP6;1 A119W) and the loop E NPV Val residue was mutated to an Ala, which is characteristic of NIP-I and the majority of other MIP channels (NIP6;1 V252A). Functional analysis of these mutant channels was performed in *Xenopus* oocytes to determine their substrate selectivity.

Figure **3.18** illustrates the results of these experiments. The NIP6;1 V252A mutant channel was indistinguishable from wild-type NIP6;1, showing no detectable water permeability, but robust glycerol permeability (Figure **3.18A** and **B**). In contrast, the NIP6;1 A119W ar/R substitution results in an acquisition of water permeability in these mutant channels with a P_f identical to NIP-I proteins such as nodulin-26, while simultaneously retaining the ability to transport glycerol

Figure 3.18: Water and glycerol permeability of NIP6;1 ar/R and NPA mutants: *Xenopus* oocytes were injected with 46 ng of cRNA encoding Nodulin-26, wild-type NIP6;1, NIP6;1 V252A, or NIP6;1 A119W mutants. These oocytes were cultured as previously described (Rivers et al., 1997) and assayed for solute permeability. **A.** Water permeability assays were performed to compare the osmotic water permeability (P_f) of Nodulin-26 (NodS-FLAG) to wild-type NIP6;1 and its mutants. Uninjected oocytes were used as negative controls. Error bars represent SEM (n=10-20). **B and C.** The glycerol permeability of wild-type and mutant NIP6;1 expressing oocytes was determined by isoosmotic uptake of radio-labeled glycerol. Nodulin-26 was used as a positive control and uninjected oocytes were used as negative controls. Error bars represent SEM (n=3 oocytes).

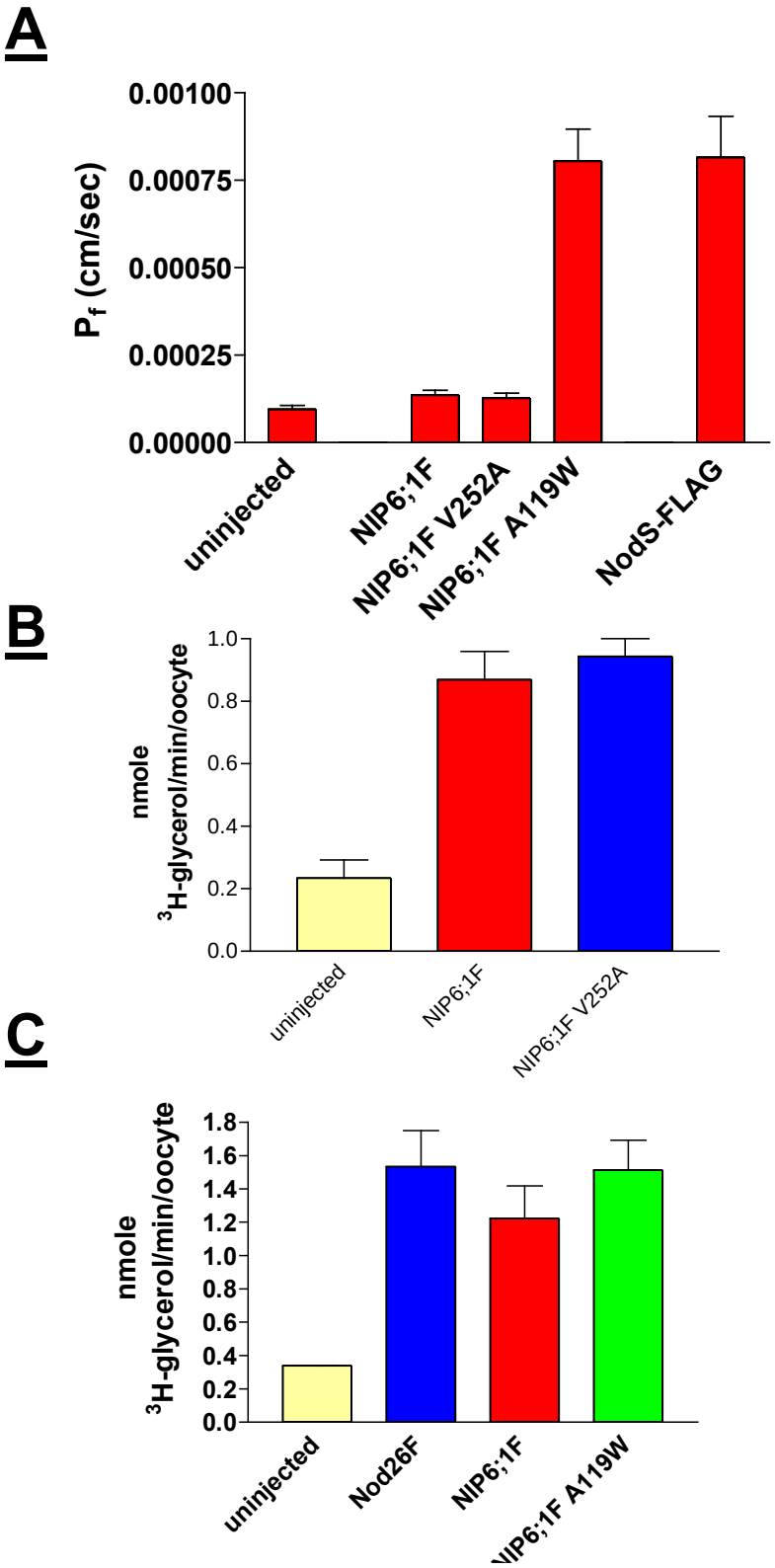
A
0.00100
0.00075
0.00050
0.00025
0.00000
P_f (cm/sec)
uninjected
NIP6;1F
NIP6;1F V252A
NIP6;1F A119W
NodS-FLAG
B
1.0
0.8
0.6
0.4
0.2
0.0
nmole
^{3}H-glycerol/min/oocyte
uninjected
NIP6;1F
NIP6;1F V252A
C
1.8
1.6
1.4
1.2
1.0
0.8
0.6
0.4
0.2
0.0
nmole
^{3}H-glycerol/min/oocyte
uninjected
Nod26F
NIP6;1F
NIP6;1F A119W

(Figure **3.18A** and **C**). Subsequent formamide and urea permeability assays indicate that AtNIP6;1 A119W-expressing oocytes are permeable to formamide, but lost the ability to transport urea (Figure **3.19A**), suggesting that the presence of this bulky Trp residue reduces the pore size sufficiently to exclude this larger solute (Figure **3.18B**). These results suggest that the substitution of Val into the C-terminal NPA motif of NIP subgroup II members does not affect function of these channels, while mutation of the ar/R H2 Ala residue to a NIP subgroup I-like Trp completely and reciprocally alters substrate selectivity between these two channels.

The finding that AtNIP6;1 is almost completely impermeable to water is somewhat surprising because the size of the AtNIP6;1 pore (Figure **3.8E**). Thus, water permeability is not simply controlled by a steric size filter. Mutagenesis of the AtNIP6;1 ar/R Ala residue to a nodulin-26 like Trp (AtNIP6;1 A119W) restores water permeability and generates a selectivity profile similar to nodulin-26 when assays are performed at 15^0 C. However, an interesting observation was made when the water transport rates as a function of temperature were analyzed for AtNIP6;1, AtNIP6;1 A119W, and nodulin-26 (Figure **3.20**).

Nodulin-26 shows a low activation energy (1.57 kcal/mol) to water transport, which is characteristic of facilitated water flow through aquaporin channels (Rivers et al., 1997; Dean et al., 1999), but AtNIP6;1 channels show a higher activation energy (12.6 kcal/ mol) that is indistinguishable from control oocytes. This high activation energy is characteristic of nonfacilitated water transport through a lipid bilayer.

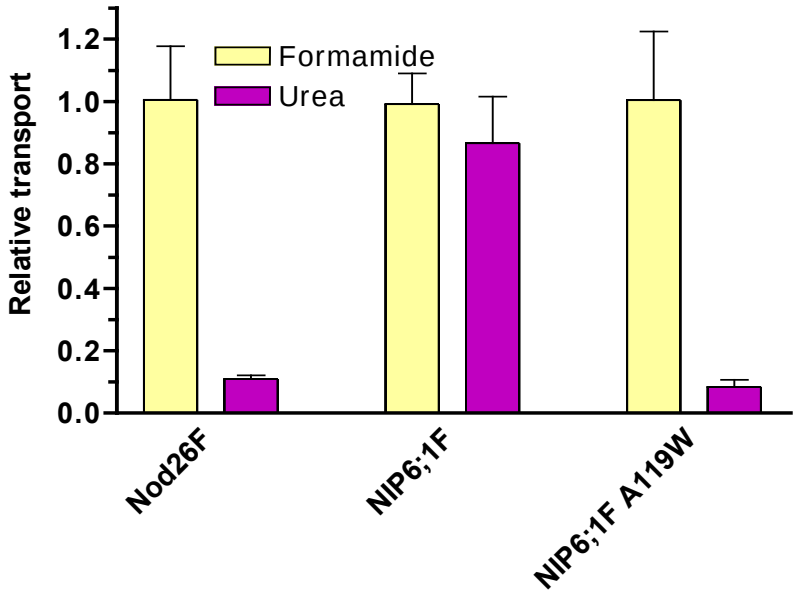

Figure 3.19: Formamide and urea permeability of AtNIP6;1 A119W:
Xenopus oocytes were injected with 46 ng of cRNA encoding Nodulin-26, wild-type NIP6;1, or NIP6;1 A119W mutants. These oocytes were cultured as previously described (Rivers et al., 1997) and assayed for solute permeability. The relative formamide and urea permeability of Nodulin-26, NIP6;1, and NIP6;1 A119W expressing oocytes was determined by video microscopy. Transport rates were standardized to the maximal formamide transport rate of each oocyte set. Error bars represent SEM (n=4-11 oocytes).

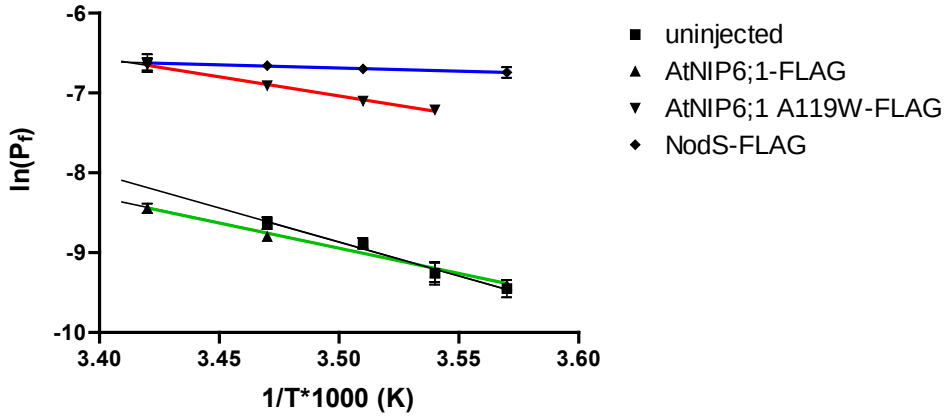

Figure 3.20: Arrhenius plot of water transport by AtNIP6;1, AtNIP6;1 A119W, and nodulin 26: 46 ng of cRNA encoding either AtNIP6;1, AtNIP6;1 A119W, or nodulin 26 was injected into *Xenopus* oocytes. The oocytes were cultured for 3 days at 18^0 C and assayed for water permeability at different temperatures using the standard video microscopy assay described previously. Activation energy curves for nodulin 26 (blue), AtNIP6;1 (green), AtNIP6;1 A119W (red), and uninjected (black) are shown. Error bars represent SEM (n=5).

AtNIP6;1 A119W shows an intermediate activation energy for water transport (9.55 kcal/mol) that is significantly lower than uninjected control oocytes, but is much higher than the activation energy observed for nodulin-26. If the AtNIP6;1 A119W mutation completely restores the water permeability properties of a NIP subgroup I protein, one would predict that the activation energy for water transport should be the same as nodulin-26. The energetic parameters for the transition state of water transport ($\Delta G^{\ddagger}$, $\Delta H^{\ddagger}$, and $\Delta S^{\ddagger}$) as well as the Arrhenius prefactor (a measure of the number of collisions in a reaction having a conformation that leads to progression to products) were calculated from the water transport rates and activation energies for each oocyte set (Table **3.4**). While the thermodynamic parameters for the transition state of NIP6;l and the NIP6;1 A119W mutant are very similar, the main difference between these channels is a 30-fold difference in the Arrhenius prefactor. This observation suggest that AtNIP6;1 A119W may be able to transport water due to an increased number of water molecules reaching the ar/R in a conformation that is more favorable for water transport compared to wild-type AtNIP6;1. However, an analysis of the water transport activation energies for nodulin 26 and AtNIP6;1 A119W indicate that significant differences exist in the water transport pathway between these proteins.

Table 3.4: Activation energy and thermodynamic analysis of AtNIP6;1 A119W

Oocyte[a]	Arrhenius pre-factor[b]	Activation energy (kcal/ mol)[b]	$\Delta G^{\ddagger}$ (kcal/ mol at 25^0 C)[c]	$\Delta H^{\ddagger}$ (kcal/mol)[c]	$\Delta S^{\ddagger}$ (e.u.)[c]
Uninjected	1.21×10^{9}	16.9	19.2	17.0	-7.38
NIP6;1	5.30×10^{5}	12.6	19.6	9.06	-35.3
NIP6;1 A119W	1.7×10^{4}	9.53	18.5	8.95	-32
Nodulin-26	2×10^{-2}	1.57	18.3	5.13	-44.9

[a] *Xenopus* oocytes were injected with 46 ng of cRNA encoding AtNIP6;1, AtNIP6;1 A119W, or nodulin-26 and the temperature dependence of water permeability was assayed. Uninjected oocytes were used as negative controls.

[b] The activation energy was calculated from the slope of Arrhenius plots from figure **3.20** and the Arrhenius pre-factor was determined from the Y-intercept.

[c] The free energy ($\Delta G^{\ddagger}$), enthalpy ($\Delta H^{\ddagger}$), and entropy ($\Delta S^{\ddagger}$) of the transition state were calculated from the activation energy and the P_f as described in Materials and Methods.

AtNIP6;1 is a plasma membrane boric acid channel in developing aerial organs of Arabidopsis[1]

While the permeability of AtNIP6;1 to various test solutes was illustrated in the previous section, the physiological solute(s) and function of this channel in vivo was not demonstrated and was pursued as the next area of investigation. Takano et al. (2006) demonstrated that AtNIP5;1, a protein that is 40 % identical to AtNIP6;1, apparently serves as a boric acid channel in root tissues (Takano et al., 2006). Boric acid is a neutral molecule at physiological pH, and is an essential micronutrient that covalently cross-links rhamnogalacturonan-II residues in the plant cell wall (O'Neill et al., 1996). Due its structural similarity to AtNIP5;1, the hypothesis that AtNIP6;1 serves as a boric acid channel was investigated.

AtNIP6;1 was expressed in *Xenopus* oocytes and was assayed for boric acid permeability by swelling-based uptake assays as well as by direct uptake assays measuring boric acid accumulation. Figure **3.21** shows the results of these experiments. Oocytes expressing AtNIP6;1 showed a linear time-dependent increase in volume when exposed to an isoosmotic bathing solution containing 200 mM boric acid (Figure **3.21A**). AtNIP5;1-expressing oocytes were included in the assay as a positive control for boric acid uptake. The boric acid-induced swelling rates for both AtNIP5;1 and AtNIP6;1-expressing oocytes were higher than uninjected oocytes, but the AtNIP6;1 swelling rate was 50% lower than that of AtNIP5;1 (Figure **3.21B**).

[1] This work was performed in collaboration with Mayuki Tanaka and Toru Fujiwara at the University of Tokyo.

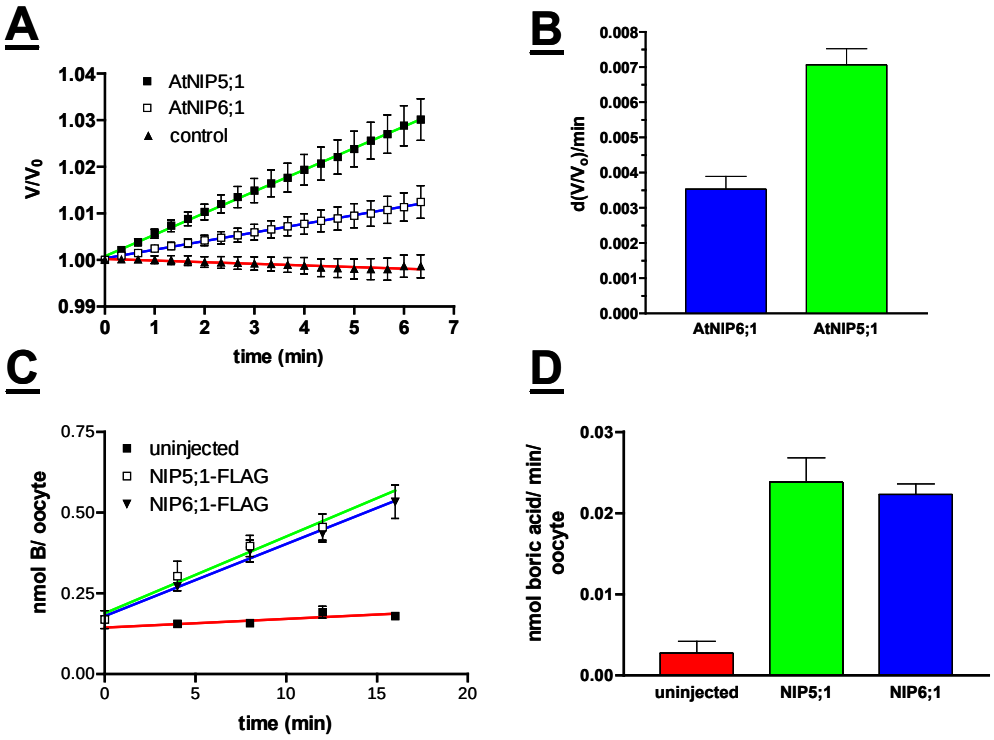

Figure 3.21: AtNIP6;1 forms a boric acid channel in *Xenopus* oocytes: *Xenopus* oocytes were injected with 46 ng of cRNA encoding AtNIP5;1 or AtNIP6;1 and cultured as previously described (Rivers et al., 1997). **A.** The time-dependent swelling of AtNIP5;1 (closed squares) and AtNIP6;1 (open squares) expressing oocytes was measured by video microscopy after exposure to an isoomotic solution containing 200 mM boric acid. Uninjected oocytes (triangles) were used as a negative control. **B.** The time-dependent swelling in panel A was used to calculate a boric acid dependent swelling rate. The error bars represent the SEM (n= 10). **C.** AtNIP5;1 (open squares) and AtNIP6;1 expressing oocytes (triangles) were assayed for boric acid permeability at various time points by direct uptake assays in 2 mM boric acid solution followed by quantitation with ICP-MS. Uninjected oocytes (closed squares) were used as negative controls. The error bars represent the SEM (n=3). **D.** The best-fit linear regression line from C was used to calculate the boric acid uptake rate. The error bars represent the standard deviation of the linear regression.

Direct uptake of boric acid was assayed by inductively-coupled plasma mass spectrometry (ICP-MS). These assays indicate that AtNIP6;1-expressing oocytes have a 10-fold higher boric acid permeability than uninjected control oocytes (Figure **3.21D**). Boric acid accumulation in these oocytes was linear with respect to time for up to 10 minutes (Figure **3.21C**), and the boric acid uptake rate was identical to the previously characterized AtNIP5;1 boric acid channel. Western blot analysis using an anti-FLAG antibody indicates that AtNIP6;1 and AtNIP5;1 are expressed at an equivalent level in oocytes (Figure **3.22B**). Overall, these data suggest that AtNIP6;1 is capable of boric acid transport.

To investigate the discrepancies between direct and swelling-induced boric acid uptake rates, AtNIP5;1 and AtNIP6;1-expressing oocytes were assayed for water permeability. Figure **3.22A** indicates that AtNIP6;1-expressing oocytes are impermeable to water, while AtNIP5;1-expressing oocytes have a water permeability that is 2-fold higher that uninjected oocytes. These results suggest that the differences in boric acid uptake rates observed by the swelling-based assay are different due to the increased water permeability of AtNIP5;1-expressing oocytes, since this assay is also dependent upon the water permeability of the oocyte plasma membrane. The results, together with those in the previous section, also suggest that AtNIP6;1 is a boric acid channel that has evolved to form a "water tight" channel, and this property may be relevant to the physiological function of AtNIP6;1.

In the previous section, it was demonstrated that the ar/R H2 alanine of NIP subgroup II proteins is a major selectivity determinant for these protein channels and discriminates them from NIP subgroup I members.

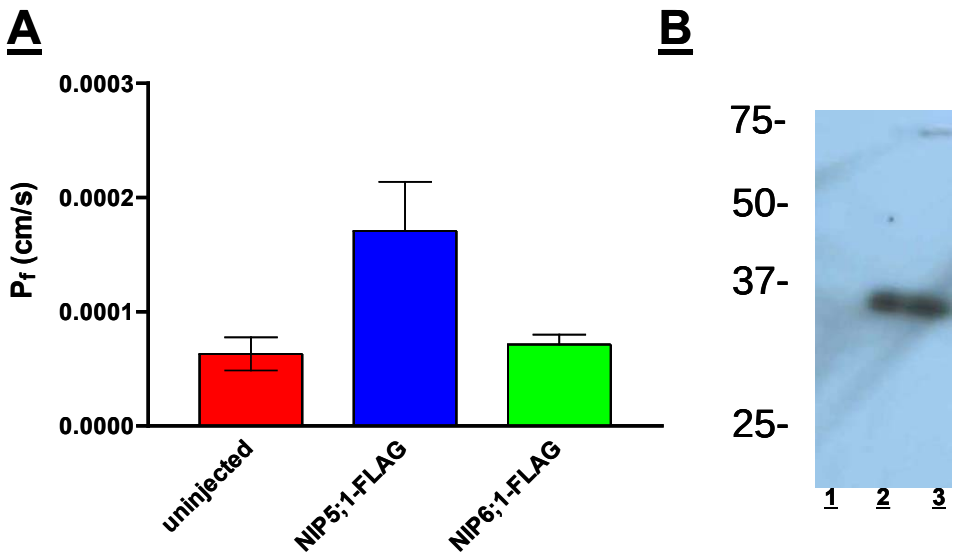

Figure 3.22: Analysis of AtNIP5;1 and AtNIP6;1 water permeability: **A.** *Xenopus* oocytes were injected with 46 nL of 1 μg/ μL AtNIP5;1-FLAG (blue bars) or AtNIP6;1-FLAG (green bars) cRNA and assayed for water permeability by video microscopy. Uninjected oocytes (red bars) were used as negative controls. Error bars represent SEM (n=6). **B.** 20 μg of AtNIP5;1-FLAG and AtNIP6;1-FLAG expressing oocyte lysate protein was separated on a 12.5% SDS-PAGE gel, blotted to PVDF, and probed with an anti-FLAG antibody to determine channel expression levels. Lane 1: uninjected oocyte lysate protein, lane 2: AtNIP5;1-expressing oocyte lysate protein, lane 3: AtNIP6;1-expressing oocyte lysate protein. The position of the molecular weight markers are shown to the left of the blot with their molecular weights indicated in kilodaltons.

To investigate the role of this residue in transport of the physiological solute boric acid (van der Waals volume = 45.5 cm^3/ mol), the permeabilities of AtNIP6;1 and AtNIP6;1 A119W were compared. Figure **3.23** indicates that the substitution of a Trp residue for the NIP6;1 H2 Ala residue causes a three-fold reduction in the boric acid transport rate of this mutant channel. These results suggest that the H2 position of the NIP subgroup II ar/R is also a critical selectivity determinant for the physiological solute boric acid

To investigate the subcellular localization of AtNIP6;1 in vivo, a C-terminal in-frame fusion of AtNIP6;1 with the green fluorescent protein (GFP) under the control of the cauliflower mosaic virus 35S RNA promoter (CaM35S) was generated and transformed into Arabidopsis plants. Analysis of the resultant transgenic plants (Figure **3.24)** show that AtNIP6;1-GFP fluorescence is present as a thin layer of fluorescence around the cell periphery, suggesting that this protein is localized to the plasma membrane. Overall, these functional and localization data suggest that AtNIP6;1 is a plasma membrane-localized, water-tight boric acid channel with a boric acid permeability similar to root-specific AtNIP5;1.

AtNIP6;1 cellular localization and transcriptional regulation by boric acid availability

Previous experiments indicate that AtNIP5;1 transcripts are induced in Arabidopsis root tissue under boric acid-limiting conditions (Takano et al., 2006). To investigate AtNIP6;1 transcriptional regulation in response to boric acid availability, AtNIP6;1 and AtNIP5;1 transcript levels were assayed by real-time PCR expression

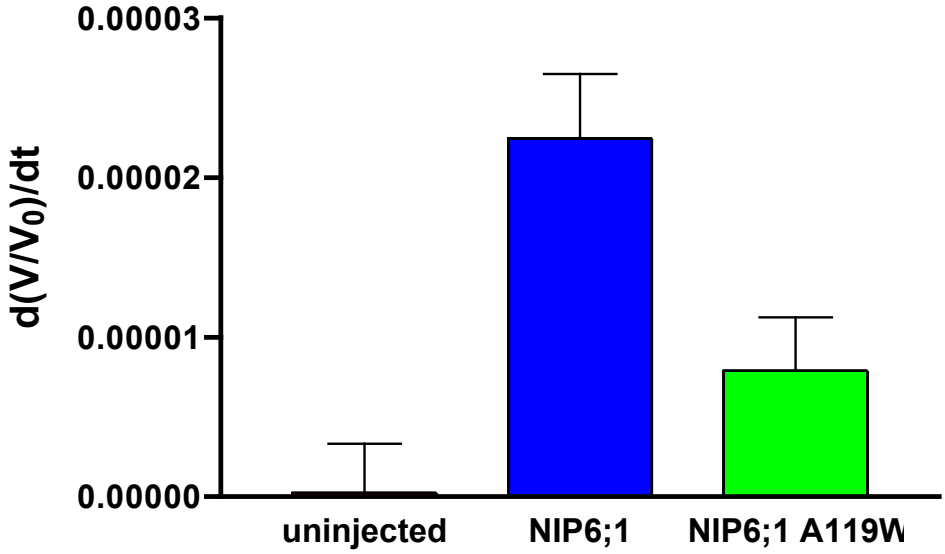

Figure 3.23: Analysis of AtNIP6;1 A119W boric acid permeability: Xenopus oocytes were injected with 46 ng of cRNA encoding wild-type AtNIP6;1 (blue bars) or the AtNIP6;1 A119W mutant (green bars). These oocytes were cultured as previously described (Rivers et al., 1997) and assayed for boric acid permeability by video microscopy. Uninjected oocytes (red bars) were used as negative controls. Error bars represent SEM (n=5-6).

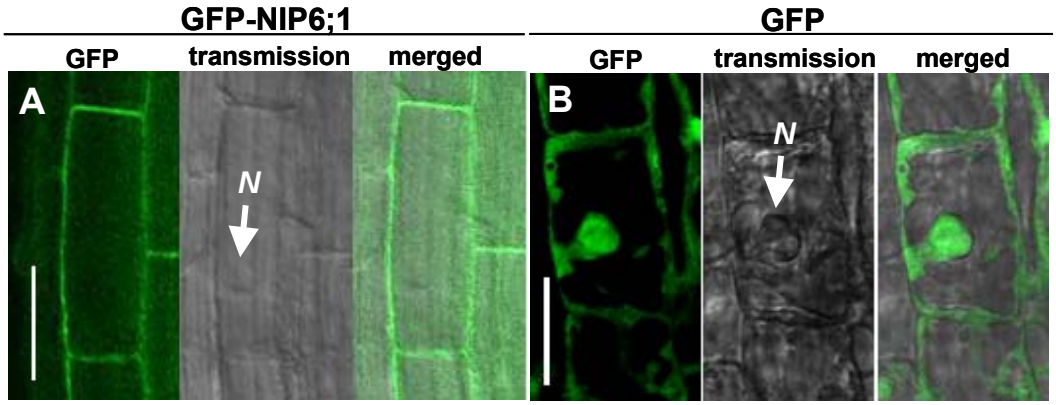

Figure 3.24: Subcellular localization of AtNIP6;1: Arabidopsis plants were transformed with constructs expressing NIP6;1-GFP or GFP alone under the control of the cauliflower mosaic virus 35S RNA promoter. The root elongation zone for each transgenic plant was examined for green fluorescence patterns. Images of GFP fluorescence (left panel), differential interference contrast (middle panel), and merged image (right panel) are shown for plants expressing GFP-NIP6;1 **(A)** and GFP alone **(B).** The position of the nucleus (N) is indicated with an arrow. Size bars indicate 50 μm.

analysis under normal and boric acid-limiting conditions. Similar to the previous findings of Takano et al. (2006), AtNIP5;1 mRNA is expressed in root tissue of young Arabidopsis seedlings, and are induced by 7-fold in response to boric acid limitation (Figure **3.25**). In contrast, AtNIP6;1 predominantly is expressed in shoot, with highest expression apparent in the stems and much lower levels observed in roots and rosette leaves. Boric acid deprivation (0.1 μM boric acid) causes a modest 1.5-fold increase in AtNIP6;1 transcript levels in the stem, but no other tissues show elevated levels of AtNIP6;1 transcript under these conditions.

The cellular expression patterns of AtNIP6;1 were investigated in greater detail by generating transgenic plants expressing β-glucuronidase under the control of the endogenous AtNIP6;1 promoter (Figure **3.26**). AtNIP6;1 promoter GUS fusion plants show AtNIP6;1 expression in stems of Arabidopsis seedlings, and in particular specific and intense staining was observed at the stem node regions (Figure **3.26A** and **B**). Further localization analysis of thin sections of GUS-stained stem nodes suggest that AtNIP6;1 is expressed in the vascular tissue (Figure **3.26C** and **D**), and high magnification images indicate that this staining pattern is consistent with AtNIP6;1 expression in xylem-phloem transfer cells (Figure **3.26F**).

The expression analysis and localization data suggest that AtNIP6;1 shows modest transcriptional up-regulation in response to boric acid deprivation and is localized to xylem-phloem transfer cells. These results also suggest that AtNIP5;1 and AtNIP6;1 play distinct roles in boron nutrition because their expression patterns do not overlap, and the extent to which these transcripts are induced by boric acid deprivation is markedly different.

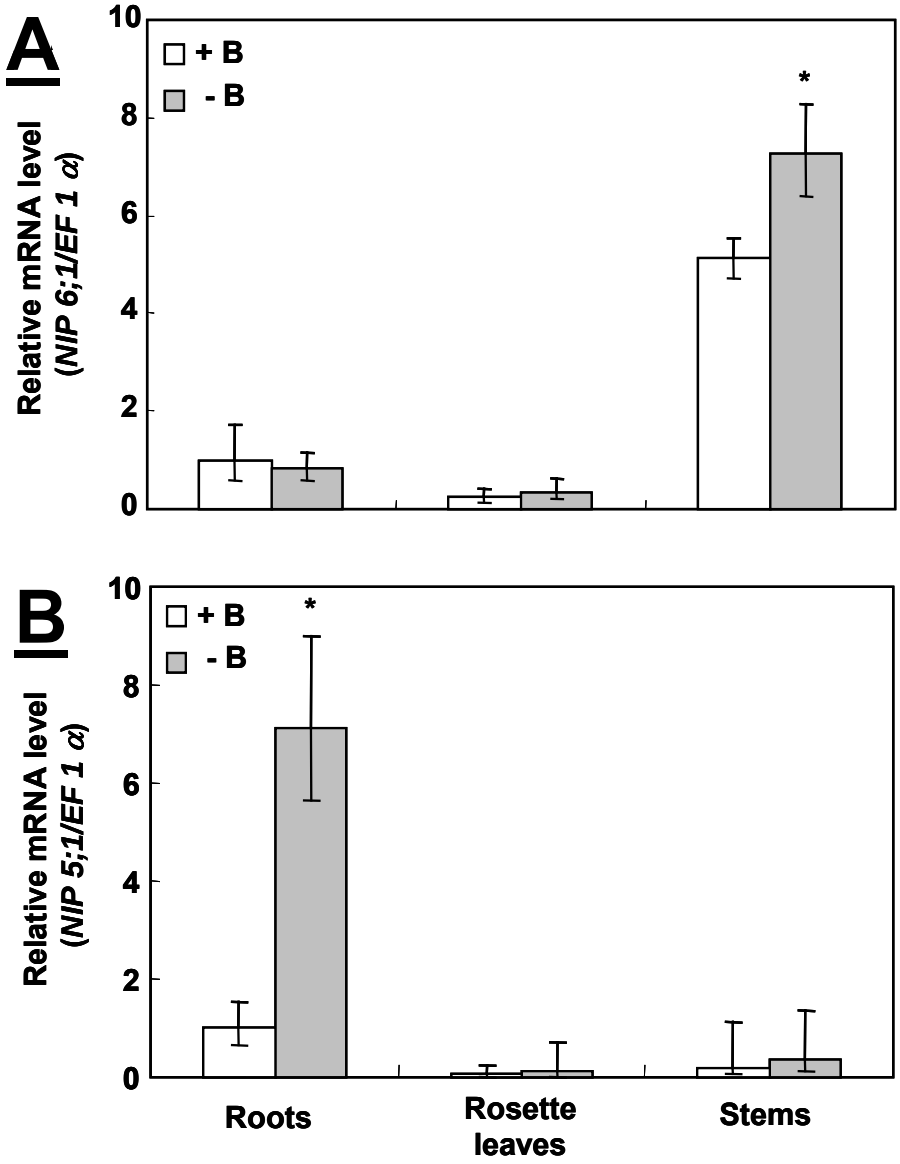

Figure 3.25: AtNIP6;1 transcript expression in response to boric acid deprivation: Wild-type Col-0 Arabidopsis plants were grown for 46 days in medium containing 100 μM boric acid (+B). Treated plants were transferred to media containing 0.1 μM boric acid for 24 hr. Total RNA was harvested from roots, rosette leaves, as well as stems and used to synthesize cDNA. Real-time PCR expression analysis was performed on these cDNA samples to quantify the relative amounts of NIP6;1 **(A)** and NIP5;1 **(B)** transcripts in each of these tissues. EF1α was used as an internal standard. Error bars represent SEM (n=3). Asterisks indicate significant differences from control ($P<0.05$; Student's t-test).

Figure 3.26: Cellular localization of AtNIP6;1 expression in transgenic AtNIP6;1 promoter-GUS fusion plants: Arabidopsis plants harboring a transgene consisting of a fusion of the promoter region of AtNIP6;1 and the coding region of β-glucuronidase (Pro-AtNIP6;1-GUS) were grown for 28 days in media supplemented with 10 μM boric acid. The expression patterns of AtNIP6;1 were assayed by exposure of the tissues to the colorimetric GUS substrate X-Gluc. Representative GUS staining patterns of whole plants **(A)** and stems **(B)** are shown with arrows indicating the vascular tissue and stem nodes, respectively. Thin sections of these tissues **(C-F)** were made and observed by light microscopy at two different magnifications. Ph = phloem, Xy = xylem. Size bars in A and B are 10 mm, C and D are 100 μm, and E and F are 50 μm.

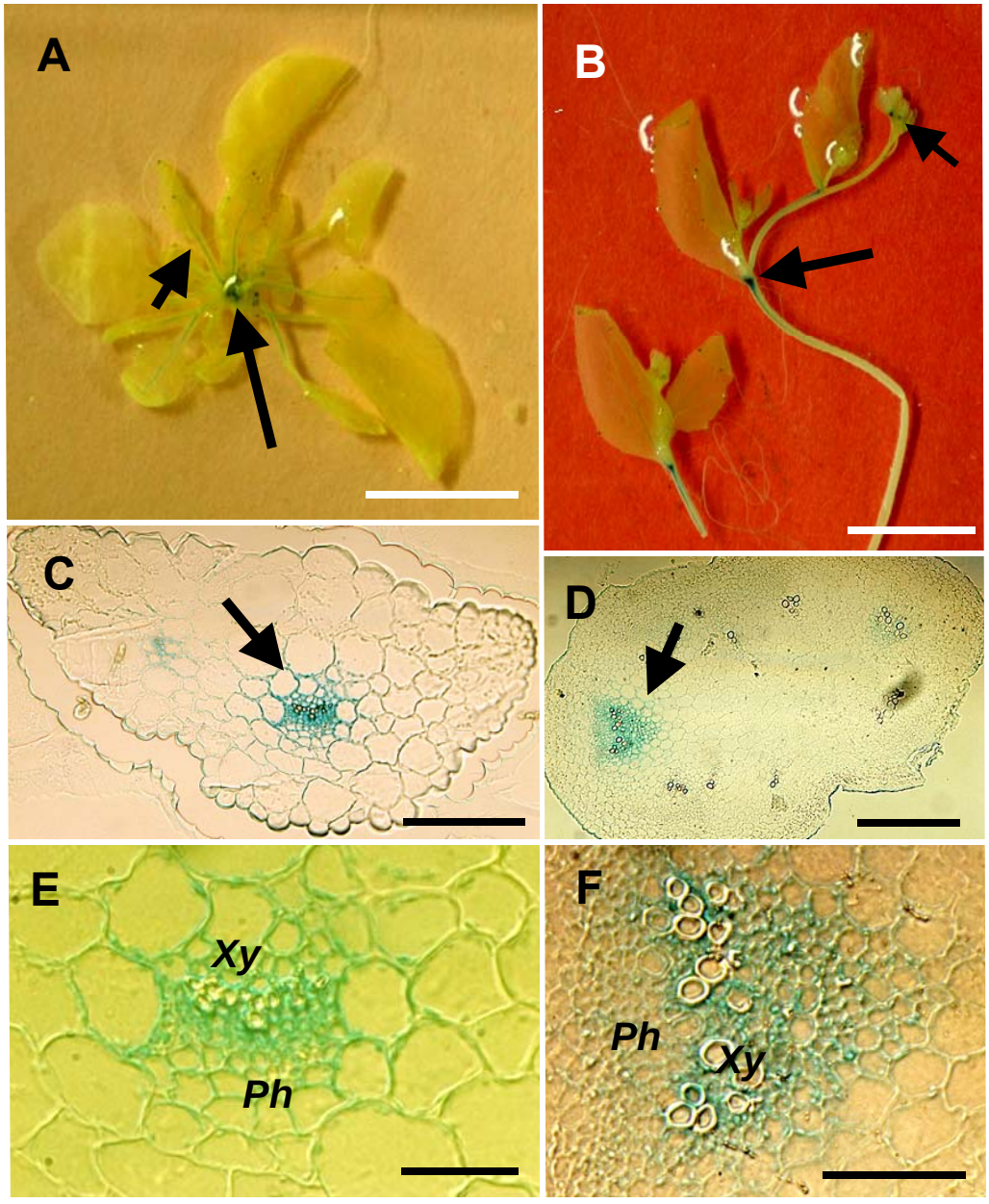
A
B
C
D
E
Xy
Ph
F
Ph
Xy

Phenotypic analysis of leaf development in AtNIP6;1 T-DNA knockout plants

To investigate the physiological function of AtNIP6;1, two independent T-DNA mutant alleles with insertions in the AtNIP6;1 gene were obtained from the SALK T-DNA insertional mutagenesis library and subjected to phenotypic analysis. Genotyping and sequencing analysis confirmed that *nip6;1-1* and *nip6;1-2* mutant lines contain a T-DNA insert in the first and fourth exons of the AtNIP6;1 gene, respectively. Figure **3.27A** and **B** show the leaf developmental phenotypes of AtNIP6;1 T-DNA mutants under normal and boric acid-limiting conditions.

When sufficient boric acid is present in the hydroponic growth media, AtNIP6;1 mutants are phenotypically indistinguishable from wild-type Arabidopsis Col-0 plants. However, AtNIP6;1 T-DNA mutant plants show obvious expansion abnormalities in the young leaves under boric acid-limiting conditions. Thin sections of young leaves isolated from wild-type and AtNIP6;1 mutant plants grown under boric acid-limiting conditions (Figure **3.27C** and **D**) revealed decreased cell expansion and a decreased volume of intracellular air spaces in the AtNIP6;1 mutant plants. This phenotype is only observed in young leaves, suggesting loss of AtNIP6;1 function may affect boric acid distribution to these sink tissues.

Boric acid-tracer analysis coupled with ICP-MS was used to investigate boric acid transport defects in AtNIP6;1 mutant plants in vivo. Plants were grown in media containing ^{11}B boric acid and then abruptly transferred to media containing ^{10}B boric acid for 24 hours. The accumulation of ^{10}B boric acid was then measured by ICP-MS in various tissues of wild-type and AtNIP6;1 mutant plants. Figure **3.28A** indicates that under these experimental conditions, both AtNIP6;1 mutant alleles show reduced

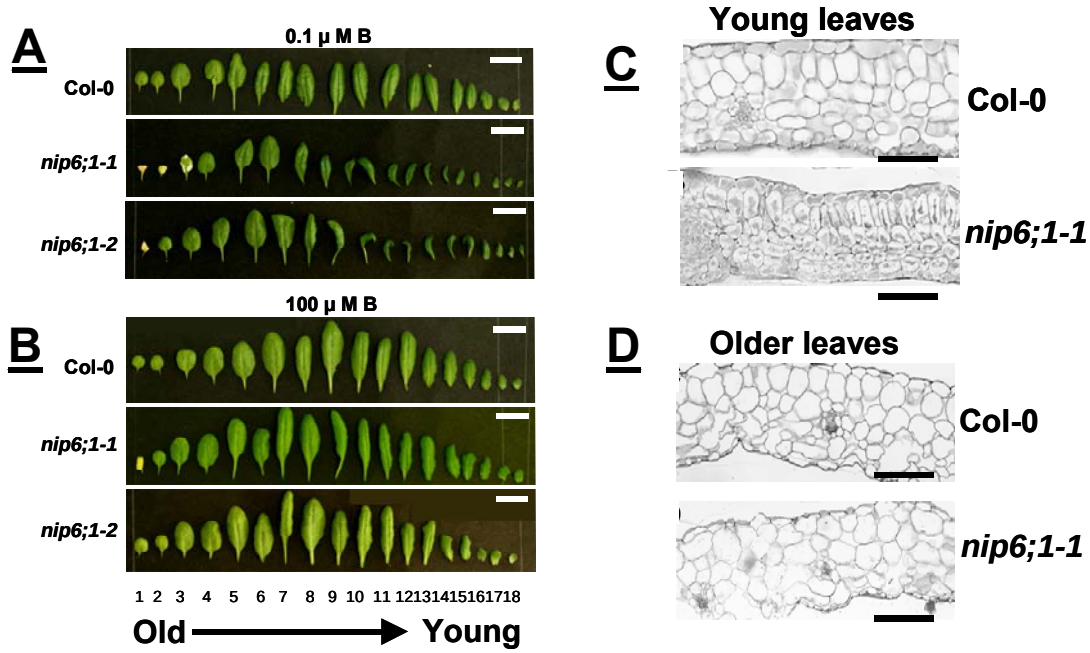

Figure 3.27: Analysis of leaf development in two T-DNA insertion alleles of AtNIP6;1: 28 day old wild-type (Col-0) Arabidopsis plants were hydroponically grown along with 2 AtNIP6;1 T-DNA insertion mutants (*nip6;1-1* and *nip6;1-2*) under conditions of boric acid deprivation (0.1 µM boric acid; **A**) or sufficient boric acid to support normal plant growth (100 µM boric acid; **B**). Leaves were dissected from the plant, numbered, and aligned according to leaf age. An arrow indicates the procession of leaf age from young to old leaves. Size bars represent 5 mm. Thin sections of young leaves **(C)** and older leaves **(D)** of wild-type as well as nip6;1-1 plants grown in media with 1 µM boric acid are shown. Size bars represent 50 µm.

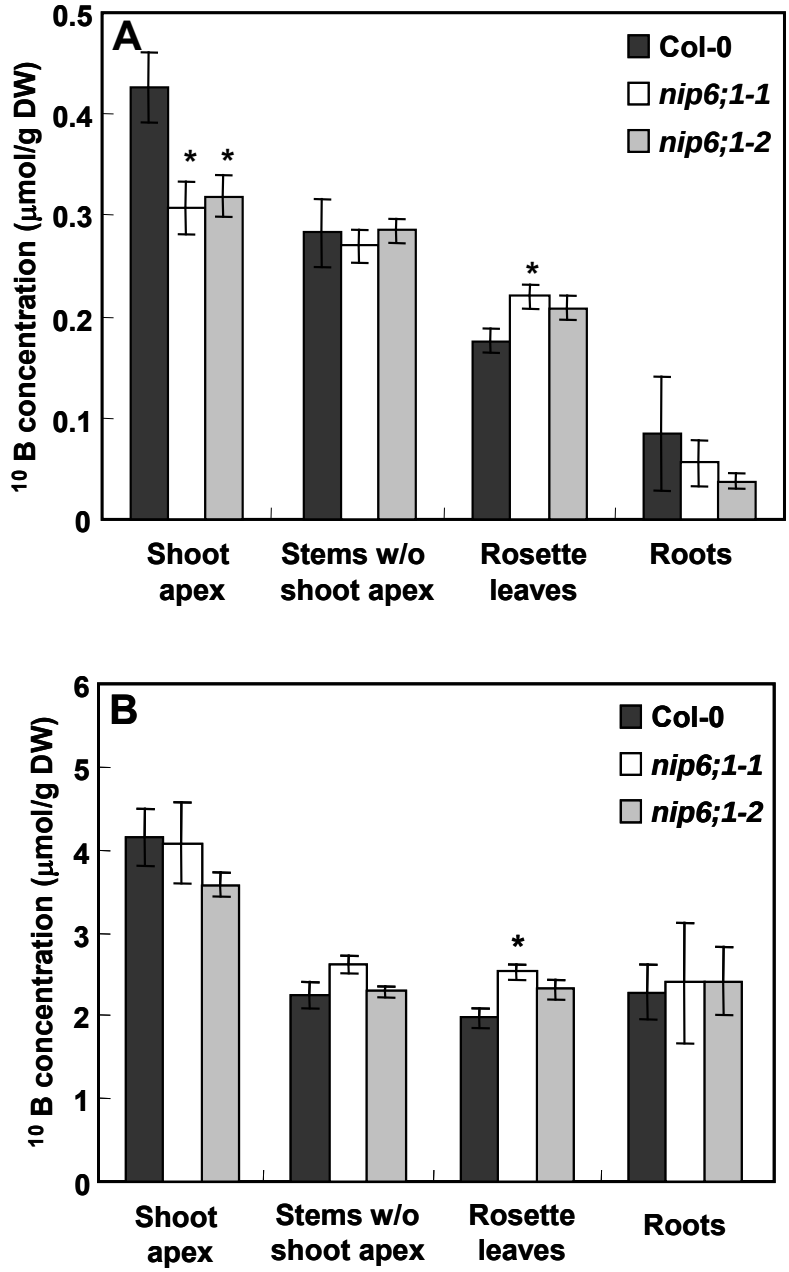

Figure 3.28: Analysis of the boric acid distribution in wild-type and AtNIP6;1 mutant alleles: Wild-type (Col-0) and AtNIP6;1 T-DNA insertion Arabidopsis plants were grown for 28 days in media containing 10 µM ^{11}B-boric acid, and then transferred to hydroponic culture in media containing 1 µM ^{11}B for 24hr. The plants were then pulsed with media containing 0.3 **(A)** or 100 **(B)** µM ^{10}B boric acid, and the uptake of this compound was quantified in plant tissues using ICP-MS. Solid black bars indicate wild-type plants, white bars indicate *nip6;1-1* mutant line, and gray bars represent *nip6;1-2* mutant line. Error bars represent standard deviation (n=3-5). Asterisks indicate significant differences from Col-0 plants as calculated by a student t-test ($P<0.05$).

boric acid transport to the shoot apex under boric acid-limiting conditions, while boric acid transport to older leaves is slightly increased. These boric acid transport defects were not observed when plants were supplied with high boric acid concentrations (Figure **3.28B**), suggesting that passive diffusion of boric acid across cell membranes is sufficient to support plant growth under these conditions.

The C-terminus of Nodulin 26 serves as a regulatory and protein interaction domain

Nodulin-26 phosphorylation and its effect on water permeability

Although the ar/R region is a critical determinant for MIP channel selectivity, the transport rates of solutes can be modulated by a variety of external stimuli, including pH (Tournaire-Roux et al., 2003), Ca^{2+} cations (Verdoucq et al., 2008), as well as post-translational phosphorylation (Johansson et al., 1998), and accumulating evidence suggests that many of these MIP regulatory sites are located in cytosolically-exposed regions of the protein. Nodulin-26 was initially described as a substrate for a symbiosome membrane-associated Calcium-Dependent Protein Kinase (CDPK; Weaver et al., 1991; Weaver and Roberts, 1992), and this kinase uniquely phosphorylates nodulin-26 on Ser 262 in the cytosolically-exposed C-terminus. To investigate the potential regulatory role of post-translational phosphorylation on nodulin-26 water permeability, functional analysis of phosphorylated and dephosphorylated nodulin 26 was performed using stopped-flow fluorimetry and *Xenopus* expression techniques.

While *Xenopus* oocytes do not express plant-specific CDPKs, the nodulin-26 C-terminus can serve as an in vitro substrate for Protein Kinase Cα (PKC) (Guenther et al., 2003), which can serve as a surrogate kinase for nodulin-26 in this heterologous expression system. Figure **3.29** demonstrates that untreated nodulin-26 expressing oocytes have a three-fold higher water permeability than control oocytes, but when these oocytes are treated with the protein phosphatase 2A inhibitor okadaic acid or with a PKC-activating phorbol ester, the nodulin 26 water permeability increased by an additional 2-3 fold. This effect is dependent on the Ser 262 phosphorylation site because a nodulin-26 phosphonull mutant (Nodulin-26 S262A) showed similar water permeability to wild-type nodulin-26 but did not show enhanced water permeability when treated with these compounds. These results suggest that phosphorylation of nodulin-26 at Ser 262 enhances the water permeability of this channel.

To investigate this regulatory modification further, nodulin-26 water permeability was assayed in isolated symbiosome membrane vesicles. Water permeability measurements can be achieved by loading these membranes with high concentrations of the volume-sensitive dye carboxyfluorescien (CF), followed by rapid exposure of the loaded membranes to a hyperosmotic solution in a stopped-flow fluorimeter (Rivers et al., 1997; Dean et al., 1999). The resulting fluorescence traces show a rapid quenching of CF fluorescence that is related to the osmotic permeability coefficient.

Before water permeability analysis was performed on isolated symbiosome membranes, it was first necessary to generate vesicles containing either phosphorylated or dephosphorylated nodulin 26. This was accomplished by 1:

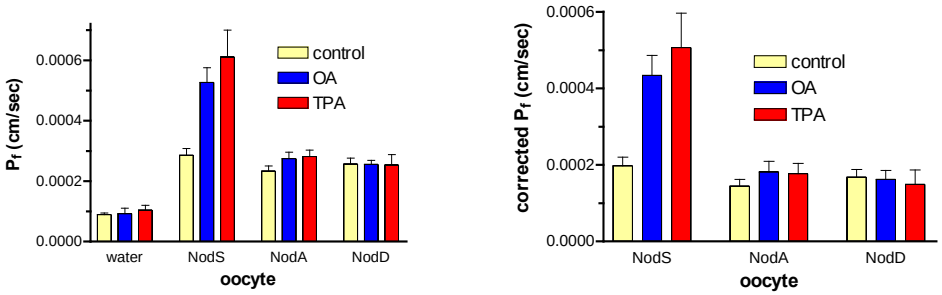

Figure 3.29: Effect of phorbol ester and okadaic acid treatments on nodulin-26 water permeability in oocytes: *Xenopus* oocytes were injected with 46 nL of 1 μg/ μL nodulin-26 or nodulin-26 S262A mutant cRNA and were assayed for water permeability without treatment (yellow bars), after incubation with 25 nM okadaic acid (blue bars), or after treatment with 10 nM TPA (phorbol 12-myristate, 13 acetate; red bars), a protein kinase C agonist. The left panel shows water permeability compared to control oocytes injected with 46 nL of DEPC water. The right panel shows oocyte permeabilities of nodulin-26 and nodulin-26 S262A after correction for changes in the basal water permeability of the oocyte plasma membrane. Error bars represent SEM (n=14 oocytes).

incubation of symbiosome membranes with Ca^{2+} and ATP, which stimulates the in situ phosphorylation of nodulin 26 by the symbiosome membrane CDPK (Weaver et al., 1991) or 2: incubation with alkaline phosphatase, which removes the phosphate from nodulin 26 (Ouyang et al., 1991). To test the success of these treatments, the symbiosome membranes were probed by Western blot analysis with antibodies specific for full-length nodulin-26 (Zhang and Roberts, 1995) as well as an antibody that specifically recognizes the Ser 262 phosphorylation site (anti-GC12P; Guenther et al., 2003). Symbiosome membranes isolated from 35-day-old soybean plants show high amounts of phosphorylated nodulin-26 when probed with this antibody, and these levels are further increased upon stimulation of the endogenous CDPK with Ca^{2+} and ATP. Preincubation of these membranes with calf intestinal alkaline phosphatase (AP) results in a loss of phosphoantibody signal, suggesting that this treatment specifically removes the Ser 262 phosphate (Figure **3.30C**).

The stopped-flow analysis of symbiosome membrane vesicles containing dephosphorylated and phosphorylated nodulin 26 is shown in figure **3.30A** and the calculated P_f is shown as a histogram in figure **3.30 B**. These results show that phosphorylation of nodulin 26 stimulates the P_f by three-fold and are in excellent agreement with the oocyte water permeability analysis. Since nodulin-26 is uniquely phosphorylated at Ser 262 (Weaver and Roberts, 1992), these results together with the results of *Xenopus* oocyte swelling assays (Figure **3.29**) strongly suggest that the decrease in water permeability of AP treated symbiosome membranes is specifically due to nodulin-26 dephosphorylation at this regulatory site.

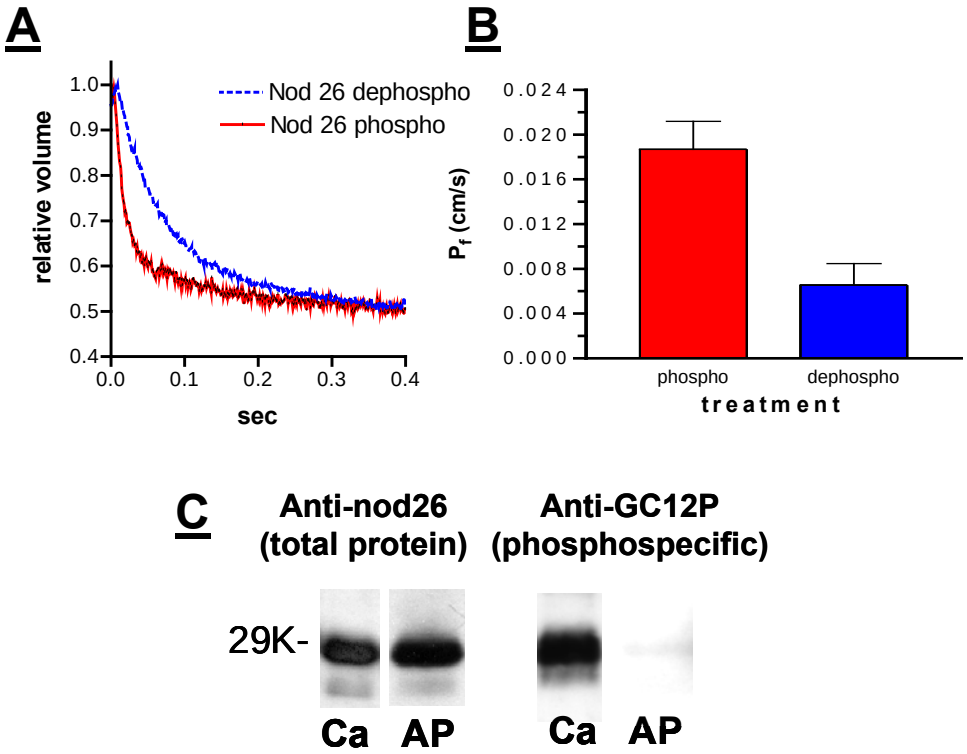

Figure 3.30: Effects of nodulin 26 phosphorylation on water permeability of isolated symbiosome membrane vesicles: **A.** Stopped-flow fluorimetry traces showing the change in internal volume of symbiosome membranes loaded with 20 mM carboxyfluorescien upon doubling the medium osmolarity. The red line represents ATP/ Ca^{2+} treated (Nodulin-26 phosphorylated) symbiosomes, while the blue dotted line represents symbiosomes pre-treated with alkaline phosphatase (dephosphorylated nodulin-26). **B.** The osmotic permeability coefficient (P_f) was calculated from stopped-flow traces similar to those in A using the osmotic permeability equation described in Materials and Methods. Error bars represent SEM (n=3). **C.** Isolated symbiosome membranes were probed by Western blot analysis using anti-nodulin 26 antibody (Zhang et al., 1995) to determine nodulin-26 whole protein levels, as well as a phosphorylation-specific antibody (anti-GC12P; Guenther et al., 2003) to determine phosphorylation status. Membranes were treated with either Ca^{2+}/ ATP to activate the endogenous symbiosome membrane CDPK, or alkaline phosphatase (AP) to remove the S262 phosphate. A 29 kDa molecular weight marker is shown to the left of the blot to indicate the position of nodulin-26.

Sequence alignment of the available NIP subgroup I sequences from Arabidopsis, corn, and rice indicate that the CDPK consensus recognition residues as well as the putative phosphorylated Ser residue are highly conserved among this subclass of NIPs (Table **3.5**), suggesting that C-terminal NIP phosphorylation may constitute a common regulatory mechanism that modulates the channel activity of these proteins.

Isolation and characterization of nodule soluble proteins that interact with the C-terminus of nodulin-26

The C-terminus of MIPs can not only regulate channel activity through posttranslational modifications, but also can affect the subcellular localization of these proteins through protein trafficking (e.g. AQP2 from mammalian tissues; Takata, 2006). In these cases, the MIP C-terminus serves as an interaction domain for proteins related to subcellular trafficking (Noda et al., 2004a; Noda et al., 2004b). Also, MIPs are often the major protein component of their resident membranes, suggesting that these proteins can serve as docking sites for the localization of soluble proteins. For example, nodulin-26 is clearly the major protein component of the symbiosome membrane, constituting 15% of the total membrane protein mass (Weaver et al., 1991; Rivers et al., 1997). This observation led to the hypothesis that nodulin-26 may serve as an interaction site for proteins in the nodule cytosol that are involved in symbiosome function.

Table 3.5: Analysis of NIP subgroup I CDPK phosphorylation sites

Gene[a]	Peptide Sequence[b]
AtNIP1;1	***I*TK**SG**S**FLK
AtNIP1;2	***I*TK**SG**S**FLK
AtNIP2;1	***F*SK**TG**S**SHK
AtNIP4;1	***L*TK**SA**S**FLR
AtNIP4;2	***L*TK**SA**S**FLR
ZmNIP1;1	***I*TK**ST**S**FLK
OsNIP1;1	***I*TK**LSG**S**FLK

[a]The gene of interest is shown. At is an abbreviation for *Arabidopsis thaliana*, Zm is an abbreviation for *Zea mays*, and Os is an abbreviation for *Oryza sativa*.

[b] The peptide sequence in each predicted protein is shown with the putative phosphorylated serine residue underlined and the CDPK consensus phosphorylation site residues in italics (hydrophobic-X-basic-X-X-Ser/Thr; Wallace et al., 2006).

To investigate the possibility that the C-terminus of nodulin-26 serves as an interaction site for proteins in the nodule infected cell cytosol, a peptide mimicking the C-terminus of nodulin-26 (CI-14 derived from LjNod26; Figure **3.31A**) was synthesized and coupled to ω-aminohexyl agarose as a solid support. A nodule soluble protein extract was chromatographed across this affinity resin, and after extensive washing, bound proteins were eluted with 6M urea. The eluate was separated on an SDS-PAGE gel to determine whether any proteins from the soluble extract bound to the CI-14 affinity column.

Figure **3.31B** indicates that a group of 38-40 kDa proteins were specifically purified on the CI-14 resin. These proteins were reproducibly eluted with denaturing urea concentrations, but were highly resistant to elution under a variety of tested conditions including low and high pH, high ionic strength (1 M NaCl), detergents, and high magnesium concentrations, suggesting that the interaction is robust. The proteins were gel excised, trypsinized, and subjected to MALDI-TOF mass fingerprint analysis to determine the identity of the purified proteins. The MALDI-TOF data presented in figure 3.31C was used to conduct a database search of the NCBI non-redundant protein library using the PROWL mass spectral identification algorithm. This search identified soybean glutamine synthetase β1 as the most likely candidate protein to produce this mass fingerprint. Additional MALDI-TOF experiments confirmed this identification with a correct identification expectation value of 6.1×10^{-5} and 56 % glutamine synthetase sequence coverage. The putative peptide fragments from this analysis are presented in Table **3.6**.

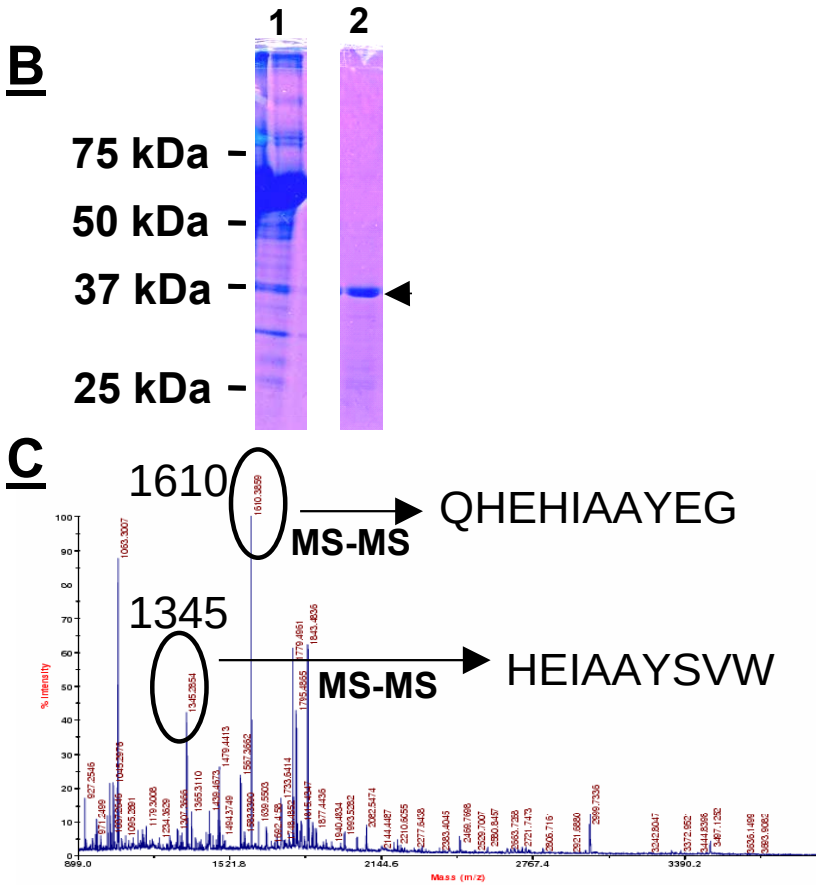

Figure 3.31: Isolation of nodule soluble proteins that interact with a nodulin-26 C-terminal peptide: **A.** The sequence of CI-14, a synthesized peptide mimicking the C-terminus of LjNod26, is shown. **B.** The CI-14 peptide was coupled to ω-aminohexyl agarose, and a nodule soluble protein fraction was chromatographed across the CI-14 agarose. Bound proteins were eluted with 6M urea, and were separated on a 12.5% (w/v) SDS-PAGE gel. Lane 1: nodule soluble fraction, Lane 2: 6M urea eluate. An arrow indicates that position of the major protein purified from this process. Molecular weight markers are indicated to the left of the gel. **C.** The area indicated by the arrow in B was gel excised, trypsinized, and subjected to MALDI-TOF mass spectrometry. Peptides corresponding to the circled mass peaks were sequenced by subsequent MS/MS analysis, and their sequences are indicated to the right of the mass peak.

Table 3.6: Summary of predicted glutamine synthetase peptides from MALDI-TOF:

Measured mass (Da)[a]	Predicted mass (Da)[a]	Error (Da)[b]	Residue indices[c]	Sequence[d]
692.392	692.385	.007	219-223	YILER
785.382	785.334	.048	327-332	GYFEDR
814.532	814.491	.041	268-275	AAIDKLGK
1436.042	1435.755	.287	39-52	TLPGPVSDPSELPK
1610.022	1609.759	.263	277-290	HKEHIAAYGEGNER
1737.602	1737.854	-.252	276-290	KHKEHIAAYGEGNER
1779.212	1778.902	.310	19-34	VIAEYIWIGGSGMMMDLR
1812.332	1812.039	.293	224-240	ITEIAGGGVVVSFDPKIPK
1843.212	1842.901	.312	296-311	HETADINTFLWGVANR
2356.362	2356.172	.190	85-106	GNNILVICDAYTPAGEPIPTNK
2512.562	2512.273	.289	85-107	GNNILVICDAYTPAGEPIPTNKR
2512.562	2512.273	.289	84-106	RGNNILVICDAYTPAGEPIPTNK
2668.442	2668.374	.068	84-107	RGNNILVICDAYTPAGEPIPTNKR
2946.632	2946.479	.153	113-137	VFSHPDVVAEVPWYGIEQEEEYTLLQK
2999.612	2999.392	.220	53-79	WNYDGSSTGQAPGEDSEVILYPQAIFR
3017.392	3017.416	-.023	138-165	DIQWPLGWPVGGFPGPQGPYYCGVGADK

[a] The experimental mass of each peptide from the MALDI-TOF experimental spectrum is shown along with the theoretical mass of the corresponding tryptic digest peptide from soybean glutamine synthetase β1. Each mass is reported in Daltons.

[b] The error between the experimental and theoretical masses of each peptide is shown

[c] The amino acids of soybean glutamine synthetase β1 corresponding to each peptide are shown

[d] The derived primary sequence of each soybean glutamine synthetase β1 peptide is shown.

MS/MS sequence analysis indicates that two peptides common to both spectral sets contain sequences corresponding to highly conserved regions of the glutamine synthetase catalytic domain (Figure **3.31C**).

To independently verify the identification of the 38-40 kDa proteins interacting with the CI-14 resin as glutamine synthetase, the ability of glutamine synthetase enzymatic activity to associate with CI-14 agarose was tested. In this experiment, nodule soluble protein extract was applied to CI-14 resin, and the bound glutamine synthetase enzymatic activity, as well as glutamine synthetase enzymatic activity remaining in the supernatant after incubation, was determined. Underivitized ω-aminohexyl agarose and ω-aminohexyl agarose coupled to an unrelated peptide (CP-13) were used as negative controls (Figure **3.32B**). Greater than 85% of the applied glutamine synthetase activity was bound by the CI-14 resin, while underived ω-aminohexyl agarose bound about 3% of the applied glutamine synthetase activity. CP-13 agarose bound 40% of the glutamine synthetase activity applied but was much less efficient at binding glutamine synthetase activity than CI-14 agarose.

As previously stated, LjNod26 is a nodulin-26 orthologue, and the CI-14 peptide was used because it was readily available as a reagent from previous antibody immunization experiments. To directly verify that glutamine synthetase interacts with the C-terminal sequence of soybean nodulin-26, a peptide comprising the entire cytosolic C-terminal domain of soybean nodulin-26 (CK-25; Figure **3.32A**) was synthesized and coupled to ω-aminohexyl agarose. As shown in figure **3.32C**, CK-25 agarose quantitatively binds glutamine

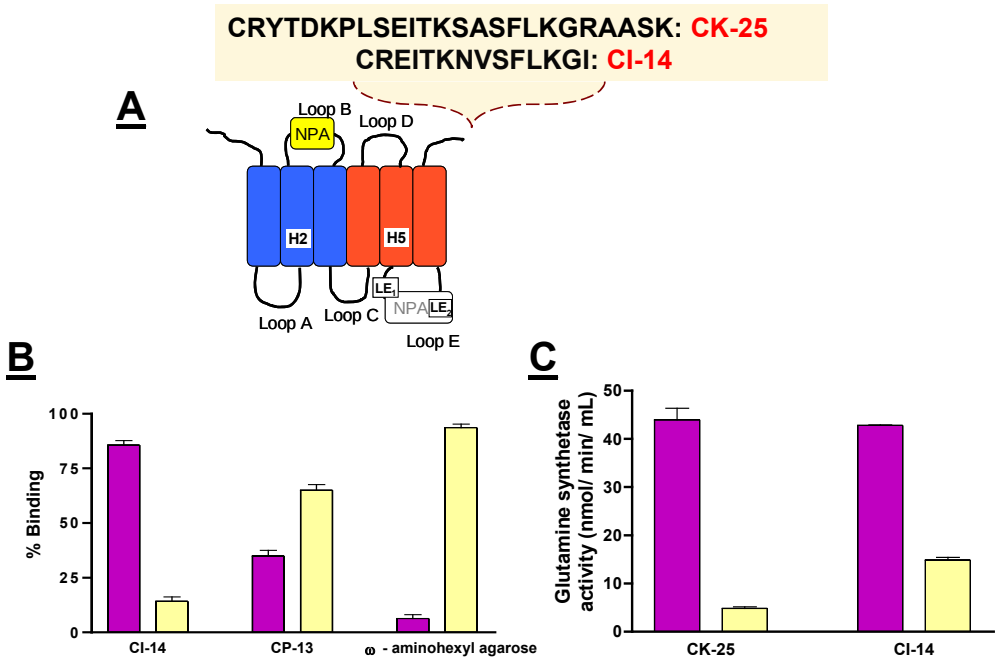

Figure 3.32: Interaction of glutamine synthetase with affinity resins: **A.** A one-dimensional topology map of nodulin-26/ LjNod26 is shown with the sequence and relative positions of the CI-14 and CK-25 peptides. **B.** 50 units of glutamine synthetase activity were incubated with CI-14 conjugated agarose. The remaining supernatant was removed, and the resin (magenta bars) as well as the supernatant (yellow bars) were assayed for glutamine synthetase activity. Experiments were standardized to % activity by dividing the activity present in each sample by the total input activity. Untreated ω-aminohexyl agarose, or agarose conjugated to an unrelated peptide (CP-13) were used as negative controls Error bars represent SEM (n=6-11). **C.** Similar resin association experiments were performed with CK-25 agarose. Magenta bars represent resin associated glutamine synthetase activity, while yellow bars represent glutamine synthetase activity remaining in the supernatant. Error bars represent SEM (n=3).

synthetase activity, suggesting that conserved amino acids present in both of these peptides constitute a glutamine synthetase binding site.

To investigate the ability of full-length nodulin-26 to interact with glutamine synthetase, assays were performed to test the specific association of the enzyme with isolated symbiosome membranes. Previous studies have indicated that symbiosome membrane isolation using the Percoll step gradient method produces vesicles with the hydrophilic nodulin-26 C-terminus on the outside of the vesicles. Symbiosome membranes were purified in this manner and were assayed for glutamine synthetase activity (Figure **3.33**). Interestingly, isolated symbiosome membranes contain a small amount of bound glutamine synthetase enzymatic activity, suggesting that this enzyme is naturally associated with symbiosome membranes and remains bound throughout the isolation procedure. Additionally, a previous proteomic analysis (Catalano et al., 2004) supports the finding that symbiosome membranes possess peripherally associated glutamine synthetase. Incubation of isolated symbiosome membrane vesicles with soluble glutamine synthetase results in additional adsorption of the enzyme activity to the symbiosome membrane sample. While these experiments show a clear association of glutamine synthetase with the symbiosome membrane, it is less apparent whether this interaction is dependent on nodulin-26. To investigate the specificity of this enzyme activity adsorption, the ability of CI-14 peptide to inhibit glutamine synthetase binding was assayed. The results of this experiment demonstrate that 10 μM CI-14 completely inhibits the adsorption of glutamine synthetase enzymatic activity to symbiosome membrane (Figure **3.33**)

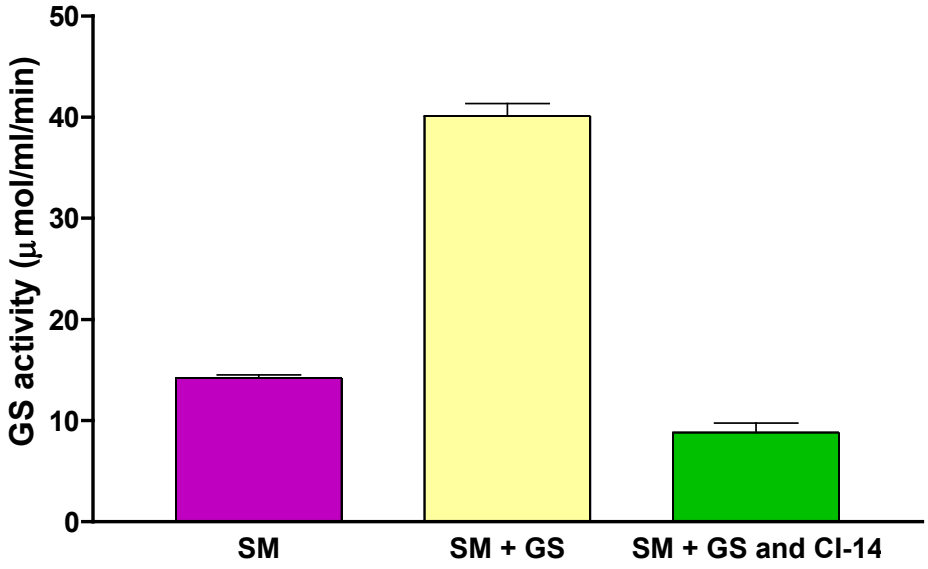

Figure 3.33: Interaction of glutamine synthetase with isolated symbiosome membranes: Isolated symbiosome membranes were assayed for associated glutamine synthetase activity after no treatment (magenta bar), after incubation with 50 units of glutamine synthetase activity (yellow bar), and after incubation with 50 units of glutamine synthetase in addition to 10 µM CI-14 peptide (green bar). Error bars represent SEM (n=3).

suggesting that the nodulin-26 C-terminus is responsible for the adsorption of glutamine synthetase activity.

Overall, these results suggest that glutamine synthetase interacts with both affinity resins that display the C-terminal peptide of nodulin-26 as well as symbiosome membranes, which contain full-length nodulin-26. Interaction specificity is demonstrated by the fact that lower amounts of glutamine synthetase activity associate with underivitized ω-aminohexyl agarose or CP-13 agarose, and that the glutamine synthetase enzymatic activity associating with symbiosome membranes can be eliminated by pre-incubation with a nodulin-26 C-terminal peptide.

To further characterize the interaction between nodulin-26 and glutamine synthetase and determine whether the interaction can potentially take place in vivo, the cytosolic glutamine synthetase isoforms expressed in the nodule were cloned and assayed for their ability to interact with nodulin-26 interaction using the split-ubiquitin yeast two-hybrid system (Obrdlik et al., 2004). Previous studies using partial cDNA sequences indicate that soybean contains at least four cytosolic glutamine synthetase isoforms that are expressed in the nodule (Morey et al., 2002). These enzymes were distinguished by their molecular weight as well as isoelectric point and were designated glutamine synthetase β_1, β_2, γ_1, and γ_2. The authors of this study were able to distinguish these genes based on DNA sequence differences in the 3' untranslated regions (3'-UTR) of the glutamine synthetase isoforms, but were not able to clone the full-length open reading frames of these proteins.

Four unique cytosolic glutamine synthetase isoforms (subsequently named *Glycine max* GS1;1 to 1;4) were cloned using from soybean nodule and root cDNA and their full length amino acid sequences are presented in Figure **3.34**. Amino acid sequence analysis of these proteins indicates that they are greater than 85% identical and are highly similar to the known glutamine synthetases Arabidopsis GLN1;1 as well as Maize GS1a, suggesting that they encode true glutamine synthetase isoforms. Sequence alignment analysis indicates that GmGS1;1 and 1;2 correspond to $GS\beta_1$ and $GS\beta_2$, respectively. GmGS1;3 and 1;4 correspond to the previously reported nodule-enhanced glutamine synthetase isoforms $GS\gamma_1$ and $GS\gamma_2$ (Morey et al., 2002).

Each cloned glutamine synthetase isoform was tested for its ability to interact with nodulin-26 in a split-ubiquitin yeast two-hybrid assay system (Obrdlik et al., 2004). In these assays, the bait protein (nodulin-26) is translationally fused to the C-terminal fragment of ubiquitin (Cub) followed by a synthetic VP-16/ LexA transcription factor. The prey proteins are translationally fused to a modified N-terminal fragment of ubiquitin (Nub) that can only interact with Cub if the bait and prey proteins are in close proximity. If the Nub and Cub fragment interact, they can reconstitute ubiquitin, which is cleaved from the protein complex by a yeast ubiquitin-specific protease, releasing the synthetic VP-16/ LexA transcription factor (Figure **3.35**). This transcription factor is then free to diffuse into the nucleus and activate β-galactosidase (β-gal) and HIS3 reporter genes under the control of the LexA promoter. Therefore, interacting proteins are characterized by the ability to grow on synthetic media lacking histidine as well as the ability to hydrolyze the β-gal substrate X-gal to form blue colonies.

Figure 3.34: Sequence alignment analysis of cloned soybean glutamine syuthetase isoforms: The sequences of GmGS1;1-1;4 were aligned with Arabidopsis glutamine synthetase 1;1 as well as *Zea mays* GS1a using the Clustal W alignment algorithm and BioEdit software. Residue identities in the sequences are colored according to the following color scheme: green; hydrophobic, blue; basic, red; acidic, salmon; serine/ threonine, yellow; proline, and purple; glycine.

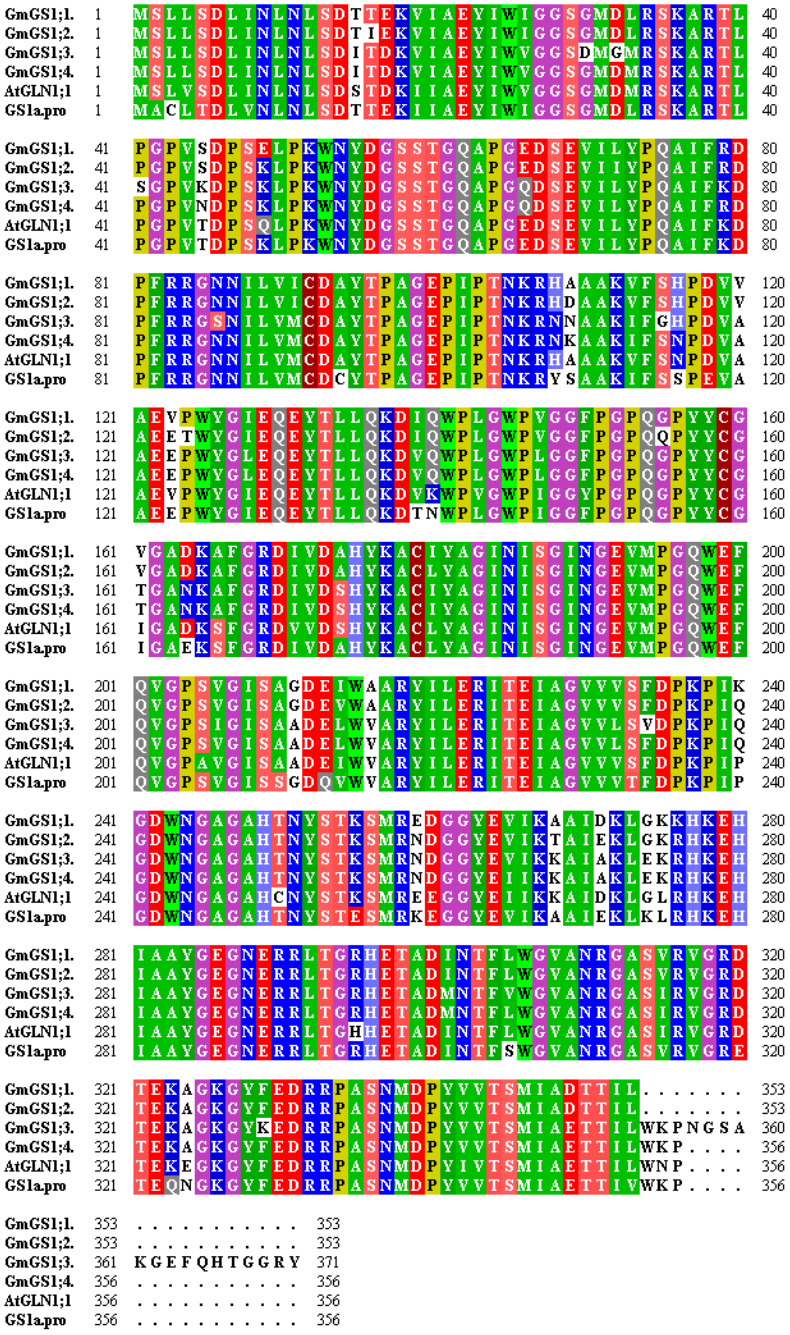
GmGS1;1. 1 MSLLSDLINLNLSDTTEKVIAEYIWIGGSGMDLRSKARTL 40
GmGS1;2. 1 MSLLSDLINLNLSDTTIEKVIAEYIWIGGSGMDLRSKARTL 40
GmGS1;3. 1 MSLLSDLINLNLSDITDKVIAEYIWVGGSDMGMRSKARTL 40
GmGS1;4. 1 MSLLSDLINLNLSDITDKVIAEYIWVGGSGMDMRSKARTL 40
AtGLN1;1 1 MSLVSDLINLNLSDSTDKIIAEYIWVGGSGMDMRSKARTL 40
GS1a.pro 1 MACLTDLVNLNLSDTTEKIIAEYIWIGGSGMDLRSKARTL 40
GmGS1;1. 41 PGPVSDPSELPKWNYDGSSTGQAPGEDSEVILYPQAIFRD 80
GmGS1;2. 41 PGPVSDPSKLPKWNYDGSSTGQAPGEDSEVIIYPQAIFRD 80
GmGS1;3. 41 SGPVKDPSKLPKWNYDGSSTGQAPGQDSEVILYPQAIFKD 80
GmGS1;4. 41 PGPVNDPSKLPKWNYDGSSTGQAPGQDSEVILYPQAIFRD 80
AtGLN1;1 41 PGPVTDPSQLPKWNYDGSSTGQAPGEDSEVILYPQAIFKD 80
GS1a.pro 41 PGPVTDPSKLPKWNYDGSSTGQAPGEDSEVILYPQAIFKD 80
GmGS1;1. 81 PFRRGNNILVICDAYTPAGEPIPTNKRHAAAKVFSHPDVV 120
GmGS1;2. 81 PFRRGNNILVICDAYTPAGEPIPTNKRHDAAKVFSHPDVV 120
GmGS1;3. 81 PFRRGSNILVMCDAYTPAGEPIPTNKRNNAAKIFGHPDVA 120
GmGS1;4. 81 PFRRGNNILVMCDAYTPAGEPIPTNKRNKAAKIFSNPDVA 120
AtGLN1;1 81 PFRRGNNILVMCDAYTPAGEPIPTNKRHAAAKVFSNPDVA 120
GS1a.pro 81 PFRRGNNILVMCDCYTPAGEPIPTNKRYSAAKIFSSPEVA 120
GmGS1;1. 121 AEVPWYGIEQEYTLLQKDIQWPLGWPVGGFPGPQGPYYCG 160
GmGS1;2. 121 AEETWYGIEQEYTLLQKDIQWPLGWPVGGFPGPQQPYYCG 160
GmGS1;3. 121 AEEPWYGLEQEYTLLQKDVQWPLGWPLGGFPGPQGPYYCG 160
GmGS1;4. 121 AEEPWYGLEQEYTLLQKDVQWPLGWPLGGFPGPQGPYYCG 160
AtGLN1;1 121 AEVPWYGIEQEYTLLQKDVKWPVGWPIGGYPGPQGPYYCG 160
GS1a.pro 121 AEEPWYGIEQEYTLLQKDTNWPLGWPIGGFPGPQGPYYCG 160
GmGS1;1. 161 VGADKAFGRDIVDAHYKACIYAGINISGINGEVMPGQWEF 200
GmGS1;2. 161 VGADKAFGRDIVDAHYKACLYAGINISGINGEVMPGQWEF 200
GmGS1;3. 161 TGANKAFGRDIVDSHYKACIYAGINISGINGEVMPGQWEF 200
GmGS1;4. 161 TGANKAFGRDIVDSHYKACIYAGINISGINGEVMPGQWEF 200
AtGLN1;1 161 IGADKSFGRDVVDSHYKACLYAGINISGINGEVMPGQWEF 200
GS1a.pro 161 IGAEKSFGRDIVDAHYKACLYAGINISGINGEVMPGQWEF 200
GmGS1;1. 201 QVGPSVGISAGDEIWAARYILERITEIAGVVVSFDPKPIK 240
GmGS1;2. 201 QVGPSVGISAGDEVWAARYILERITEIAGVVVSFDPKPIQ 240
GmGS1;3. 201 QVGPSIGISAADELWVARYILERITEIAGVVLSVDPKPIQ 240
GmGS1;4. 201 QVGPSVGISAADELWVARYILERITEIAGVVLSFDPKPIQ 240
AtGLN1;1 201 QVGPAVGISAADEIWVARYILERITEIAGVVVSFDPKPIP 240
GS1a.pro 201 QVGPSVGISSGDQVWVARYILERITEIAGVVVTFDPKPIP 240
GmGS1;1. 241 GDWNGAGAHTNYSTKSMREDGGYEVIKAAIDKLGKKHKEH 280
GmGS1;2. 241 GDWNGAGAHTNYSTKSMRNDGGYEVIKTAIEKLGKRHKEH 280
GmGS1;3. 241 GDWNGAGAHTNYSTKSMRNDGGYEVIKKAIAKLEKRHKEH 280
GmGS1;4. 241 GDWNGAGAHTNYSTKSMRNDGGYEIIKKAIAKLEKRHKEH 280
AtGLN1;1 241 GDWNGAGAHCNYSTKSMREEGGYEIIKKAIDKLGLRHKEH 280
GS1a.pro 241 GDWNGAGAHTNYSTESMRKEGGYEVIKAAIEKLKLRHKEH 280
GmGS1;1. 281 IAAYGEGNERRLTGRHETADINTFLWGVANRGASVRVGRD 320
GmGS1;2. 281 IAAYGEGNERRLTGRHETADINTFLWGVANRGASVRVGRD 320
GmGS1;3. 281 IAAYGEGNERRLTGRHETADMNTFVWGVANRGASIRVGRD 320
GmGS1;4. 281 IAAYGEGNERRLTGRHETADMNTFLWGVANRGASIRVGRD 320
AtGLN1;1 281 IAAYGEGNERRLTGHHETADINTFLWGVANRGASIRVGRD 320
GS1a.pro 281 IAAYGEGNERRLTGRHETADINTFSWGVANRGASVRVGRE 320
GmGS1;1. 321 TEKAGKGYFEDRRPASNMDPYVVTSMIADTTIL..... 353
GmGS1;2. 321 TEKAGKGYFEDRRPASNMDPVVVTSMIADTTIL..... 353
GmGS1;3. 321 TEKAGKGYKEDRRPASNMDPVVVTSMIAETTILWKPNGSA 360
GmGS1;4. 321 TEKAGKGYFEDRRPASNMDPYVVTSMIAETTILWKP.... 356
AtGLN1;1 321 TEKEGKGYFEDRRPASNMDPYIVTSMIAETTILWNP.... 356
GS1a.pro 321 TEQNGKGYFEDRRPASNMDPVVVTSMIAETTIVWKP.... 356
GmGS1;1. 353 353
GmGS1;2. 353 353
GmGS1;3. 361 KGEFQHTGGRY 371
GmGS1;4. 356 356
AtGLN1;1 356 356
GS1a.pro 356 356

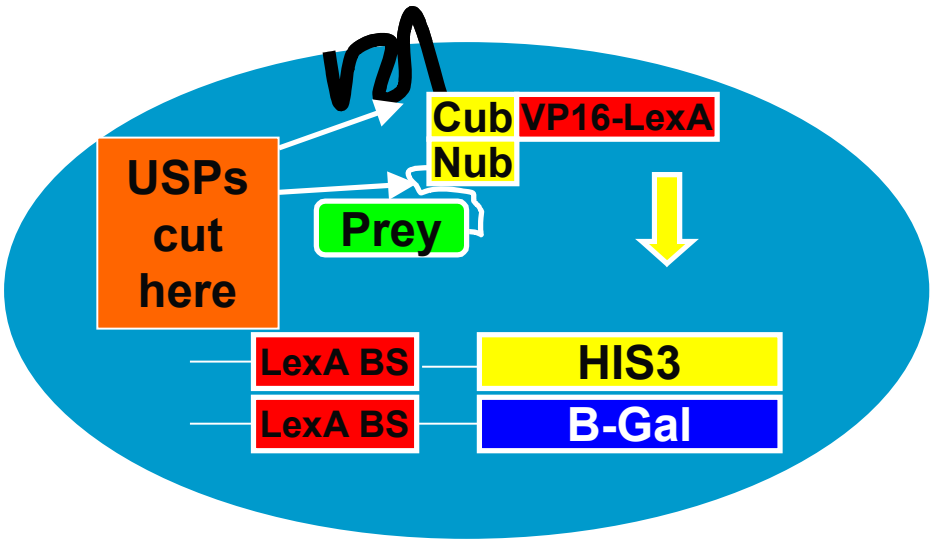

Figure 3.35: Split-ubiquitin yeast two-hybrid methodology: Bait (black line) and prey (green) open reading frames were cloned as described in Materials and Methods into the pMetYCgate and pNXgate32 vectors, respectively. pMetYCgate translationally fuses the bait protein to the C-terminal fragment of ubiquitin (Cub) followed by a synthetic VP16-LexA transcription factor, while the pNXgate32 vector fuses the prey protein to NubG, the N-terminal fragment of ubiquitin with an Ile to Gly mutation. This mutation reduces the basal affinity of the N-terminal fragment for the C-terminal fragment so that they will only reconstitute ubiquitin when the bait and prey proteins are in close proximity (i.e. during a protein interaction). If the two proteins interact, the ubiquitin fragments will form a functional ubiquitin molecule that is released by ubiquitin-specific proteases. This proteolysis event releases the VP16-LexA transcription factor, which diffuses into the nucleus to activate LexA binding sites controlling the expression of the HIS3 and β-galactosidase reporter genes. Once these genes are activated, the yeast strains can produce β-galactosidase, which can be assayed colorimetrically in the presence of X-gal. In addition, HIS3 gene expression is assayed by the ability of each yeast strain to grow on media lacking histidine.

Figure **3.36** illustrates the results of this experiment. Nodulin-26 forms homotetramers like many other MIPs (Fu et al., 2000; Sui et al., 2001; Harries et al., 2004; Tornroth-Horsefield et al., 2006), and AtKAT1 (an Arabidopsis potassium channel) has also been demonstrated to form oligomers by this method (Obrdlik et al., 2004). Therefore, the subunit-subunit interactions between monomers of these proteins serve as excellent positive controls and are among the most robust interactions reported in the interaction screen. The homooligomerization results also suggest that both of these proteins are properly expressed and folded in the yeast heterologous system. Additionally, the wild-type ubiquitin N-terminal fragment serves as a system control because it constitutively interacts with the C-terminal fragment and activates both reporter genes without a prey protein attached (Figure **3.36**). The results of this experiment also demonstrate that each of the four glutamine synthetase isoforms isolated from soybean nodule cDNA are capable of interacting with nodulin-26, as indicated by β-gal and His- growth assays, but none of these isoforms interacted with the Arabidopsis KAT1 potassium channel (AtKAT1).

These results suggest that soybean glutamine synthetase isoforms are capable of interacting specifically with full-length nodulin-26, implying that this interaction is biologically relevant.

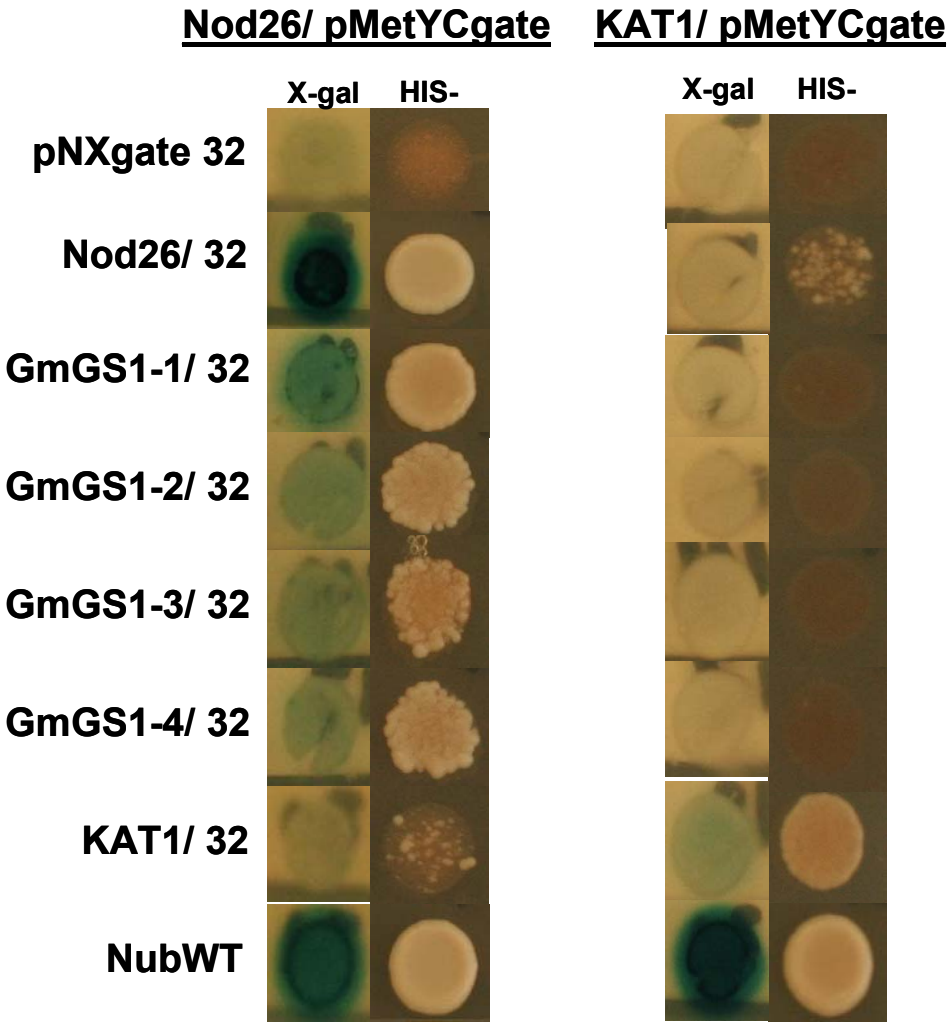

Figure 3.36: Split-ubiquitin two-hybrid screen for interactions between nodulin-26 and specific soybean glutamine synthetase isoforms: The nodulin-26 cDNA was translationally fused to the C-terminal fragment of ubiquitin followed by a synthetic VP-16/ LexA transcription factor. This construct was transformed into yeast strains harboring β-gal and HIS3 reporter genes under the control of the LexA promoter as well as a candidate interacting protein fused to the N-terminal fragment of ubiquitin. Each panel shows β-gal and HIS3 reporter activation for a variety of co-transformed prey plasmids indicated to the left. The Arabidopsis KAT potassium channel was used as a negative control. The homo-oligomerization of KAT1 and nodulin-26 were used as positive controls.

Aphid MIPs involved in gut metabolism and osmoregulation[2]

Metabolic and osmoregulatory concerns arising from aphid feeding behavior

The common pea aphid (*Acyrithrosiphon pisum*) is a hemipteran insect that feeds solely on a diet of plant phloem sap, making this organism a concern for agricultural productivity. Plant phloem sap has an osmotic pressure that is up to four-fold higher than that of the aphid body fluids, and most of the osmolarity can be attributed to sucrose, which is present in concentrations of up to 1 M in phloem sap (Fisher, 2000). In addition, phloem sap does not contain essential amino acids and vitamins that are necessary for aphid metabolism. Due to the chemical composition of this phloem sap and the fact that aphids use this fluid as their sole food source, these insects are presented with two fundamental problems. The high concentrations of sucrose in the phloem sap make this fluid greatly hyperosmotic compared to the aphid tissues, suggesting that osmoregulatory mechanisms must be present in the aphid digestive system to prevent water loss to the gut. Aphids must also be able to produce the essential amino acids, nucleotides, and vitamin-derived cofactors necessary for metabolism, even though they are not present in their food source.

To circumvent these apparent problems, aphids have developed osmoregulatory and metabolic strategies to maintain the ability to live on phloem sap as a sole carbon source. The sucrose in phloem sap is hydrolyzed to fructose and glucose by a gut-localized α-sucrase (Cristofoletti et al., 2003; Price et al., 2007). The fructose is quantitatively assimilated for aphid metabolism, while the glucose is polymerized in the gut and exctreted as honeydew. The transformation of glucose

[2] This work was performed in collaboration with Ally Shakesby and Angela Douglas at the University of York.

monomers to a polymer combined with the rapid metabolism of fructose effectively reduces the osmolarity of the ingested food source providing one mechanism to reduce the osmolarity in the aphid gut. The architecture of the gut itself suggests a putative "water-cycling" mechanism because of the close juxtaposition of the stomach and distal intestine. The close proximity of these digestive tract regions would allow for rapid water flow between the stomach and distal intestine, and in the case of aphids with α-glucosidase activity in the gut, the direction of water transport would be from the distal intestine to the stomach. However, the molecular details of this proposed mechanism remain unknown.

Aphids must also find a source of essential amino acids because their diet does not provide these compounds, and they are crucial for protein synthesis. As a result, aphids form a symbiotic relationship with bacteria of the *Buchnera* genus, and house these bacteria in a specialized group of cells called bacteriocytes (Nakabachi et al., 2005). Inside these cells, *Buchnera* are surrounded by an insect-derived membrane termed the bacteriocyte membrane where these bacteria generate essential amino acids, vitamin derived co-factors, and nucleotide sugars (Douglas, 2006). In exchange, the aphids provide the bacteria with a reduced carbon source, and the proteins on the bacteriocyte membrane must necessarily control this process.

Because both of these developmental adaptations that allow aphids to survive on their unique diet require multiple transport systems, an expressed sequence tag (EST) database generated from gut and bacteriocyte sequences was screened for the presence of transporter genes. Two sequences were isolated from this screen that possess six putative transmembrane domains and the hallmark NPA motifs that are

characteristic of the MIP superfamily. These sequences were named *Acyrthrosiphon pisum* AQP1 and AQP2 (ApAQP1 and ApAQP2), and the following sections describe the function of each of these channels in the context of aphid physiology.

Homology modeling and functional analysis of ApAQP1 and ApAQP2

Homology models of ApAQP1 and ApAQP2 show good agreement with the overall MIP topology, with RMS deviations of 0.88 and 1.04 angstroms from the bovine AQP1 template, respectively (Figure **3.37A**). An analysis of the ApAQP1 ar/R regions indicates that ApAQP1 contains a Phe residue at the H2 position, a His at H5, an Ala at LE_1, and an Arg residue at LE_2. The ApAQP1 H2, H5, and LE_2 ar/R residues are identical to the amino acids observed in the AQP1 template (Figure **3.37B**), but ApAQP1 contains an Ala residue at LE_1, which is a Cys residue in the bovine AQP1 crystal structure. This residue substitution is not likely to alter the function of ApAQP1 because the peptide backbone carbonyl oxygen of the LE_1 ar/R residue usually serves as a hydrogen bond acceptor for the transported water molecule. These results indicate that ApAQP1 contains all of the selectivity determinants to serve as a water-selective channel and predict that ApAQP1 will form a high conductance water channel. In contrast, the ApAQP2 ar/R region consists of a Phe residue at H2, a Ser at H5, an Asn at LE_1, and an Arg residue at LE_2 (Figure **3.37C**). These observations suggest that ApAQP2 has a novel ar/R region that is not typical of animal MIPs, and that this protein may be permeable to unconventional MIP solutes.

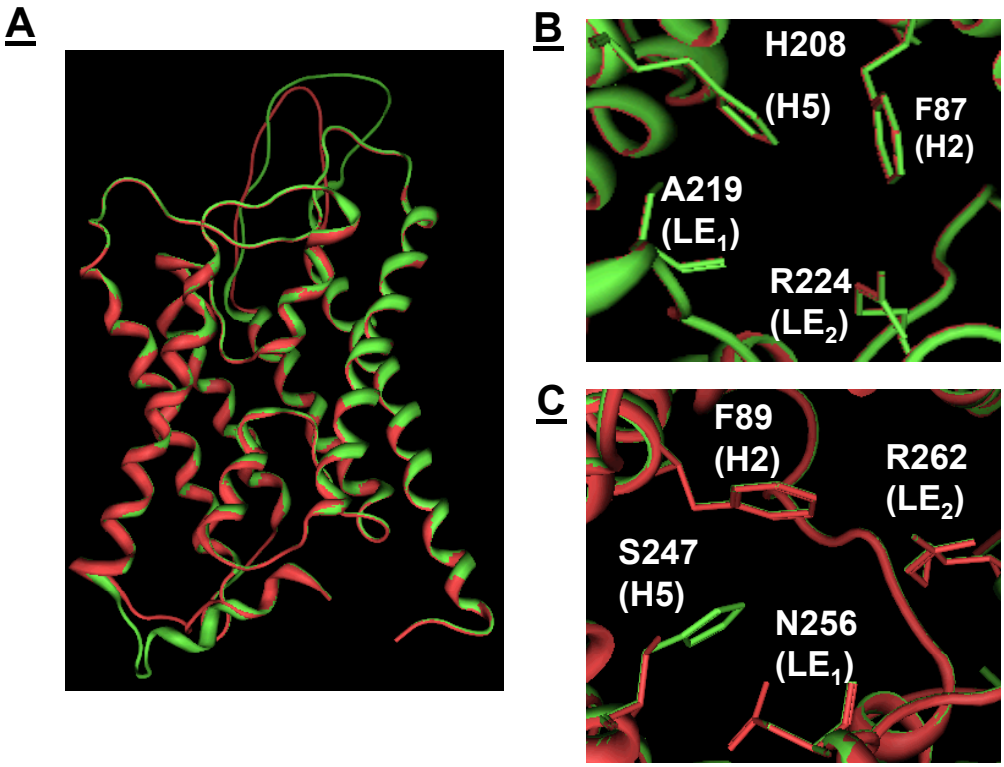

Figure 3.37: Homology modeling and structural analysis of aphid MIPs: Homology models of ApAQP1 and ApAQP2 were generated using the MOE software and bovine AQP1 (1J4N; Sui et al., 2001) as a template. **A.** A representative superposition of the ApAQP1 homology model (red) and the AQP1 experimental structure (green) is shown. Homology models were used to examine the structure of the ApAQP1 (B) and ApAQP2 (C) ar/R regions by superimposing these residues onto the corresponding AQP1 residues. Amino acids of the ar/R region are identified by their single letter amino acid code and residue indices. The H2, H5, LE_1, and LE_2 positions of the ar/R region are indicated in parenthesis.

Functional analysis studies of ApAQP1 and ApAQP2 in *Xenopus* oocytes largely support these conclusions. ApAQP1 show the classical properties of water-selective aquaporins (Preston et al., 1992). For example, ApAQP1-expressing oocytes show a 15-fold increase in water permeability of the oocyte plasma membrane, and this water permeability is inhibited by 66% after treatment with the classical aquaporin inhibitor mercury (II) chloride (Figure **3.38A**). ApAQP1-expressing oocytes also have a decreased activation energy for water transport (3 kcal/ mol) compared to uninjected control oocytes (20 kcal/ mol; Figure **3.38B**). Taken together, these data show that the water permeability exhibited by ApAQP1-expressing oocytes is protein-mediated. Radiolabeled glycerol uptake assays also indicate that the ApAQP1 channel is not permeable to glycerol (Figure **3.38C**). These results suggest that ApAQP1 is a classical water-selective aquaporin channel that is impermeable to larger solutes.

Functional analysis of ApAQP2-expressing oocytes indicates that expression of this channel increases the water permeability of the oolemma by 20-fold. However, this water permeability is not sensitive to $HgCl_2$ or other inhibitors of aquaporin-mediated transport like silver nitrate (Figure **3.39A**). By using the previously described swelling-based assay, a more comprehensive investigation of ApAQP2 substrate selectivity revealed that ApAQP2-expressing oocytes are permeable to an array of linear polyols, including mannitol, ribitol, galacitol, and sorbitol (Figure **3.40B**). ApAQP2 was equally permeable to four, five, as well as six carbon polyols and had virtually no preference to hydroxyl group stereochemistry.

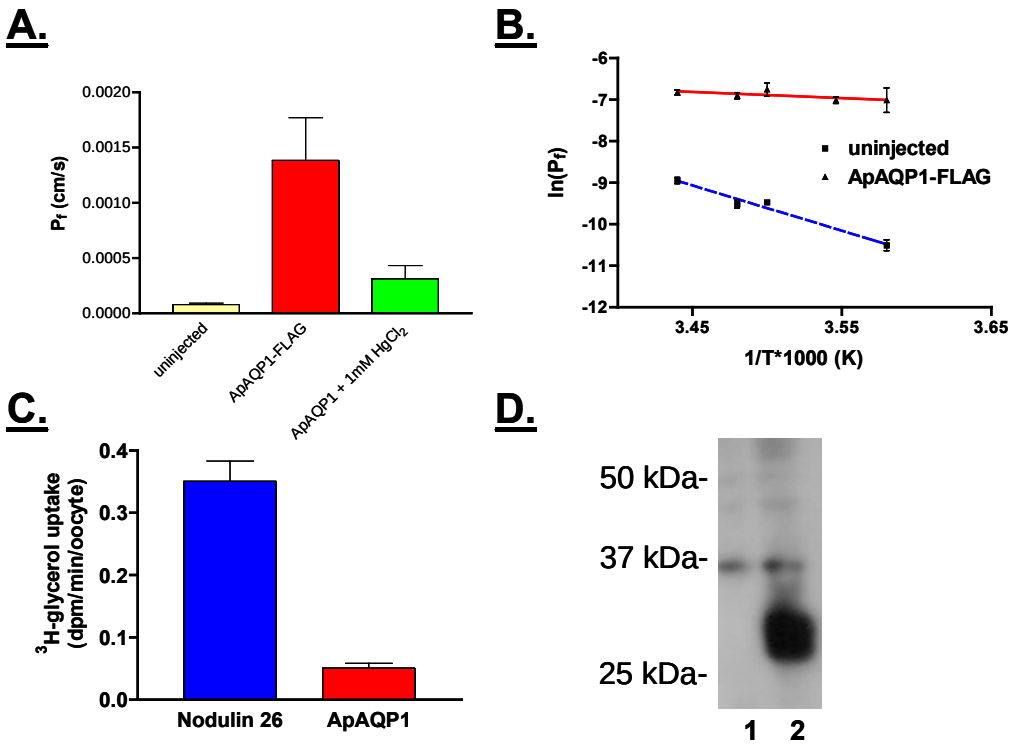

Figure 3.38: Functional analysis of ApAQP1: *Xenopus* oocytes were injected with 46 ng of ApAQP1 cRNA, cultured as previously described (Rivers et al., 1997), and assayed for water and solute permeability. **A.** Uninjected negative control oocytes (yellow bars) and ApAQP1 expressing oocytes (red bars) were assayed for water permeability by video microscopy. ApAQP1 expressing oocytes were also treated with 1 mM $HgCl_2$ for five minutes prior to assay to investigate the mercury-dependent inhibition of water permeability (green) bars. **B.** The activation energy for water transport of uninjected (dashed blue line and squares) and ApAQP1 expressing oocytes (solid red line and triangles) was assayed. The best-fit linear regression from the Arrhenius plot above was used to calculate the activation energy. Error bars represent SEM (n=6-8 oocytes). **C.** ApAQP1 was assayed for radio-isotopic uptake of glycerol (red bars) as described in materials and methods. Nodulin-26 was used as a positive control (blue bars). Error bars represent SEM (n=9). **D.** Ten micrograms of oocyte lysate protein from uninjected controls (lane 1) and ApAQP1- expressing oocytes (lane 2) were subjected to Western blot analysis using an anti-FLAG antibody. The positions of the molecular weight markers are indicated to the left of the blot.

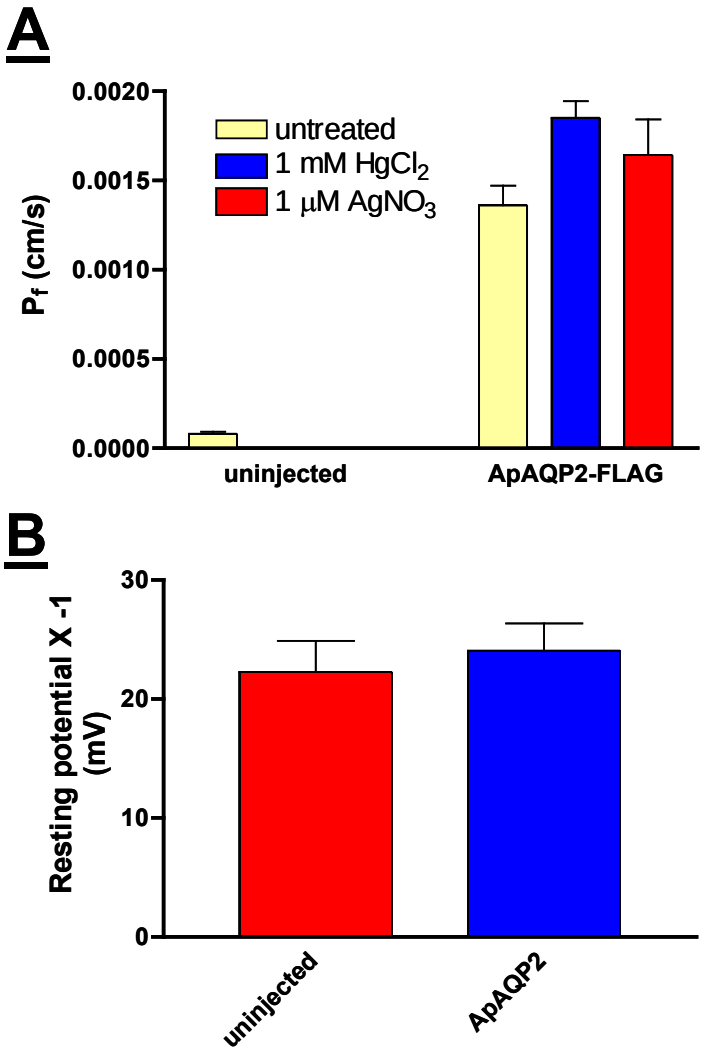

Figure 3.39: Water transport analysis of ApAQP2: *Xenopus* oocytes were injected with 46 ng of ApAQP2 cRNA and assayed for water as well as solute permeability. **A.** The water permeability of ApAQP2-expressing oocytes was assayed using a standard osmotic permeability assay (Guenther and Roberts, 2000). ApAQP2-expressing oocytes were also treated with the water channel inhibiting compounds $HgCl_2$ (blue bars) and $AgNO_3$ (red bars). Uninjected oocytes were used as negative controls. Error bars represent standard deviation (n=6-9 oocytes). **B.** Resting membrane potentials for ApAQP2-expressing (blue bar) and uninjected oocytes (red bar) were recorded. Error bars represent SEM (n=3-4).

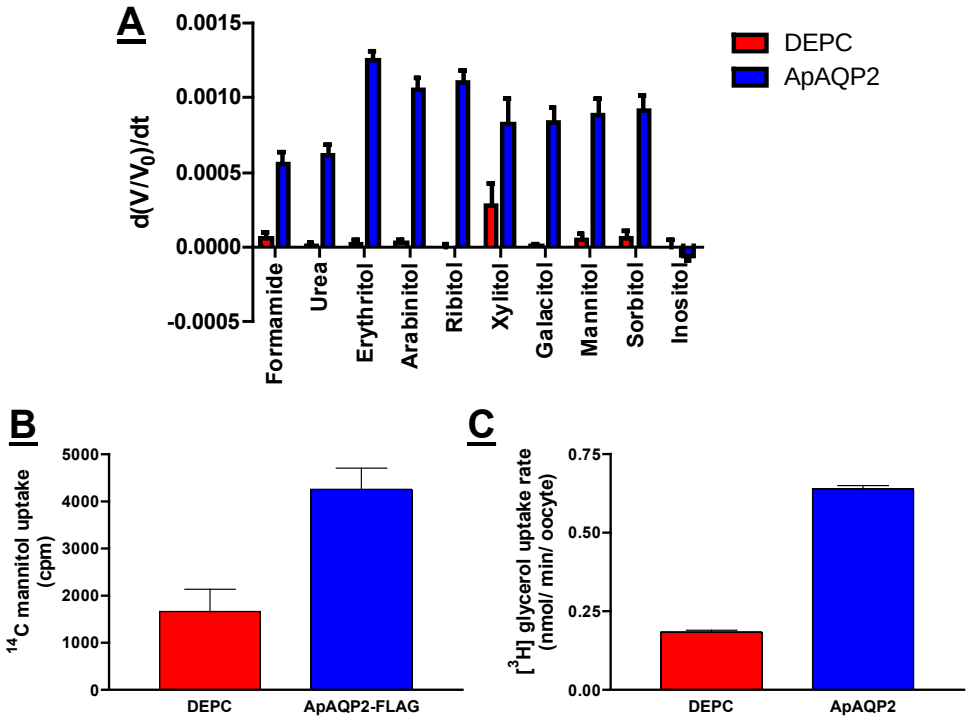

Figure 3.40: Analysis of ApAQP2 solute permeability: *Xenopus* oocytes were injected with 46 ng of ApAQP2 cRNA and assayed for solute permeability. **A.** ApAQP2-expressing oocytes (blue bars) were assayed for permeability to various solutes by video microscopy using the general oocyte swelling assay described in materials and methods. Oocytes injected with 46 nL of DEPC treated water (red bars) were used as negative controls. ApAQP2-expressing oocytes (blue bar) were assayed for mannitol (**B**) and glycerol (**C**) permeability by direct uptake of radio-labeled solute. Oocytes injected with 46 nL of DEPC water (red bar) were used as negative controls. Error bars represent SEM (n=3).

In addition, ApAQP2 was permeable to the uncharged test compounds formamide and urea. The permeability of these compounds is slightly lower than those observed in the polyol series, and these differences in permeability are most likely due to the different shape, and chemical composition of these test substrates. These oocytes were not permeable to the cyclic polyol inositol, suggesting that the ApAQP2 pore is only large enough to accommodate these polyols in their linear form. ApAQP2 permeability to mannitol and glycerol were verified by direct uptake analyses of these radiolabeled substrates. Figure **3.40B** and **C** indicate that ApAQP2-expressing oocytes are 2.5-3 fold more permeable to mannitol and glycerol than negative control oocytes, further supporting that the transported substrates observed in the video microscopy oocyte swelling experiments are transported by ApAQP2. To ensure these novel permeabilities were not due to nonviable oocytes or a compromised oocyte membrane, the resting potentials of uninjected as well as ApAQP2-expressing oocytes were measured (Figure **3.39B**). All oocytes possessed inwardly negative resting potentials between –22 and –25 mV, consistent with the reported membrane potential values of viable oocytes (Dascal, 1987).

These results suggest that ApAQP2 is a high conductance water channel that is also permeable to a defined range of linear polyols. This diversity of transported substrates is unprecedented and highlights the novelty of the ApAQP2 channel. In addition, comparison of ApAQP1 and ApAQP2 substrate selectivity profiles indicate that these proteins are functionally distinct, with ApAQP1 forming a water-selective channel, and ApAQP2 forming a multifunctional water/ solute channel.

Tissue localization suggests roles for ApAQP1 and ApAQP2 in aphid osmoregulation and metabolism

To investigate the cellular localization of the ApAQP1 and ApAQP2 transcripts, complementary in situ hybridization and real-time PCR expression analysis experiments were performed. Real-time PCR analysis was performed using cDNA samples from aphid heads, guts, bacteriocytes, embryos, and fat bodies to quantitate the relative amounts of ApAQP1 and ApAQP2 transcripts in each of these tissues. Figure **3.41A** indicates that ApAQP1 is highly expressed in gut tissue and to a lesser extent in embryo tissue, while ApAQP2 is mainly expressed in isolated bacteriocytes as well as fat bodies (Figure **3.41B**).

In situ hybridization experiments using ApAQP1 and ApAQP2 antisense probes were performed to determine the spatial expression pattern of each transcript in these tissues. Figure **3.42** illustrates a representative in situ hybridization experiment of isolated aphid guts and embryos using an ApAQP1 probe. ApAQP1 is highly expressed in the stomach and distal intestine of the gut, as well as a pair of anterior structures in the embryo that are tentatively identified as the salivary glands (Figure **3.42A** and **B**). In contrast, ApAQP2 is expressed in the embryonic gut in the same region as the bacteriocyte tissue (Figure **3.42C**). The in situ hybridization as well as real-time PCR expression analysis data indicate that ApAQP1 and ApAQP2 have non-overlapping spatial expression patterns. Combined with the distinct functional properties of the two proteins, this work suggests that these proteins may play unique roles in aphid physiology.

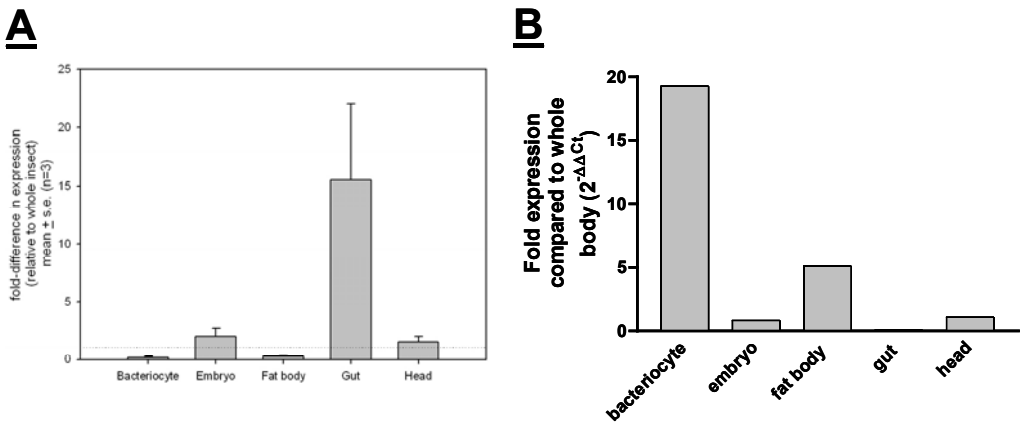

Figure 3.41: Real-time PCR analysis of ApAQP1 and ApAQP2 in aphid tissues: Total RNA was isolated from various aphid tissues (bacteriocytes, embryos, fat bodies, guts, and heads), reverse transcribed to cDNA, and used to quantitate the relative expression of ApAQP1 **(A)** and ApAQP2 **(B)** by real-time PCR expression analysis. Transcripts were standardized to three different reference genes as expression controls and normalized to expression of the tested gene in whole aphid bodies. Error bars represent SEM (n=3).

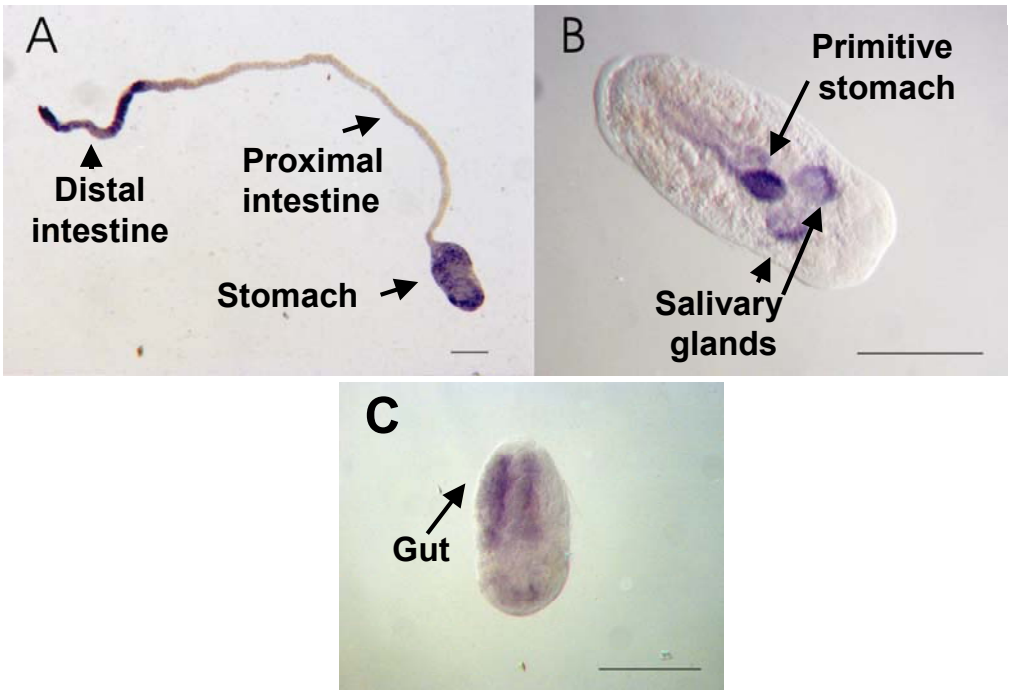

Figure 3.42: Tissue localization of ApAQP1 and ApAQP2 by in situ hybridization: An antisense alkaline phosphatase-labeled ApAQP1 probe was hybridized to dissected gut tissue **(A)** and aphid embryos **(B)**. The positions of the stomach, proximal intestine, distal intestine, and salivary glands are indicated. The size bar in A and B are 100 μm. **C.** An antisense alkaline phosphatase labeled ApAQP2 probe was hybridized to aphid embryos. The location of the primitive gut is indicated. The size bar represents 50 μm.

RNAi mediated knockdown of ApAQP1 indicates that this protein is involved in gut osmoregulation

Since ApAQP1 is expressed in both the stomach and distal intestine (Figures **3.41** and **3.42**), it is possible that this water channel is involved in the the osmoregulation of these two gut compartments as discussed in the introduction. Therefore, reduction of ApAQP1 protein levels should alter the osmoregulatory balance between the gut contents and the aphid hemolymph, and this osmoregulatory dysfunction should be manifested as changes in the hemolymph osmolarity. To test this hypothesis, aphids were fed dsRNA complimentary to ApAQP1 in order to reduce ApAQP1 expression levels, and the hemolymph osmolarity of these insects was measured.

Real-time PCR expression analysis of aphids fed on a diet containing 1 μg/μL ApAQP1 dsRNA indicates that ApAQP1 transcript levels in these insects decreased by 50% after 24 hrs of treatment (Figure **3.43A**). However, the ApAQP1 transcript levels began to increase after 48 hours of treatment and continued to increase for the remaining 3 days of the expression analysis experiment. The body weight of aphids administered ApAQP1 dsRNA or GFP dsRNA was not affected during the time course of the experiment indicating that these insects were healthy and did not lose large amounts of body water during the course of the experiment (Figure **3.43B**). Hemolymph osmolarity analysis indicated that ApAQP1 dsRNA-treated aphids had significantly increased hemolymph osmolarities compared to GFP

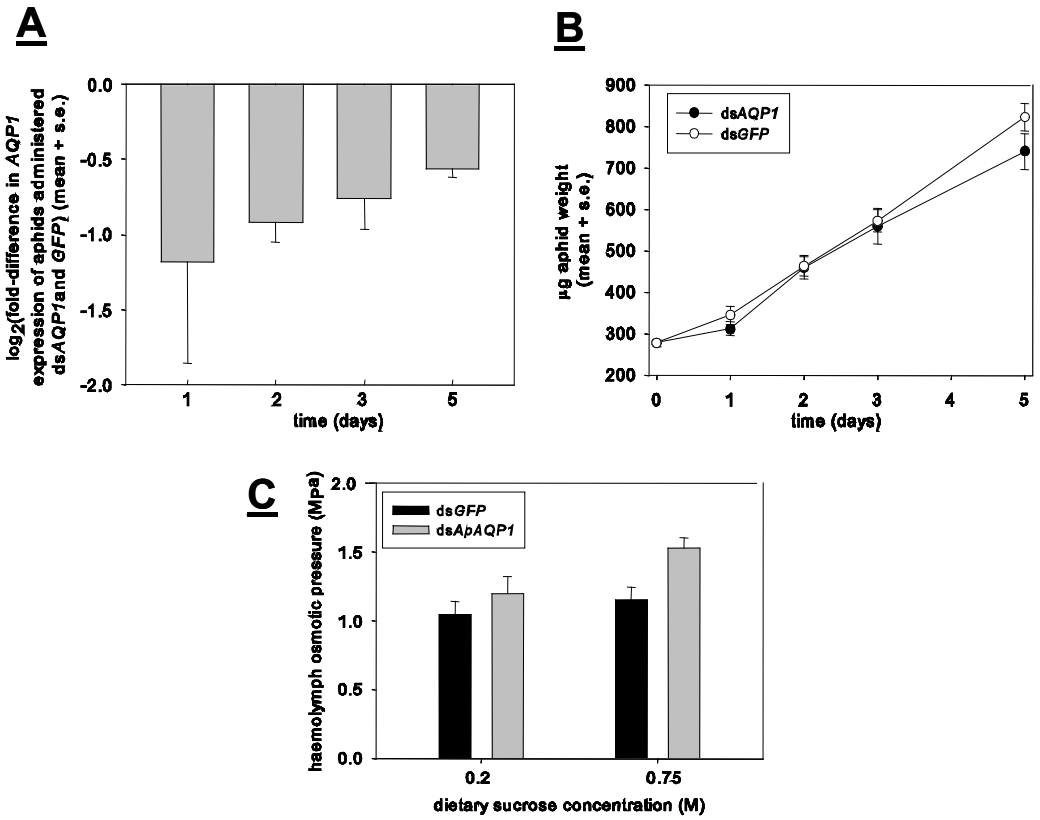

Figure 3.43: ApAQP1 is involved in aphid gut osmoregulation: **A.** Total RNA was isolated from 6-day-old aphids after feeding on a diet containing 1 µg/µL ApAQP1 dsRNA, converted to cDNA, and analyzed for ApAQP1 expression by real-time PCR expression analysis. Timepoints were taken at the number of days indicated, and Ct values were standardized to β-tubulin. Relative expression was compared to aphids administered GFP dsRNA. Error bars represent SEM (n=3). **B.** Aphid body weights were measured over the time course of the knockdown experiment. Error bars represent SEM (n=10-12). **C.** Changes in the hemolymph osmolarity in GFP dsRNA-fed aphids (black bars) and ApAQP1 dsRNA-fed aphids (gray bars) is shown at isoosmotic (0.2 M) and hyperosmotic (0.75 M) sucrose concentrations.

dsRNA-fed aphid controls, and this osmolarity increase was exacerbated by feeding the aphids on a hyperosmotic diet (Figure **3.43C**). These results suggest that even small decreases in ApAQP1 transcript levels result in a disruption of the osmotic balance between the hemolymph and the gut.

Chapter IV

Discussion

Modeling and phylogeny of MIP pore structures: the ar/R selectivity filter

Early analyses of MIPs from animal and microbial sources showed that they generally possess a limited number of ar/R regions with conserved features of either aquaporins or glyceroporins (Thomas et al., 2002). From the present study, it is clear that this paradigm is not adequate to explain the diversity of ar/R regions in all species, and particularly in higher plants. For example, phylogenetic analysis and protein homology modeling of Arabidopsis MIPs suggests greater structural diversity in the pore-determinant sequences, and that the various plant MIPs can be separated into at least 8 distinct ar/R subgroups that are likely to aid in determining the pore architecture and functional properties of each protein. The structural an functional significance of each ar/R subgroup is discussed below.

The TIP and NIP subgroups:

A conserved feature of all NIPs and TIPs characterized, and a characteristic that fundamentally distinguishes them from PIPs as well as most mammalian and microbial aquaporins, is the presence of a conserved aliphatic residue (Ile or Val) at the H5 position of the ar/R region in place of the conventional His residue. TIPs can be further distinguished from NIPs by the residues found at the H2 ar/R position. In the large majority of MIPs, H2 is a hydrophobic aromatic residue (Figures **3.11** and

3.12), but in TIPs, a hydrophilic residue occupies this position. In the case of TIP subgroups I and II, this residue is a highly conserved His. The conserved His/ Ile pair at the H2 and H5 positions of these TIPs is in contrast to most water-specific aquaporins (H2 hydrophobic/ aromatic and H5 His), in that the chemical characteristics of the H2 and H5 positions seem to be reversed. Nevertheless, analysis of the TIP molecular models suggests that the ar/R region remains the zone of narrowest constriction, and likely forms a substrate selectivity filter in these proteins. In this regard, it is interesting to note that MIPs are proposed to have arisen from an ancient gene duplication event (Reizer et al., 1993), and that H2 is homologous to the symmetrically related H5 position. In the case of plant TIPs, the inversion of these residues relative to the majority of animal and microbial aquaporins would conserve the properties of the ar/R region and allow these residues to form similar contacts with transported substrates in three-dimensional space despite having a different locations in the primary sequence.

A comparison of the NIP subgroup I ar/R region (Nodulin-26 like) with those of TIP ar/R group II shows that the key difference is the substitution of a Trp for His at the H2 position. A comparison of the ar/R regions of these subgroups shows that the presence of the Trp at H2 combined with the Val at H5 and the Ala residue at LE_1 results in a wider pore diameter and a nonpolar van der Waals interaction surface for interaction with the methylene backbone of glycerol. In addition, the NIP subgroup I ar/R region has a hydrophilic surface (LE_1 carbonyl and LE_2 Arg sidechain) to facilitate hydrogen bonding to glycerol hydroxyl groups as well as to transported water molecules. This proposed mechanism sharply contrasts from the mechanism

proposed for mammalian and microbial aquaglyceroporins that have an ar/R region that is similar to *E. coli* GlpF, with a Gly at H5 and a Phe or Tyr at LE_1 (Thomas et al., 2002) and could represent a divergent solution to the formation of an aquaglyceroporin channel in plants. Since all characterized members of the NIP subgroup I are aquaglyceroporins (reviewed in Wallace et al., 2006), it is argues that the H2 position may be a critical determinant of NIP and TIP substrate selectivity. This hypothesis is supported by functional analysis experiments that were performed in this study.

Homology modeling and phylogenetic analyses performed as part of this study reveal that the NIP subfamily in terrestrial plants is divided into two distinct pore subfamilies: NIP subgroup I and NIP subgroup II. The ar/R region of NIP subgroup II members differs from that of NIP subgroup I members by a single nonconservative substitution of an Ala for the highly conserved Trp at H2. This substitution results in a doubling of the predicted pore diameter, and permits the permeation of larger solutes. Another unusual feature of NIP subgroup II members is the presence of an Ala to Val substitution in the C-terminal NPA motif, which increases the hydrophobicity and decreases the pore diameter at the NPA region. The effect of this substitution on the selectivity of NIP subgroup II channels and the distinct biological function of these channels will be discussed in greater detail in the following sections.

An interesting observation of the TIP group I ar/R region is the presence of a highly conserved and unusual Val for Arg substitution at the LE_2 position of the ar/R region. The Arg residue at this position is highly conserved in the vast majority of

MIP superfamily members (Park and Saier, 1996; Froger et al., 1998; Engel et al., 2000; Figure **3.11**) and plays a multifunctional role in MIP substrate selectivity. This residue provides hydrogen bonds to transported water in water-selective MIPs (Sui et al., 2001; Savage et al., 2003; Horsefield et al., 2008) as well as to glycerol in aquaglyceroporins (Fu et al., 2000; Newby et al., 2008). Further, in both aquaporins and aquaglyceroporins, the Arg residue also serves as an electrostatic barrier to block transport of positive ions (de Groot and Grubmuller, 2001). In comparison to other plant aquaporins, the modeled ar/R region of TIP subgroup I members shows a reduced capacity to form hydrogen bonds with transported water due to the loss of the Arg at LE_2. Based on the proposed mechanism of the ar/R region in facilitating water transport (Sui et al., 2001; de Groot and Grubmuller, 2001), it could be argued that TIP subgroup I members would exhibit a reduced unitary water conductance rate compared to classical aquaporins with an Arg at the LE_2 position. Indeed, this hypothesis is supported by the observation that the substitution of a Val for Arg at this residue in *E. coli* AqpZ abrogates water transport (Borgnia et al., 1999). However, it is clear that the archetype of the TIP I subfamily (AtTIP1;1) forms a robust water channel upon expression in *Xenopus* oocytes and likely performs this function in tonoplasts in vivo (Maurel et al., 1993). It is possible that water transport through TIP I channels may be dependent upon other ar/R residues as well as residues outside the ar/R region to form contacts with transported water molecules. Structural elucidation of TIP subgroup I members should help to resolve how this unusual proposed pore structure results in a functional water channel.

The PIP subgroup:

Based on homology modeling, the PIP family stands alone as the plant MIP family that most resembles mammalian and microbial aquaporins with respect to conservation of the ar/R region. This family is the only group of plant MIPs that possess the characteristic conserved His at H5, which has been implicated in providing both the steric and hydrogen bonding character to the ar/R region that results in water selectivity (Sui et al., 2001; Savage et al., 2003; Horsefield et al., 2008). Consistent with this observation, functional analysis of most PIP subfamily members indicate that they form water channels upon expression in *Xenopus* oocytes (Kammerloher et al., 1994; Johansson et al., 1998; Chaumont et al., 2000; Li et al., 2000; Katsuhara et al., 2002; Tournaire-Roux et al., 2003; Fetter et al., 2004; Ohrui et al., 2007; Vandeleur et al., 2008). However, a disparity in the transport rates within the PIP subfamily has been observed. PIP1 members form low water conductance channels, while PIP2 members are high conductance water channels (Chaumont et al., 2000). This distinction is intriguing because PIP1 and PIP2 channels not only have identical ar/R residues, but also share complete sequence identity with respect to all residue lining the putative pore, and these residues are highly similar to the pore residues in bovine AQP1. These observations would suggest that the two classes of PIPs should have identical transport selectivities and rates. In this regard, it is important to note that the ar/R region may be one of several determinants that control water or solute flow through the MIP pore. For example, heterotetramerization of PIP1 and PIP2 members, phosphorylation, and pH have all been demonstrated to

regulate the water permeability of PIP water channels and the structural basis for these gating effects will be discussed further in following sections.

The SIP subgroup:

The SIPs are a unique subset of MIPs characterized by an unusually high pI due to the large amount of basic residues at their carboxyl termini (Johanson and Gustavsson, 2002). Based on sequence similarity, the SIP subfamily in Arabidopsis can be divided into two subclasses, SIP1 (with two members) as well as SIP2 (with a single member), and these subdivisions are conserved in other plants (Chaumont et al., 2001; Sakurai et al., 2005). AtSIP1;1, AtSIP1;2, and AtSIP2;1 were recently demonstrated to be localized to the endoplasmic reticulum (Ishikawa et al., 2006). Heterologous expression of these proteins in yeast followed by functional analysis also indicates that SIP subgroup I channels are permeable to water, while SIP subgroup II channels are not. These analyses are interesting because the ar/R region of SIP subgroup I members is much more hydrophobic that that of SIP subgroup II members, suggesting that the mechanism for water transport in these channels may be distinct. An analysis of public microarray data (Zimmerman et al., 2004) suggests that the Arabidopsis SIP subgroup members are mainly expressed in pollen and siliques, suggesting an undefined role for these proteins in these reproductive tissues in planta.

As originally observed by Johanson and Gustavsson (2002), the SIP subfamily is distantly phylogenetically related to the MIP family, and these proteins contain many nonconservative substitutions in critical regions of the protein, including the

ar/R region. These observations suggest that SIPs may have functional roles outside of water transport that remain to be discovered and also suggest that SIPs may not adhere to the canonical MIP fold. Furthermore, the first NPA motif of each SIP is distinct from other MIPs, with a conserved Thr or Cys substitution replacing the Ala residue of this highly conserved sequence. The structure of PfAQP (Newby et al., 2008) is the only MIP of known structure that contains similar substitutions in the NPA regions, and it was demonstrated in this structure that other residue substitutions throughout the pore collaborate to maintain the same three-dimensional positions of the critical asparagine residues in the NPA region of this pore. Whether a similar mechanism occurs in the SIP subfamily remains to be determined.

Additional plant ar/R region diversity in plants species other than Arabidopsis:

The publication of the Arabidopsis ar/R modeling study discussed above (Wallace and Roberts, 2004) led to subsequent analyses of the MIPs in other model plant systems, including *Physcomitrella patens*, corn, and rice (Bansal and Sankararamakrishnan, 2007; Danielson and Johanson, 2008). These modeling experiments continue to highlight the diversity of MIP ar/R regions in the plant kingdom. A comparative modeling study using all of the MIP isoforms from the corn and rice genomes (Bansal and Sankararamakrishnan, 2007) indicated that the NIP, TIP, and SIP subfamilies in these species contain a total of 5 novel ar/R regions that were not represented in the Arabidopsis genome. The rice genome contains an additional TIP and 3 NIP ar/R regions that are unique to this organism. Since corn and rice are monocotyledonous plants, these additional ar/R subgroups may be

involved in transport processes that are not essential in dicotyledonous plants like Arabidopsis, suggesting functional diversification of the MIP family even within different higher plant species.

Analysis of the ar/R regions of the MIPs in the moss (*Physcomitrella patens*) genome indicates that this organism has entire subclasses of MIP ar/R regions that are less commonly observed in vascular land plants. These unique subclasses include the hybrid intrinsic proteins (HIPs), which contain a histidine at both the H2 and H5 ar/R positions and therefore have characteristics of both TIPs and PIPs (Danielson and Johanson, 2008). In addition, these authors observed a new class of MIP termed the XIPs, which contain ar/R residues that are similar to TIPs and NIPs, but have a conserved glutamine residue at the H2 position. These MIPs are present in other mosses as well as in some higher plant such as poplar, suggesting that in some cases they were conserved in higher plant evolution. Both the PIP and TIP family ar/R regions are absolutely conserved in the moss genome, and contain the FHTR and HIAR residue combinations, respectively. These observations, coupled with the diverse number of ar/R regions observed in the TIP family of Arabidopsis, rice, and corn, suggest that TIP family ar/R diversity developed after the emergence of vascular land plants. Finally, it is interesting to note that moss stands out as an evolutionarily "simple" organism that contains a large number of MIPs with great ar/R region diversity. This observation was used to forward the hypothesis that various MIPs were lost during the course of land plant evolution at both the transition to vascular plant anatomy as well as the divergence of monocotyledonous and dicotyledonous plants (Daniels and Johanson, 2008). It could also be postulated that

these lost ar/R groups were no longer necessary after these transitions, and that the ar/R regions of the standard TIP, NIP, and SIP subfamilies have continued to evolve to compensate for any new MIP substrates that might arise.

Phylogenetic analysis of the ar/R region

To conduct a larger analysis of the selectivity-determining ar/R region across the MIP superfamily, a database of 1000 sequences were assembled from the NCBI database consisting of protein sequences from multiple eukaryotic and prokaryotic kingdoms. This analysis resulted in the identification of 92 unique ar/R regions, and many of the sequences harboring these novel ar/R regions occur in taxa outside of the plant kingdom. This observation suggests that multiple organisms may have utilized the core MIP fold to develop specialized transporters of a variety of substrates besides water by varying the amino acids at the ar/R region. This hypothesis is further supported by functional analysis of a novel insect MIP that forms a multifunctional polyol channel in this study.

An analysis of the most common ar/R regions in the dataset revealed that sequences containing the FHTR, FHCR, FHAR, and FHSR ar/R regions (letters denote the single letter amino acid code for the H2, H5, LE_1, and LE_2 ar/R positions, respectively) constitute the majority of sequences in the dataset. Multiple examples of each of these ar/R regions were found in all kingdoms examined. Since MIPs containing these ar/R residues have been repeatedly demonstrated to form water-selective channels (Preston et al., 1992; Fushimi et al., 1993; Jung et al., 1994a; Calamita et al., 1995; Chaumont et al., 2000), the prevalence of these ar/R regions

suggest that water-selective channels were highly conserved during evolution and are essential to osmotic homeostasis in all organisms.

The plant TIP subgroup-like ar/R regions HIGR, HIAV, and HIAR are also highly represented in the sequence analysis dataset. MIPs containing these ar/R regions also are documented water channels, but these proteins are multifunctional and are also permeable to physiologically relevant alternative solutes like ammonia and urea (Klebl et al., 2003; Jahn et al., 2004; Holm et al., 2005; Loque et al., 2005; Dynowski et al., 2008). Interestingly, mammalian AQP8 isoforms have been demonstrated to phylogenetically group with plant TIP isoforms (Zardoya, 2005), and an analysis of the AQP8 ar/R region indicates that it falls in to the HIAR family. AQP8 has also been recently characterized as an ammonia channel (Jahn et al., 2004; Holm et al., 2005; Saparov et al., 2007) on the mitochondrial inner membrane of mammalian cells (Calamita et al., 2005; Calamita et al., 2007), suggesting that plants as well as animals have conserved this MIP functional class, but use the proteins to accomplish different tasks. However, AQP8 appears to be an isolated case because all other mammalian aquaporins adhere to the classical FHCR paradigm characteristic of AQP1.

It is also of interest to note that MIPs with ar/R regions that are characteristic of aquaglyceroporin transport properties (WVAR, FGYR, WGYR) are also highly represented. Interestingly, each of these ar/R regions shows kingdom specificity. The WVAR ar/R region is characteristic of NIP subgroup I proteins, which are only observed in plant species, FGYR containing sequences are all derived from vertebrate organisms, and the WGYR sequences are only found in bacteria or protists. The

proposed mechanisms of selectivity for these types of aquaglyceroporins are fundamentally different (Thomas et al., 2002; Wallace and Roberts, 2004; Wallace and Roberts, 2005), suggesting that each of these groups of organisms have developed MIPs with ar/R regions that allow for simultaneous water and glycerol transport.

The observed frequency of structurally similar amino acids at each position of the ar/R region was also determined, and this analysis provides at least three interesting structural implications concerning MIP evolution. First, structurally similar amino acid categories have distinct frequencies of occurrence in the position of the ar/R region that they occupy. For example, large aromatic residues are almost always observed at the H2 or LE_1 position of the ar/R region, consistent with all known structures of MIPs (Fu et al., 2000; Sui et al., 2001; Savage et al., 2003; Harries et al., 2004; Tornroth-Horsefield et al., 2006; Newby et al., 2008). Aromatic residues are observed at the LE_1 position of GlpF-like aquaglyceroporin channels (Fu et al., 2000; Newby et al., 2008), and this type of amino acid is almost always accompanied by a Gly at the ar/R H5 position to avoid steric hindrance (Fu et al., 2000). Interestingly, the frequencies of Gly at H5 and an aromatic at the LE_1 position of the ar/R are nearly identical, suggesting that these substitutions have co-evolved due to steric concerns.

A second implication of the ar/R amino acid frequencies is that certain amino acids are not tolerated at the ar/R region. An exquisite example of this phenomenon occurs at the LE_2 position of the ar/R region. Arg is present at this position in 91.4 % of the sequences in the dataset, but Lys is not observed at any position of the ar/R

region despite the fact that both of these residues are positively charged and have fairly similar chemical properties. This strict preference for Arg may result from the need to form bidentate hydrogen bonding networks with the transported solute, similar to those observed in the GlpF and AQP1 structures (Fu et al., 2000; Sui et al., 2001). In addition, only three sequences out of the 1000 observed contain acidic residues in any of the four ar/R region positions. The positively charged Arg residue has been suggested in a number of molecular dynamics studies to form an electrostatic barrier to positively charged ions (de Groot and Grubmuller, 2001; de Groot et al., 2003), and the maintenance of this electrostatic barrier is essential for preserving proton gradients across cellular membranes (de Groot and Grubmuller, 2001). The presence of an acidic residue could neutralize the positive charge at the LE_1 Arg, rendering it ineffective as a cation exclusion filter. In addition, the presence of an electrostatic bond across the ar/R region could result in pore occlusion and the resulting channel would be impermeable to all solutes.

A third and final implication of these amino acid frequencies suggests that during the course of MIP evolution, only certain amino acids were tolerated at discreet positions of the ar/R region. This hypothesis was tested by observing the frequency of individual ar/R regions that differ by a single amino acid substitution. These data suggest that nonconservative substitutions at a certain ar/R position are most likely to retain a new amino acid that is within the apparent preferences observed within the phylogenetic distribution. For example, many water-selective aquaporin type ar/R regions (FHAR, FHCR, FHGR, FHSR) have a corresponding ar/R region in which the H5 position has been substituted to a β-branched amino acid

(FIAR, FICR, FIGR, FISR). Both His and β-branched amino acids are frequently observed, suggesting that these ar/R regions could have functionally evolved by the substitution of one amino acid in the ar/R region. In support of this hypothesis, the only characterized MIP with an ar/R sequence in this family (the archaeal MIP AqpM contains the ar/R sequence FISR), has been functionally characterized as an aquaglyceroporin (Kozono et al., 2003), and the structure of this protein has been determined revealing the molecular architecture of this ar/R region at the atomic level (Lee et al., 2005). The H5 Ile substitution characteristic of AqpM is also observed in other archaeal aquaporins (Lee et al., 2005), suggesting that this divergent amino acid has been conserved in the evolution of these organisms for a specific functional purpose. These bacteria use H_2S as a terminal electron acceptor in their electron transport chains, and it has been hypothesized that this molecule is the physiological substrate of AqpM-like MIPs and that the Ile substitution serves to increase the size of the ar/R constriction to allow this molecule to pass through the protein channel (Lee et al., 2005). In addition to this study, other structural analyses of ar/R substitutions that influence substrate specificity agree very well with the hypothesis presented above (Wallace et al., 2002; Wallace and Roberts, 2005; Beitz et al., 2006).

Structural and functional determinants of NIP and TIP transport

The amino acids in the ar/R region of NIP subgroup I and II as well as TIP subgroup II differ principally in the residue occupying the H2 position (TIP subgroup II = His, NIP subgroup I = Trp, NIP subgroup II = Ala). As a result, these channels

provided a unique system to investigate the effects of single ar/R substitutions on protein function, and to determine the divergent transport properties of previously uncharacterized NIP subgroup II channels. The outcome of protein engineering experiments performed as part of this study support the finding that the H2 position of the ar/R region is the major determinant of transport selectivity in these protein families.

NIP subgroup I members are permeable to water, formamide, glycerol, and ammonia, but not the larger test solute urea (Rivers et al., 1997; Weig et al., 1997; Dean et al., 1999; Guenther and Roberts, 2000; Niemietz and Tyerman, 2000; Weig and Jakob, 2000; Guenther et al., 2003). These functional properties can potentially be explained by the conserved amino acids of the NIP subgroup I ar/R region. The Trp and Arg residues are conserved features of glyceroporins and generate the amphipathic contacts necessary to interact with glycerol at the ar/R filter (Fu et al., 2000). Analysis of the nodulin-26 homology model using the computational pore-sizing algorithm HOLE predicts that the Val and Ala side chains at the H5 and LE_1 positions of the ar/R region would provide a wider pore aperture compared to water-selective aquaporins, allowing the passage of larger substrates like glycerol. In contrast, water-selective aquaporins, such as AQP1, have a conserved His residue at H5. Together with the conserved Arg residue at the LE_2 position of the ar/R region, these residues provide a narrower constriction that contains multiple hydrogen bonding sites for the transported water molecule. The substitutions in the NIP subgroup I ar/R region would generate a wider pore diameter with a reduced potential to form hydrogen bonds. These pore properties may be responsible for the lower

intrinsic water transport rate of nodulin-26 compared to AQP1 (Zeidel et al., 1992; Rivers et al., 1997; Dean et al., 1999). Consistent with this prediction, the results of thermodynamic transition state analysis of water transport through nodulin-26 and AQP1 in this study indicates a difference in the $\Delta H^{\ddagger}$ of water transport between nodulin-26 and AQP1 by about the energy of a single hydrogen bond (4-8 kJ/ mol). These data are in agreement with the substitution of a Val for His in nodulin-26, which would eliminate a single hydrogen bond donor in the ar/R region.

While the NIP subgroup II ar/R region shares many of the same properties as the NIP subgroup I ar/R, it contains a single nonconservative substitution of Ala at the H2 position for the highly conserved Trp in NIP subgroup I and virtually all other characterized aquaglyceroporins. On the basis of modeling, the structural consequence of this substitution is predicted to be an increase in the pore diameter of the NIP subgroup II ar/R region and a decrease in the hydrophobicity of the ar/R region.

As mentioned previously, AtNIP6;1 also contains an Ala to Val substitution in the second NPA motif. Similar substitutions have been observed in both the ar/R region and NPA regions in other Arabidopsis NIP subgroup II members (i.e. AtNIP5;1), as well as NIPs isolated from *Atriplex nummularia* (Cabello-Hurtado and Ramos, 2004), corn (Chaumont et al., 2001), and rice (Sakurai et al., 2005) suggesting that these features might be typical of NIP subgroup II members. HOLE analysis indicates that in contrast to most known MIP structures, the narrowest constriction of the AtNIP6;1 pore occurs at the NPA region, and this structural feature probably results from the Val substitution at the C-terminal NPA motif.

Functional analysis of AtNIP6;1 as well as soybean nodulin-26 indicates that both of these NIPs are highly permeable to glycerol as well as formamide and transport these solutes at similar rates. However, AtNIP6;1 differs substantially from nodulin-26 in that it exhibits no measurable water permeability and shows the ability to transport larger solutes, such as urea, that are excluded from the nodulin 26 pore. To investigate the structural features of the NIP subgroup II pore that are responsible for these unique transport properties, site-directed mutagenesis of the two unusual conserved residues (i.e. Val in the second NPA and Ala in the H2 position of the ar/R region) was performed to exchange these residues for their NIP subgroup I counterparts. Surprisingly, the substitution of Ala for Val 252 resulted in an AtNIP6;1 protein that was functionally identical to wild-type with respect to transport rates and substrate selectivity of all tested solutes. This result suggests that the substitution of a bulkier Val for Ala at this position is not important for determining the transport selectivity profile of AtNIP6;1 with respect to the assayed substrates.

In contrast, the substitution of a Trp for Ala at the H2 position of the putative AtNIP6;1 ar/R region (AtNIP6;1 A119W) had a dual effect on channel activity. The A119W mutant acquired the ability to facilitate water transport with a P_f identical to NIP subgroup I members like nodulin-26. Additionally, the substitution of the bulkier Trp residue provides a greater size restriction on transport, resulting in the exclusion of urea, again similar to NIP subgroup I members.

The extremely low water permeability of AtNIP6;1 is perplexing considering that the modeled ar/R region, which is large enough to accommodate approximately two water molecules. Furthermore, the ar/R region of AtNIP6;1 contains all of the

putative hydrogen bond donors and acceptors that are present in NIP subgroup I members (the backbone carbonyl of Ala in LE_1 and the guanido group of Arg at LE_2 are conserved in both nodulin-26 and AtNIP6;1), suggesting that AtNIP6;1 should be capable of transporting water at a rate similar to nodulin-26. In fact, a mutant of AQP1 in which the H2 Phe and H5 His are mutated to Ala residues shows a wider predicted pore, rapid and facilitated water transport, as well as the ability to transport urea and glycerol (Beitz et al., 2006). The structural mechanism for the observed low water permeability of AtNIP6;1 remains unknown, but it could arise from several different sources. A gating mechanism has been proposed to account for the low water permeability of GlpF (Tajkhorshid et al., 2002), in which the Trp sidechain at the H2 position of the ar/R moves when it comes in contact with glycerol to allow the solutes to pass through the pore. In this scheme, water cannot open the gate, but it is cotransported with glycerol, accounting for the low but measurable water permeability of GlpF.

An alternative hypothesis is the possibility of a gating domain provided by loop or terminal sequences outside of the pore. For example, the glycerol transport function of the yeast aquaglyceroporin Fps1 is gated by large hydrophilic domains in the N and C termini by a proposed "ball and chain mechanism" (Tamas et al., 2003; Hedfalk et al., 2004; Karlgren et al., 2004; Thorsen et al., 2006). In support of this hypothesis, NIP subgroup II members have unique extended amino-terminal domains that could potentially serve as external gates in a similar fashion.

To gain insight into a possible mechanism for the observed low water transport of NIP subgroup II members it is also instructive to examine other

aquaporins with low intrinsic water permeability. For example, in the case of the mammalian lens specific aquaporin (AQP0), a separate gating mechanism is observed, in which two Tyr residues form a second constriction within the pore that serves to decrease the occupancy time of water in this region (Gonen et al., 2004; Harries et al., 2004; Jensen et al., 2008). While these tyrosine residues are not conserved in NIP subgroup II members, a similar but structurally divergent mechanism could exist within the NIP subgroup II channel. In order to identify potential pore gating residues or additional constrictions, further protein engineering approaches and ultimately the structural elucidation of AtNIP6;1 (or another representative NIP subgroup II member) is needed.

A final hypothesis on the basis of the low water permeability of AtNIP6;1 is based on thermodynamic considerations. In this model, it is possible that AtNIP6;1 may not be able to properly organize water at the ar/R region because of the large predicted pore diameter. This hypothesis is based on the observation that robust water channels, such as AQP1, have a Phe residue at the H2 position of the ar/R region that is proposed to position the transported water such that maximal hydrogen bonding overlap occurs between the various hydrogen bond donors and acceptors (Sui et al., 2001). Aquaporin water transport shows a strong entropic component compared to water transport through a bare lipid bilayer, with a highly negative $\Delta S^{\ddagger}$ and a low positive $\Delta H^{\ddagger}$, suggesting that organization in the transport process is essential. Thermodynamic transition state analysis of water transport through AtNIP6;1 does indicate that the $\Delta S^{\ddagger}$ for water transport is less negative compared to the value observed for nodulin-26. In addition, the Arrhenius exponential prefactor (a

measure of the number of molecular collisions that lead to successful transport events) differs by seven orders of magnitude between these channels. Interestingly, the AtNIP6;1 A119W mutant shows a greater temperature dependence on water transport compared to nodulin-26, suggesting that this mutant is not functionally identical to NIP subgroup I members at all temperatures and that other structural features that lead to a decrease in water transport rate may become influential as the temperature increases. While the observations of Beitz and co-workers (Beitz et al., 2006) discussed above are in contradiction to this hypothesis, the authors did not perform a careful analysis of the thermodynamic parameters for water transport and they performed their mutagenesis experiments on a channel that normally conducts water, suggesting that undiscovered structural determinants may be present and maintain the water permeability of these mutant channels in the absence of key ar/R residues. However, it should be explicitly stated that low water permeability is a common characteristic of MIP channels that have large predicted pore diameters based on the results of the present study with NIP subgroup II members as well as those with other representative MIP channels (Fu et al., 2000; Takano et al., 2006; Ma et al., 2006; Yamaji et al., 2008).

A comparison of the NIP and TIP subgroups indicates that the principal difference between their ar/R amino acids lies at the H2 position. In TIP subfamily members, this position is occupied by a highly conserved His residue that would serve to increase the hydrophilicity and hydrogen bonding potential of the TIP ar/R, similar to AQP1 and other water-selective channels. Indeed, TIPs form high conductance water channels in *Xenopus* oocytes (Maurel et al., 1993; Chaumont et

al., 1998; Higuchi et al., 1998; Sarda et al., 1999; Schuurmans et al., 2003; Daniels et al., 2006), but these proteins are functionally distinct from NIPs because they are impermeable to glycerol. In the present study, site-directed mutagenesis was used to convert the H2 ar/R Trp of the *Lotus japonicus* nodulin-26 orthologue LjNod26 to a TIP-like His residue. The results of this transport analysis support this hypothesis, and it was observed that this mutant channel is permeable to water, but loses the ability to transport glycerol. Overall, these data strongly suggest that the H2 position of the ar/R region is a key structural determinant that functionally differentiates NIP and TIP subgroup members. It should be noted that some members of the TIP subfamily are capable of transporting other solutes like urea and ammonia (Klebl et al., 2003; Loque et al., 2005; Dynowski et al., 2008), suggesting that other properties of the TIP pore could lead to this divergent selectivity. Nevertheless, it is clear that selectivity for water and glycerol of these separate groups of plant MIPs (NIP subgroup I, NIP subgroup II, and TIPs) may be largely determined by a single residue at the H2 position of the ar/R region, with a His for TIP aquaporins, a Trp for NIP subgroup I aquaglyceroporins, and an Ala for NIP subgroup II glyceroporins that are incapable of water transport (Figure **4.1**).

AtNIP6;1 plays a role in boric acid distribution to developing aerial tissues

Boric acid is an essential micronutrient for plant development, and this compound forms covalent linkages between rhamnogalacturonan-II residues in the plant cell wall (O'Neill et al., 2001; O'Neill et al., 2004). Uptake of boric acid by plant cells was originally postulated to occur by passive diffusion, due to the fact that

Figure 4.1: Role of the H2 ar/R residue in NIP and TIP substrate selectivity: The substrate selectivity of NIPs with various substitutions at the H2 position of the ar/R region are shown. Transport data are corrected for the basal water and glycerol permeability of uninjected oocytes. The proteins represented are soybean nodulin-26, Arabidopsis NIP6;1, NIP6;1 A119W, LjNod26 (the Lotus japonicus nodulin-26 orthologue LIMP2), and the LjNod26 W77H mutant. The single letter amino acid code of the amino acids composing each ar/R region are shown above the transport data for each protein in the following order: H2, H5, LE_1 and LE_2. The water permeability data **(A)** and glycerol permeability data **(B)** are normalized to transport rates for nodulin-26. Error bars represent SEM.

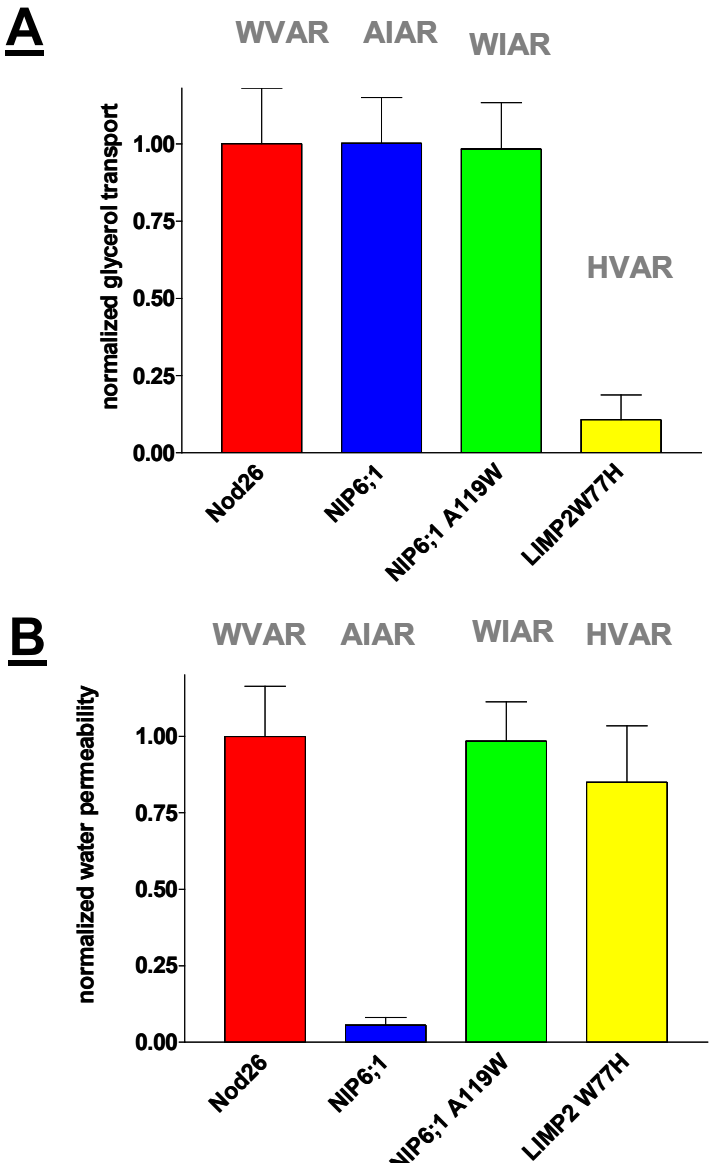
A
WVAR
AIAR
WIAR
HVAR
normalized glycerol transport
1.00
0.75
0.50
0.25
0.00
Nod26
NIP6;1
NIP6;1 A119W
LIMP2W77H
B
WVAR
AIAR
WIAR
HVAR
normalized water permeability
1.00
0.75
0.50
0.25
0.00
Nod26
NIP6;1
NIP6;1 A119W
LIMP2 W77H

it is a neutral molecule at physiological pH (pKa = 9.24) and it has a high ether/ water partition coefficient (Raven, 1980). This idea was challenged by the fact that the boric acid permeability of plant membranes is much higher than predicted from previous theoretical calculations and permeability experiments using ideal lipid bilayers (Dordas and Brown, 2000; Dordas et al., 2000). Several lines of evidence suggest that boric acid transport in plants involves a protein-based component, including dramatic differences in species-specific accumulation of boric acid (Nable, 1988), and a reduced activation energy for boric acid transport in isolated plant plasma membranes vesicles (Dordas et al., 2000). In addition, boric acid transport in isolated plant plasma membranes is sensitive to mercurial compounds, suggesting the possible involvement of MIPs.

Recently, both secondary and passive boric acid transport systems have been elucidated in plants (Takano et al., 2002; Takano et al., 2006; Nakagawa et al., 2007; Tanaka et al., 2008) and yeast (Nozawa et al., 2006; Takano et al., 2007). The Arabidopsis BOR1 gene encodes a protein that represents a secondary active transporter that is expressed in roots, and is transcriptionally regulated by boric acid availability. The AtBOR1 protein is proposed to transfer boric acid from the root epidermis cells into the xylem, so that this essential compound can be distributed to growing tissues via the transpiration stream (Takano et al., 2002). The finding that rice contains a BOR1 homologue (OsBOR1) that shows very similar transcriptional regulation, functional transport properties, and the knockout phenotype suggests that this mechanism is the general function for these transporters (Nakagawa et al., 2007).

The first indication that NIP subgroup II members may form boric acid channels cam from a microarray analysis indicating that AtNIP5;1, an Arabidopsis NIP subgroup II, member is transcriptionally induced in plants experiencing boric acid deprivation. Subsequent analysis demonstrated that AtNIP5;1 is expressed in Arabidopsis roots only under conditions of boric acid deprivation and serves as a channel for boric acid in *Xenopus* oocytes (Takano et al., 2006). An analysis of AtNIP5;1 T-DNA mutant plants revealed that these plants are phenotypically indistinguishable when 100 μM boric acid is included in the growth media, but when these plants were subjected to boric acid deprivation primary root growth was drastically inhibited. Using boric acid tracer uptake analysis, the authors also demonstrated that boric acid transport into the root tissue was reduced by up to 75 % in AtNIP5;1 knockout plants (Takano et al., 2006).

AtNIP6;1 is 66.4 % identical to AtNIP5;1 at the amino acid level, and contains identical amino acid residues at the selectivity-determining ar/R region (Table **3.8**), suggesting that AtNIP6;1 may be capable of transporting boric acid like AtNIP5;1, and that the NIP subgroup II ar/R region may be uniquely designed for metalloid transport. Functional comparison in *Xenopus* oocytes indicates that AtNIP6;1 is capable of transporting boric acid across the oocyte membrane at an identical rate compared to AtNIP5;1. Similar to previous observations with other NIPs, the boric acid transport associated with AtNIP5;1 and AtNIP6;1 is inhibited by mercurial compounds, providing a molecular basis for the previously observed mercury sensitivity in isolated plant membranes. Further evidence for specific transport of boric acid mediated by AtNIP6;1 is illustrated by the fact that AtNIP6;1

A119W shows a drastically inhibited rate of boric acid transport, suggesting that the Ala residue at the ar/R H2 position is also a critical structural determinant for boric acid permeability of NIP subgroup II proteins.

Subcellular localization experiments of transgenic plants expressing an AtNIP6;1-GFP translational fusion indicate that this protein is localized to the plasma membrane. Taken together, the localization and transport data suggest that AtNIP6;1 functions as a plasma membrane-localized boric acid channel in plant cells. One possible explanation for the water-tight properties of AtNIP6;1 is its plasma membrane localization. The plasma membrane generally possesses an intrinsically low water permeability compared to internal membranes, which is largely mediated by the regulation of PIP isoforms (reviewed in Maurel et al., 2008). The transport properties of AtNIP6;1 allow robust uptake of boric acid, while maintaining a low intrinsic P_f of the plasma membrane.

GUS staining in 10-day-old AtNIP6;1 promoter:: GUS fusion transgenic Arabidopsis seedlings was observed in the first nodes, petioles, and leaf veins, while GUS staining in 28-day-old plants was observed at the base of flowers and siliques as well as in the nodal regions, veins, and petioles of the young rosette leaves. GUS staining in the petioles and veins disappeared when the leaves matured, while staining in the nodal regions was constant. These developmentally-dependent expression profiles suggest that AtNIP6;1 plays a role in boric acid distribution to young rosette leaf tissue to support normal cell wall development.

This hypothesis was supported by phenotypic analysis of AtNIP6;1 T-DNA insertional mutants. The symptoms of boric acid deficiency are generally observed in

young tissues, and defects in young leaf expansion are a classical symptom of this deficiency. The main cause of these developmental defects is impaired cell elongation due to a loss of cell wall integrity (Dell and Huang, 1997). Under boric acid-limiting conditions, root elongation is severely inhibited in AtNIP5;1 T-DNA insertional mutants (Takano et al., 2006), and this study indicates that a similar phenomenon occurs in the young leaves of AtNIP6;1 knockout plants. Under low boric acid conditions, the young leaves of AtNIP6;1 mutant plants show a reduced cell size as well as the absence of intercellular air spaces, suggesting that the defective leaf growth phenotype is due to inhibition of cell elongation rather than decreased cell divisions.

While the expansion of young leaf tissue was inhibited under boric acid limiting conditions in AtNIP6;1 mutant plants, this inhibition was only observed at certain stages of vegetative growth. During the first two weeks of development, AtNIP6;1 mutant plants are phenotypically normal under boric acid-limiting conditions, suggesting that passive diffusion of boric acid across the lipid bilayer (or another unidentified boric acid transporter/ channel) can supply the aerial tissues with enough boric acid to support normal plant growth. In contrast, the growth of young rosette leaves emerging after several weeks of development was retarded in AtNIP6;1 mutant plants under boric acid-limiting conditions, suggesting that this channel becomes essential to these young tissues as the leaf system becomes larger.

Boric acid tracer analysis demonstrated that short-term ^{10}B uptake into the shoot apices is inhibited in AtNIP6;1 mutant plants under low boric acid conditions, but not under high boric acid conditions., suggesting that this compound is not

effectively distributed to sink tissues in the AtNIP6;1 mutant plants. These findings suggest that AtNIP6;1 is crucial for distribution of boric acid to developing aerial tissues under low boric acid conditions. The fact that the developmental phenotype of AtNIP6;1 knockout plants are only observed at low boric acid conditions is consistent with a model in which a facilitated pathway is needed only when boric acid concentrations prohibit rapid uptake by a diffusive mechanism.

AtBOR1 is not only involved in xylem loading of boric acid in the root tissue, but also in boric acid distribution to young rosette leaves. The Arabidopsis *bor1-1* mutant showed reduced growth rates and developmental abnormalities in young rosette leaves (Noguchi et al., 1997; Takano et al., 2002), and boric acid tracer experiments showed that higher amounts of boric acid were transported to young rosette leaves compared to older leaves in wild-type plants, but not in the *bor1-1* mutant. These observations suggest that boric acid is preferentially transported to young tissues via AtBOR1 under boric acid-limiting conditions (Takano et al., 2002). In the root tissue, AtNIP5;1 is involved in boric acid acquisition , while AtBOR1 is involved in xylem loading of this compound. Similarly, transport of boric acid through AtNIP6;1 and AtBOR1 at different points may be required for efficient partitioning of boric acid to young developing leaves.

This analysis provides evidence for the role of AtNIP6;1 in xylem-phloem transfer of boric acid. AtNIP6;1 is expressed at branching points (stem nodal regions) as well as junction areas (the base of flowers and siliques), which are known sites of xylem-phloem transfer (Marschner, 1995; Offler et al,. 2002; Royo et al., 2007). Localization and functional analysis experiments indicate that AtNIP6;1 would serve

as an efficient boric acid channel in these areas, while phenotypic analysis as well as in vivo measurements of boric acid transport in AtNIP6;1 mutant plants indicate that the boric acid transport defects in these plants are localized to the young developing aerial tissues. These observations strongly support the hypothesis that AtNIP6;1 is involved in preferential transport of boric acid to sink tissues in the shoot via xylem-phloem transfer. A model describing this process is presented in figure **4.2**. In this diagram, cells between the xylem and phloem are grouped into two subtypes: companion cells/ phloem parenchyma and xylem parenchyma cells. In wild-type plants, AtNIP6;1 is expressed in companion cells and this channel facilitates the rapid diffusion of boric acid towards the phloem and on to the developing young leaf tissue, but in AtNIP6;1 mutant plants, this process would be at least one order of magnitude slower due to passive diffusion of boric acid through the cell membrane.

NIP subgroup II members transport a variety of metalloid compounds

Boric acid belongs to the metalloid class of elements, which additionally include arsenic, silicon, antimony, and germanium. Like boric acid, each of these elements form weak Lewis acids in solution and contain three to four hydroxyl groups, suggesting that these compounds may be structurally related to polyhydroxyl alcohols such as glycerol (Porquet and Filella, 2007).

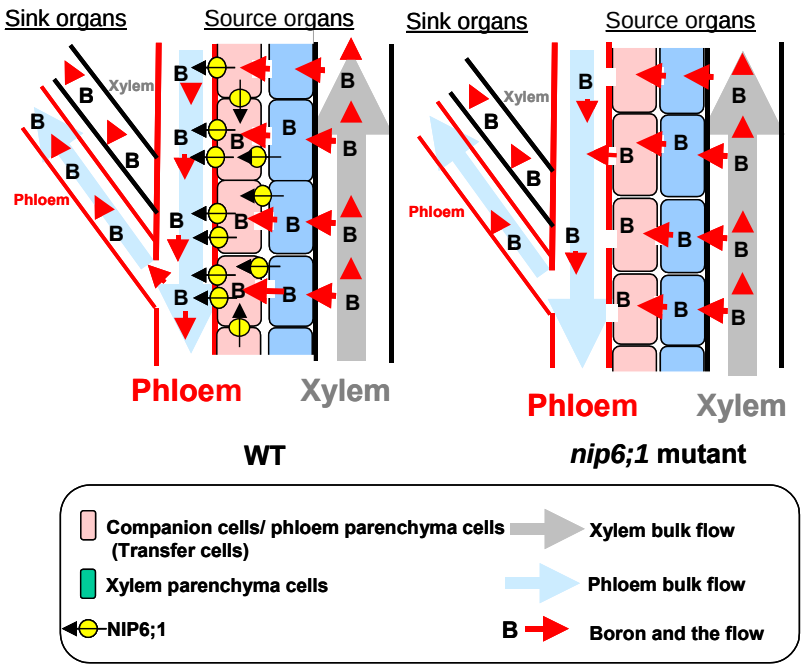

Figure 4.2: Model for NIP6;1 involvement in distribution of boric acid to growing aerial tissues: A model is presented to describe a role for NIP6;1 in boric acid distribution to developing young organs. Boric acid is normally transported to aerial organs through the xylem, and this compound must pass through the xylem-phloem transfer cells to reach the phloem. NIP6;1 provides a low energy pathway for the diffusion of boric acid through these cells, allowing boric acid to rapidly reach the phloem and sink tissues under boric acid-limiting conditions. In the nip6;1 mutants, this low energy pathway is absent, and boric acid must passively diffuse through the xylem-phloem transfer cell membrane to reach sink tissues, resulting in reduced distribution to developing aerial tissues.

In addition to boric acid, members of NIP subgroup II have recently been demonstrated to transport a variety of metalloid compounds, suggesting that metalloid transport is a common physiological function for these proteins in plants.

Evidence for the involvement of NIP subgroup II members in silicic acid uptake came from the analysis of the *Lsi1* and *Lsi6* low silicon uptake mutations in rice. Both of these mutants were isolated in a genetic screen for plants resistant to the toxic silicic acid analogue germanium. *Lsi1* mutants show reduced accumulation of silicic acid, which leads to increased susceptibility of these plants to a variety of pathogens as well as decreased fertility (Ma et al., 2006). In contrast, *Lsi6* mutants show decreased levels of silicon in the aerial tissues, and a reduction of silicon deposition in the leaf tissue (Yamaji et al., 2008). The *Lsi1* and *Lsi6* genetic lesions were mapped to the OsNIP2;1 and OsNIP2;2 genes, respectively (Ma et al., 2006; Yamaji et al., 2008). OsNIP2;1 is expressed in the root tissue of rice plants and serves as a plasma-membrane localized channel that was permeable to silicic acid and germanium when assayed in *Xenopus* oocytes (Ma et al., 2006). A single point mutation in the OsNIP2;1 (*Lsi1*) gene as well as RNAi-mediated knockdown of the transcript suggest that this channel serves as a physiologically relevant silicon transporter, due to the observation that these mutations cause decreased silicon uptake, increased susceptibility to various pathogens, and a drastically reduced grain yield (Ma et al., 2006).

In contrast, OsNIP2;2 is expressed in the aerial tissues, and Lsi6 mutant rice plants show a distinct defect in the translocation of silicon to the aerial tissues (Yamaji et al., 2008). Parallels exist between the AtNIP5;1/ AtNIP6;1 boric acid

translocation model in Arabidopsis and the OsNIP2;1/ OsNIP2;2 silicon translocation model in rice. In these corresponding models, AtNIP5;1 and OsNIP2;1 are analogous channels for boric acid and silicic acid that acquire these nutrients from the soil and transport them into the root epidermis (Takano et al., 2006; Ma et al., 2006). Once these compounds reach the root epidermis cells, they are loaded into the xylem by AtBOR1 (boric acid) or the corresponding silicic acid active transporter Lsi2 (Ma et al., 2007). These metalloid compounds are translocated from the root to aerial tissues along the transpiration stream, and are distributed to aerial organs by the concerted effort of channel mediated (AtNIP6;1/ Lsi6) and active transport (AtBOR1/ Lsi2) mechanisms (Takano et al., 2002; Ma et al., 2007; Yamaji et al., 2008).

It is also of interest to note that silicic acid differs from boric acid in that it contains four hydroxyl groups, instead of the three hydroxyl groups. An examination of the predicted ar/R residues in known silicic acid and boric acid NIP channels shows that silicic acid-transporting NIPs have a slightly modified ar/R region amino acids that are most likely necessary to transport this structurally divergent substrate. While AtNIP6;1 and many other NIP subgroup II members contain an Ala at H2, Ile/ Val at H5, Ala/ Gly at LE_1, and an Arg residue at LE_2, the documented silicic acid channels contain a single nonconservative substitution of a Ser residue at the H5 ar/R position (Ma et al., 2006; Yamaji et al., 2008). This substitution is also observed in three NIP subgroup II members (ZmNIP2-1, ZmNIp2-2, and ZmNIP2-3) from maize, which is also a silicon-accumulating plant.

In contrast to boric acid and silicic acid, other metalloid compounds such as $As(OH)_3$ and $Sb(OH)_3$ are toxic and serve no useful purpose in plants. Nevertheless,

these compouinds are also among the newly demonstrated substrates for NIP subgroup II channels (Bienert et al., 2008; Isayenkov and Maathius, 2008). By using a yeast expression system and toxicity screening, Bienert and co-workers (2008) were able to demonstrate that NIP subgroup II members from Arabidopsis, rice, and *Lotus japonicus* bidirectionally transport arsenous acid [$As(OH)_3$]. Interestingly, it was necessary to truncate the N-terminus of AtNIP5;1 and AtNIP6;1, as well as their *Lotus japonicus* orthologues, to observe arsenous acid transport in yeast. It was suggested that this observation is due to reduced expression and mistargeting of full-length NIPs in yeast, but preliminary analysis of arsenous acid transport in *Xenopus* oocytes expressing full-length AtNIP6;1 and AtNIP5;1 suggest that the full-length channels are actually incapable of transporting this compound even when they are expressed (Wallace and Roberts, unpublished). One hypothesis that emerges from these observations is that the N-terminus of some NIP subgroup II members may serve as a gating domain to allow transport of boric acid, while simultaneously excluding the toxic analogous metalloid compound arsenous acid. This hypothesis is further supported by the observation that the arsenous acid permeability of yeast Fps1 is regulated by a large N-terminal gating domain (Wysocki et al., 2001). Yeast Hog1p MAP kinase participates in the yeast response to hypoosmotic shock by phosphorylating Fps1 at a site within the N-terminal domain (Thorsen et al., 2006; Mollapour and Piper, 2007) and regulating its glycerol transport activity. Interestingly, Hogl also responds to arsenous acid and regulates Fps1-mediated arsenic uptake through this channel (Thorsen et al., 2006). It is interesting to note that NIPs homologous to AtNIP5;1 and AtNIP6;1 always contain extended N-

terminal domains that contain multiple MAP kinase concensus phosphorylation motifs (P-X-S/T-P), suggesting that the mechanism observed in the yeast Fps1 arsenic resistance system may have evolved to allow regulation of essential or beneficial metalloid compounds in plants.

Although it is an essential nutrient, boric acid also becomes toxic to plants (Miwa et al., 2007) and yeast (Nozawa et al., 2006) at elevated concentrations. To avoid boric acid toxicity, boric acid transporters such as AtBOR1 are down-regulated from the plasma membrane and degraded when plants cells are exposed to high concentrations of boric acid (Takano et al., 2005). Putative regulatory domains in the N-terminus of NIP subgroup II members could also serve to regulate the boric acid permeability of these channels in response to these conditions to avoid potential boric acid toxicity in the plant, or possibly to direct and compartmentalize excess boric acid.

AtNIP7;1 represents a specialized case of a NIP subgroup II gene product. Phylogenetic analysis indicates that this NIP is distinct from AtNIP5;1 as well as AtNIP6;1, and transport analyses show that it has a distinct metalloid selectivity profile. For example, Sb transport was only documented in AtNIP7;1, while this channel showed a very low measured permeability to arsenous acid (Bienert et al., 2008). Conflicting results were obtained in an analysis of AtNIP7;1 T-DNA insertional mutants, which demonstrated increased resistance to arsenic suggesting a possible transport function for As in vivo (Isayenkov and Maathius, 2008). While these results suggest that AtNIP7;1 is permeable to both arsenous acid and $Sb(OH)_3$, the physiological relevance of these substrates is subject to discussion because public

microarray data indicates that AtNIP7;1 is maximally expressed in the developing floral tissue (Zimmerman et al., 2004) and could not serve as a putative toxic metalloid uptake/ extrusion system. A more detailed analysis of the transport functions and the physiological role of AtNIP7;1 in Arabidopsis will be necessary to determine the substrate selectivity of this unique NIP subgroup II member.

Uptake of metalloid compounds was not observed for NIP subgroup I members, suggesting that these proteins play a functionally distinct role in plant membrane transport role. Analysis of the boric acid permeability in the AtNIP6;1 A119W mutant suggests that these differences in permeability are directly related to the composition of the ar/R region, and suggest that the Ala residue at the H2 position of the ar/R is a key determinant for metalloid selectivity. Metalloid compounds were initially suggested to structurally mimic glycerol (Porquet and Filella, 2007), which is a common MIP substrate, but functional analysis of NIP subgroup I and II suggests that this model is oversimplified. For example, AtNIP1;1 and AtNIP1;2 are NIP subgroup I members that are documented aquaglyceroporins (Weig et al., 1997; Weig and Jakob, 2000), but are unable to transport $As(OH)_3$ or $Sb(OH)_3$ (Bienert et al., 2008). Atomic models of NIP subgroup I and II members will most likely be necessary to determine the mechanism for selectivity between metalloid compounds and glycerol in these unique channels.

The analysis of AtNIP6;1 presented in this study as well as many recent studies discussed in this section underscore the importance of NIP subgroup members as physiological metalloid transporters in plants. MIP-mediated arsenic transport has been documented in bacteria and yeast for a number of years (Liu et al., 2004; Meng

et al., 2004). It is interesting to note that a MIP homologue in *Sinorhizobium meliloti* (AqpS; Yang et al., 2005) is present in the arsenic resistance operon of this bacterium and is essential for arsenic detoxification, suggesting that arsenic detoxification by MIPs in unicellular organisms is critical to their survival. Angiosperms utilize greater amounts of boric acid in their cell walls than bryophytes, and it has been suggested that borate cross-linked rhamnogalacturonan II residues were necessary for the upright growth of land plants (Matsunaga et al., 2004). It is also interesting to suggest that NIP subgroup I members may have evolved from ancient arsenous acid efflux channels in bacteria to acquire boric acid during plant evolution. Recently, NIP subgroup members that contain the canonical NIP subgroup II ar/R sequence were observed in the genome of moss (*Physcomitrella patens*; Danielson and Johanson, 2008), which does not utilize high amounts of boric acid, supporting this hypothesis for NIP evolution.

Post-translational modifications affect the water permeability of nodulin-26

A large number of MIPs are subject to regulation by posttranslational phosphorylation events, and the effects on channel activity vary from stimulation in the case of plants MIPs such as α-TIP (Maurel et al., 1995), as well as SoPIP2 (Johansson et al., 1998; Tornroth-Horsefield et al., 2006), to inhibition of water transport in AQP4 (Han et al., 1998; Zelinina et al., 2002). In addition, phosphorylation of MIPs has been demonstrated to alter the membrane localization and trafficking of these proteins in plant and animal cells (Nielsen et al., 1995; Fushimi et al., 1997; Kamsteeg et al., 2000; Madrid et al., 2001; Kosugi-Tanaka et al.,

2006; Prak et al., 2008). The present study demonstrates that phosphorylation of nodulin-26 at Ser 262 enhances its water permeability when heterologously expressed in *Xenopus* oocytes as well as in purified symbiosome membrane vesicles. This finding supports previous data indicating that the incubation of symbiosome membrane vesicles with ATP coincides with an increase in P_f (Niemietz and Tyerman, 2000). LjNod26 is also phosphorylated by CDPK at the analogous position (Ser 262), suggesting that CDPK phosphorylation is a common feature of symbiosome-specific NIPs (Guenther and Roberts, 2000). The CDPK consensus phosphorylation sequence surrounding Ser 262 in nodulin-26 is highly conserved among NIP subgroup I members (Table **3.5**), suggesting that phosphorylation by CDPK may represent a common mechanism for regulation of this NIP class.

Using an antibody generated against the phosphorylated Ser 262 epitope of nodulin-26, it was previously demonstrated that nodulin-26 phosphorylation is subject to regulation by developmental control as well as environmental cues (Guenther et al., 2003). Nodulin-26 protein levels appear during nodule organogenesis as early as 16 days after infection, coinciding with the early stages of infected cell development, including breakdown of the central vacuole and a burst of membrane biosynthesis, which is necessary to accommodate the expanding infected cell size as well as the development of symbiosome membranes (Verma and Hong, 1996). Phosphorylation of nodulin-26 lags behind synthesis of the protein and reaches steady state levels at approximately 25 days after infection. During this phase of nodule development, the infected cell matures and the bacteroids become fully differentiated signaling the onset of nitrogen fixation. Nodulin-26 phosphorylation is maintained at a steady state

level in mature nitrogen-fixing nodules, but becomes dephosphorylated at later stages (post 53 days) when nodule senescence generally occurs. These results suggest that nodulin-26 phosphorylation is developmentally regulated during the nodule life cycle, and that an increased phosphorylation status during the mature nitrogen fixation phase of nodule development is necessary for nodulin-26 function.

The phosphorylation status of nodulin-26 during the mature nitrogen fixation phase can also be altered by abiotic stresses that affect water homeostasis. Nodulin-26 phosphorylation levels increase in response to salinity as well as drought stress (Guenther et al., 2003), and it is interesting to note that these conditions are associated with a concomitant increase in cytosolic Ca^{2+} concentrations (Knight et al., 1997) that would lead to activation of the symbiosome-associated CDPK that phosphorylates nodulin-26. Nodulin-26 protein levels did not change under either of these conditions, suggesting that changes in water permeability at the symbiosome membrane are completely posttranslationally regulated through nodulin-26 phosphorylation (Guenther et al., 2003).

Because nodulin-26 phosphorylation on Ser 262 stimulates water transport, at least two modes of regulation are possible. During normal nitrogen fixation, phosphorylation could represent a means of regulating the water and solute permeability of the symbiosome membrane during times of high metabolic activity to maintain an osmotic balance. Secondly, in conditions of severe osmotic stress, nodulin-26 may play an additional role in adaptation of the infected cell to these stresses. Plant CDPKs are involved in a wide range of physiological processes including Ca^{2+} signaling during bacterial initiation of the nitrogen fixation symbiosis,

biotic as well as abiotic stress adaptation, pollen development, nitrogen metabolism, and hormone signaling (Cheng et al., 2002; Harper et al., 2004; Harper and Harmon, 2005). Thus, there appears to be significant overlap between processes that may involve NIPs (Wallace et al., 2006) and many of the processes that are regulated by CDPKs. In addition to the regulation of channel permeability, other potential roles of phosphorylation must be considered, such as MIP trafficking and protein interactions.

In light of the fact that nodulin-26 water permeability is enhanced by phosphorylation, it is essential to understand that posttranslational modifications and regulatory domains serve as crucial determinants outside of the ar/R region that affect MIP function. In addition to phosphorylation, MIPs are regulated by Ca^{2+} ions (Yasui et al., 1999a; Nemeth-Cahalan and Hall, 2000; Nemeth-Cahalan and Hall, 2004; Verdoucq et al., 2008) as well as pH (Gerbeau et al., 2002; Tournaire-Roux et al., 2003). The recently determined X-ray crystal structure of *Spinacea oleracea* PIP2;1 (SoPIP2; Tornroth-Horsefield et al., 2006) suggests a comprehensive structural mechanism for several of these regulatory posttranslational modifications. The authors observed that a network of residues from the N-terminus (Asp 28 and Glu 31) as well as a His residue from loop D (His 193) serve to reversibly open and close the channel in response to these stimuli. When His 193 is protonated, it tightly interacts with Asp 28, causing a large conformational change in loop D resulting in physical occlusion of the pore by Leu 197. Modulation by divalent cations also occurs through the closure of loop D, but in this case the divalent metal directly interacts with Asp 28 and Glu 31. This interaction results in a similar conformational change in which loop D occludes the pore, and this structural state is maintained by a

hydrogen bonding network between Arg residues in loops B and D (Tornroth-Horsefield et al., 2006).

Phosphorylation of the loop B residue Ser 115 has the opposite effect and serves to stabilize loop D in the open state, allowing water channel activation. The C-terminal phosphorylation site of SoPIP2;1 (Ser 274), which is analogous to the phosphorylation site of nodulin-26, is proposed to act in a similar manner, but in this case the interaction occurs through transactivation (i.e. the phosphorylation site of one monomer opens loop D in an adjacent monomer). Interestingly, loop D of nodulin-26 is devoid of His residues, but it does contain an Arg residue that could potentially interact with the phosphate on Ser 262 through a similar transactivation mechanism. However, the pKa of the Arg guanido group is normally around 12.8, suggesting that this residue has a constitutive positive charge at this position that would argue against pH regulation of nodulin-26.

The structural basis for pH regulation of the low water permeability of AQP0 from mammalian lens cells has also been structurally investigated. Atomic structural studies performed on AQP0 indicate that this protein can exist in an open or closed conformation, and the equilibrium between these two states is determined by the pH of the solution (Gonen et al., 2004; Harries et al., 2004). The closed state of AQP0 was observed at pH 6 via electron diffraction experiments, and this structure indicates that the AQP0 pore constricts to a diameter of 1.96 angstroms over a 10-angstrom length along the pore axis (Gonen et al., 2004). This general pore constriction seems to be mediated by subtle movements of the amino acids lining the pore. The "open" state structure of AQP0 was determined at pH 10 by X-ray diffraction, and this

structure suggests that the conformation is similar to the pore characteristics observed in bovine AQP1 (Harries et al., 2004). This AQP0 structure also elucidated the presence of two Tyr residues (Tyr 23 and Tyr 149) that form a gate on the cytosolic side of the pore. The structures generated in these two studies were subject to speculation because the "open" conformation was observed at a more basic pH, where AQP0 water channel activity is usually inhibited (Nemeth-Cahalan and Hall, 2000; Nemeth-Cahalan et al., 2004). An examination of the crystallographic B-factors suggested that Tyr 149 was highly mobile (Gonen et al., 2004), and subsequent molecular dynamics simulations suggest that the Tyr 23/ Tyr 149 gate serves as the primary structural basis for the low water permeability of AQP0 (Jensen et al., 2008) by physically occluding the pore and reducing water occupancy at this region of the channel.

The regulatory mechanism proposed for AQP0 is fundamentally different from the mechanism observed in SoPIP2;1, and phylogenetic analysis reveals that the Tyr residues involved are conserved in AQP0-like proteins from a variety of different organisms (Harries et al., 2004), but are not found in other water-selective channels like AQP1 that have a constitutively high water permeability. These results suggest that this type of regulation is probably suited for proteins that normally maintain a low water permeability, but may need to slightly increase the water permeability under certain physiological conditions. This hypothesis is further supported by the observation that the Tyr residues responsible for the AQP0 gating mechanism are thought to have arisen recently in evolution (Zardoya, 2005).

Protein interactions among MIPs have also emerged as a source of MIP regulation. For example, the previously discussed low water permeability of plant PIP1 isoforms can be modulated by heterotetramer formation between PIP1 and PIP2 isoforms (Fetter et al., 2004; Mahdieh et al., 2008; Vandeleur et al., 2008), resulting in an increase in PIP1 water permeability. This increase in water permeability was linked to an increase in the plasma membrane trafficking efficiency of PIP1-PIP2 heterotetramers in oocytes, suggesting that the increase in water permeability is due to a combination of structural effects and an increase in the number of water channels on the oolemma (Fetter et al., 2004). These observations suggest that the various MIPs expressed in different plant cells types may interact with each other to form heterogenous channels according to the needs of the plant cell.

The structural models of MIP posttranslational regulation have several interesting implications. It is widely accepted that permeable MIP substrates pass through the same conduction pathway in a given protein (i.e. water and glycerol would pass through the same pore in nodulin-26). Therefore, it is reasonable to suggest that a posttranslational modification that regulates the permeability of one solute for a channel regulates the permeability of all other solutes for that channel. In the case of SoPIP2;1, the structural mechanism is based on physical occlusion of the conduction pore by loop D, suggesting that substrates besides water (i.e. H_2O_2; Dynowski et al., 2008) will also become impermeable when this structural element interacts with the pore. It is also interesting to note that there are no examples of a posttranslational modification altering the selectivity of a given MIP channel. This observation suggests that there is an interplay between the ar/R region and the

regulatory domains of MIP channels in which the ar/R region controls the selectivity of the channel, while the regulatory domains modulate the permeability of solutes that are allowed to pass through this selectivity filter. Again, this model is in agreement with the structural model of aquaporin gating suggested for SoPIP2;1 (Tornroth-Horsefield et al., 2006) because there are no alterations in the ar/R region conformation, or the general pore conformation for that matter.

The C-terminus of nodulin-26 serves as a protein interaction domain for glutamine synthetase

Since the original identification of nodulin-26 over 20 years ago (Fortin et al., 1987), the function of this channel in the context of the nodule has been debated. In addition to its identification as an aquaglyceroporin (Rivers et al., 1997; Dean et al., 1999), nodulin-26 has been proposed to serve as a symbiosome membrane ion channel (Weaver et al., 1994; Lee et al., 1995), as a malate channel (Ouyang et al., 1991), and as a channel for uncharged ammonia (Niemietz and Tyerman, 2000). As an aquaglyceroporin, nodulin-26 has also been proposed to serve as a low energy barrier for water and osmolytes within the infected cell, to aid in cell volume regulation as well as the adaptation to a variety of osmotic stresses (Guenther et al., 2003). A growing body of evidence suggests that some additional MIP functions may arise from the formation of protein interactions involved in the specific membrane targeting (Noda et al., 2004a; Noda et al., 2004b; Noda et al., 2005) and regulation (Rose et al., 2008; Reichow and Gonen, 2008). In light of these observations, a

biochemical screen was designed to isolate nodulin-26 interacting proteins from the nodule cytosol using peptide affinity resins that mimic the C-terminus of nodulin-26.

Chromatography on CI-14-coupled ω-aminohexyl agarose resulted in the isolation of a group of 38-40 kDa proteins that were subsequently identified by peptide mass fingerprinting as a family of cytosolic glutamine synthetases from soybean. Glutamine synthetase is a homooctameric enzyme (M_w of octamer = 376,000 Da) that catalyzes the ATP-dependent ligation of ammonia and glutamate to form glutamine. This enzymatic reaction is the committed step to assimilation of the ammonia released from symbiosome membrane during symbiotic nitrogen fixation (Miflin and Habash, 2002). Ammonia permeability assays of isolated symbiosome membranes as well as reconstituted nodulin-26 proteoliposomes (Niemietz and Tyerman, 2000; Niemietz, Tyerman, and Roberts, unpublished data) suggest that nodulin-26 serves as a channel for the ammonia substrate of glutamine synthetase, implying that the interaction between these proteins is physiologically relevant. Glutamine synthetase enzymatic activity was also observed to specifically adsorb to resins displaying the CI-14 peptide as well as resins displaying a peptide encompassing the entire C-terminus of nodulin-26 (CK-25). In contrast, underivitized ω-aminohexyl agarose failed to adsorb glutamine synthetase activity, and a resin coupled to an unrelated peptide corresponding to the C-terminus of Arabidopsis SIP2;1 showed reduced adsorption of this enzyme activity. These results unequivocally identify the interacting proteins as glutamine synthetase isoforms, and also suggest that their interaction is selective for nodulin-26 C-terminal peptides. Interestingly, preliminary experiments suggest that glutamine synthetase also

interacts with the GC-12P peptide, which mimics the phosphorylated C-terminus of nodulin-26 and thus the influence of phosphorylation on the interaction remains an open question.

Analysis of isolated symbiosome membranes indicates that a small but measureable amount of glutamine synthetase enzymatic activity co-purifies with the symbiosome membranes. This result is in agreement with a previous proteomic analysis that identified glutamine synthetase associated with the symbiosome membrane of *Medicago truncatula* nodules (Catalano et al., 2004) and suggests that glutamine synthetase associates with the symbiosome membrane. An additional binding of glutamine synthetase activity was observed upon incubation of purified glutamine synthetase with the symbiosome membrane preparation. If it is assumed that glutamine synthetase isoforms have an average specific activity of 75 μmol/ min/ mg protein and that the average molecular weight of the GS octamer is 376 kDa (McParland et al., 1976), then the amount of adsorbed glutamine synthetase activity shown in figure **3.33** exactly corresponds to a stoichiometry of 1 GS monomer interacting with 1 nodulin-26 monomer. The adsorption of glutamine synthetase to symbiosome membranes was quantitatively inhibited by the addition of 10 μM soluble CI-14 peptide, suggesting that the C-terminus of nodulin-26 serves as a primary interaction site for glutamine synthetase. These results also indicate that glutamine synthetase is capable of interacting with full-length nodulin-26.

Cytosolic glutamine synthetases form a small, highly conserved gene family in Arabidopsis (Ishiyama et al., 2004a), rice (Ishiyama et al., 2004b), as well as in soybean (Morey et al., 2002), and isolated glutamine synthetase isoforms show a K_m

for ammonia that varies over three orders of magnitude, despite the fact that these proteins share greater than 85 % amino acid identity (Ishiyama et al., 2004a; Ishiyama et al., 2004b). To investigate the isoform specificity of the interaction between nodulin-26 and glutamine synthetase, the full-length sequences of the four glutamine synthetase isoforms expressed in the nodule (Morey et al., 2002) were cloned and analyzed. GmGS1;1 and GmGS1;2 correspond to the $GS\beta_1$ and $GS\beta_2$ sequences that were previously reported (Morey et al., 2002), indicating that these isoforms are expressed in both the root as well as the nodule. GmGS1;3 and GmGS1;4 correspond to the nodule-specific glutamine synthetase isoforms $GS\gamma_1$ and $GS\gamma_2$. Split-ubiquitin yeast two-hybrid analysis indicates that each of these isoforms interacts with nodulin 26.

As stated previously, accumulating evidence suggests that nodulin-26 can serve as an ammonia channel (Niemietz and Tyerman, 2000). The common cellular localization and utilization of ammonia as a substrate suggest that the interaction between these two proteins may be physiologically relevant. One possible model is that the interaction of nodulin-26 and glutamine synthetase could serve as a "metabolic funnel" for fixed nitrogen assimilation in the cytosol (Figure **4.3**). In this model, it is noted that fixed nitrogen can be released from the symbiosome by one of at least three pathways. Ammonium ion can be transported across the symbiosome membrane through the nonselective cation channel, while uncharged NH_3 can passively diffuse through the membrane or can be released by facilitated diffusion through nodulin-26.

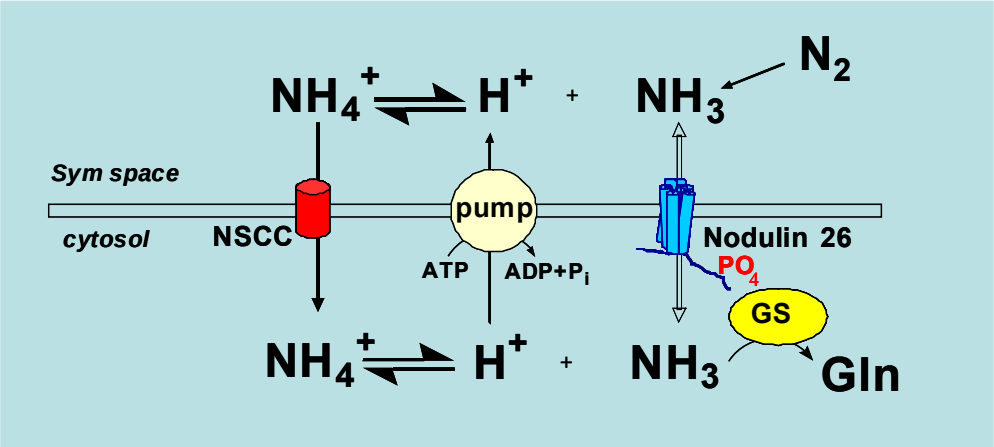

Figure 4.3: Model for the glutamine synthetase/ nodulin-26 interaction in symbiotic nitrogen assimilation: As atmospheric dinitrogen is reduced, ammonia accumulates in the symbiosome space. This compartment is acidified by a proton pumping ATPase that creates an equilibrium between fixed ammonia and charged ammonium ion. The ammonium ion can leave the symbiosome through a non-selective cation channel, while ammonia can pass through nodulin-26 or passively through the symbiosome membrane. Glutamine synthetase bound to the C-terminal tail of nodulin-26 could serve to assimilate ammonia/ ammonium leaving the symbiosome through any one of these pathways. In addition, the glutamine synthetase could prevent ammonia from re-traversing the symbiosome membrane and futile ammonia cycling.

An interaction between nodulin-26 and glutamine synthetase would localize this critical assimilatory enzyme to the surface of the symbiosome, facilitating the assimilation of the ammonia transported across the membrane through nodulin-26. Since nodulin-26 constitutes 10-15 % of the symbiosome membrane protein, it would also serve to increase the local concentration of glutamine synthetase in the vicinity of the membrane so that the enzyme would have direct and immediate access to NH_3/ NH_4^+ that leaves the symbiosome through the other efflux pathways.

The importance of this association may stem from the observation that high concentrations of ammonia/ ammonium are extremely toxic to plants due to a proposed "ammonia futile cycling" mechanism. In this situation, ammonium ion is transported into the plant cell from the extracellular space into the cytosol via high affinity ammonium transporters (D'Apuzzo et al., 2004; Yuan et al., 2007). The extracellular space pH is generally more acidic than the neutral cytosol, so a small fraction of the ammonium ion will lose a proton and pass through the plasma membrane as uncharged ammonia, resulting in the net transport of a proton from the extracellular space to the cytosol (Britto et al., 2001). The direction of proton transport in this case is against the gradient established by the plasma membrane H^+-ATPases and results in the net hydrolysis of ATP.

A similar situation could exist at the symbiosome membrane, due to the acidic pH of the symbiosome space and the high concentrations of ammonium that accumulate during active nitrogen fixation (Streeter, 1989). The interaction of nodulin-26 with glutamine synthetase could also serve to inhibit this futile cycling process. Nodulin-26 serves as the lowest energy pathway for ammonia transport

across the symbiosome membrane, and there is some evidence that the vestibules of MIPs are able to increase the local concentration of their substrates (Lu et al., 2003). Therefore, the ammonia approaching nodulin-26 for re-entry into the symbiosome space could be converted to glutamine by glutamine synthetase before it has time to traverse the membrane and dissipate the proton gradient. Future molecular genetics experiments using transient transformation of soybean nodules by *Agrobacterium rhizogenes*-mediated transformation may provide more detail concerning the physiological effects of the nodulin-26/ glutamine synthetase interaction in each of these processes.

Aquaporins are involved in aphid gut osmoregulation

In the present study, we have extended our work on MIP/ AQP structure and function to the analysis of conventional (ApAQP1) and unusual (ApAQP2) MIPs from insects using aphids as a test system. ApAQP1 modeling and functional analyses suggest that this protein is similar in structure and function to mammalian AQP1. Superposition of the ApAQP1 homology model into the experimental structure of AQP1 indicates that all of the ApAQP1 ar/R residues are identical to the residues observed in AQP1, with the exception of Ala-218. The Cys at the LE_1 position of the AQP1 ar/R region contributes a peptide backbone carbonyl oxygen as a hydrogen bonding acceptor to the transported water molecule (Sui et al., 2001), and the substitution of Ala in the ApAQP1 ar/R region should not affect the three-dimensional hydrogen bonding network that is needed for rapid water transport.

Indeed, other water-selective aquaporins, such as mammalian AQP4, contain an Ala residue at this position and are capable of rapid water transport (Thomas et al., 2002). Overall, structural analysis suggests that ApAQP1 contains all of the amino acid determinants necessary for rapid water-selective transport.

This conclusion is supported by the functional analysis of ApAQP1. *Xenopus* oocytes expressing this channel show all of the hallmarks of aquaporin-mediated water transport, including an 18-fold increase in the water permeability of the oolemma, a low activation for water transport (3 kcal/ mol), and inhibition of water transport by the classical aquaporin inhibitor mercury chloride.

In addition to its functional properties as a water-selective aquaporin, the localization of the ApAQP1 transcript in the common pea aphid supports its potential role in mediating rapid osmotically-induced transmembrane water movements between the stomach and distal intestine. The osmotic gradient that is generated between these two compartments directly results from a reduction in the osmotic pressure of the gut contents, and this metabolic transformation is mediated by a sucrase-transglucosidase that is localized to the proximal intestine (Price et al., 2007). Consistent with the identification of ApAQP1 sequences in EST libraries prepared from both guts and salivary glands of aphids (Sabater-Munoz et al., 2006), in situ hybridization experiments using an ApAQP1 probe show large amounts of ApAQP1 in the stomach and distal intestine of adult aphids. Anatomically, these gut regions are in close juxtaposition and an enhanced P_f of both regions would facilitate transcellular water flow from the distal intestine to the stomach in response to the osmotic gradient between these two tissues (Figure **4.4**). In various insects, water-

transporting aquaporins mediate rapid water movement and partitioning. For example, aquaporins are associated with the tracheoles, where they play a crucial role in controlling water movement during gas exchange (Pietrantonio et al., 2000; Duchesne et al., 2003), and in the Malphigian tubules, where these proteins mediate the flux of water into the tubule lumen to form primary urine (Kaufmann et al., 2005; Spring et al., 2007).

Complementary insight into the function of ApAQP1 was obtained from RNAi studies, which demonstrated that the RNAi-mediated reduction in ApAQP1 gene expression correlated with a significant elevation in the osmotic pressure of the aphid hemolymph. This result was the predicted effect of depressed water cycling in the gut and suggests that even a modest and temporary decrease in ApAQP1 expression is sufficient to disrupt gut osmoregulation. The increase in hemolymph osmotic pressure caused by RNAi was not associated with reduced aphid performance or abnormal development, suggesting that the osmotic effects were a consequence of the treatment and not a non-specific effect of abnormal insect growth. Overall, the function, localization, and consequences of reduced gene expression suggest that ApAQP1 is a water-selective channel involved in a homeostatic water-cycling mechanism that transfers water from the distal intestine to the stomach and contributes to osmoregulation of the pea aphid gut.

Figure 4.4: A model for ApAQP1 involvement in aphid gut osmoregulation: The anatomy of the aphid gut is shown. The gut contains a simple stomach followed by proximal and distal regions of the intestine. The expression domains of ApAQP1 are shown in blue corresponding to the regions that display the highest ApAQP1 in situ hybridization signal. The areas of the intestine containing α-sucrase/ sugar polymerizing activities are also indicated. As sucrose ingested from the phloem enters the stomach, the high concentrations of this compound result in a hyperosmotic environment compared to the aphid tissues. When sucrose enters the intestine, it is hydrolyzed and the glucose residues by the activity of the α-sucrase in the proximal intestine. This enzymatic transformation decreases the osmolarity of the fluid entering the distal intestine, making this compartment hypoosmotic to the stomach. Water is transported from the distal intestine to the stomach (red arrow) resulting in the conservation of osmotic homeostasis and fluid conservation.

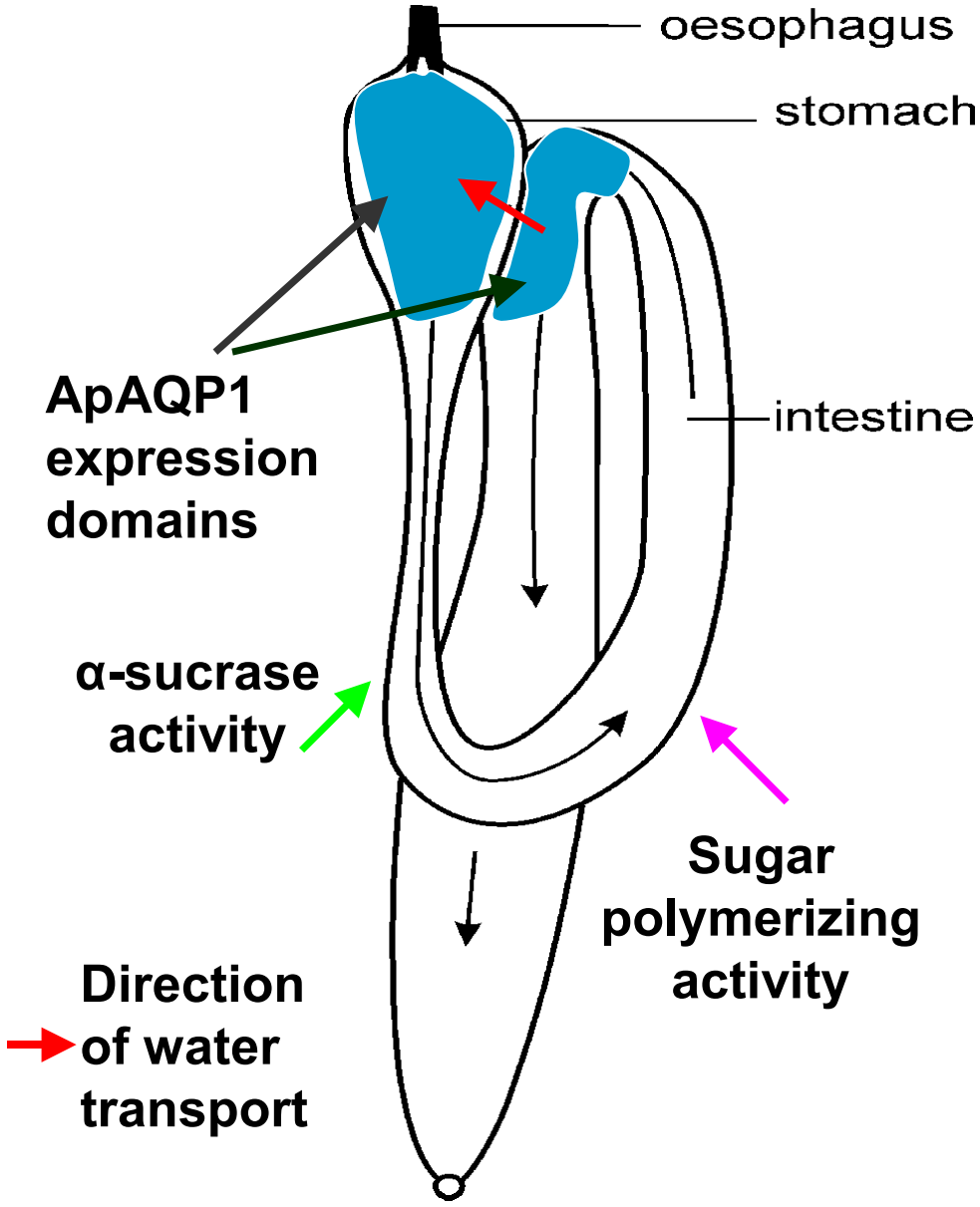
oesophagus
stomach
intestine
ApAQP1
expression
domains
α-sucrase
activity
Sugar
polymerizing
activity
Direction
of water
transport

ApAQP2 is a novel multifunctional MIP located in symbiotic bacteriocyte cells

The structural diversity of insect aquaporins has previously been observed (reviewed in Campbell et al., 2008), but these studies have not focused on the selectivity-determining regions in insect MIPs. Homology modeling of ApAQP2 indicates that this protein has a completely novel ar/R region, consisting of a Phe at H2, a Ser at H5, an Asn at LE_1, and the highly conserved Arg residue at LE_2. These substitutions lead to a widening of the pore compared to the AQP1 template, and the Asn residue substitution at LE_1 projects a side-chain amide group into the pore, suggesting that this residue may form bidentate hydrogen bonding interactions with transported substrates in a similar manner to the Arg residue at LE_2.

Functional analysis of ApAQP2 in *Xenopus* oocytes indicates that this protein is highly permeable to water, inducing a 20-fold increase in the water permeability of the oolemma. In contrast to ApAQP1, the ApAQP2 water permeability is not sensitive to mercury chloride or silver nitrate, a recently characterized inhibitor of MIP water channels (Niemietz and Tyerman, 2002). Although the majority of MIP channels are inhibited by mercury chloride, there are certainly examples of water-selective aquaporins that are insensitive to mercury (Daniels et al., 1994; Hasegawa et al., 1994; Biela et al., 1999). The most astonishing feature of the ApAQP2 selectivity profile is the permeability of this protein to polyols with no apparent preference to size or stereochemistry. GlpF has been demonstrated to transport ribitol in addition to glycerol, but this channel shows remarkable stereoselectivity in that it is relatively

impermeable to the C-3 epimer xylitol and is completely impermeable to mannitol (Fu et al., 2000). A comparative structural analysis of the GlpF and ApAQP2 ar/R regions suggests that ApAQP2 is more promiscuous in its selection of substrates based on the wider aperture and increased number of hydrogen bonding sites in the ApAQP2 ar/R region. However, it should be noted that ApAQP2 is a selective channel in that it does not transport the cyclic 6 carbon polyol inositol. In addition, *Xenopus* oocytes that express ApAQP2 have basal resting potentials that are indistinguishable from control oocytes suggesting that ApAQP2 does not transport ions.

Real-time PCR expression analysis indicates that ApAQP2 is expressed in the aphid bacteriocyte cells that house the obligate symbiont *Buchnera aphidicola*. A symbiosis exists between aphids and *Buchnera*, in which these intracellular bacteria synthesize the essential amino acids that are not provided in the aphid diet of plant phloem sap (Wilkinson et al., 2007). The genome sequence of *Buchnera* is now available (Shigenobu et al., 2000), and highlights the interdependence of these endosymbionts with aphids. *Buchnera* have become so dependent on their aphid hosts that they have discarded the majority of the genes that are unnecessary to perform the task of synthesizing essential amino acids. These bacteria contain the biosynthetic pathways for all essential amino acids, but lack the genes necessary to produce nonessential amino acids, which are often present in high concentrations within the phloem sap (Sandstrom and Moran, 2001). In addition, *Buchnera* has lost genes for several essential processes, such as 1: producing energy in the TCA cycle, 2: synthesizing lipids for membrane integrity, 3: regulating osmotic homeostasis, 4:

intracellular signaling, and 5: most of the protein machinery necessary for transcriptional regulation (Shigenobu et al., 2000). These observations suggest that this organism is a minimalistic symbiont that has abandoned essential pathways, instead relying on its host. It is interesting to note that these bacteria do retain a homologue of the *E. coli* mtlA mannitol transporter (Grisafi et al., 1989; White and Jacobson, 1990) as well as a GlpF homologue, suggesting that these organisms must import a carbon source from the aphid host in order to survive. Due to the extreme evolutionary pressure to remove any genes from the *Buchnera* genome that do not contribute to the symbiosis (Shigenobu et al., 2000; Gil et al., 2002; van Ham et al., 2003; Tamames et al., 2007), and the permeability of ApAQP2 to mannitol as well as glycerol, a model can be proposed in which ApAQP2 is localized to the bacteriocyte membrane, where this protein transports mannitol or glycerol (or both) into the bacteriocyte space. MtlA catalyzes the transport of mannitol into the cell while simultaneously phosphorylating this compound to form mannitol-6-phosphate (M6P). M6P can be directly converted to fructose-6-phosphate (F6P) by the activity of M6P-dehydrogenase (which is present in the *Buchnera* genome; Shigenobu et al., 2000), and the resulting F6P is metabolized in glycolysis. In addition, glycerol could be transported through ApAQP2 followed by the *Buchnera* GlpF homologue to serve as an osmolyte for osmotic homeostasis. Osmoregulation is essential due to the high osmolarity of the aphid food source in the nearby gut tissue (Douglas, 2006), as well as the fact that *Buchnera* are mechanically fragile due to the lack of cell wall biosynthetic enzymes (Shigenobu et al., 2000). Further subcellular localization

experiments are necessary to verify the location of ApAQP2 within the cell and to test the validity of this model.

In the 1000 sequences observed in the phylogenetic analysis presented in this study, ApAQP2 is one of only two sequences that contain the unusual Asn substitution at the LE_1 position of the ar/R region. The second sequence is an uncharacterized aquaporin from the dog tick (*Dermacentor variables*), and is identical to ApAQP2 at the ar/R region, with the exception of a Met substitution at the H5 position. It is interesting to note that both aphids and the common dog tick contain obligate intracellular gut bacteria (Rymaszewska, 2007), although the role that these bacteria play in the dog tick life cycle is unknown. It could be suggested that this tick MIP has a similar substrate specificity to ApAQP2 and could be involved in the tick-bacteria symbiosis, although the nature of the metabolic exchange is unknown.

List of references

Aerts, T., Xia, J. Z., Slegers, H., de Block, J., and Clauwaert, J. (1990). Hydrodynamic characterization of the major intrinsic protein from the bovine lens fiber membranes: extraction in n-octyl-β-glucoside and evidence for a tetrameric structure. *J. Biol. Chem.* **265**: 8675-8680.

Agmon, N. (1995). The Grotthuss mechanism. *Chem. Phys. Letters* **244**: 456-462.

Agre, P., and Kozono, D. (2003). Aquaporin water channels: molecular mechanisms for human diseases. *FEBS Lett*. **555**: 72-78.

Aharon, R., Shahak, Y., Wininger, S., Bendov, R., Kapulnik, Y., and Galili, G. (2003). Overexpression of a plasma membrane aquaporin in transgenic tobacco improves plant vigor under favorable growth conditions but not under drought or salt stress. *Plant Cell* **15**: 439-447.

Alonso, J. M., Stepanova, A. N., Leisse, T. J., Kim, C. J., Chen, H., Shinn, P., Stevenson, D. K., Zimmerman, J., Barajas, P., Cheuk, R., Gadrinab, C., Heller, C., Jeske, A., Koesema, E., Meyers, C. C., Parker, H., Prednis, L., Ansari, Y., Choy, N., Deen, H., Geralt, M., Hazari, N., Hom, E., Karnes, M., Mulholland, C., Ndubaku, R., Schmidt, I., Guzman, P., Aguilar-Henonin, L., Schmid, M., Weigel, D., Carter, D. E., Marchand, T., Risseeuw, E., Brogden, D., Zeko, A., Crosby, W. L., Berry, C. C., and Ecker, J. R. (2003). Genome-wide insertional mutagenesis of *Arabidopsis thaliana*. *Science* **301**: 653-657.

Andreev, I. M., Dubrovo, P. N., Krylova, V. V., and Izmailov, S. F. (1999). Functional identification of ATP-driven Ca^{2+} pump in the peribacteroid membrane of broad bean root nodules. *FEBS Lett*. **447**: 49-52.

Bansal, A., and Sankararamakrishnan, R. (2007). Homology modeling of major intrinsic proteins in rice, maize, and Arabidopsis: comparative analysis of transmembrane helix association and aromatic/ arginine selectivity filters. *BMC Struct. Biol*. **7**: 27-44.

Barrieu, F., Chaumont, F., and Chrispeels, M. J. (1998). High expression of the tonoplast aquaporin ZmTIP1 in epidermal and conducting tissues in maize. *Plant Physiol*. **117**: 1153-1163.

Beitz, E., Wu, B., Holm, L.M., Schultz, J. E., and Zeuthen, T. (2006). Point mutations in the aromatic/ arginine region in aquaporin-1 allow passage of urea, glycerol, ammonia, and protons. *Proc. Natl. Acad. Sci. USA* **103**: 269-274.

Biela, A., Grote, K., Otto, B., Hoth, S., Hedrich, R., and Kaldenhoff, R. (1999). The *Nicotinia tabacum* plasma membrane aquaporin NtAQP1 is mercury-insensitive and permeable for glycerol. *Plant J*. **18**: 565-570.

Bienert, G. P., Thorsen, M., Schussler, M. D., Nilsson, H. R., Wagner, A., Tamas, M. J., and Jahn, T. P. (2008). A subgroup of plant aquaporins facilitate the bi-directional diffusion of $As(OH)_3$ and $Sb(OH)_3$ across membranes. *BMC Biol*. **6**: 26-41.

Bonhivers, M., Carbrey, J. M., Gould, S. J., and Agre, P. (1998). Aquaporins in *Saccharomyces*: genetic and functional distinctions between laboratory and wild-type strains. *J. Biol. Chem*. **273**: 27565-27572.

Borgnia, M. J., Kozono, D., Calamita, G., Maloney, P. C., and Agre, P. (1999). Functional reconstitution and characterization of AqpZ, the *E. coli* water channel protein. *J. Mol. Biol*. **291**: 1169-1179.

Borstlap, A. C. (2002) Early diversification of plant aquaporins. *Trends Plant Sci*. **7**: 529-530.

Bourguet, J., Chevalier, J., and Hugon, J. S. (1976) Alterations in membrane-associated particle distribution during antidiuretic challenge in frog urinary bladder epithileum. *Biophys. J*. **16**: 627-639.

Brahm, J. (1982) The diffusional water permeability of human erythrocytes and their ghosts. *J. Gen. Physiol*. **79**: 791-819.

Britto, D. T., Siddiqui, M. Y., Glass, A. D., and Kronzucker, H. J. (2001). Futile transmembrane NH_4^+ cycling: a cellular hypothesis to explain ammonium toxicity in plants. *Proc. Natl. Acad. Sci. USA* **98**: 4255-4258.

Brown, D., and Orci, L. (1983). Vasopressin stimulates formation of coated pits in rat kidney collecting ducts. *Nature* **302**: 253-255.

Cabello-Hurtado, F., and Ramos, J. (2004). Isolation and functional analysis of the glycerol permease activity of two new nodulin-like intrinsic proteins from salt stressed roots of the halophyte *Atriplex nummularia*. *Plant Sci*.**166**: 633-640.

Calamita, G., Bishai, W. R., Preston, G. M., Guggino, W. B., and Agre, P. (1995). Molecular cloning and characterization of AqpZ, a water channel from *Eschericia coli*. *J. Biol. Chem*. **270**: 29063-29066.

Calamita, G., Ferri, D., Gena, P., Liquori, G. E., Cavalier, A., Thomas, D., and Svelto, M. (2005). The inner mitochondrial membrane has aquaporin-8 water channels and is highly permeable to water. *J. Biol. Chem*. **280**: 17149-17153.

Calamita, G., Moreno, M., Ferri, D., Silvestri, E., Roberti, P., Schiavo, L., Gena, P., Svelto, M., and Goglia, F. (2007). Triiodothyronine modulates the expression of aquaporin-8 in rat liver mitochondria. *J. Endocrinol*. **192**: 111-120.

Campbell, E. M., Ball, A., Hoppler, S., and Bowman, A. S. (2008). Invertebrate aquaporins: a review. *J. Comp. Physiol*. **178**: 935-955.

Carbrey, J. M., Bonhivers, M., Boeke, J. D., and Agre, P. (2001). Aquaporins in *Saccharomyces*: characterization of a second functional water channel protein. *Proc. Natl. Acad. Sci. USA* **98**: 1000-1005.

Catalano, C. M., Lane, W. S., and Sherrier, D. J. (2004). Biochemical characterization of symbiosome membrane proteins from *Medicago truncatula* root nodules. *Electrophoresis* **25**: 519-531.

Chaumont, F., Barrieu, F., Herman, E. M., and Chrispeels, M. J. (1998). Characterization of a maize tonoplast aquaporin expressed in zones of cell division and elongation. *Plant Physiol.* **117**: 1143-1152.

Chaumont, F., Barrieu, F., Jung, R., and Chrispeels, M. J. (2000). Plasma membrane intrinsic proteins from maize cluster in two sequence subgroups with differential water transport activity. *Plant Physiol*. **122**: 1025-1034.

Chaumont, F., Barrieu, F., Wojick, E., Chrispeels, M. J., and Jung, R. (2001). Aquaporins constitute a large and highly divergent protein family in maize. *Plant Physiol*. **125**: 1206-1215.

Cheng, S. H., Willmann, M. R., Chen, H. C., and Sheen, J. (2002). Calcium signaling through protein kinases: the Arabidopsis calcium-dependent protein kinase gene family. *Plant Physiol*. **129**: 469-485.

Chrispeels, M. J., and Maurel, C. (1994). Aquaporins: the molecular basis of facilitated water movement through living plant cells? *Plant Physiol*. **105**: 9-13.

Clough, S. J., and Bent, A. F. (1998). Floral dip: a simplified method for *Agrobacterium*-mediated transformation of *Arabidopsis thaliana*. *Plant J*. **16**: 735-743.

Cohen, B. E. (1975). The permeability of liposomes to nonelectrolytes I: activation energies for permeation. *J. Membr. Biol*. **20**: 205-234.

Corzo, J., Santamaria, M., and Gutierrez-Navarro, A. M. (1997). Transient energy coupling between rhizobia and legume cells mediated by the peribacteroid membrane ATPase proton pump. *Biosci. Rep*. **17**: 389-400.

Cristofoletti, P. T., Ribiero, A. F., Deraison, C., Rahbe, Y., and Terra, W. R. (2003). Midgut adaptation and digestive enzyme distribution in a phloem feeding insect, the pea aphid *Acyrthosiphon pisum*. *J. Insect Physiol*. **49**: 11-24.

Curtis, M. D., and Grossniklaus, U. (2003). A gateway cloning vector set for high-througput functional analysis of genes in planta. *Plant Physiol*. **133**: 462-469.

Daniels, M. J., Mirkov, T. E., and Chrispeels, M. J. (1994). The plasma membrane of *Arabidopsis thaliana* contains a mercury-insensitive aquaporin that is a homologue of the tonoplast water channel protein TIP. *Plant Physiol*. **106**: 1325-1333.

Daniels, M. J., Chaumont, F., Mirkov, T. E., and Chrispeels, M. J. (1996). Characterization of a new vacuolar membrane aquaporin sensitive to mercury at a unique site. *Plant Cell* **8**: 587-599.

Daniels, M. J., Chrispeels, M. J., and Yeager, M. (1999). Projection structure of a plant vacuole membrane aquaporin by electron cryo-crystallography. *J. Mol. Biol*. **294**: 1337-1349.

Daniels, M. J., Wood, M. R., and Yeager, M. (2006). In vivo functional assay of a recombinant aquaporin in *Pichia pastoris*. *Appl. Environ. Microbiol*. **72**: 1507-1514.

Danielson, J.A., and Johanson, U. (2008). Unexpected complexity of the aquaporin gene family in the moss *Physcomitrella patens*. *BMC Plant Biol*. **8**: 45-60.

D'Apuzzo, E., Rogato, A., Simon-Rosin, U., El Alaoui, H., Barbulova, A., Betti, M., Dimou, M., Katinakas, P., Marquez, A., Marini, A. M., Udvardi, M. K., and Chiurazzi, M. (2004). Characterization of three functional high-affinity ammonium transporters in *Lotus japonicus* with differential transcriptional regulation and spatial expression. *Plant Physiol*. **134**: 1763-1774.

Dascal, N. (1987). The use of *Xenopus* oocytes for the study of ion channels. *CRC Crit. Rev. Biochem*. **22**: 317-387.

Day, D. A., Poole, P. S., Tyerman, S. D., and Rosendahl, L. (2001). Ammonia and amino acid transport across symbiotic membranes in nitrogen-fixing legume nodules. *Cell. Mol. Life Sci*. **58**: 61-71.

Deamer, D. W., Mahon, E. H., and Bosco, G. (1994). Self-assembly and function of primitive membrane structures. Early life on earth. Nobel symposium No. 84, ed. By S. Bengston (Columbia University Press, New York, 1994)

Dean, R. M., Rivers, R. L., Zeidel, M. L., and Roberts, D. M. (1999). Purification and functional reconstitution of soybean nodulin 26, an aquaporin with water and glycerol transport properties. *Biochemistry* **38**: 347-353.

Deen, P. M., Verdijk, M. A., Knoers, N. V., Wieringa, B., Monnens, L. A., van Os, C. H., and van Oost, B. A. (1994). Requirement of human renal water channel aquaporin-2 for vasopressin-dependent concentration of urine. *Science* **264**: 92-95.

de Groot, B. L., and Grubmuller, H. (2001). Water permeation across biological membranes: mechanism and dynamics of aquaporin-1 and GlpF. *Science* **294**: 2353-2357.

de Groot, B. L., Frigato,T., Helms, V., and Grubmuller, H. (2003). The mechanism of proton exclusion in the aquaporin-1 water channel. *J. Mol. Biol*. **333**: 279-293.

de Grotthuss, C. J. T. (1806) Sur la decomposition de l'eau et des corps qu'elle tient en dissolution a l'aide de l'eletricite galvanique. *Ann. Chim*. **58**: 54-74.

Dell, B., and Huang, L. (1997). Physiological response of plants to low boron. *Plant Soil* **193**: 103-120.

Denker, B. M., Smith, B. L., Kuhajda, F. P., and Agre, P. (1988). Identification, purification, and partial characterization of a novel M_r 28,000 integral membrane protein from erythrocytes and renal tubules. *J. Biol. Chem*. **263**: 15634-15642.

Dicker, S. E., and Elliot, A. B. (1967). Water uptake by *Bufo melanosticus*, as affected by osmotic gradients, vasopressin, and temperature. *J. Physiol*. **190**: 359-370.

Dordas, C., and Brown, P. (2000). Permeability of boric acid across lipid bilayers and factors affecting it. *J. Membr. Biol*. **175**: 95-105.

Dordas, C., Chrispeels, M. J., and Brown, P. H. (2000). Permeability and channel-mediated transport of boric acid across membrane vesicles isolated from squash roots. *Plant Physiol*. **124**: 1349-136.

Douglas, A.E. (2006) Phloem-sap feeding by animals: problems and solutions. *J. Exp. Bot*. **57**: 747-754.

Duchesne, L., Hubert, J. F., Verbavatz, J. M., Thomas, D., and Pietrantonio, P. V. (2003). Mosquito (*Aedes aegypti*) aquaporin, present in tracheolar cells, transports water, not glycerol, and forms orthogonal arrays in *Xenopus* oocyte membranes. *Eur. J. Biochem*. **270**: 422-429.

Dynowski, M., Mayer, M., Moran, O., and Ludewig, U. (2008). Molecular determinants of ammonia and urea conductance in plant aquaporin homologues. *FEBS Lett*. **582**: 2458-2462.

Echevarria, M., Windhager, E. E., Tate, S. S., and Frindt, G. (1994). Cloning and expression of AQP3, a water channel from the medullary collecting duct of rat kidney. *Proc. Natl. Acad. Sci. USA* **91**: 10997-11001.

Engel, A., Fujiyoshi, Y., and Agre, P. (2000). The importance of aquaporin water channel protein structures. *EMBO J*. **19**: 800-806.

Fedorova, E., Thomson, R., Whitehead, L. F., Maudoux, O., Udvardi, M.K., and Day, D. A. (1999). Localization of H^+-ATPases in soybean root nodules. *Planta* **209**: 25-32.

Fetter, K., Van Wilder, V., Moshelion, M., and Chaumont, F. (2004). Interactions between plasma membrane aquaporins modulate their water channel activity. *Plant Cell* **16**: 215-228.

Finkelstein, A. (1987). *Water Movement Through Lipid Bilayers, Pores, and Plasma Membranes, Theory and Reality*. Wiley and Sons, New York.

Fischbarg, J., Kuang, K. Y., Hirsch, J., Lecuona, S., Rogozinski, L., Silverstein, S. C., and Loike, J. (1989). Evidence that the glucose transporter serves as a water channel in J774 macrophages. *Proc. Natl. Acad. Sci. USA* **86**: 8397-8401.

Fischbarg, J., Kuang, K. Y., Vera, J. C., Arant, S., Silverstein, S. C., Loike, J., and Rosen, O. M. (1990). Glucose transporters serve as water channels. *Proc. Natl. Acad. Sci. USA* **87**: 3244-3247.

Fisher, D. B. (2000). Long distance transport. In: Buchanan, B. B., Gruissem, W., and Jones, R. L. (Eds), Biochemistry and Molecular Biology of Plants. American Society of Plant Physiologists, Rockville, MD., pp. 730-784.

Fortin, M. G., Morrison, N. A., and Verma, D. P. (1987). Nodulin-26, a peribacteroid membrane nodulin is expressed independently of the development of the peribacteroid compartment. *Nucleic Acids Res*. **15**: 813-824.

Francis, P., Chung, J. J., Yasui, M., Berry, V., Moore, A., Wyatt, M. K., Wistow, G., Bhattacharya, S. S., and Agre, P. (2000a). Functional impairment of lens aquaporin in two families with dominantly inherited cataracts. *Hum. Mol. Genet*. **9**: 2329-2334.

Francis, P., Berry, V., Bhattacharya, S., and Moore, A. (2000b). Congenital progressive polymorphic cataract caused by a mutation in the major intrinsic protein of the lens, MIP (AQP0). *Br. J. Opthamol*. **84**: 1376-1379.

Froger, A., Tallur, B., Thomas, D., and Delamarche, C. (1998). Prediction of the functional residues in water channels and related proteins. *Protein Sci*. **7**: 1458-1468.

Fu, D., Libson, A., Miercke, L.J., Weitzmann, C., Nollert, P., Krucinski, J., and Stroud, R.M. (2000). Structure of a glycerol-conducting channel and the basis for its selectivity. *Science* **290**: 481-486.

Fujiwara, T., Hirai, M. Y., Chino, M., Komeda, Y., and Naito, S. (1992). Effects of sulfur nutrition on expression of the soybean seed storage protein genes in transgenic petunia. *Plant Physiol*. **99**: 263-268.

Fushimi, K., Uchida, S., Hara, Y., Hirata, Y., Marumo, F., and Sasaki, S. (1993). Cloning and expression of apical membrane water channel of rat kidney collecting tubule. *Nature* **361**: 549-552.

Fushimi, K., Sasaki, S., and Marumo, F. (1997). Phosphorylation of serine 256 is required for cAMP-dependent regulatory exocytosis of the aquaporin-2 water channel. *J. Biol. Chem*. **272**: 14800-14804.

Gerbeau, P., Guclu, J., Ripoche, P., and Maurel, C. (1999). Aquaporin Nt-TIPa can account for the high permeability of tobacco cell vacuolar membrane to small neutral solutes. *Plant J*. **18**: 577-587.

Gerbeau, P., Amodeo, G., Henzler, T., Santoni, V., Ripoche, P., and Maurel, C. (2002). The water permeability of Arabidopsis plasma membrane is regulated by divalent cations and pH. *Plant J*. **30**: 71-81.

Gil, R., Sabater-Munoz, B., Latorre, A., Silva, F. J., and Moya, A. (2002). Extreme genome reduction in Buchnera spp.: toward the minimal genome needed for symbiotic life. *Proc. Natl. Acad. Sci. USA* **99**: 4454-4458.

Gonen, T., Sliz, P., Kistler, J., Cheng, Y., and Walz, T. (2004). Aquaporin-0 membrane junctions reveal the structure of a closed water pore. *Nature* **429**: 193-197.

Gorin, M. B., Yancey, S. B., Cline, J., Revel, J. P., and Horwitz, J. (1984). The Major Intrinsic Protein (MIP) of the bovine lens fiber membrane: characterization and structure based on cDNA cloning. *Cell* **39**: 39-59.

Grisafi, P. L., Scholle, A., Sugiyama, J., Briggs, C., Jacobson, G. R., and Lengeler, J. W. (1989). Deletion mutants of the *Eschericia coli* K-12 mannitol permease: dissection of transport-phosphorylation, phospho-exchange, and mannitol-binding activities. *J. Bacteriol*. **171**: 2719-2727.

Guenther, J. F., and Roberts, D. M. (2000). Water-selective and multifunctional aquaporins from *Lotus japonicus* nodules. *Planta* **210**: 741-748.

Guenther, J. F., Chanmanivone, N., Galetovic, M. P., Wallace, I. S., Cobb, J. A., and Roberts, D. M. (2003). Phosphorylation of soybean nodulin 26 on serine 262 enhances water permeability and is regulated developmentally and by osmotic signals. *Plant Cell* **15**: 981-991.

Guerrero, F. D., Jones, J. T., and Mullet, J. E. (1990). Turgor-responsive gene transcription and RNA levels increase when pea shoots are wilted: sequence and expression of three inducible genes. *Plant Mol. Biol*. **15**: 11-26.

Han, Z., Wax, M. B., and Patil, R. V. (1998). Regulation of aquaporin-4 water channels by phorbol ester-dependent protein phosphorylation. *J. Biol. Chem*. **273**: 6001-6004.

Harper, J. F., Brenton, G., and Harmon, A. (2004). Decoding Ca^{2+} signals through plant protein kinases. *Annu. Rev. Plant Biol*. **55**: 263-288.

Harper, J. F., and Harmon, A. (2005). Plants, symbiosis, and parasites: a calcium signaling connection. *Nat. Rev. Mol. Cell. Biol*. **6**: 555-566.

Harries, W. E., Akhavan, D., Miercke, L. J., Khademi, S., and Stroud, R. M. (2004). The channel architecture of aquaporin-0 at 2.2 angstrom resolution. *Proc. Natl. Acad. Sci. USA* **101**: 14045-14050.

Harris, H. W. Jr., Handler, J. S., and Blumenthal, R. (1990). Apical membrane vesicles of ADH-stimulated toad bladder are highly water permeable. *Am. J. Physiol*. **258**: F237-243.

Hasegawa, H., Ma, T., Skach, W., Matthay, M. A., and Verkman, A. S. (1994). Molecular cloning of a mercurial-insensitive water channel expressed in selected water-transporting tissues. *J. Biol. Chem*. **269**: 5497-5500.

Hedfalk, K., Bill, R. M., Mullins, J. G., Karlgren, S., Filipsson, C., Bergstrom, J., Tamas, M. J., Rydstrom, J., and Hohmann, S. (2004). A regulatory domain in the C-terminal extension of the yeast glycerol channel Fps1p. *J. Biol. Chem*. **279**: 14954-14960.

Heller, K. B., Lin, E. C., and Wilson, T. H. (1980). Substrate specificity and transport properties of the glycerol facilitator of *Eschericia coli*. *J. Bacteriol*. **144**: 274-278.

Higuchi, T., Suga, S., Tsuchiya, T., Hisada, H., Morishima, S., Okada, Y., and Maeshima, M. (1998). Molecular cloning, water channel activity, and tissue specific expression of two isoforms of radish vacuolar aquaporin. *Plant Cell Physiol*. **39**: 905-913.

Hofte, H., Hubbard, L., Reizer, J., Ludevid, D., Herman, E. M., and Chrispeels, M. J. (1992). Vegetative and seed-specific forms of tonoplast intrinsic protein in the vacuolar membrane of *Arabidopsis thaliana*. *Plant Physiol*. **99**: 561-570.

Hohmann, I., Bill, R. M., Kayingo, I., and Prior, B. A. (2000). Microbial MIP channels. *Trends Microbiol*. **8**: 33-38.

Holm, L.M., Jahn, T.P., Moller, A.L., Schjoerring, J.K., Ferri, D., Klaerke, D.A., and Zeuthen, T. (2005). NH_3 and NH_4^+ permeability in aquaporin-expressing *Xenopus* oocytes. *Pflugers Arch*. **450**: 415-428.

Horsefield, R., Norden, K., Fellert, M., Backmark, A., Tornroth-Horsefield, S., Terwisscha van Scheltinga, A. C., Kvassman, J., Kjellbom, P., Johanson, U., and Neutze, R. (2008). High resoltution X-ray structure of aquaporin 5. *Proc. Natl. Acad. Sci. USA* **105**: 13327-13332.

Huang, C. G., Lamitina, T., Agre, P., and Strange, K. (2007). Functional analysis of the aquaporin gene family in *Caenorhabditis elegans*. *Am. J. Physiol. Cell. Physiol*. **292**: C1867-1873.

Isayenkov, S. V., and Maathius, F. J. (2008). The *Arabidopsis thaliana* aquaglyceroporin AtNIP7;1 is a pathway for arsenite uptake. *FEBS Lett*. **582**: 1625-1628.

Ishibashi, K., Sasaki, S., Fushimi, K., Uchida, S., Kuwahara, M., Saito, H., Furukawa, T., Nakajima, K., Yamaguchi, Y., and Gojobori, T. (1994). Molecular cloning and expression of a member of the aquaporin family with permeability to glycerol and urea in addition to water expressed at the basolateral membrane of kidney collecting duct cells. *Proc. Natl. Acad. Sci. USA* **91**: 6269-6273.

Ishibashi, K., Kuwahara, M., Gu, Y., Kageyama, Y., Toshaka, A., Suzuki, F., Marumo, F., and Sasaki, S. (1997). Cloning and functional expression of a new water channel abundantly expressed in the testis permeable to water, glycerol, and urea. *J. Biol. Chem*. **272**: 20782-20786.

Ishikawa, F., Suga, S., Uemura, T., Sato, M.H., and Maeshima, M. (2006). Novel type aquaporin SIPs are mainly localized to the ER membrane and show cell-specific expression in *Arabidopsis thaliana*. *FEBS Lett*. **579**: 5814-5820.

Ishiyama, K., Inoue, E., Watanabe-Takahashi, A., Obara, M., Yamaya, T., and Takahashi, H. (2004a). Kinetic properties and ammonium-dependent regulation of cytosolic enzymes of glutamine synthetase in Arabidopsis. *J. Biol. Chem*. **279**: 16598-16605.

Ishiyama, K., Inoue, E., Tabuchi, M., Yamaya, T., and Takahashi, H. (2004b). Biochemical background and compartmentalized functions of cytosolic glutamine synthetase for active ammonium assimilation in rice roots. *Plant Cell Physiol*. **45**: 1640-1647.

Jahn, T. P., Moller, A. L., Zeuthen, T., Holm, L. M., Klaerke, D. A., Moshin, B., Kuhlbrandt, W., and Schjoerring, J. K. (2004). Aquaporin homologues in plants and mammals transport ammonia. *FEBS Lett*. **574**: 31-36.

Jap, B. K., and Li, H. (1995). Structure of the osmo-regulated H_2O-channel, AQP-CHIP, in projection at 3.5 angstrom resolution. *J. Mol. Biol*. **251**: 413-420.

Jaubert-Possamai, S., Le Trionnaire, G., Bonhomme, J., Christophides, G. K., Rispe, C., and Tagu, D. (2007). Gene knockdown by RNAi in the pea aphid *Acyrthrosiphon pisum*. *BMC Biotechnol*. **7**: 63-71.

Jauh, G. Y., Fischer, A. M., Grimes, H. D., Ryan, C. A. Jr., and Rogers, J. C. (1998). delta-Tonoplast intrinsic protein defines unique plant vacuole functions. *Proc. Natl. Acad. Sci. USA* **95**: 12995-12999.

Javot, H., Lauvergeat, V., Santoni, V., Martin-Laurent, F., Guclu, J., Vinh, J., Heyes, J., Franck, K. I., Schaffner, A. R., Bouchez, D., and Maurel, C. (2003). Role of a single aquaporin isoform in root water uptake. *Plant Cell* **15**: 509-522.

Jensen, M. O., Park, S., Tajkhorshid, E., and Schulten, K. (2002). Energetics of glycerol conduction through aquaglyceroporin GlpF. *Proc. Natl. Acad. Sci*. **99**: 6731-6736.

Jensen, M. O., Dror, R. O., Xu, H., Borhani, D. W., Arkin, I. T., Eastwood, M. P., and Shaw, D. E. (2008). Dynamic control of slow water transport by aquaporin-0: implications for hydration and junction stability in the eye lens. *Proc. Natl. Acad. Sci. USA* **105**: 14430-14435.

Johanson, U., Karlsson, M., Johansson, I., Gustavsson, S., Sjovall, S., Fraysse, L., Weig, A. R., and Kjellbom, P. (2001). The complete set of genes encoding major intrinsic proteins in Arabidopsis provides a framework for a new nomenclature for major intrinsic proteins in plants. *Plant Physiol*. **126**: 1358-1369.

Johanson, U., and Gustavsson, S. (2002). A new subfamily of major intrinsic proteins in plants. *Mol. Biol. Evol*. **19**: 456-461.

Johansson, I., Larsson, C., Ek, B., and Kjellbom, P. (1996). The major integral proteins of spinach leaf plasma membranes are putative aquaporins and are phosphorylated in response to Ca^{2+} and apoplastic water potential. *Plant Cell* **8**: 1181-1191.

Johansson, I., Karlsson, M., Shukla, V. K., Chrispeels, M. J., Larsson, C., and Kjellbom, P. (1998). Water transport activity of the plasma membrane aquaporin PM28A is regulated by phosphorylation. *Plant Cell* **10**: 451-459.

Johnson, K. D., Herman, E. M., and Chrispeels, M. J. (1989). An abundant highly conserved tonoplast protein in seeds. *Plant Physiol*. **91**: 1006-1013.

Johnson, K. D., Hofte, H., and Chrispeels M. J. (1990). An intrinsic tonoplast protein of storage vacuoles in seeds is structurally related to a bacterial solute transporter (GlpF). *Plant Cell* **2**: 525-532.

Jung, J. S., Bhat, R. V., Preston, G. M., Guggino, W. B., Baraban, J. M., and Agre, P. (1994a). Molecular characterization of an aquaporin cDNA from brain: candidate osmoreceptor and regulator of water balance. *Proc. Natl. Acad. Sci. USA* **91**: 13052-13056.

Jung, J. S., Preston, G. M., Smith, B. L., Guggino, W. B., and Agre, P. (1994b). Molecular structure of the water channel through aquaporin CHIP: the hourglass model. *J. Biol. Chem*. **269**: 14648-14654.

Kachadorian, W. A., Levine, S. D., Wade, J. B., Di Scala, V. A., and Hays, R. M. (1977). Relationship of aggregated intramembranous particles to water permeability in vasopressin-treated toad urinary bladder. *J. Clin. Invest*. **59**: 576-581.

Kaiser, B. N., Finnegan, P. M., Tyerman, S. D., Whitehead, L. F., Bergerson, F. J., Day, D. A., and Udvardi, M .K. (1998). Characterization of an ammonium transport protein from the peribacteroid membrane of soybean nodules. *Science* **281**: 1202-1206.

Kaiser, B. N., Moreau, S., Castelli, J., Thomson, R., Lambert, A., Bogliolo, S., Puppo, A., and Day, D. A. (2003). The soybean NRAMP homologue, GmDMT1, is a symbiotic divalent metal transporter capable of ferrous ion transport. *Plant J*. **35**: 295-304.

Kammerloher, W., Fischer, U., Piechottka, G. P., and Schaffner, A. R. (1994). Water channels in the plant plasma membrane cloned by immunoselection from a mammalian expression system. *Plant J*. **6**: 187-199.

Kamsteeg, E. J., Heijnen, I., van Os, C. H., and Deen, P. M. (2000). The subcellular localization of an aquaporin-2 tetramer depends on the stoichiometry of phosphorylated and nonphosphorylated monomers. *J. Cell Biol*. **151**: 919-930.

Karlgren, S., Filipsson, C., Mullins, J. G., Bill, R. M., Tamas, M. J., and Hohmann, S. (2004). Identification of the residues controlling transport through the yeast aquaglyceroporin Fps1using a genetic screen. *Eur. J. Biochem*. **271**: 771-779.

Karlsson, M., Johansson, I., Bush, M., McCann, M. C., Maurel, C., Larsson, C., and Kjellbom, P. (2000). An abundant TIP expressed in mature highly vacuolated cells. *Plant J*. **21**: 83-90.

Katsuhara, M., Akiyama, Y., Koshio, K., Shibasaka, M., and Kasamo, K. (2002). Functional analysis of water channels in barley roots. *Plant Cell Physiol*. **43**: 885-893.

Kaufmann, N., Mathai, J. C., Hill, W. G., Dow, J. A., Zeidel, M. L., and Brodsky, J. L. (2005). Developmental expression and biophysical characterization of a *Drosophila melanogaster* aquaporin. *Am. J. Physiol. Cell. Physiol*. **289**: C397-407.

Kelly, K. (1996). Multiple sequence and structural alignment in MOE. Chemical Computing Group. http://www.chemcomp.com/Journal_of_CCG/Features/align.htm

Kelly, K., and Labute, P. (1996). The A* search and applications to sequence alignment. Chemical Computing Group. http://www.chemcomp.com/ Journal_of_CCG/Articles/astar.htm

Kikawada, T., Saito, A., Kanamori, Y., Fujita, M., Snigorska, K., Watanabe, M., and Okuda, T. (2008). Dehydration-inducible changes in expression of two aquaporins in the sleeping chironomid (*Polypedilium vanderplanki*). *Biochim. Biophys. Acta* **1778**: 514-520.

Klebl, F., Wolf, M., and Sauer, N. (2003). A defect in the yeast plasma membrane urea transporter Dur3p is complemented by CpNIP1, a Nod26-like protein from zucchini (*Cucurbita pepo L.*), and by *Arabidopsis thaliana* delta –TIP or gamma-TIP. *FEBS lett.* **547**: 69-74.

Knight, H., Trewavas, A. J., and Knight, M. R. (1997). Calcium signaling in *Arabidopsis thaliana* responding to drought and salinity. *Plant J.* **12**: 1067-1078.

Kosugi-Tanaka, C., Li, X., Yao, C., Akamatsu, T., Kanamori, N., and Hosoi, K. (2006). Protein kinase A-regulated membrane trafficking of a green fluorescent protein-aquaporin 5 chimera in MDCK cells. *Biochim. Biophys. Acta* **1763**: 337-344.

Koyama, N., Ishibashi, K., Kuwahara, M., Inase, N., Ichioka, M., Sasaki, S., and Marumo, F. (1998). Cloning and functional expression of human aquaporin-8 cDNA and analysis of its gene. *Genomics* **54**: 169-172.

Kozono, D., Ding, X., Iwasaki, I., Meng, X., Kamagata, Y., Agre, P., and Kitagawa, Y. (2003). Functional expression and characterization of an archaeal aquaporin AqpM from *Methanothermobacter marburgensis*. *J. Biol. Chem*. **278**: 10649-10656.

Kuriyama, H., Kawamoto, S., Ishida, N., Ohno, I., Mita, S., Matsuzawa, Y., Matsubara, K., and Okubo, K. (1997). Molecular cloning and expression of a novel human aquaporin from adipose tissue with glycerol permeability. *Biochem. Biophys. Res. Commun*. **241**: 53-58.

Laemmli, U. K. (1970). Cleavage of structural proteins during the assembly of the head of bacteriophage T4. *Nature* **227**: 680-685.

Lee, J. K., Kozono, D., Remis, J., Kitagawa, Y., Agre, P., and Stroud, R. M. (2005). Structural basis for conductance by the archaeal aquaporin M at 1.68 angstroms. *Proc. Natl. Acad. Sci. USA* **102**: 18932-18937.

Lee, J. W., Zhang, Y., Weaver, C. D., Shomer, N. H., Louis, C. F., and Roberts, D. M. (1995). Phosphorylation of nodulin 26 on serine 262 affects its voltage-sensitive channel activity in planar lipid bilayers. *J. Biol. Chem*. **270**: 27051-27057.

Levitt, M. (1992). Accurate modeling of protein modeling by automatic segment matching. *J. Mol. Biol*. **226**: 507-533.

Li, L., Li, S., Tao, Y., and Kitagawa, Y. (2000). Molecular cloning of a novel water channel from rice: its products expression in *Xenopus* oocytes and involvement in chilling tolerance. *Plant Sci*. **154**: 43-51.

Lian, H. L., Yu, X., Ye, Q., Ding, X., Kitagawa, Y., Kwak, S. S., Su, W. A., and Tang, Z. C. (2004). The role of aquaporin RWC3 in drought avoidance in rice. *Plant Cell Physiol*. **45**: 481-489.

Limpens, E., and Bisseling, T. (2003). Signaling in symbiosis. *Curr. Opin. Plant Biol*. **6**: 343-350.

Liu, Q., Umeda, M., and Uchimaya, H. (1994). Isolation and expression analysis of two rice genes encoding the major intrinsic protein. *Plant Mol. Biol*. **26**: 2003-2007.

Liu, L. H., Ludewig, U., Gassert, B., Frommer, W. B., and von Wiren, N. (2003). Urea transport by nitrogen-regulated tonoplast intrinsic proteins in Arabidopsis. *Plant Physiol*. **133**: 1220-1228.

Liu, Z., Boles, E., and Rosen, B. P. (2004). Arsenic trioxide uptake by hexose permeases in *Saccharomyces cerevisiae*. *J. Biol. Chem*. **279**: 17312-17318.

Loque, D., Ludewig, U., Yuan, L., and von Wiren, N. (2005). Tonoplast intrinsic proteins AtTIP2;1 and AtTIP2;3 facilitate NH_3 transport into the vacuole. *Plant Physiol*. **137**: 671-680.

Lu, D., Grayson, P., and Schulten, K. (2003). Glycerol conductance and physical asymmetry of the *Eschericia coli* glycerol facilitator. *Biophys. J*. **85**: 2977-2987.

Luyten, K., Albertyn, J., Skibbe, W. F., Prior, B. A., Ramos, J., Thevelein, J. M., and Hohmann, S. (1995). Fps1, a member of the MIP family of channel proteins, is a facilitator for glycerol uptake and efflux and is inactive under osmotic stress. *EMBO J*. **14**: 1360-1371.

Ma, J. F., Tamai, K., Yamaji, N., Mitani, N., Konishi, S., Katsuhara, M., Ishiguro, M., Murata, Y., and Yano, M. (2006). A silicon transporter in rice. *Nature* **440**: 688-691.

Ma, J. F., Yamaji, N., Mitani, N., Tamai, K., Konishi, S., Fujiwara, T., Katsuhara, M., and Yano, M. (2007). An efflux transporter of silicon in rice. *Nature* **448**: 209-212.

Ma, T., Yang, B., and Verkman, A. S. (1997). Cloning of a novel water and urea-permeable aquaporin from mouse expressed strongly in colon, placenta, liver, and heart. *Biochem. Biophys. Res. Commun*. **240**: 324-328.

Macey, R. I., and Farmer, R. E. (1970). Inhibition of water and solute permeability in human red cells. *Biochim. Biophys. Acta* **211**: 104-106.

Macey, R. I. (1984). Transport of water and urea in red blood cells. *Am. J. Physiol*. **246**: C195-203.

Madrid, R., Le Maout, S., Barrault, M. B., Janvier, K., Benichou, S., and Merot, J. (2001). Polarized trafficking and surface expression of the AQP4 water channel are coordinated by serial and regulated interactions with different clathrin-adaptor complexes. *EMBO J*. **20**: 7008-7021.

Mahdieh, M., Mostajeron, A., Horie, T., and Katsuhara, M. (2008). Drought stress alters water relations and expression of PIP-type aquaporin genes in *Nicotinia tabacum* plants. *Plant Cell Physiol*. **49**: 801-813.

Malone, M., and Tomos, A. D. (1992). Measurement of gradients of water potential in elongating pea stems by pressure probe and picoliter osmometry. *J. Exp. Bot*. **43**: 1325-1331.

Malz, S., and Sauter, M. (1999). Expression of two PIP genes in rapidly growing internodes of rice is not primarily controlled by meristem activity or cell expansion. *Plant Mol. Biol*. **40**: 985-995.

Manley, G. T., Fujimura, M., Ma, T., Noshita, N., Filiz, F., Bollen, A. W., Chan, P., and Verkman, A. S. (2000). Aquaporin-4 deletion in mice reduces brain edema after acute water intoxication and ischemic stroke. *Nat. Med*. **6**: 159-163.

Marschner, H. (1995). Mineral nutrition of higher plants, 2nd edition. San Diego, CA. Academic Press.

Martre, P., Morillon, R., Barrieu, F., North, G. B., Nobel, P. S., and Chrispeels, M. J. (2002). Plasma membrane aquaporins play a significant role during recovery from water deficit. *Plant Physiol*. **130**: 2101-2110.

Marx, D., Tuckerman, M. E., Hutter, J., and Parrinello, M. (1999). The nature of the hydrated excess proton in water. *Nature* **397**: 601-604.

Matsunaga, T., Ishii, T., Matsumoto, S., Higuchi, M., Darvill, A., Albersheim, P., and O'Neill, M. A. (2004). Occurrence of the primary cell wall polysaccharide rhamnogalacturonan II in pteridophytes, lycophytes, and bryophytes: implications for the evolution of vascular plants. *Plant Physiol*. **134**: 339-351.

Maurel, C., Reizer, J., Schroeder, J. I., and Chrispeels, M. J. (1993). The vacuolar membrane protein gamma-TIP creates water specific channels in *Xenopus* oocytes. *EMBO J*. **12**: 2241-2247.

Maurel, C., Reizer, J., Schroeder, J. I., Chrispeels, M. J., and Saier, M. H. Jr. (1994). Functional characterization of the *Escherichia coli* glycerol facilitator, GlpF, in *Xenopus* oocytes. *J. Biol. Chem*. **269**: 11869-11872.

Maurel, C., Kado, R.T., Guern, J., and Chrispeels, M. J. (1995). Phosphorylation regulates the water channel activity of the seed-specific aquaporin alpha-TIP. *EMBO J*. **14**: 3028-3035.

Maurel, C. (1997). Aquaporins and water permeability of plant membranes. *Annu. Rev. Plant Physiol. Plant Mol. Biol*. **48**: 399-429.

Maurel, C., Javot, H., Lauvergeat, V., Gerbeau, P., Tournaire, C., Santoni, V., and Heyes, J. (2002). Molecular physiology of aquaporins in plants. *Int. Rev. Cytol*. **215**: 105-148.

Maurel, C., Verdoucq, L., Luu, D. T., and Santoni, V. (2008). Plant aquaporins: membrane channels with multiple integrated functions. *Annu. Rev. Plant Biol*. **59**: 595-624.

McParland, R. H., Guevara, J. G., Becker, R. R., and Evans, H. J. (1976). The purification and properties of the glutamine synthetase from the cytosol of Soya-bean root nodules. *Biochem. J*. **153**: 597-606.

Meinild, A. K., Klaerke, D. A., and Zeuthen, T. (1998). Bidirectional water fluxes and specificity for small hydrophilic molecules in aquaporins 0-5. *J. Biol. Chem*. **273**: 32446-32451.

Meng, Y. L., Liu, Z., and Rosen, B. P. (2004). As(III) and Sb(III) uptake by GlpF and efflux by ArsB in *Eschericia coli*. *J. Biol. Chem*. **279**: 18334-18341.

Miflin, B. J., and Habash, D. Z. (2002). The role of glutamine synthetase and glutamate dehydrogenase in nitrogen assimilation and possibilities for improvement in nitrogen utilization of crops. *J. Exp. Bot*. **53**: 979-987.

Miwa, K., Takano, J., Omori, H., Seki, M., Shinozaki, K., and Fujiwara, T. (2007). Plants tolerant of high boron levels. *Science* **318**: 1417.

Mollapour, M., and Piper, P. W. (2007). Hog1 mitogen-activated protein kinase phosphorylation targets the yeast Fps1 aquaglyceroporin for endocytosis, thereby rendering cells resistant to acetic acid. *Mol. Cell. Biol*. **27**: 6446-6456.

Moreau, S., Thomson, R. M., Kaiser, B. N., Trevakis, B., Guerinot, M. L., Udvardi, M. K., Puppo, A., and Day, D. A. (2002). GmZIP1 encodes a symbiosis-specific zinc transporter in soybean. *J. Biol. Chem*. **277**: 4738-4746.

Morey, K. J., Ortega, J. L., and Sengupta-Gopalan, C. (2002). Cytosolic glutamine synthetase in soybean is encoded by a multigene family, and the members are regulated in an organ-specific and developmental manner. *Plant Physiol*. **128**: 182-193.

Morgan, T., and Berliner, R. W. (1968). Permeability of the loop of Henle, vasa recta, and collecting duct to water, urea, and sodium. *Am. J. Physiol*. **215**: 108-115.

Muramatsu, S., and Mizuno, T. (1989). Nucleotide sequence of the region encompassing the glpKF operon and its upstream region containing a bent DNA sequence of *Eschericia coli*. *Nucleic Acids Res*. **17**: 4378.

Nakabachi, A., Shigenobu, S., Sakazume, N., Shiraki, T., Hayashizaki, Y., Carninci, P., Ishikawa, H., Kudo, T., and Fukatsu, T. (2005). Transcriptome analysis of the aphid bacteriocyte, the symbiotic host cell that harbors and endocellular mutualistic bacterium, *Buchnera*. *Proc. Natl. Acad. Sci. USA* **102**: 5477-5482.

Nakagawa, Y., Hanaoka, H., Kobayashi, M., Miyoshi, K., Miwa, K., and Fujiwara, T. (2007). Cell-type specificity of the expression of OsBOR1, a rice efflux boron transporter gene, is regulated in response to boron availability for efficient boron uptake and xylem loading. *Plant Cell* **19**: 2624-2635.

Nemeth-Cahalan, K. L., and Hall, J. E. (2000). pH and calcium regulate the water permeability of aquaporin-0. *J. Biol. Chem*. **275**: 6777-6782.

Nemeth-Cahalan, K. L., Kalman, K., and Hall, J. E. (2004). Molecular basis of pH and Ca^{2+} regulation of aquaporin water permeability. *J. Gen. Physiol*. **123**: 573-580.

Newby, Z. E., O'Connell, J. 3rd, Robles-Colmenares, Y., Khademi, S., Miercke, L. J., and Stroud, R. M. (2008). Crystal structure of the aquaglyceroporin PfAQP from the malarial parasite *Plasmodium falciparum*. *Nat. Struct. Mol. Biol*. **15**: 619-625.

Nielsen, S., Chou, C. L., Marples, D., Christensen, E. I., Kishore, B. K., and Knepper, M. A. (1995). Vasopressin increases water permeability of kidney collecting duct by inducing translocation of aquaporin-CD water channels to plasma membrane. *Proc. Natl. Acad. Sci. USA* **92**: 1013-1017.

Niemietz, C. M., and Tyerman, S. D. (2000). Channel-mediated permeation of ammonia gas through the peribacteroid membrane of soybean nodules. *FEBS Lett*. **465**: 110-114.

Niemietz, C. M., and Tyerman, S. D. (2002). New potent inhibitors of aquaporins: silver and gold compounds inhibit aquaporins of plant and human origin. *FEBS Lett*. **531**: 443-447.

Noda, Y., Horikawa, S., Furukawa, T., Hirai, K., Katayama, Y., Asai, T., Kuwahara, M., Katagiri, K., Kinashi, T., Hattori, M., Minato, N., and Sasaki, S. (2004a). Aquaporin-2 trafficking is regulated by PDZ-domain containing protein SPA-1. *FEBS Lett*. **568**: 139-145.

Noda, Y., Horikawa, S., Katayama, Y., and Sasaki, S. (2004b). Water channel aquaporin-2 directly binds actin. *Biochem. Biophys. Res. Commun*. **322**: 740-745.

Noda, Y., Horikawa, S., Katayama, Y., and Sasaki, S. (2005). Identification of a multiprotein "motor" complex binding to water channel aquaporin-2. *Biochem. Biophys. Res. Commun*. **330**: 1041-1047.

Noguchi, K., Yasumori, M., Imai, T., Naito, S., Matsunaga, T., Oda, H., Hayashi, H., Chino, M., and Fujiwara, T. (1997). bor1-1, and *Arabidopsis thaliana* mutant that requires a high level of boron. *Plant Physiol*. **115**: 901-906.

Nozawa, A., Takano, J., Kobayashi, M., von Wiren, N., and Fujiwara, T. (2006). Roles of BOR1, DUR3, and FPS1 in boron transport and tolerance in *Saccharomyces cerevisiae*. *FEMS Microbiol. Lett*. **262**: 216-222.

Obermeyer, G., and Tyerman, S. D. (2005). NH_4^+ currents across the peribacteroid membrane of soybean: macroscopic and microscopic properties, inhibition by Mg^{2+}, and temperature dependence indicate a subpicosiemens channel finelyregulated by divalent cations. *Plant Physiol*. **139**: 1015-1029.

Obrdlik, P., El-Bakkoury, M., Hamacher, T., Cappellaro, C., Vilarino, C., Fleischer, C., Ellerbrok, H., Kamuzini, R., Ledent, V., Blaudez, D., Sanders, D., Revuelta, J. L., Boles, E., Andre, B., and Frommer, W. B. (2004). K^+ channel interactions detected by a genetic system optimized for systematic studies of membrane protein interactions. *Proc. Natl. Acad. Sci. USA* **101**: 12242-12247.

Offler, C.E., McCurdy, D. W., Patrick, J. W., and Talbot, M. J. (2002). Transfer cells: cells specialized for a special purpose. *Annu. Rev. Plant Biol*. **54**: 431-454.

Ohrui, T., Nobira, H., Sakata, Y., Taji, T., Yamamoto, C., Nishida, K., Yamakawa, T., Sasuga, Y., Yaguchi, Y., Takenaga, H., and Tanaka, S. (2007). Foliar trichome and aquaporin aided water uptake in a drought resistant epiphyte *Tillandsia ionatha Planchon*. *Planta* **227**: 47-56.

Oldroyd, G. E., and Downie, J. A. (2008). Coordinating nodule morphogenesis with rhizobial infection in legumes. *Annu. Rev. Plant Biol*. **59**: 519-546.

O'Neill, M. A., Warrenfeltz, D., Kates, K., Pellerin, P., Doco, T., Darvill, A. G., and Albersheim, P. (1996). Rhamnogalacturonan-II, a pectic polysaccharide in the walls of growing plant cell, forms a dimer that is covalently cross-linked by a borate ester: in vitro conditions for the formation and hydrolysis of the dimer. *J. Biol. Chem*. **271**: 22923-22930.

O'Neill, M. A., Eberhard, S., Albersheim, P., and Darvill, A. G. (2001). Requirement of borate cross-linking of cell wall rhamnogalacturonan-II for Arabidopsis growth. *Science* **294**: 846-849.

O'Neill, M. A., Ishii, T., Albersheim, P., and Darvill, A. G. (2004). Rhamnogalacturonan-II: structure and function of a borate cross-linked cell wall pectic polysaccharide. *Annu. Rev. Plant Biol*. **55**: 109-139.

Ouyang, L. J., Udvardi, M. K., and Day, D. A. (1990). Specificity and regulation of the dicarboxylate carrier on the perbacteroid membrane of soybean nodules. *Planta* **182**: 434-444.

Ouyang, L. J., Whelan, J., Weaver, C. D., Roberts, D. M., and Day, D. A. (1991). Protein phosphorylation stimulates the rate of malate uptake across the perbacteroid membrane of soybean nodules. *FEBS Lett*. **293**: 188-190.

Paganelli, C. V., and Solomon, A. K. (1957). The rate of exchange of tritiated water across the human red cell membrane. *J. Gen. Physiol*. **41**: 258-277.

Park, J. H., and Saier, M. H. Jr. (1996). Phylogenetic characterization of the MIP family of transmembrane channel proteins. *J. Membr. Biol*. **153**: 171-180.

Pietrantino, P. V., Jagge, C., Keeley, L. L., and Ross, L. S. (2000). Cloning of an aquaporin-like cDNA and in situ hybridization in adults of the mosquito *Aedes aegypti* (Diptera: Culicidae). *Insect Mol*. Biol. **9**: 407-418.

Porquet, A., and Filella, M. (2007). Structural evidence of the similarity of $Sb(OH)_3$ and $As(OH)_3$ with glycerol: implications for their uptake. *Chem. Res. Toxicol*. **20**: 1269-1276.

Prak, S., Hem, S., Boudet, J., Viennois, G., Sommerer, N., Rossignol, M., Maurel, C., and Santoni, V. (2008). Multiple phosphorylations in the C-terminal tail of plant plasma membrane aquaporins: role in subcellular trafficking of AtPIP2;1 in response to salt stress. *Mol. Cell. Proteomics* **7**: 1019-1030.

Preston, G. M., and Agre, P. (1991). Isolation of the cDNA for erythrocyte integral membrane protein of 28 kilodaltons: member of an ancient channel family. *Proc. Natl. Acad. Sci. USA* **88**: 1110-1114.

Preston, G. M., Carroll, T. P., Guggino, W. B., and Agre, P. (1992). Appearance of water channels in *Xenopus* oocytes expressing red cell CHIP28 protein. *Science* **256**: 385-387.

Price, D. R., Karley, A. J., Ashford, D. A., Isaacs, H. V., Pownall, M. E., Wilkinson, H. S., Gatehouse, J. A., and Douglas, A. E. (2007). Molecular characterization of a candidate gut sucrase in the pea aphid, *Acyrthosiphon pisum*. *Insect Biochem. Mol. Biol*. **37**: 307-317.

Promeneur, D., Kwon, T. H., Yasui, M., Kim, G. H., Frokiar, J., Knepper, M. A., Agre, P., and Nielsen, S. (2000). Regulation of AQP6 mRNA and protein expression in rats in

response to altered acid-base or water balance. *Am. J. Physiol. Renal Physiol*. **279**: F1014-1026.

Qi, X., Tai, C. Y., and Wasserman, B. P. (1995). Plasma membrane intrinsic proteins of *Beta vulgaris L*. *Plant Physiol*. **108**: 387-392.

Quigley, F., Rosenberg, J. M., Shachar-Hill, Y., and Bohnert, H. J. (2001). From genome to function: the Arabidopsis aquaporins. *Genome Biol*. **3**: 1-17.

Raina, S., Preston, G. M., Guggino, W. B., and Agre, P. (1995). Molecular cloning and characterization of an aquaporin cDNA from salivary, lacrimal, and respiratory tissues. *J. Biol. Chem*. **270**: 1908-1912.

Rao, Y., Jan, L. Y., and Jan, Y. N. (1990). Similarity of the product of *Drosophila* neurogenic big brain to transmembrane channel proteins. *Nature* **345**: 163-167.

Raven, J.A. (1980). Short and long distance transport of boric acid in plants. *New Phytol*. **84**: 231-249.

Reichow, S. L., and Gonen, T. (2008). Noncanonical binding of calmodulin to aquaporin-0: implications for channel regulation. *Structure* **16**: 1389-1398.

Reizer, J., Reizer, A., and Saier, M. H. Jr. (1993). The MIP family of integral membrane channel proteins: sequence comparisons, evolutionary relationships, reconstructed pathway of evolution, and proposed functional differentiation of the two repeated halves of the proteins. *Crit. Rev. Biochem. Mol. Biol*. **28**: 235-257.

Ren, G., Cheng, A., Reddy, V., Melnyk, P., and Mitra, A. K. (2000). Three-dimensional fold of the human AQP1 water channel determined at 4 angstrom resolution by electron crystallography of two-dimensional crystals embedded in ice. *J. Mol. Biol*. **301**: 369-387.

Ren, G., Reddy, V. S., Cheng, A., Melnyk, P., and Mitra, A. K. (2001). Visualization of a water-selective pore by electron crystallography in vitreous ice. *Proc. Natl. Acad. Sci. USA* **98**: 1398-1403.

Rivers, R. L., Dean, R. M., Chandy, G., Hall, J. E., Roberts, D. M., and Zeidel, M. L. (1997). Functional analysis of nodulin 26, an aquaporin in soybean root nodule symbiosomes. *J. Biol. Chem*. **272**: 16256-16261.

Roberts, D. M., and Tyerman, S. D. (2002). Voltage-dependent cation channels permeable to NH_4^+, K^+, and Ca^{2+} in the symbiosome membrane of the model legume *Lotus japonicus*. *Plant Physiol*. **128**: 370-378.

Rose, K. M., Wang, Z., Magrath, G. N., Hazard, E. S., Hildebrandy, J. D., and Schey, K. L. (2008). Aquaporin 0-calmodulin interaction and the effect of aquaporin 0 phosphorylation. *Biochemistry* **47**: 339-347.

Roth, E., Jeon, K., and Stacey, G. (1988). Homology in endosymbiotic systems: The term "symbiosome". Molecular genetics of plant microbe interactions (eds), Palacios, R., Verma, D. P. S., ADS Press, St. Paul. 220-225.

Royo, J., Gomez, E., and Hueros, G. (2007). Transfer cells. In Endosperm development and molecular biology. Plant Cell monographs series, A. Olsen, ed. Berlin; Springer-Verlag, pp. 73-90.

Ruiter, R. K., van Eldik, G. J., van Herpen, M. M., Schrauwen, J. A., and Wullems, G. J. (1997). Expression in anthers of two genes encoding *Brassica oleracea* transmembrane channel proteins. *Plant Mol. Biol*. **34**: 163-168.

Rymaszewska, A. (2007). Symbiotic bacteria in oocyte and ovarian cell mitochondria of the tick *Ixodes ricinus*: biology and phylogenetic position. *Parasitol. Res*. **100**: 917-920.

Sabater-Munoz, B., Legai, F., Rispe, C., Bonhomme, J., Dearden, P., Dossat, C., Duclert, A., Gauthier, J. P., Ducray, D. G., Hunter, W., Dang, P., Kambhampti, S., Martinez-Torrez, D., Cortes, T., Moya, A., Nakabachi, A., Philippe, C., Prunier-Leterme, N., Rahbe, Y., Simon, J.C., Stern, D. L., Wincker, P., and Tagu, D. (2006). Large-scale gene discovery in the pea aphid *Acyrthosiphon pisum* (hemiptera). *Genome Biol*. **7**: R21-31.

Saboori, A. M., Smith, B. L., and Agre, P. (1988). Polymorphism in the M_r 32,000 Rh protein purified from Rh(D)-positive and –negative erythrocytes. *Proc. Natl. Acad. Sci. USA* **85**: 4042-4045.

Sakr, S., Alves, G., Morillon, R., Maurel, K., Decourteix, M., Guilliot, A., Fleurat-Lessard, P., Julien, J. L., and Chrispeels, M. J. (2003). Plasma membrane aquaporins are involved in winter embolism recovery in walnut tree. *Plant Physiol*. **133**: 630-641.

Sakurai, J., Ishikawa, F., Yamaguchi, T., Uemura, M., and Maeshima, M. (2005). Identification of 33 rice aquaporin genes and analysis of their expression and function. *Plant Cell Physiol*. **46**: 1568-1577.

Sambrook, J., Fritsch, E. F., and Maniatis, T. (1989). Molecular cloning: a laboratory manual. Cold Spring Harbor Laboratory Press, Cold Spring Harbor, N. Y.

Sandal, N. N., and Marcker, K. A. (1988). Soybean nodulin 26 is homologous to the major intrinsic protein of the bovine lens fiber membrane. *Nucleic Acids Res*. **16**: 9347.

Sandstrom and Moran (2001)

Saparov, S. M., Liu, K., Agre, P., and Pohl, P. (2007). Fast and selective ammonia transport by aquaporin-8. *J. Biol. Chem*. **282**: 5296-5301.

Sarda, X., Tousch, D., Ferrare, K., Cellier, F., Alcon, C., Dupuis, J. M., Casse, F., and Lamaze, T. (1999). Characterization of closely related delta-TIP genes enconding aquaporins which are differentially expressed in sunflower roots upon water deprivation through exposure to air. *Plant Mol. Biol.* **40**: 179-191.

Saterlee, J. S., and Sussman, M. R. (1998). Unusual membrane-associated protein kinases in higher plants. *J. Membr. Biol*. **164**: 205-213.

Savage, D. F., Egea, P. F., Robles-Colmenares, Y., O'Connel, J. D. 3rd, and Stroud, R. M. (2003). Architecture and selectivity in aquaporins: 2.5 angstrom X-ray structure of Aquaporin Z. *PLoS Biol*. **1**: 334-340.

Schuurmans, J. A., van Dongen, J. T., Rutjens, B. P., Boonman, A., Pieterse, C. M., and Borstlap, A. C. (2003). Members of the aquaporin family in the developing pea seed coat include representatives of the PIP, TIP and NIP subfamilies. *Plant Mol. Biol*. **53**: 633-645.

Shen, L., Shrager, P., Girsch, S. J., Donaldson, P. J., and Peracchia, C. (1991). Channel reconstitution in liposomes and planar bilayers with HPLC-purified MIP26 of bovine lens. *J. Membr. Biol*. **124**: 21-32.

Shibagaki, N., Rose, A., McDermott, J. P., Fujiwara, T., Hayashi, H., Yoneyama, T., and Davies, J. P. (2002). Selenate-resistant mutants of Arabidopsis thaliana identify Sultr1;2, a sulfate transporter required for efficient transport of sulfate into roots. *Plant J*. **29**: 475-486.

Shiels, A., Mackay, D., Bassnett, S., Al-Ghoul, K., and Kuszak, J. (2001). Disruption of lens fiber cell architecture in mice expressing a chimeric AQP0-LTR protein. *FASEB J*. **14**: 2207-2212.

Shigenobu, S., Watanabe, H., Hattori, M., Sasaki, Y., and Ishikawa, H. (2000). Genome sequence of the endocellular bacterial symbiont of aphids *Buchnera* sp. APS. *Nature* **407**: 81-86.

Sidel, V. W., and Solomon, A. K. (1957). Entrance of water into human red cells under an osmotic pressure gradient. *J. Gen. Physiol*. **41**: 243-257.

Smart, O. S., Goodfellow, J. M., and Wallace, B. A. (1993). The pore dimensions of gramicidin A. *Biophys. J*. **65**: 2455-2460.

Smith, B. L., and Agre, P. (1991). Erythrocyte M_r 28,000 transmembrane protein exists as a multisubunit oligomer similar to channel proteins. *J. Biol. Chem*. **266**: 6407-6415.

Sogami, M., Era, S., Murakami, M., Seo, Y., Watari, H., and Uyesaka, N. (2001). Application of transition state theory to water transport across cell membranes. *Biochim. Biophys. Acta* **1511**: 42-48.

Solomon, A. K., Chasan, B., Dix, J. A., Lukacovic, M. F., Toon, M.R., and Verkman, A. S. (1983). The aqueous pore in the red cell membrane: band 3 as a channel for anions, cations, nonelectrolytes, and water. *Ann. N. Y. Acad. Sci*. **414**: 97-124.

Spring, J. H, Robichaux, S. R., Kaufmann, N., and Brodsky, J. L. (2007). Localization of a Drosophila DRIP-like aquaporin in the malphigian tubules of the house cricket, *Acheta domesticus*. *Comp. Biochem. Physiol. A Mol. Integr. Physiol*. **148**: 92-100.

Streeter, J. G. (1989). Estimation of ammonium concentration in the cytosol of soybean nodules. *Plant Physiol*. **90**: 779-782.

Sui, H., Han, B. G., Lee, J. K., Walian, P., and Jap, B. K. (2001). Structural basis of water-specific transport through the AQP1 water channel. *Nature* **414**: 872-878.

Sweet, G., Gandor, C., Voegele, R., Wittekindt, N., Beuerle, J., Truniger, V., Lin, E. C., and Boos, W. (1990). Glycerol facilitator of *Eschericia coli*: cloning of GlpF and identification of the GlpF product. *J. Bacteriol*. **172**: 424-430.

Tajkhorshid, E., Nollert, P., Jensen, M. O., Miercke, L. J., O'Connell, J., Stroud, R. M., and Schulten, K. (2002). Control of the selectivity of the aquaporin water channel by global orientational tuning. *Science* **296**: 525-530.

Takano, J., Noguchi, K., Yasumori, M., Kobayashi, M., Gajdos, Z., Miwa, K., Hayashi, H., Yoneyama, T., and Fujiwara, T. (2002). Arabidopsis boron transporter for xylem loading. *Nature* **420**: 337-340.

Takano, J., Miwa, K., Yuan, L., von Wiren, N., and Fujiwara, T. (2005). Endocytosis and degradation of BOR1, a boron transporter of *Arabidopsis thaliana*, regulated by boron availability. *Proc. Natl. Acad. Sci. USA* **102**: 12276-12281.

Takano, J., Wada, M., Ludewig, U., Schaaf, G., von Wiren, N., and Fujiwara, T. (2006). The Arabidopsis major intrinsic protein NIP5;1 is essential for efficient boron uptake and plant development under boron limitation. *Plant Cell* **18**: 1498-1509.

Takano, J., Kobayashi, M., Noda, Y., and Fujiwara, T. (2007). *Saccharomyces cerevisiae* Bor1p is a boron exporter and a key determinant of boron tolerance. *FEMS Microbiol. Lett*. **267**: 230-235.

Takata, K. (2006). Aquaporin-2 (AQP2): its intracellular compartment and trafficking. *Cell. Mol. Biol*. **52**: 34-39.

Tamames, J., Moya, A., and Valencia, A. (2007). Modular organization in the reductive evolution of protein-protein interaction networks. *Genome Biol*. **8**: R94-102.

Tamas, M. J., Karlgren, S., Bill, R. M., Hedfalk, K., Allegri, L., Ferreira, M., Thevelein, J. M., Rydstrom, J., Mullins, J. G., and Hohmann, S. (2003). A short regulatory domain restricts glycerol transport through yeast Fps1p. *J. Biol. Chem.* **278**: 6337-6345.

Tanaka, M., Wallace, I. S., Takano, J., Roberts, D. M., and Fujiwara, T. (2008). NIP6;1 is a boric acid channel for preferential transport of boron to growing shoot tissue in Arabidopsis. *Plant Cell* Epublication ahead of print.

Thellin, O., Zorzi, W., Lakaye, B., De Borman, B., Coumans, B., Hennen, G., Grisar, T., Igout, A., and Heinen, E. (1999). Housekeeping genes as internal standards: use and limits. *J. Biotechnol*. **75**: 291-295.

Thomas, D., Bron, P., Ranchy, G., Duchesne, L., Cavalier, A., Rolland, J.P., Raguenes-Nicol, C., Hubert, J. F., Haase, W., and Delamarche, C. (2002). Aquaglyceroporins, one channel for two molecules. *Biochem. Biophys. Acta* **1555**: 181-186.

Thorsen, M., Di, Y., Tangemo, C., Morillas, M., Ahmadpour, D., Van der Does, C., Wagner, A., Johansson, E., Boman, J., Posas, F., Wysocki, R., and Tamas, M. J. (2006). The MAPK Hog1p modulates Fps1p-dependent arsenite uptake and tolerance in yeast. *Mol. Biol. Cell* **17**: 4400-4410.

Tornroth-Horsefield, S., Wang, Y., Hedfalk, K., Johanson, U., Karlsson, M., Tajkhorshid, E., Neutze, R., Kjellbom, P. (2006). Structural mechanism of plant aquaporin gating. *Nature* **439**: 688-694.

Tournaire-Roux, C., Sutka, M., Javot, H., Gout, E., Gerbeau, P., Luu, D.T., Bligny, R., and Maurel, C. (2003). Cytosolic pH regulates root water transport during anoxic stress through gating of aquaporins. *Nature* **425**: 393-397.

Tsai, S. T., Zhang, R. B., and Verkman, A. S. (1991). High channel-mediated water permeability in rabbit erythrocytes: characterization in native cells and expression in *Xenopus* oocytes. *Biochemistry* **30**: 2087-2092.

Tuckerman, M. E., Marx, D., Klein, M., and Parrinello, M. (1997). On the quantum nature of the shared proton in hydrogen bonds. *Science* **275**: 817-820

Tyerman, S. D., Whitehead, L. F., and Day, D. A. (1995). A channel-like transporter for NH_4^+ on the symbiotic interface of N_2-fixing plants. *Nature* **378**: 629-632.

Udvardi, M. K., and Day, D. A. (1989). Electrogenic ATPase activity on the peribacteroid membrane of soybean (*Glycine max L.*) root nodules. *Plant Physiol*. **90**: 982-987.

Udvardi, M. K., and Day, D. A. (1990). Ammonia (C-methylamine) transport across the bacteroid and peribacteroid membranes of soybean root nodules. *Plant Physiol*. **94**: 71-76.

Udvardi, M. K., and Day, D. A. (1997). Metabolite transport across symbiotic membranes of legume nodules. *Annu. Rev. Plant Physiol. Plant Mol. Biol*. **48**: 493-523.

Van Aelst, L., Hohmann, S., Zimmermann, F. K., Jans, A. W., and Thevelein, J. M. (1991). A yeast homologue of the bovine lens fiber MIP gene family complements the growth defect of a *Saccharomyces cerevisiae* mutant on fermentable sugars but not its defect in glucose-induced RAS-mediated cAMP signaling. *EMBO J*. **10**: 2095-2104.

Vandeleur, R. K., Mayo, G., Sheldon, M. C., Gilliham, M., Kaiser, B. N., and Tyerman, S. D. (2008). The role of PIP aquaporins in water transport through roots: diurnal and drought stress responses reveal different strategies between isohydric and anisohydric cultivars of grapevine. *Plant Physiol*. Epublication ahead of print.

Vandesompele, J., De Preter, K., Pattyn, F., Poppe, B., Van Roy, N., De Paepe, A., and Speleman, F. (2002). Accurate normalization of real-time quantitative RT-PCR data by geometric averaging of multiple internal control genes. *Genome Biol*. **3**: 34-46.

van Ham, R. C., Kamerbeek, J., Palacios, C., Rausell, C., Abascal, F., Bastolla, U., Fernandez, J. M., Jimenez, L., Postigo, M., Silva, F. J., Tamames, J., Viguera, E., Latorre, A., Valencia, A., Moran, F., and Moya, A. (2003). Reductive genome evolution in *Buchnera aphidicola*. *Proc. Natl. Acad. Sci. USA* **100**: 581-586.

van Hoek, A. N., Hom, M. L., Luthjens, L. H., de Jong, M. D., Dempster, J. A., and van Os, C. H. (1991.) Functional unit of 30 kDa for proximal tubule water channels as revealed by radiation inactivation. *J. Biol. Chem*. **266**: 16633-16635.

van Hoek, A. N., and Verkman, A. S. (1992). Functional reconstitution of isolated erythrocyte water channel CHIP28. *J. Biol. Chem*. **267**: 18267-18269.

van Lieburg, A. F., Verdijk, M. A., Knoers, V. V., van Essen, A. J., Proesmans, W., Mallmann, R., Monnens, L. A., van Oost, B. A., van Os, C. H., and Deen, P. M. (1994). Patients with autosomal nephrogenic diabetes insipidus homozygous for mutations in aquaporin-2 water-channel gene. *Am. J. Hum. Genet*. **55**: 648-652.

Verdoucq, L., Grondin, A., and Maurel, C. (2008). Structure-function analysis of plant aquaporin AtPIP2;1 gating by divalent cations and protons. *Biochem. J*. **415**: 409-416.

Verma, D. P., and Hong, Z. (1996). Biogenesis of the peribacteroid membrane in root nodules. *Trends Microbiol*. **4**: 364-368.

Vincill, E. D., Szcsyglowski, K., and Roberts, D. M. (2005). GmN70 and LjN70: Anion transporters of the symbiosome membrane of nodules with a transport preference for nitrate. *Plant Physiol*. **137**: 1435-1444.

Vizuete, M. L., Venero, J. L., Vargas, C., Ilundain, A. A., Echevarria, M., Machado, A., and Cano, J. (1999). Differentail upregulation of aquaporin-4 mRNA expression in reactive astrocytes after brain injury: potential role in brain edema. *Neurobiol. Dis*. **6**: 245-258.

Wade, J. B., Stetson, D. L., and Lewis, S. A. (1981). ADH action: evidence for a membrane shuttle mechanism. *Ann. N. Y. Acad. Sci*. **372**: 106-117.

Wallace, I. S., Wills, D. M., Guenther, J. F., and Roberts, D. M. (2002). Functional selectivity for glycerol of the nodulin 26 subfamily of plant membrane intrinsic proteins. *FEBS lett*. **523**: 109-112.

Wallace, I. S., and Roberts, D. M. (2004). Homology modeling of representative subfamilies of Arabidopsis major intrinsic proteins: Classification based on the aromatic/ arginine selectivity filter. *Plant Physiol*. **135**: 1059-1068.

Wallace, I. S., and Roberts, D. M. (2005). Distinct transport selectivity of two structural subclasses of the nodulin 26-like intrinsic protein family of plant aquaglyceroporin channels. *Biochemistry* **44**: 16826-16834.

Wallace, I. S., Choi, W. G., and Roberts, D. M. (2006). The structure, function, and regulation of the nodulin 26-like intrinsic protein family of plant aquaglyceroporins. *Biochem. Biophys. Acta* **1758**: 1165-1175.

Walz, T., Tittmann, P., Fuchs, K. H., Muller, D. J., Smith, B. L., Agre, P., Gross, H., and Engel, A. (1996). Surface topographies at subnanometer-resolution reveal asymmetry and sidedness of aquaporin-1. *J. Mol. Biol*. **264**: 907-918.

Weaver, C. D., Crombie, B., Stacey, G., and Roberts, D. M. (1991). Calcium-dependent phosphorylation of symbiosome membrane proteins from nitrogen-fixing soybean nodules: evidence for phosphorylation of nodulin-26. *Plant Physiol*. **95**: 222-227.

Weaver, C. D., and Roberts, D. M. (1992). Determination of the site of phosphorylation of nodulin 26 by the calcium-dependent protein kinase from soybean nodules. *Biochemistry* **31**: 8954-8959.

Weaver, C. D., Shomer, N. H., Louis, C. F., and Roberts, D. M. (1994). Nodulin 26, a nodule-specific symbiosome membrane protein from soybean, is an ion channel. *J. Biol. Chem*. **269**: 17858-17862.

Weig, A., Deswarte, C., and Chrispeels, M. J. (1997). The major intrinsic protein family of Arabidopsis has 23 members that form three distinct groups with functional aquaporins in each group. *Plant Physiol*. **114**: 1346-1357.

Weig, A. R., and Jakob, C. (2000). Functional identification of the glycerol permease activity of *Arabidopsis thaliana* NLM1 and NLM2 proteins by heterologous expression in *Saccharomyces cerevisiae*. *FEBS lett*. **481**: 293-298.

White, D. W., and Jacobson, G. R. (1990). Molecular cloning of the C-terminal domain of *Eschericia coli* D-mannitol permease: expression, phosphorylation, and complementation with the C-terminal permease deletion proteins. *J. Bacteriol*. **172**: 1509-1515.

White, H. L., and Rolf, D. (1963). Diffusion of tritiated water into collecting duct urine in the dog. *Am. J. Physiol*. **205**: 715-717.

Wilkinson, T. L., Ashford, D. A., Pritchard, J., and Douglas, A. E. (1997). Honeydew sugars and osmoregulation in the pea aphid *Acyrthosiphon pisum*. *J. Exp. Biol*. **200**: 2137-2143.

Wilkinson, T. L., Koga, R., and Fukatsu, T. (2007). Role of host nutrition in symbiont regulation: impact of dietary nitrogen on proliferation of obligate and facultative bacterial endosymbionts of the pea aphid *Acyrthosiphon pisum*. *Appl. Environ. Microbiol*. **73**: 1362-1366.

Wysocki, R., Chery, C. C., Wawrzycka, D., Van Hulle, M., Cornelis, R., Thevelein, J. M., and Tamas, M. J. (2001). The glycerol channel Fps1p mediates the uptake of arsenite and antimonite in *Saccharomyces cerevisiae*. *Mol. Microbiol*. **40**: 1391-1401.

Xu, D., Xu, Y., and Uberbacher, E. C. (2000). Computational tools for protein modeling. *Curr. Protein Pept. Sci*. **1**: 1-21.

Yamaguchi-Shinozaki, K., and Shinozaki, K. (1993). Characterization of the expression of a dessication-responsive rd29 gene of *Arabidopsis thaliana* and analysis of its promoter in transgenic plants. *Mol. Gen. Genet*. **236**: 331-340.

Yamaji, N., Mitatni, N., and Ma, J. F. (2008). A transport regulating silicon distribution in rice shoots. *Plant Cell* **20**: 1381-1389.

Yamamoto, Y. T., Cheng, C. L., and Conkling, M. A. (1990). Root-specific genes from tobacco and Arabidopsis homologous to an evolutionarily conserved gene family of membrane channel proteins. *Nucleic Acids Res*. **18**: 7449.

Yang, H. C., Cheng, J., Finan, T. M., Rosen, B. P., and Bhattacharjee, H. (2005). Novel pathway for arsenic detoxification in the legume symbiont *Sinorhizobium meliloti*. *J. Bacteriol*. **187**: 6991-6997.

Yanochko, G. M., and Yool, A. J. (2002). Regulated cationic channel function in *Xenopus* oocytes expressing Drosophila Big Brain. *J. Neurosci*. **22**: 2530-2540.

Yasui, M., Hazama, A., Kwon, T. H., Nielsen, S., Guggino, W. B., and Agre, P. (1999a). Rapid gating and anion permeability of an intracellular aquaporin. *Nature* **402**: 184-187.

Yasui, M., Kwon, T. H., Knepper, M. A., Nielson, S., and Agre, P. (1999b). Aquaporin-6: an intracellular water channel protein in renal epithelia. *Proc. Natl. Acad. Sci. USA* **96**: 5808-5813.

Yuan, L., Loque, D., Kojima, S., Rauch, S., Ishiyama, K., Inoue, E., Takahashi, K., von Wiren, N. (2007). The organization of high-affinity ammonium uptake in Arabidopsis roots depends on the spatial arrangement and biochemical properties of AMT1-type transporters. *Plant Cell* **19**: 2636-2652.

Zampighi, G. A., Kreman, M., Boorer, K. J., Loo, D. D., Bezanilla, F., Chandy, G., Hall, J. E., and Wright, E. M. (1995) A method for determining the unitary functional capacity of cloned channels and transporters expressed in *Xenopus laevis* oocytes. *J. Membr. Biol*. **148**: 65-78.

Zhang, T., and Roberts, D. M. (1995). Expression of soybean nodulin 26 in transgenic tobacco: targeting to the vacuolar membrane and the effects on floral and seed development. *Mol. Biol. Cell* **6**: 109-117.

Zardoya, R. (2005). Phylogeny and evolution of the major intrinsic protein family. *Biol. Cell* **97**: 397-414.

Zeidel, M. L., Ambudkar, S. V., Smith, B. L., and Agre, P. (1992). Reconstitution of functional water channels in liposomes containing purified red cell CHIP28 protein. *Biochemistry* **31**: 7436-7440.

Zelinina, M., Zelenin, S., Bondar, A. A., Brismar, H., and Aperia, A. (2002). Water permeability of aquaporin-4 is decreased by protein kinase C and dopamine. *Am. J. Physiol. Renal Physiol*. **283**: F309-318.

Zhang, R. B., Logee, K. A., and Verkman, A. S. (1990). Expression of mRNA coding for kidney and red cell water channels in *Xenopus* oocytes. *J. Biol. Chem*. **265**: 15375-15378.

Zhang, R., Alper, S. L., Thorens, B., and Verkman, A. S. (1991). Evidence from oocyte expression that the erythrocyte water channel is distinct from band 3 and the glucose transporter. *J. Clin. Invest*. **88**: 1553-1558.

Zimmerman, P., Hirsch-Hoffman, M., Hennig, L., and Gruissem, W. (2004). GENEVESTIGATOR Arabidopsis microarray database and analysis toolbox. *Plant Physiol*. **136**: 2621-2632.

VITA

Ian Stuart Wallace was born in Memphis, Tennessee on March 21st, 1982. He graduated from Memphis University School in May of 2000 and entered the University of Tennessee the following August as an undergraduate. As a freshman, Ian was initially employed by Wesley D. Wicks in the Biochemistry, Cellular, and Molecular Biology Department as well as Dr. David Baker in the Chemistry department. He began his work in Dr. Daniel Roberts' lab in 2001 by characterizing the residues involved in substrate selectivity for *Lotus japonicus* nodulin 26. This simple project led to the initiation of a broader study of the selectivity regions in Arabidopsis Major Intrinsic Proteins that served as the foundation for his graduate work. Ian received his B. S. at the University of Tennessee in 2003 and graduated Cum Laude.

Ian chose to stay at the University of Tennessee and continue the work that he initiated as an undergraduate. He began graduate school in August of 2004 and received his Ph. D. in December of 2008. During his graduate school tenure, he continued his work on the selectivity of major intrinsic proteins, as well as initiated a number of collaborative projects characterizing aphid aquaporins and determining the physiological solutes of nodulin 26-like proteins in Arabidopsis. In total, his research led to seven publications in the primary literature (see below)

Publications

Wallace, I. S., Wills. D. M., Guenther, J. F., and Roberts, D. M. (2002). Functional selectivity for glycerol of the nodulin 26 subfamily of plant membrane intrinsic proteins. *FEBS lett*. **523**: 109-112.

Guenther, J. F., Chanmanivone, N., Galetovic, M. P., **Wallace, I. S.**, Cobb, J. A., and Roberts, D. M. (2003). Phosphorylation of soybean nodulin 26 on serine 262 enhances water permeability and is regulated developmentally and by osmotic signals. *Plant Cell* **15**: 981-991.

Wallace, I. S., and Roberts, D. M. (2004). Homology modeling of representative subfamilies of Arabidopsis major intrinsic proteins: Classification based on the aromatic/arginine selectivity filter. Special Arabidopsis Issue *Plant Physiol*. **135**: 1059-1068.

Wallace, I. S., and Roberts, D. M. (2005). Distinct transport selectivity of two structural subclasses of the nodulin-like intrinsic protein family of plant aquaglyceroporin channels. *Biochemistry* **44**: 16826-16834.

Wallace, I. S., Choi, W. G., and Roberts, D. M. (2006). The structure, function, and regulation of the nodulin 26-like intrinsic protein family of plant aquaglyceroporins. *Biochim. Biophys. Acta* **1758**: 1165-1175.

Tanaka, M., **Wallace, I. S.**, Takano, J., Roberts, D. M., and Fujiwara, T. (2008). NIP6;1 is a boric acid channel for preferential transport of boron to growing shoot tissues in Arabidopsis. *Plant Cell* **20**: 2860-2875.

Shakesby, A. J., **Wallace, I. S**., Isaacs, H. V., Pritchard, J., Roberts, D. M., and Douglas, A. E. (2008). A water-specific aquaporin involved in aphid osmoregulation. *Insect Biochem. Mol*. Biol. Published online

Honors and awards

Graduate:

1. Recipient of the Science Alliance Award for excellence in graduate research (2008).
2. Recipient of the Wright Research Fellowship Award for recognition of outstanding graduate research (2006)
3. Recipient of the Alexander Hollaender Award for excellence in graduate research (2005)
4. National Science Foundation Graduate Research Fellowship (2005)

Undergraduate:

1. American Society of Plant Biologists Summer Undergraduate Research Fellowship (SURF) Award (2003)
2. Phi Beta Kappa (2003)
3. Barry M. Goldwater Scholarship (2002)
4. Rhenium Chemistry Fellowship (2001)
5. Fred M. Roddy Scholarship (2001)